Molecular-Scale Mechanistic Investigation of Asphaltene Precipitation and Deposition Control Using Chemical Inhibitors

By
©Ali Ghamartale

A thesis submitted to the school of Graduate Studies in partial fulfilment of the requirements for the degree of

Doctor of Philosophy

Faculty of Engineering and Applied Science
Memorial University of Newfoundland

October, 2022

St. John’s, Newfoundland and Labrador
Canada

ABSTRACT

Asphaltene stability can be perturbed during oil production and transportation, leading to asphaltene precipitation and deposition. Chemical inhibitors are usually added to the crude oil to postpone asphaltene deposition. The interaction and potential bonds between asphaltene and inhibitor molecules describe the mechanisms and efficiency of inhibitors during the prevention of precipitation and deposition. As the asphaltene type varies from oil to oil, screening, designing, and developing inhibitors for a target oil are necessary. The screening process of selecting an effective inhibitor will be much more efficient if actual inhibition mechanisms are known. Although chemical inhibitors have been used in the industry for a long time, understanding of interaction mechanisms between asphaltenes and chemical inhibitors is vital in developing an efficient inhibitor. Disclosing the interaction mechanisms using an experimental strategy needs high technology tools, and it is demanding and costly. This research aims to develop a simulation workflow to understand the interaction between asphaltene molecules, inhibitors, and surfaces, which will help to figure out the main prevention/aggregation mechanisms during precipitation and deposition. In this study, molecular dynamics (MD), an advanced computational chemistry method, is employed to analyze the inhibitory effect of *n*-octylphenol (OP) and two 1-Butyl-3-methylimidazolium ionic liquids for three different asphaltene structures. The employed asphaltene structures include one archipelago and two continentals. Based on the knowledge gaps, we first study the impact of asphaltene structure, inhibitor concentration, pressure, and temperature on the efficiency of asphaltene aggregation inhibitors. Then, the impact of inhibitors on asphaltene binding arrangement during the aggregation process is investigated. Finally, we explore the inhibitory effect of chemicals on asphaltene deposition in the calcite pore. The asphaltene

aggregation, aggregate characterization, and deposit characterization are studied in oil bulk and confined oil systems (pore structure) to meet the objectives.

This thesis begins with an extensive literature review, and the first sets of simulations focus on the impact of asphaltene structures during the precipitation process. In this section, systems with singular and binary asphaltene types in *n*-heptane are simulated in the absence and presence of OP, as a surfactant inhibitor. The results show that the OP can delay the aggregation of the continental asphaltene with the potential of forming hydrogen bonds. It is also concluded that the average aggregation number needs to be coupled with the gyration radius analysis to evaluate the hierarchical paradigm of asphaltene aggregation. After that, a sensitivity analysis is conducted to investigate important aspects such as the inhibitor concentration, thermodynamic condition, and computational hardware. This part aims to optimize the screening and designing of inhibitors from both technical and economic viewpoints. It is concluded that a minimum inhibitor concentration is needed so that the inhibitor appears to be impactful. It also shows that in the pressure range of 1-60 bar, OP has the most inhibitory effect at 30 bar since the asphaltene-asphaltene aggregation energies are extremely high at 1 bar such that the asphaltene-inhibitor energy can not cope with this situation. In comparison, the asphaltene-asphaltene interaction energy is extremely reduced at 60 bar such that the aggregates are already unstable even in the absence of OP. OP is most impactful at 360 K in the temperature range of 300-360 K. The significant impact of the inhibitor on aggregate shape in this study motivates us to study the detailed arrangement of asphaltene aggregation, which is directly related to the strength and stability of the aggregation. Therefore, we concentrate on more mechanistic details by investigating the impact of two types of inhibitor, including surfactant and ionic liquid, on the asphaltene binding arrangement. The outcome reveals the OP mainly forms bonding through hydrogen bonds, and the quadrupole-quadrupole interaction

between the OP benzene ring and asphaltene core is weaker than the quadrupole-quadrupole between asphaltenes. In contrast, the ionic liquid reduces the asphaltene stacking association as the cation part of ionic liquids approaches the aromatic core of the asphaltene and beats the quadrupole-quadrupole interaction between asphaltenes. In the next step, the asphaltene deposition is studied when asphaltene-heptane is placed in a calcite pore without/with chemical inhibitors. According to the results, the OP adsorbs on the calcite surface and reduces LJ and Coulomb energies between asphaltene and calcite by 400 and 1000 kJ/mol, respectively, which reduces the asphaltene deposition on the surface. The selected ionic liquid has a short alkyl tail on its cation, which cannot provide a hindrance layer near the calcite surface. The combination of two inhibitors minimizes the precipitation and deposition of asphaltene when OP to IL ratio is 3:1. At this ratio, the aggregation number reduces from 20 to less than 10, and the deposition rate reduces from 1 to 0.8 compared to the case with no inhibitor. This thesis is a pioneering study to demystify the asphaltene-inhibitor behaviors during asphaltene precipitation and deposition, which can provide a useful workflow to screen, select, and design the effective inhibitor for the target crude oil (and asphaltene) besides saving time and money for the industry with effective pre-selection instead of conducting trial and error lab tests.

ACKNOWLEDGMENTS

I would like to express my sincere appreciation to those who gave me absolute support and invaluable advice and recommendations. This work would never be a success without the mutual collaboration of many people.

First and foremost, I would like to emphasize the role of my supervisor, Dr. Sohrab Zendehboudi and express my sincere gratitude and thanks to him. His magnificent visions and guidance have always inspired me. I greatly appreciate Dr. Nima Rezaei for his continued support and guidance toward my thesis completion. I was lucky to collaborate with Dr. Nima during my PhD who was not only a colleague for technical questions but also a great mentor/friend who taught me how to behave professionally and prepared me morally for my future career.

Most importantly, none of this would have been possible without the love and support of my family. Words cannot express my appreciation for my parents and my lovely sister. Although there was miles distance between us, they motivated me, encouraged me, advised me and kept me in their prays every day, which I will never be able to appreciate enough.

Last but not least, I would like to thank the Natural Sciences and Engineering Research Council of Canada (NSERC), Memorial University (NL, Canada), InnovateNL, and Equinor (formerly Statoil) Canada for their financial support.

“This dissertation is dedicated to my parents and my sister.”

Table of Contents

LIST OF TABLES

LIST OF FIGURES

1. CHAPTER ONE

Introduction and Methodology

1.1 Background

Asphaltene is the heaviest, most polarizable, and the best surface-active component among the crude oil constituents [1]. Asphaltene is defined as a specie that is soluble in aromatic solvents (such as toluene, benzene, or pyridine) but insoluble in alkanes (such as *n*-pentane or *n*-heptane) [2, 3]; this means asphaltene does not have a unique structure. Asphaltene fraction is made of a range of components, varying from oil to oil. For instance, if asphaltenes of different oils have a comparable solubility, the chemical properties can be completely different [4]. The precipitation and deposition of asphaltenes in the production and transportation of the crude oil cause production interruption via formation damage, and wellbore and production equipment plugging [5, 6]. The asphaltene damage can be handled using physical and chemical approaches before and after precipitation/deposition. Solvent wash and scrapers are typical examples of chemical and physical treatments for asphaltene treatment after its deposition. Nevertheless, prevention is always more effective than treatment since it reduces production interruption and costs. The application of chemical inhibitors in preventing asphaltene precipitation and deposition has been proven on the industrial scale; however, screening and designing an effective inhibitor for the target oil and asphaltene are still a challenge for the industry. Since the chemical treatment is a significant investment, such processes require detailed investigation before the operation to ensure the project's success. Systematic investigations can be conducted using experimental and computational approaches. The experimental works need high technology devices, and the experimental tests are usually expensive and time consuming, while the computational approach such as advanced computational chemistry tools can predict the material behaviors at molecular scale with an acceptable accuracy through an easy and inexpensive manner.

The asphaltene molecules are known for having either one polycyclic aromatic hydrocarbon cores (named continental type) or two polycyclic aromatic hydrocarbon cores (named archipelago type). Two asphaltene molecules can have an attractive force through induced dipole-induced dipole (due to resonance bonds) and dipole-dipole (due to heteroatoms) [7]. Gray et al. [8] demonstrated that the π-π stacking is not the dominant force for asphaltene aggregation. They stated that Brønsted acid-base interactions, hydrogen bonding, metal coordination complexes, and interactions between cycloalkyl and alkyl groups (to form hydrophobic pockets) are also responsible for asphaltene aggregation forces. Therefore, asphaltenes bond to each other with either of three configurations, including face-to-face, edge-on, and offset π-stacked. The chemical inhibitors also come in various types and structures. They can be surfactants, polymers, nanoparticles, ionic liquids, vegetable oils or oil derivatives. The chemical inhibitors, such as surfactants, can attach to asphaltene molecules through various bonding and prevent asphaltene self-aggregation. Inhibitors can be suspended in the oil environment, such as nanoparticles, and keep the asphaltene suspended for a longer duration by adsorbing them on their top. The inhibitors such as vegetable oil and oil derivatives can also postpone the asphaltene aggregation by changing the mixture's composition, and eventually changing the phase envelope and the asphaltene envelope of target fluids. Various inhibitors have different influential parameters, which are listed in Table 1-1.

Table 1-1. Influential parameters on inhibition mechanisms: dependent parameters.

	Dependent Parameters				
	Surfactants	**Polymers**	**Nanoparticles**	**Ionic liquids**	**Oil products**
Inhibitor influential parameters	Type and number of functional groups	Polymerization degree	Surface chemistry and charge	Functional groups	SARA ratio
	Size and number of alkyl tails	Type and number of functional groups	Specific surface	Size of alkyl tail	H/C
	Acidity	Molecular weight	Shape and Size	Charge density	API Polarity Solubility

Recently, researchers put efforts into revealing the asphaltene aggregation mechanisms in different scenarios using molecular dynamics (MD). The knowledge gap in understanding the asphaltene-inhibitor interactions, and the importance of component structure and functional groups in both asphaltene and chemical inhibitors need to be extensively investigated for better screening and designing of suitable chemical inhibitors for the target oil. Ideally, the asphaltene inhibitors should be able to adhere to the asphaltene particles and keep them suspended in the solution. For instance, the asphaltene polyaromatic core should bind to the chemical inhibitors instead of the asphaltene-asphaltene self-aggregation and keep the asphaltene molecules separated [9]. Also, the heteroatoms in the asphaltene structure should form hydrogen bonds with chemicals, which have N-H, O-H, and F-H bonds, and keep the asphaltenes separated. The heteroatoms and metal particles that induce polarity on the asphaltene molecules allow acid-base interactions with the polar head of inhibitors which can be another inhibitory mechanism [9]. These characteristics and bonding properties are related to the asphaltene and chemical inhibitors' structures. Therefore, both asphaltene and inhibitor should have suitable structures and functional groups to keep asphaltene suspended and dispersed in the carrying fluid [9].

The wide variations of inhibitor types in the market allow engineers and researchers to select the most efficient inhibitor, although the variations make the screening process complex when all aspects are considered. A few important aspects of asphaltene inhibitor selection are stated in the following. Some significant factors need to be considered; for instance, inhibitors such as polymers may lose their efficiency with increasing temperature, while the others' efficiency may increase by increasing temperature, such as some ionic liquids. Also, fluid and asphaltene characteristics, including polarity and acidity, are key parameters when using ionic surfactant inhibitors [9]. Crude oil acidity and the asphaltene polarity can limit the applicability of the inhibitors with a particular

charge or acidity [9]. Therefore, the success of inhibitors application significantly depends on the pre-screening and designing suitable inhibitors for the target asphaltene and oil.

MD simulation is a powerful tool for investigating physical phenomena at a molecular scale. MD considers molecular interactions and calculates the properties of (bio)chemical systems, such as temperature, pressure, and energy between molecules over the simulation period. In MD simulation, constituents of the physical systems and atoms interact through interatomic forces based on the atomic forcefield model. Each atom in the system is influenced by the potential energy (partial charge) of other atoms, and the system energy is calculated based on the relative positions of the particles and the selected forcefield. This important feature considers the intramolecular energies as contributions of the potential energy from bonds' length, bend angles, and dihedrals angles; the intermolecular energies are accounted by van der Waals and electrostatic [10]. Various forcefields such as polymer-consistent forcefield (PCFF), constant valence forcefield (CVFF), condensed-phase-optimized molecular potential for atomistic simulation studies (COMPASS) forcefield, assisted model building with energy refinement (AMBER) forcefield, chemistry at Harvard macromolecular mechanics (CHARMM-27) forcefield, GROningen molecular simulation (GROMOS96) forcefield, and OPLS-AA forcefield have been developed. Among the mentioned forcefields, GROMOS96 and OPLS-AA are the most popular ones for modeling organic compounds. Not all the forcefields are available in every MD software, and the best forcefield may need to be selected based on the selected simulation software. The accuracy of the selected forcefield may need to be validated with either experimental results or previous valid simulation results. In fact, MD has been used to estimate the equilibrium properties such as density or enthalpy of mixtures. It is practical to investigate the transport properties such as mass transfer (and/or diffusion) coefficients, heat transfer coefficient (thermal conductivity), and momentum

transfer coefficient (viscosity). MD can simulate physical properties such as interfacial tension, solubility, adsorption, and aggregation. However, it needs to be coupled with another modeling strategy, such as quantum mechanics, when a chemical reaction produces a new component (molecule) in the system. Typically, four statistical states are considered in MD, which can be implemented based on the test conditions, including 1) constant number of particles, volume, and energy (NVE), 2) constant number of particles, volume, and temperature (NVT), 3) constant number of particles, pressure, and temperature (NPT); and 4) constant chemical potential, volume, and temperature (μVT) [10].

The molecular dynamics method has been developed to calculate the physical properties of the chemicals and their mixtures based on structures and molecular interactions (e.g., solubility and self-aggregation). There are various commercial and open-source software to perform MD simulations. Materials Studio, which belongs to the Biovia Company, is a commercial software. Other open-source software packages to implement MD simulation include NAMD, GROMACS, AMBER SUITE, and LAMMPS. MD has been successfully employed to model asphaltene precipitation [11-33], and asphaltene deposition on calcite [34-36] and silica [21, 35] surfaces. Also, MD is able to model interfacial properties in the presence of different substances such as asphaltene [23, 37-42], asphaltene and resin [43], emulsifier [43], and demulsifier of water/oil emulsion [44]. Recently, the MD approach has been used to model asphaltene aggregation during enhanced oil recovery (EOR) processes such as water injection [45-47] and gas injection [48]. However, the interactions of asphaltene and inhibitors have not been studied comprehensively. It is vital to disclose the inhibitory mechanisms of inhibitors; this helps in effectively screening and designing new chemical inhibitors. Also, the molecular interactions of asphaltene and inhibitor

near surfaces have never been studied using computational methods to the best of our knowledge, while it is important to figure out the inhibitor efficiency during the asphaltene deposition.

This research is dedicated to filling the above-mentioned knowledge gaps and providing a better understanding and approach for screening and designing chemical inhibitors. Therefore, as the first objective of this research, the MD technique is adopted to reveal the asphaltene-inhibitor interaction during the precipitation of various asphaltene structures in the presence of a chemical inhibitor. In addition, the same technique is adopted to explore the impact of an inhibitor concentration, temperature, and pressure during the asphaltene precipitation as the second objective of this research. During the previous simulation, the importance and impact of chemical inhibitors on asphaltene binding arrangement were indirectly realized. Therefore, the effects of various chemical inhibitors on the type of binding arrangements between asphaltene molecules during the precipitation process are studied as the third main objective of this research. Finally, the asphaltene-inhibitor interaction is studied for various asphaltene and inhibitor types during the deposition of asphaltene molecules in a calcite pore using the MD technique. To obtain the goal of this study, the energies between molecules and asphaltene aggregates characteristics are assessed during asphaltene precipitation and deposition.

The current study shows the applicability of MD in revealing the effective mechanisms of real-world problems, particularly in the asphaltene flow assurance concern. This method can be incorporated into screening, selecting, and designing effective and new inhibitors for asphaltene precipitation and deposition. This work is a pioneer study in screening and designing effective inhibitors for the target oil and asphaltene. This thesis consists of four manuscripts (either published or under review for publication), briefly described in Figure 1-1 and listed below:

The second chapter is published in the Journal of Energy & Fuels and is dedicated to studying the asphaltene-inhibitor interaction for the systems that carry individual and binary types of asphaltene, focusing on the impact of asphaltene type and structure. The results of this study are validated by a recent study [30]. The highlights of this study are the discussion of the aggregation criteria during the simulation, followed by discussing the research outcomes from two main research groups working on asphaltene and asphaltene-inhibitor interactions [7, 30, 31, 49]. The third chapter is published in the Journal of Molecular Liquids and is a follow-up to the first study by assessing the inhibitor concentration and thermodynamic conditions on the inhibitor efficiency and asphaltene-inhibitor interactions. In this work, parallel computing and GPU hardware are incorporated to minimize the simulation time compared to regular simulation using CPUs.

The fourth chapter is submitted to the Journal of Chemical Engineering Science and is devoted to studying the coordination of asphaltene and asphaltene binding types during their aggregation. This study tries to fill the molecular knowledge gap of binding arrangements and intermolecular network formations between the asphaltenes and inhibitors, limiting the design and preparation of chemical inhibitors. This study uses the radial distribution function, the aggregate shape index, and the angle and distance between the molecules to explore the asphaltene binding arrangement manipulation in the presence of different inhibitors. This work introduces a new method of distinguishing the various types of asphaltene binding arrangements.

The fifth chapter is a manuscript accepted to be published in the Journal of Industrial & Engineering Chemistry Research. This research manuscript focuses on asphaltene precipitation and deposition in the calcite pore when the carrying fluid is *n*-heptane in the absence and presence of inhibitors. This work studies the impact of two types of inhibitors, including surfactant and ionic

liquid, both individually and as a mixture, during the asphaltene deposition. The last chapter covers the summary, conclusions, and recommendations for future work.

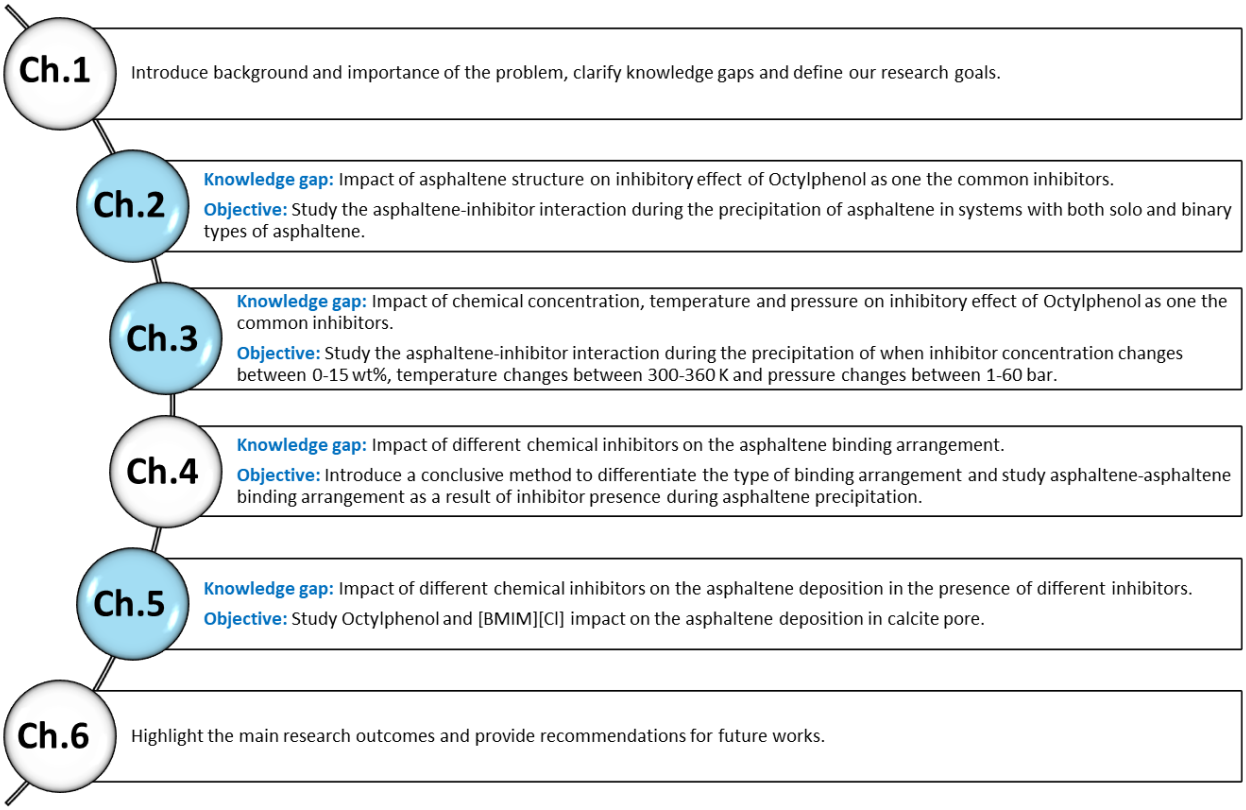

Figure 1-1. The summary of the main objectives and contributions of each chapter. The lighted chapters are published.

1.2 Methodology

In this research, we employed GROMACS, open-source software that is free and easy to access for future reference. It is also available on ComputeCanada, a huge cluster available in Canada, and we could run our simulation on numerous CPUs and GPUs depending on our need and cluster availability. AMBER, CHARMM-27, GROMOS96, and OPLS-AA are available forcefield on GROMCAS software. In the literature review, various molecular forcefields are assessed, including AMBER, OPLS, CHARMM, and GROMOS forcefields to predict and compare

thermodynamic properties of liquid benzene with experimental results. The results have demonstrated that OPLS-AA can produce more accurate results for organic compounds compared with other forcefields [50]. Also, based on our literature review, OPLS-AA forcefield has been used usually in asphaltene studies and generated trustable results. Therefore, we decided to use OPLS-AA forcefield with GROMACS software in our studies.

The molecular structure of a component is required for any molecular level simulation. The asphaltene part of the crude oil consists of molecules with different structures. Two methods are suggested in the literature to find the representative chemical structure of the asphaltene molecules. The first analytical method is based on elemental analysis and NMR tests. In this technique, the hypothetical structure has a stronger association tendency [19]. The second method to develop asphaltene structures is generating structure using Monte Carlo simulation and quantitative molecular representation (QMR), in which the structure is chosen based on the least deviation from experimental data [51, 52]. Headen et al. [31] conducted a comprehensive survey about the types of asphaltene structures and introduced four structures and we adopted two of them in our study [20, 29, 30, 52].

In this study, we used three different hypothetical asphaltene structures. The hypothetical asphaltene structure A1 is of archipelago type. The other two asphaltene structures, A2 and A3, are of the continental type. We use the asphaltene structures A1 and A3 from Headen et al. [31] as we could validate our results. Similar to the study by Goual et al. [53], we modify the asphaltene structure A3 by substituting an aromatic group with pyridine and replacing a methyl group with a hydroxyl group to create A2. Therefore, A2 can form hydrogen bonds, while the asphaltene structure A3 lacks such a capability. The asphaltene structures and more detail are demonstrated in Chapter 2.

To the best of our knowledge, surfactants (in particular, phenol-based) are known as a potential type of inhibitor based on techno-economic perspectives. Inhibitor screening studies show that octylphenol, nonylphenol, and ethoxylated nonylphenol are the most effective surfactants for preventing asphaltene aggregation [54]. The ionic liquid is a novel and more environmentally friendly type of asphaltene inhibitor. Phenols can form hydrogen bonds, and ionic liquids can have cation-quadrupole interaction with asphaltene polyaromatic cores. Therefore, we considered *n*-Octylphenol (OP) and two ionic liquids including 1-butyl-3-methylimidazolium bromide ([BMIM][Br]), and 1-butyl-3-methylimidazolium chloride ([BMIM][Cl]) for further investigation.

1.2.1 MD simulation in the bulk of fluids

The component structures can be built as a pdb file using various software such as Avogadro and Gaussview. We built the asphaltenes and Octylphenol structures and adopted the structure of ionic liquids from the literature [55]. Subsequently, the structures are optimized using Gaussian09 software at the ground state and their atoms' partial charges are also calculated using ESP or electrostatic potential approach. Quantum mechanics calculation with density functional theory (B3LYP) method and 6-31g(d,p) basis set are applied for structural optimization [56]. The electrostatic potential is an accurate and standard method used to estimate the atoms' partial charge [57]. MKTOP [58] is used to generate topology files for the molecules based on the OPLS-AA forcefield. MKTOP considers all bonds, non-bonds, and improper dihedrals for the aromatic ring in the output file. However, the output results may need a few corrections on atom type and partial charge, which should be conducted manually. Finally, the optimized pdb file and topology file or itp files are ready to be imported to GROMACS software.

A cubic box with 15×15×15 nm3 dimension is built for all simulation runs to reduce the possible overlap between molecules. The box size will change when we set temperature and pressure and

run NPT ensemble based on the material type, quantity, intermolecular interactions and the thermodynamic conditions that lead to convergence and precise estimation of physical properties (such as density). Afterward, the respective number of each molecule based on the designed concentration of asphaltene and inhibitor will randomly be distributed in the box.

After distributing the molecules in the box, the system is ready to start the simulation. The steepest descent method minimizes the initial configuration for 10000 steps to relax the system. A velocity rescaling thermostat [59] is used in NVT for 100 ps to reach the desired temperature. Velocity rescaling thermostat and Berendsen barostat [60] are used in NPT for 1 ns to adjust the box size and density at the designed temperature and pressure. The production runs are conducted using the Nose-Hoover thermostat [61, 62] and Parrinello−Rahman barostat [63] to maintain the system temperature and pressure for 120 ns. Leapfrog algorithm [64] is employed to integrate the equation of motion for all NVT, NPT, and production runs. The time step is fixed at 2 fs as an optimal time step in all simulation runs [29]. The outputs, including the atom position, energy, temperature, pressure, and density, are recorded every 10 ps. The long-range electrostatic interactions are governed by the particle-mesh Ewald (PME) algorithm [65, 66], for which the cutoff radius of the van der Waals and Coulomb interactions is fixed at 1.2 nm. Periodic boundary conditions are employed to approximate an extensive system, and all bond lengths are kept rigid using the LINCS algorithm [67]. Finally, suitable analyses will be conducted using energy and atoms' coordination as two main outputs of the simulation. The analyses related to each project are described in each chapter in detail.

1.2.2 MD simulation in the pore filled with fluid (confined box)

The simulation setting, when the box is confined, is generally similar to the case where there is no confinement with a few amendments. First, the solid atoms must be restrained as the solid's

molecule will not move. As the box is confined, the box size cannot change, meaning the NPT ensemble is not applicable. Therefore, in our study, NVT simulation using a velocity rescaling thermostat will be used for 100 ps to adjust system temperature at the desired temperature, and the production run will be performed based on the NVT for 60 ns as the last step for data sampling.

As mentioned, the box size is fixed in the confined simulation; hence, we need to adjust the space in the confined area with the correct volume for our fluid at the desired pressure and temperature. Afterward, we are able to design the surface slab' size based on the measured volume and target pore opening. Our approach to finding the correct volume was simulating the fluid out of a confined space at the designed pressure and temperature, similar to the bulk simulation and extracting the final volume as an input for simulation in the confined area. Hence, we will implement energy minimization, 100 ps NVT and 1 ns NPT, extracting the final volume and considering that as the volume of the confined area or the pore volume. Considering the measured volume and calcite pore opening, which we designed to be 10 nm, the calcite slab is constructed by splitting calcite along the (104) crystallographic surface of a calcite unit cell using Materials Studio software with 11.477 nm × 9.275 nm × 2.240 nm dimensions. The pore is constructed by placing one layer of slab on top of the other with a 10 nm pore opening. We also adopted the forcefield suggested by Xiao and co-workers as it was used to model the calcite surfaces in the literature with satisfactory results [68]. Finally, suitable analyses will be conducted using energy and atoms' coordination as two main outputs of the simulation. The analyses related to each project are described in each chapter in detail.

REFERENCES

1. Mullins, O.C., The asphaltenes. Annual review of analytical chemistry, 2011. 4: p. 393-418.

2. Adams, J.J., Asphaltene adsorption, a literature review. Energy & Fuels, 2014. 28(5): p. 2831-2856.
3. Subramanian, S., S. Simon, and J. Sjöblom, Asphaltene precipitation models: a review. Journal of Dispersion Science and Technology, 2016. 37(7): p. 1027-1049.
4. Luo, P., X. Wang, and Y. Gu, Characterization of asphaltenes precipitated with three light alkanes under different experimental conditions. Fluid Phase Equilibria, 2010. 291(2): p. 103-110.
5. Kokal, S.L. and S.G. Sayegh. Asphaltenes: The cholesterol of petroleum. in Middle East Oil Show. 1995. Society of Petroleum Engineers.
6. Leontaritis, K.J. and G.A. Mansoori, Asphaltene deposition: a survey of field experiences and research approaches. Journal of Petroleum Science and Engineering, 1988. 1(3): p. 229-239.
7. Mullins, O.C., The modified Yen model. Energy & Fuels, 2010. 24(4): p. 2179-2207.
8. Gray, M.R., et al., Supramolecular assembly model for aggregation of petroleum asphaltenes. Energy & Fuels, 2011. 25(7): p. 3125-3134.
9. Ghamartale, A., et al., Asphaltene Deposition Control by Chemical Inhibitors: Theoretical and Practical Prospects. 2021: Elsevier Science.
10. Seyyedattar, M., S. Zendehboudi, and S. Butt, Molecular dynamics simulations in reservoir analysis of offshore petroleum reserves: A systematic review of theory and applications. Earth-science reviews, 2019. 192: p. 194-213.
11. Rogel, E., Studies on asphaltene aggregation via computational chemistry. Colloids and Surfaces A: Physicochemical and Engineering Aspects, 1995. 104(1): p. 85-93.

12. Sheu, E.Y., Self-association of asphaltenes, in Structures and dynamics of asphaltenes. 1998, Springer. p. 115-144.
13. Rogel, E., Simulation of interactions in asphaltene aggregates. Energy & Fuels, 2000. 14(3): p. 566-574.
14. Murgich, J., J. Rodríguez, and Y. Aray, Molecular recognition and molecular mechanics of micelles of some model asphaltenes and resins. Energy & Fuels, 1996. 10(1): p. 68-76.
15. Murgich, J. and O.P. Strausz, Molecular mechanics of aggregates of asphaltenes and resins of the Athabasca oil. Petroleum science and technology, 2001. 19(1-2): p. 231-243.
16. Pacheco-Sánchez, J., I. Zaragoza, and J. Martínez-Magadán, Asphaltene aggregation under vacuum at different temperatures by molecular dynamics. Energy & fuels, 2003. 17(5): p. 1346-1355.
17. Pacheco-Sánchez, J., I. Zaragoza, and J. Martínez-Magadán, Preliminary study of the effect of pressure on asphaltene disassociation by molecular dynamics. Petroleum science and technology, 2004. 22(7-8): p. 927-942.
18. Takanohashi, T., S. Sato, and R. Tanaka, Structural relaxation behaviors of three different asphaltenes using MD calculations. Petroleum science and technology, 2004. 22(7-8): p. 901-914.
19. Carauta, A.N., et al., Modeling solvent effects on asphaltene dimers. Energy & fuels, 2005. 19(4): p. 1245-1251.
20. Ungerer, P., et al., Sensitivity of the aggregation behaviour of asphaltenes to molecular weight and structure using molecular dynamics. Molecular Simulation, 2014. 40(1-3): p. 115-122.

21. Fang, T., et al., Study on the asphaltene precipitation in CO2 flooding: a perspective from molecular dynamics simulation. Industrial & Engineering Chemistry Research, 2018. 57(3): p. 1071-1077.

22. Liu, B., et al., Mechanism of asphaltene aggregation induced by supercritical CO 2: insights from molecular dynamics simulation. RSC advances, 2017. 7(80): p. 50786-50793.

23. Kuznicki, T., J.H. Masliyah, and S. Bhattacharjee, Molecular dynamics study of model molecules resembling asphaltene-like structures in aqueous organic solvent systems. Energy & Fuels, 2008. 22(4): p. 2379-2389.

24. Jian, C., T. Tang, and S. Bhattacharjee, Probing the effect of side-chain length on the aggregation of a model asphaltene using molecular dynamics simulations. Energy & fuels, 2013. 27(4): p. 2057-2067.

25. Gao, F., et al., Molecular dynamics simulation: the behavior of asphaltene in crude oil and at the oil/water interface. Energy & fuels, 2014. 28(12): p. 7368-7376.

26. Silva, H.S., et al., Molecular dynamics study of nanoaggregation in asphaltene mixtures: Effects of the N, O, and S heteroatoms. Energy & Fuels, 2016. 30(7): p. 5656-5664.

27. Sodero, A.C., et al., Investigation of the effect of sulfur heteroatom on asphaltene aggregation. Energy & Fuels, 2016. 30(6): p. 4758-4766.

28. Mehana, M., M. Fahes, and L. Huang, Asphaltene Aggregation in Oil and Gas Mixtures: Insights from Molecular Simulation. Energy & Fuels, 2019. 33(6): p. 4721-4730.

29. Headen, T.F., E.S. Boek, and N.T. Skipper, Evidence for asphaltene nanoaggregation in toluene and heptane from molecular dynamics simulations. Energy & Fuels, 2009. 23(3): p. 1220-1229.

30. Sedghi, M., et al., Effect of asphaltene structure on association and aggregation using molecular dynamics. The Journal of Physical Chemistry B, 2013. 117(18): p. 5765-5776.
31. Headen, T., et al., Simulation of asphaltene aggregation through molecular dynamics: Insights and limitations. Energy & Fuels, 2017. 31(2): p. 1108-1125.
32. Javanbakht, G., et al., Molecular polydispersity improves prediction of asphaltene aggregation. Journal of Molecular Liquids, 2018. 256: p. 382-394.
33. Headen, T.F. and M.P. Hoepfner, Predicting Asphaltene Aggregate Structure from Molecular Dynamics Simulation: Comparison to Neutron Total Scattering Data. Energy & Fuels, 2019. 33(5): p. 3787-3795.
34. Headen, T.F. and E.S. Boek, Potential of mean force calculation from molecular dynamics simulation of asphaltene molecules on a calcite surface. Energy & fuels, 2011. 25(2): p. 499-502.
35. Mohammed, S. and G. Gadikota, The role of calcite and silica interfaces on the aggregation and transport of asphaltenes in confinement. Journal of Molecular Liquids, 2019. 274: p. 792-800.
36. Mohammed, S. and G. Gadikota, The influence of CO2 on the structure of confined asphaltenes in calcite nanopores. Fuel, 2019. 236: p. 769-777.
37. Mikami, Y., et al., Molecular dynamics simulations of asphaltenes at the oil–water interface: from nanoaggregation to thin-film formation. Energy & Fuels, 2013. 27(4): p. 1838-1845.
38. Jian, C., et al., A molecular dynamics study of the effect of asphaltenes on toluene/water interfacial tension: surfactant or solute? Energy & fuels, 2018. 32(3): p. 3225-3231.

39. Lv, G., et al., The properties of asphaltene at the oil-water interface: A molecular dynamics simulation. Colloids and Surfaces A: Physicochemical and Engineering Aspects, 2017. 515: p. 34-40.

40. Mohammed, S. and G.A. Mansoori, Effect of CO2 on the interfacial and transport properties of water/binary and asphaltenic oils: insights from molecular dynamics. Energy & fuels, 2018. 32(4): p. 5409-5417.

41. Mohammed, S. and G.A. Mansoori, Molecular insights on the interfacial and transport properties of supercritical CO2/brine/crude oil ternary system. Journal of Molecular Liquids, 2018. 263: p. 268-273.

42. Teklebrhan, R.B., et al., Initial partition and aggregation of uncharged polyaromatic molecules at the oil–water interface: a molecular dynamics simulation study. The Journal of Physical Chemistry B, 2014. 118(4): p. 1040-1051.

43. Song, S., et al., Molecular Dynamics Study on Aggregating Behavior of Asphaltene and Resin in Emulsified Heavy Oil Droplets with Sodium Dodecyl Sulfate. Energy & fuels, 2018. 32(12): p. 12383-12393.

44. Liu, J., Y. Zhao, and S. Ren, Molecular dynamics simulation of self-aggregation of asphaltenes at an oil/water interface: formation and destruction of the asphaltene protective film. Energy & Fuels, 2015. 29(2): p. 1233-1242.

45. Yaseen, S. and G.A. Mansoori, Molecular dynamics studies of interaction between asphaltenes and solvents. Journal of Petroleum Science and Engineering, 2017. 156: p. 118-124.

46. Yaseen, S. and G.A. Mansoori, Asphaltene aggregation due to waterflooding (A molecular dynamics study). Journal of Petroleum Science and Engineering, 2018. 170: p. 177-183.

47. Yaseen, S. and G.A. Mansoori, Asphaltene aggregation onset during high-salinity waterflooding of reservoirs (a molecular dynamic study). Petroleum Science and Technology, 2018. 36(21): p. 1725-1732.

48. Khalaf, M.H. and G.A. Mansoori, Asphaltenes aggregation during petroleum reservoir air and nitrogen flooding. Journal of Petroleum Science and Engineering, 2019. 173: p. 1121-1129.

49. Sedghi, M. and L. Goual. Molecular dynamics simulations of asphaltene dispersion by limonene and PVAc polymer during CO 2 flooding. in SPE International Conference and Exhibition on Formation Damage Control. 2016. Society of Petroleum Engineers.

50. Fu, C.-F. and S.X. Tian, A comparative study for molecular dynamics simulations of liquid benzene. Journal of chemical theory and computation, 2011. 7(7): p. 2240-2252.

51. Boek, E.S., D.S. Yakovlev, and T.F. Headen, Quantitative molecular representation of asphaltenes and molecular dynamics simulation of their aggregation. Energy & Fuels, 2009. 23(3): p. 1209-1219.

52. Strausz, O.P., T.W. Mojelsky, and E.M. Lown, The molecular structure of asphaltene: an unfolding story. Fuel, 1992. 71(12): p. 1355-1363.

53. Goual, L., et al., Asphaltene aggregation and impact of alkylphenols. Langmuir, 2014. 30(19): p. 5394-5403.

54. !!! INVALID CITATION !!! 6, 7, 8, 9, 10, 11, 12, 13.

55. Doherty, B., et al., Revisiting OPLS Force Field Parameters for Ionic Liquid Simulations. J Chem Theory Comput, 2017. 13(12): p. 6131-6145.

56. Parr, R.G., Density functional theory of atoms and molecules, in Horizons of Quantum Chemistry. 1980, Springer. p. 5-15.

57. Campañá, C., B. Mussard, and T.K. Woo, Electrostatic potential derived atomic charges for periodic systems using a modified error functional. Journal of Chemical Theory and Computation, 2009. 5(10): p. 2866-2878.

58. Ribeiro, A.A., B.A. Horta, and R.B.d. Alencastro, MKTOP: a program for automatic construction of molecular topologies. Journal of the Brazilian Chemical Society, 2008. 19(7): p. 1433-1435.

59. Bussi, G., D. Donadio, and M. Parrinello, Canonical sampling through velocity rescaling. The Journal of chemical physics, 2007. 126(1): p. 014101.

60. Berendsen, H.J., et al., Molecular dynamics with coupling to an external bath. The Journal of chemical physics, 1984. 81(8): p. 3684-3690.

61. Nosé, S., A molecular dynamics method for simulations in the canonical ensemble. Molecular physics, 1984. 52(2): p. 255-268.

62. Hoover, W.G., Canonical dynamics: Equilibrium phase-space distributions. Physical review A, 1985. 31(3): p. 1695.

63. Parrinello, M. and A. Rahman, Strain fluctuations and elastic constants. The Journal of Chemical Physics, 1982. 76(5): p. 2662-2666.

64. Hockney, R.W., S. Goel, and J. Eastwood, Quiet high-resolution computer models of a plasma. Journal of Computational Physics, 1974. 14(2): p. 148-158.

65. Darden, T., D. York, and L. Pedersen, Particle mesh Ewald: An N· log (N) method for Ewald sums in large systems. The Journal of chemical physics, 1993. 98(12): p. 10089-10092.

66. Essmann, U., et al., A smooth particle mesh Ewald method. The Journal of chemical physics, 1995. 103(19): p. 8577-8593.

67. Hess, B., et al., LINCS: a linear constraint solver for molecular simulations. Journal of computational chemistry, 1997. 18(12): p. 1463-1472.

68. Xiao, S., S.A. Edwards, and F. Gräter, A new transferable forcefield for simulating the mechanics of CaCO3 crystals. The Journal of Physical Chemistry C, 2011. 115(41): p. 20067-20075.

2. CHAPTER TWO

New Molecular Insights into Aggregation of Pure and Mixed Asphaltenes in the Presence of *n*-Octylphenol Inhibitor

Preface

A version of this manuscript has been published in the Energy & Fuels 34.10 (2020): p. 13186. Ghamartale, A., Rezaei, N. and Zendehboudi, S. are the authors of this paper. Ghamartale, with the insight from co-authors, designed and developed the simulation using molecular dynamics (MD) models. All three authors contributed to the design of the manuscript structure. The literature review, execution of the models and comparison were mainly conducted by the first author, Ali Ghamartale. The first draft of the paper was also prepared by the first author and extensively revised by Rezaei. The feedback comments from co-author Sohrab Zendehboudi and journal reviews were applied by the first author. Both Rezaei and Zendehboudi supervised the first author through the project and edited the manuscript.

ABSTRACT

Asphaltene stability can be perturbed during the oil production and transportation, leading to asphaltene precipitation and deposition. Chemical inhibitors are usually added to the oil phase to postpone asphaltene deposition. The chemical bonding between asphaltene and inhibitor molecules, and the steric hindrance are the key mechanisms of aggregation inhibition. Nevertheless, the interaction mechanisms between asphaltenes and chemical inhibitors still need more research investigations. In this paper, we use an advanced computational chemistry tool, molecular dynamics (MD), to analyze the inhibitory effect of *n*-octylphenol (OP) on three different asphaltene structures at 1 bar and 300 K. To meet the objectives, the asphaltene aggregation and aggregates characterization in both cases of pure and mixed asphaltenes are studied. It is concluded that the archipelago asphaltene (A1) does not aggregate appreciably in the absence of OP; nevertheless, OP reduces the aggregation. The OP is more effective in reducing the aggregation rate for the continental asphaltene with hydroxyl and pyridine groups (A2), which is due to the formation of strong hydrogen bonds between asphaltene-OP, compared to the aromatic stacking between asphaltene-asphaltene. The presence of hydrogen bonds significantly changes the characteristics of aggregates in both scenarios: in the absence and presence of OP. Hence, OP shows less efficiency for the continental asphaltene case without hydrogen bond privilege (A3). For the mixed asphaltene systems, OP considerably lowers the aggregation rate in the case of having A2 and A3; the higher relative portion of OP to A2 is the main reason for this behavior. This study reveals that the OP can be an effective inhibitor, depending on the portion of different types of asphaltenes in the crude oil. The same strategy can be used to screen proper inhibitors or inhibitor mixtures for various types of asphaltenes.

Keywords: Asphaltene precipitation; Chemical inhibitor; Molecular dynamics simulation; Molecules' interaction; Asphaltene aggregation; Aggregate characterization

2.1 INTRODUCTION

Although the governmental and international entities have promoted the use of renewable energy as an alternative to fossil fuels, a recent report by International Energy Agency 2019 predicts an increased oil demand of 106 mb/d in 2040 according to the Stated Policies Scenario [1].

The production of oil is challenged by various factors such as sand production, water production, and the deposition of crude oil constituents such as asphaltenes, wax, and hydrates. Asphaltene is composed of a range of molecules with a variety of structures; it is commonly defined as a part of crude oil that is soluble in aromatic solvents and insoluble in aliphatic solvents. The asphaltene deposition occurs upon a change in thermodynamic conditions during hydrocarbon production and transportation [2]. Based on the solubility theory, the asphaltene is soluble in oil at reservoir conditions [3]. A decrease in pressure and temperature during the oil production, or a change in the composition during improved oil recovery/enhanced oil recovery (IOR/EOR) can destabilize the asphaltene, causing asphaltene precipitation and deposition [4, 5]. When the thermodynamic condition approaches the onset of asphaltene stability, the asphaltene molecules begin to agglomerate as nanoaggregates. The asphaltene nanoaggregates further aggregate to form asphaltene clusters. The entire process of solid phase formation from liquid phase is known as precipitation. Upon flocculation, larger asphaltene clusters deposit on a solid surface through sedimentation [6]. This process can happen at reservoir, near wellbore, or in tubing, and also in surface facilities; the asphaltene deposition imposes production and process challenges, such as

increased pressure drop, reduced oil production rate, and increased operating costs for the asphaltene removal.

Different physical and chemical methods are used to inhibit or mitigate the problems originated from asphaltene precipitation and deposition. The preventive approaches are more cost-effective than the treatment methods to remove depositions because the preventative strategies allow oil production to some extent [7-9]. Although the chemical methods bring more environmental impacts (compared to the physical methods), they are commonly applied in practice as a preventive approach due to their higher performance and better economic perspectives. The chemical inhibitors are added to the crude oil before asphaltene precipitation (or deposition) to keep the asphaltenes suspended within a broad range of thermodynamic conditions. Different types of chemicals including surfactants [10], polymers [11], nanoparticles [12], ionic liquids [13], and organic solvents have been proposed as asphaltene inhibitors. Generally, the chemical structure of inhibitors includes polar moieties that attach to the asphaltene molecules; the non-polar moieties cause steric repulsion, hindering the aggregation of asphaltene molecules, and suspending them in the solution [14]. Surfactants are considered a promising type of chemical inhibitors for asphaltenes in the literature [14-16]. Although controversial behaviours have been noticed for some ionic surfactant inhibitors such as dodecyl benzenesulfonic acid (DBSA) [15, 16] and salicylic acid [9]; the nonionic surfactants such as phenols are an efficient and economical category of surfactants. Octylphenol, nonylphenol, and ethoxylated nonylphenol are usually considered as effective asphaltene inhibitors based on inhibitor screening [4, 10, 14, 17-22]. Although phenols are recognized as proper surfactants in terms of inhibition efficiency and economic prospect, they are not generally used as pure due to various technical and non-technical aspects, and usually, they will be mixed with specific asphaltene solvents and diesel to be used in industrial/field-scale [23].

For instance, they should be used with solvents as dispersive media that facilitate the mass transfer to the oil phase due to a reduction in the viscosity [2,3]. Another reason is that using a concentrated surfactant is prone to forming micelles that can be easily lost in the reservoir (through adsorption) without reaching the oil phase. Using a solvent helps inject it at concentrations below the critical micelle concentration (CMC). In addition, pure surfactants (e.g., phenols) are still relatively expensive [2,3]. Based on the Millipore Sigma, 500 mg of 4-octylphenol is 63.4 CAD [24], while 100 mg of 4-nonylphenol is 87.9 CAD [25]. This shows that the 4-octylphenol is cheaper than 4-nonylphenol. Please note that these quantities are far away from field sale requirements; the surfactant price (in terms of $/kg) is expected to decrease substantially for larger quantities.

The asphaltene aggregation and inhibitory mechanisms have been mostly investigated using experimental studies and thermodynamic modeling methods such as equations of state (EoSs); however, both methods suffer from drawbacks. The laboratory tests require relatively expensive materials and tools and are prone to safety risks due to high pressure and temperature conditions. The EoS approach requires parameter tuning (through a fitting procedure) and often considers asphaltenes as pseudo-component with hypothetical properties. In addition, both methods are not able to properly explore the molecular mechanisms. Recently, the application of artificial intelligence has been revitalized in oil industry, including the prediction of asphaltene precipitation (and/or deposition) [26]. Although this method can provide promising results, it needs a large dataset for development of a reliable model, which is computationally demanding and expensive. Also, collecting enough reliable data under various process and thermodynamic conditions for training and testing phases of artificial neural network modeling is not always feasible.

Molecular dynamics (MD) simulation has been employed to model different phenomena, such as asphaltene aggregation and the impact of inhibitors on the aggregation, at the molecular scale, to

better understand the governing mechanisms. In 1995, Rogel [27] used MD to simulate the asphaltene aggregation for the first time. Rogel considered a 3-asphaltene molecule model in both toluene and *n*-heptane (nC_7) in a small cubic box (3 nm×3 nm×3 nm) for a simulation time of 45 ps. They confirmed increasing tendency of asphaltene to form dimer when the amount of nC_7 increases. After significant improvement in the computational capability of computers, researchers are able to conduct simulation runs in larger scale and longer simulation periods. Table 2-1 shows a summary of the progress in the MD studies of asphaltene aggregation and their progress over time. There are only a few studies on the application of MD simulation on the inhibitory efficiency of surfactants in asphaltene aggregation in the literature. In 2011, Headen et al. [28] studied the effect of limonene as an aggregation inhibitor for asphaltenes within a range of temperature (300–400 K) and pressure (100–200 bar) for the first time. They used GROMACS software and all-atom optimized potentials for liquid simulations (OPLS-AA) force-field. Six asphaltene molecules with 7 wt% concentration in carbon dioxide (CO_2) were considered, using a simulation time of 20 ns. Limonene reduced the aggregation of asphaltenes in the asphaltene-CO_2 system, significantly. The minimum aggregation was observed at 350 K and 150 bar. Although they investigated the influence of temperature and pressure on the inhibition efficiency, the effects of asphaltene structure, inhibitor concentration, and solvent type were not studied. Goual et al. [10] studied the impact of *n*-octylphenol (OP) at 300 K and 1 bar on a similar asphaltene structure as that used by Headen et al. [28]. Changes in asphaltene structure include a substitution of an aromatic ring with a pyridine, and a methyl group with a hydroxyl group. In their study, GROMACS 4.5.5 software and OPLS-AA force-field were employed. Goual et al. [10] used 36 asphaltene molecules with a concentration of 6.6 wt% in nC_7, and a simulation time of 150 ns. They concluded that the OP interacts with the hydroxyl group and restricts asphaltene self-aggregation; they found that it is

possible for the inhibitor molecules to self-aggregate, too. The self-aggregation of OP decreased its effectiveness as an asphaltene inhibitor. They also observed that the OP forms fewer hydrogen bonds with pyridine groups than the hydroxyl groups; this was in agreement with their experimental results [10]. Goual and Sedghi [16] compared the effect of dodecylbenzene acid (DBSA) and OP on the aggregation of a similar asphaltene structure used in their previous work (without hydroxyl group) at 300K and 1 bar. They used the same software, force-field, and asphaltene molecule number and concentration, and 80 ns simulation time. The main objective of their study was to find the reasons for the contradictory performances of DBSA as an asphaltene inhibitor at different conditions. The asphaltene-DBSA interaction energy was 15 times stronger than Asp-OP due to the formation of acid-base bonds between the asphaltene and DBSA as well as the formation of hydrogen bonds in asphaltene-DBSA system. They concluded that the high electrostatic attraction energy between the asphaltene-DBSA pairs is the main reason for the formation of larger asphaltene aggregation size in the presence of DBSA, compared to the case without inhibitor addition. Sedghi and Goual [29] studied the inhibitory efficiency of limonene and polyvinyl acetate (PVAc) with concentrations 10–30% and 1–5%, respectively, on asphaltene aggregation at 308 K and 300 bar. They employed GROMACS 5.1.0 and OPLS-AA force-field to simulate aggregation of 200 asphaltene molecules with 4 wt% concentration in CO_2 for 80 ns simulation time. They used two continental asphaltene structures with and without hydroxyl group. Limonene was more effective for the case of asphaltene with hydroxyl group, while PVAc was more suitable for the asphaltene without the hydroxyl group. For both inhibitors, asphaltene aggregation decreased by increasing the concentration of inhibitors. Nevertheless, the solubility of PVAc in CO_2 decreased by attaching to the asphaltenes, which revived with the addition of limonene. In 2019, Tirjoo et al. [30] screened the effectiveness of six different inhibitors including

linear DBSA, limonene, oleic acid, stearic acid, diethylene triamine-penta methylene phosphonic acid (DETPMP), and poly-phosphino carboxylic acid (PPCA) for a continental asphaltene at 298 K and 100 bar. In their study, Materials Studio 6.0 software and COMPASS force-field were employed to simulate the asphaltene aggregation for 100 ps simulation time. It was concluded that limonene is a weak inhibitor due to the lack of polar groups, but linear DBSA is a strong inhibitor due to the possession of the SO_3 polar groups, causing an acid-base interaction with the asphaltene molecules. For the same reason, steric acid was a more effective inhibitor than oleic acid. DETPMP was considered as the strongest inhibitor among all tested inhibitors; it increased the minimum distance of asphaltene-asphaltene (Asp-Asp) from 3 Å to 7 Å. They found an optimum number of inhibitor molecules, using five molecules of asphaltene with 14.3 wt% in toluene. The optimum number of inhibitors for DBSA, oleic acid, DETPMP, and PPCA was five; this optimum number was three for limonene and ten for stearic acid. They claimed that the number of inhibitor molecules increases the chance of inhibitor to self-aggregate through hydrogen bonding.

Despite MD simulation studies on asphaltene inhibitors, some effects are overlooked. For example, the effects of temperature, pressure, asphaltene structure, and polydispersity of asphaltene structure are expected to be significant on asphaltene aggregation, but they are not investigated adequately. To the best of our knowledge, the effect of inhibitor on asphaltene structure especially for the archipelago asphaltene type has not been explored yet. In addition, the polydispersity in asphaltene structures has not been studied yet, and needs to be considered in MD simulation studies of asphaltene-inhibitor for attaining more realistic and reliable simulation results [31-33]. Thus, more research investigations regarding the impacts of aggregate size, density, and shape on asphaltene-inhibitor behaviors should be conducted.

Table 2-1. Asp-Asp aggregation studies using MD

Asphaltene source	Type of asphaltene	Space	T (K) (P in bar)	t (ns)	Software (Force-field)	Remarks	Ref
Venezuelan crude	1 Continental	Toluene, nC_7	-	0.045	Biosym Tech. Inc (PCFF)	• Asp solubility parameter decreases with increasing the aggregation number	[27]
Ratawi vacuum residue	Continentals with 3 to 11 aromatic cores (mean 7 rings)	Toluene	-	0.25	Cerius2 (DREIDING, MOPAC6)	• No Asp self-aggregation at 0.15 wt% Asp • Offset-stacking configuration at 5% Asp	[34]
-	Various types of continentals	Vacuum, toluene, pyridine, tetrahydrofuran, naphthalene	-	0.1	Insight II (CVFF)	• vdW π–π interactions are the major mechanism for Asp self-association	[35]
Average crude of Kuwait, California, and France	1 Continental	Vacuum system	298–400	0.1	Cerius2 (COMPASS)	• Lower aggregation number and Mw at a higher temperature	[36]
Average crude of Kuwait, California, and France	1 Continental	Toluene and nC_5	300 (10–10000)	-	Cerius2 (COMPASS)	• Asp aggregates dissociate in toluene by decreasing but not in pentane	[37]
Khafji, Maya, and Iranian-light crudes	Continental and archipelago	Decalin and 1-methylnaphthalene	373–673	0.1–0.3	Cerius2 (DREIDING 2.02)	• Peripheral alkyl chains and heteroatom functional groups stabilize the aggregates. • Decalin is more effective than 1-methylnaphthalene to dissociate Asp aggregates.	[38]
-	2 Continentals	Toluene, *i*-butane, nC_4, and nC_7	323–573	0.1–0.3	Accelrys Discover Program (CVFF)	• Asp-Asp aggregation in toluene<$iC4$<$nC4$< nC_7 • Aggregation decreases for all solvents when temperature is increased.	[39]
Hypothetical	2 Continentals and 1 archipelago	Toluene, nC_7, and water	298 (1)	10	GROMACS (GROMOS)	• Asp stacking affinity order: nC_7>water> toluene	[40]
QMR Generated	1 Continental and 1 archipelago	Toluene and nC_7	300–350	20	GROMACS (OPLS-AA)	• The Asp forms dimer and trimer reversibly in both toluene and nC_7 while asphaltene aggregates and aggregate form were more persistence lasted longer in nC_7	[41]
Hypothetical	8 Continentals	Toluene and nC_7	300 (1)	80	GROMACS (OPLS-AA)	• The aggregation energy increases when the number of aromatic rings in Asp core increases • The number and length of the peripheral alkyl chains in asphaltene structures are not effective parameters. • Heteroatoms in the aromatic core increase the aggregation energy, compared to adding that to heteroatom in the side chain.	[42]
Based on Violanthrone-78	4 Continentals	Water	300 (1)	60	GROMACS (GROMOS)	• Asp with short and long side chains self-aggregate with different mechanisms.	[43]
Prototypical	2 Continentals	Oil (alkanes and aromatics)	298	200	GROMACS (GROMOS)	• Carboxyl group result face-to-face Asp aggregation configuration	[44]

Heavy Arabian crude	2 Continentals and 1 archipelago	Toluene and nC_7	350 (1)	15	LAMMPS (PCFF)	• Carboxylate groups result face-to-face and also T-shape configuration (due to steric repulsion of anionic group). • The continental Asp type shows high aggregation in nC_7 but not in toluene (larger core, higher attraction). • The archipelago type shows no aggregation in either solvents.	[45]
Kuwait crude, Indonesian coal	2 Continental categories	Toluene	298 (1)	60	GROMACS (GROMOS)	• Substituting heteroatoms does not change Asp aggregation. • Adding carboxylic group changes the Asp aggregation affinity due to hydrogen bond.	[46]
Prototypical	1 Continental category	Toluene	298 (1)	150	GROMACS (GROMOS)	• The sulfur heteroatoms in the side chain cause long-range interactions. • The sulfur heteroatoms in the core reduce aggregation.	[47]
Venezuelan crude	1 Continental	Oil (a saturate, an aromatic, and a resin) and CO_2	323 (150)	20	GROMACS (CHARMM)	• CO_2 affects Asp aggregation in crude mixture. • CO_2 extracts other molecules prevents other oil molecules (saturates, aromatic and resins) to be involved in asphaltene aggregation, causing a denser aggregate.	[48]
QMR generated, Arabian heavy crude	2 Continentals and 2 archipelagos	Toluene and nC_7	300 (1)	80 & 500	GROMACS (OPLS-AA)	• Considering Asp polydispersity improves modeling results. • The archipelago type Asp has lower solubility in toluene than the continental type. • Resin reduces the cluster density and radius of gyration, increasing Asp solubility.	[31]
Hypothetical	1 Continental	Resin, dodecane, and CO_2	373 (200–400)	10	Materials Studio (COMPASS)	• The Asp aggregation energy reduces when increasing pressure.	[49]
Hypothetical	Various types of continentals	nC_7	300 (1)	20 & 200	GROMACS (OPLS-AA)	• Considering Asp polydispersity improves results on the size, shape, and configuration of aggregates. • The minimum number of Asp is 375 molecules to observe all possible aggregates configurations/structures.	[32]
QMR generated	1 Continental and 1 archipelago	C_1, C_3, CO_2, nC_7, and toluene	285–400 (300–500)	100	GROMACS (GROMOS)	• The solubility of the continental Asp type increases in pure toluene and binary solvent mixtures of toluene. • The solubility of the archipelago Asp type is not affected by methane or propane in the system. • Aggregation become larger with pressure and become smaller with temperature.	[50]
QMR generated, Arabian heavy crude	2 Continentals and 1 archipelago	Vacuum and 1-methylnaphthalene	300–453 (1)	80 &400	GROMACS (OPLS-AA)	• The accuracy of the MD simulation results is limited by the cell size and run-time.	[33]

In this study, we conduct MD simulation runs to investigate the effect of OP, as a surfactant asphaltene inhibitor, for three different structures of asphaltenes at 300 K and 1 bar. The selected asphaltenes include archipelago, continental, and modified continental type that are simulated as individual and binary systems. In all systems, nC_7 is considered as the base fluid and the concentration of asphaltene is constant and equal to 7 wt%. In systems containing OP, the concentration of OP is 7 wt%. To analyze asphaltene-inhibitor interactions, we consider visualization, interaction energy including Lennard-Jones (LJ), Coulomb and hydrogen bond, number of aggregations, gyration radius (for the aggregates), aggregate density, and aggregate shape. The cluster analysis is used for the first time in asphaltene-inhibitor simulation.

The structure of this manuscript is organized as follows: after the Introduction, in Section 2.2, we review the theory of molecular dynamics, different force-fields, and analysis methods. Section 2.3 is dedicated to the methods for building asphaltene molecules in the simulation framework as well as the assumptions and settings considered to build the simulation box itself and to conduct MD simulation runs. Section 2.4 includes the validation phase, verification of the scripted code with built-in tools in GROMACS, and the results and discussions for both single- and binary- types of asphaltenes. In both cases, the asphaltene aggregation analysis and aggregate characterization analysis are performed. Finally, Section 2.5 summarizes the main conclusion remarks from our study. Our findings can help researchers to design more effective inhibitors for asphaltene-crude oil systems.

2.2 THEORY OF COMPUTATIONAL APPROACH

MD simulation is a powerful tool to investigate physical phenomena at a molecular scale. It can be combined with quantum mechanics/molecular mechanics to model various chemical reaction systems for broad ranges of process and thermodynamic conditions. MD considers molecular interactions and calculates the properties of (bio)chemical systems, including temperature, pressure,

energy, and the distribution of molecules' positions and velocities over the simulation period. The intra- and inter-molecular potentials are assigned to the atoms and molecules based on the selected force-field, and the coordination and velocity changes are calculated based on the Newton motion law. MD has been successfully employed to model asphaltene precipitation [27, 31-52], and asphaltene deposition on calcite [53-55] and silica [49, 54]. Also, MD is able to model interfacial properties in the presence of different substances such as asphaltene [40, 56-61], asphaltene and resin [62], emulsifier [62], and demulsifier of water/oil emulsion[63]. MD has been used to estimate the solubility parameter for asphaltenes in different solvents [30, 64], diffusion coefficients [40, 55, 65, 66], and hydrate stability and dissociation [67-69]. Recently, the MD approach has been used to model asphaltene aggregation during enhanced oil recovery (EOR) processes such as water injection [70-72] and gas injection [73]. The focus of the current study is on the inhibition of asphaltene aggregation. There are a few research studies about surfactants [10, 16, 28-30] and polymers [11, 29, 30, 74] as asphaltene aggregation inhibitor, using MD.

2.2.1 Force-field

Researchers use different force-fields to simulate hydrocarbon interactions at various thermodynamic conditions while performing MD simulation runs. The common force-fields used for the hydrocarbon systems include polymer-consistent force-field (PCFF) [27, 45], constant valence force-field (CVFF) [35, 39, 63], condensed-phase-optimized molecular potential for atomistic simulation studies (COMPASS) force-field [30, 36, 37, 49, 64], assisted model building with energy refinement (AMBER) force field [75], chemistry at Harvard macromolecular mechanics (CHARMM-27) force-field [48], GROningen molecular simulation (GROMOS96) force-field [40, 43, 44, 46, 47, 50, 57, 58, 62], and OPLS-AA force-field [10, 11, 16, 28, 29, 31, 33, 41, 42, 53-56, 59, 60, 70-74, 76]. GROMOS and OPLS-AA are the most common force-fields

while dealing with hydrocarbons. In 2011, Fu and Tian [77] assessed a variety of molecular force-fields, including OPT-FF, AMBER 03, general AMBER force field (GAFF), OPLS-AA, OPLS-CS, CHARMM27, GROMOS 53A5, and GROMOS 53A6 in prediction of the experimentally available thermodynamic properties of liquid benzene; the OPLS-AA was recommended as the best force-field. Based on the results of Fu and Tian's study and previous studies on asphaltenes [10, 16, 29, 42, 70, 77-79], we choose OPLS-AA force-field, which is available in GROMACS software. The total energy in this force-field is based on the summation of three intramolecular potentials related to the stretching of bonds, bending of angles, and torsion of dihedral angles. The force-field also considers contributions from intermolecular interactions, namely; vdW (that is represented by Lennard-Jones 6-12 potential), and electrostatic (ES) (that is represented by Coulomb potential). The force-field is given below [80]:

$$k = \sum_{bond} \frac{1}{2} k_{ij} (r - r_0)^2 + \sum_{angle} \frac{1}{2} k_{ijk} (\theta - \theta_0)^2 + \sum_{dihedral} k_{ijkl} (1 + \cos(m\varphi - \delta)) + \sum_{LJ} 4\varepsilon_{ij} \left[\left(\frac{\sigma_{ij}}{r_{ij}} \right)^{12} - \left(\frac{\sigma_{ij}}{r_{ij}} \right)^{6} \right] + \sum_{Coulomb} \frac{q_i q_j}{4\pi\varepsilon_0} \frac{1}{r_{ij}} \quad (2.1)$$

where k is the atomic potential energy; k_{ij} refers to the force constant for bonds; k_{ijk} introduces the force constant for angle; and k_{ijkl} represents the force constant for dihedral angles. r_0, θ_0, and $m\varphi$ denote the initial bond length, angle, and dihedral, respectively; the parameter δ adjusts phase degree in the dihedral potential; σ is the radial distance (from a molecule) where the potential energy is zero ; r_{ij} is the distance between charges; ε_{ij} resembles the potential well depth; ε_0 is the permittivity of vacuum; and q refers to the charge of each atom.

2.2.2 Molecule Trajectory

One of the MD outputs is the trajectory of molecules in the simulation box throughout the simulation run-time (reported in *.xtc* and *.trr* file). This file can be used to measure any position-

related calculation and to visualize molecules' movement versus time using Visual Molecular Dynamics (VMD) software [81] and NGLview package [82]. The visualization of the molecules' movement can provide researchers with better insights into interactions between molecules at a molecular scale.

2.2.3 Energy Calculation

One of the simulation outputs is energy file (*.edr* file), which includes box dimension, thermodynamic properties, and contributions from different types of energy in the system. Van der Waals (vdW), electrostatic (ES), and hydrogen bond (HB) are the main intermolecular energies between the asphaltene molecules. The vdW force is a non-bonding interaction that is related to the geometry and polarizability of molecules. Molecules with a larger size and surface area have a greater polarizability and more chance to form vdW interactions. This implies that the electron cloud for larger molecules tends to be distorted as a change of electrostatic environment. ES is another non-bonding interaction form, which is related to the polarity of interacting molecules. The existence of heteroatom (in asphaltene) shrinks the electron cloud and significantly affects polarity [83]. Hydrogen bond is a type of vdW interaction (dipole-dipole interaction), which occurs between a hydrogen (an electropositive atom) attached to oxygen, nitrogen, or fluorine, and a nearby and highly electronegative atom. Hydrogen bond is an attractive interaction, which is stronger than vdW interactions; it is, however, weaker than covalent or ionic bonds [84]. These three intermolecular interaction energies between Asp-Asp and Asp-inhibitor (OP) can be calculated using the built-in tools in GROMACS; these energies explain the interaction preferences between inhibitor and different asphaltene molecules, and aggregation mechanisms. The vdW and ES energies are calculated with *gmx energy*, and HB is calculated with *gmx hbond*.

2.2.4 Aggregation Number

The aggregation of the asphaltene molecules can be quantified in terms of a criterion for a binary distance between them. There are three possibilities for such criteria: 1) the distance between the closest atoms on two adjacent molecules; 2) the distance between a certain atom of two adjacent molecules; and 3) the distance between the center-of-mass (COM) of two molecules. Researchers have commonly used the first criteria [31] or the third one [42]; they employed a certain cut-off distance for systems including asphaltene and crude oil. In this study, we use the distance between the closest atoms and apply a cut-off threshold of 0.35 nm as a criterion for asphaltene aggregation. This particular cut-off was used previously for similar asphaltene structures but without hydrogen bonds [31, 50]; it is applicable in our study because the range of hydrogen bond length is between 0.27–0.33 nm [85]. The *gmx clustsize* module in GROMACS calculates the number-averaged aggregation number g_n (see Eq. (2)). Here, we use *z*-averaged aggregation numbers, g_z, to calculate the aggregate size (see Eq. (3)), which is more reliable and accurate. We script a code in python using the MDAnalysis package [86, 87] that takes *.gro* and *.xtc* files as the outputs of GROMACS simulation, and calculates the aggregation number. The results of the code are compared with GROMACS' results for validation purpose. The corresponding formulas for determination of aggregation number are given below:

$$g_n = \frac{\sum_i n_i . g_i}{\sum_i g_i} \tag{2.2}$$

$$g_z = \frac{\sum_i n_i g_i^3}{\sum_i n_i g_i^2} \tag{2.3}$$

In the above equations, n_i denotes the number of aggregates containing g_i monomers. *i* starts from 2, implying it does not consider monomers individually.

2.2.5 Aggregate Size

The radius of gyration (R_g) represents the size of macromolecules in a solution. It is used to measure the aggregate size independent of its shape during the simulation. In this study, MDAnalysis and the following equation are used to calculate the radius of gyration:

$$R_g^2 = \frac{1}{N}\sum_{k=1}^{N}(r_k - r_{cm})^2 \tag{2.4}$$

where r_k is the position vector of atom k; and r_{cm} introduces the position vector of the aggregate COM.

2.2.6 Aggregate Shape

The shape of aggregates is an important factor, showing how the inhibitors bond the asphaltenes; it also identifies the aggregate shape in the presence of an inhibitor. Three indices can be used to identify the 3D morphology of the aggregates including: 1) relative shape anisotropy (asphericity); 2) shape factor; and 3) ratio of principal moments (shape index), which are related to the principal moments of the gyration tensor (λ_1, λ_2, and λ_3) [31]. The dimensionality and symmetry of the aggregates are estimated with the relative shape anisotropy, κ^2 (see Eq. (6)). The range of relative shape anisotropy is between 0 and 1; κ^2=0 applies for a perfectly spherical chain, while κ^2=1 applies for a linear chain. The shape factor (S), which is defined by Eq. (5), is another measure to characterize the shape of aggregates. This parameter can be between -0.25 and 2. Negative values refer to oblate shapes, while positive values indicate prolate shapes; a shape factor of zero value shows a spherical shape for aggregates. The definitions of the shape factor (S) and relative shape anisotropy (κ^2) are provided below:

$$S = 27\frac{\prod_{i=1}^{3}(\lambda_i - \lambda)}{(\sum_{i=1}^{3}\lambda_i)^3} \tag{2.5}$$

$$\kappa^2 = 1 - 3\frac{(\lambda_1\lambda_2 + \lambda_2\lambda_3 + \lambda_3\lambda_1)}{(\lambda_1 + \lambda_2 + \lambda_3)^2} \quad (2.6)$$

The two indices r_1 and r_2 are defined as $r_1 = (\lambda_1/\lambda_2)^{0.5}$ and $r_2 = (\lambda_2/\lambda_3)^{0.5}$; while the principal moment is in the following order $\lambda_1>\lambda_2>\lambda_3$. Aggregates are considered spherical if both r_1 and r_2 are equal to one; they are of oblate shape if only r_1 is equal to one, and they are of prolate shape when only r_2 is equal to one.

2.2.7 Aggregate Density

The density of aggregates is an index to understand how much the inhibitors have penetrated into the asphaltene aggregates. The mass of the aggregates is calculated from the mass of each atom of asphaltene molecules (m_i) in the aggregates. The volume of each aggregate is approximated by an "effective" ellipsoid with the same principal moments of the gyration tensor [31]. Based on this definition, ellipsoid axes would be considered equal to $5\lambda_1$, $5\lambda_2$, and $5\lambda_3$. Therefore, the aggregate volume ($V_{aggregate}$) and density ($\rho_{aggregate}$) respectively, are obtained as follows:

$$V_{aggregate} = \frac{4}{3}\pi\sqrt{5^3\lambda_1\lambda_2\lambda_3} \quad (2.7)$$

$$\rho_{aggregate} = \frac{\sum_i m_i}{V_{aggregate}} \quad (2.8)$$

It is worth noting that since the target is the investigation of asphaltene aggregates, only asphaltene molecules (not nC$_7$ and OP) are considered to determine the asphaltene aggregation number, aggregate size, aggregate shape, and aggregate density.

2.3 SIMULATION/MODELING METHODOLOGY

2.3.1 Choosing Asphaltene and Inhibitor Structure

The molecular structure of a component is required for any molecular level simulation. There are two general structural types for the asphaltenes: continental and archipelago. Both structure types include unsaturated polar aromatics, heteroatoms (e.g., nickel, vanadium, nitrogen, oxygen, and sulfur), and alkyl chains either in the molecule (archipelago structure) or around the molecule (continental structure) [88]. The continental type has one core, consisting of 4–15 aromatics rings with one or more aliphatic chains. The archipelago structure has multiple small cores that are connected with aliphatic chains. The asphaltene part of the crude oil consists of molecules with different structures. Two methods are suggested in the literature to find the representative chemical structure of the asphaltene molecules. The first analytical method is based on elemental analysis and NMR tests. In this technique, the hypothetical structure is the one with a stronger association tendency [39]. The second method to propose the asphaltene structures is automatically obtained from Monte Carlo simulation and quantitative molecular representation (QMR); thus, it is chosen based on the least deviation from experimental data [89, 90]. Headen et al. [31] conducted a comprehensive survey about the types of asphaltene structures and introduced four different structures [41, 42, 45, 90].

In this study, we adopt three different hypothetical asphaltene structures as shown in Figure 2-1. The hypothetical asphaltene structure A1 that is shown in Figure 2-1(a) is of archipelago type. The other two asphaltene structures are of the continental type, A2 and A3, in Figure 2-1(b) and (c), respectively. We use the asphaltene structures A1 and A3 from Headen et al. [31]. Similar to the study by Goual et al. [10], we modify the asphaltene structure A3 by substituting an aromatic group with pyridine and replacing a methyl group with a hydroxyl group, to create A2 (as seen in Figure

2-1(b)). Therefore, A2 is able to form hydrogen bonds, while the asphaltene structure A3 lacks such a capability.

(a) A1 (Mw = 1250 g/mol, dipole moment = 3.64 Debye)

(b) A2 (Mw = 730 g/mol, dipole moment = 4.44 Debye)

(c) A3(Mw = 727 g/mol, dipole moment = 1.2 Debye)

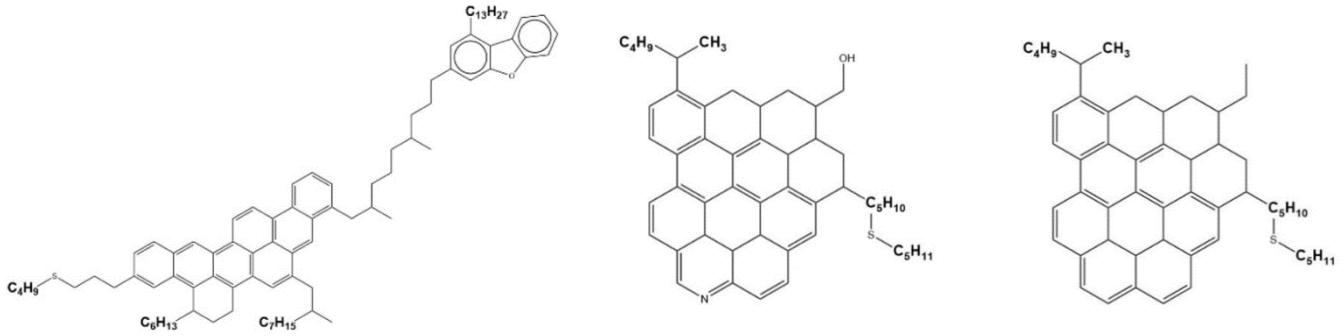

Figure 2-1. Chemical structure of the asphaltenes used in this study: (a) A1, (b) A2, and (c) A3.

The asphaltene part of the crude oil comprises a range of molecules with different structures. We need to include various types of molecules that exist in the oil to generate more reliable results from molecular simulation runs. In fact, it is impossible to define all asphaltene structures in oil phase while conducting MD simulation. Thus, a few common structures (three structures in the current study) are suggested in the modeling. Based on the literature [41-45], the MD simulation results are more accurate and logical if we consider a mixture of asphaltene molecules as more possible interactions between molecules can be taken into account.

We choose *n*-octylphenol (OP) as an asphaltene inhibitor. OP has a polar head, which is capable of forming aromatic stacks, and hydrogen bonds (from hydroxyl group). It also contains an alkane tail that is long enough to provide steric repulsion. Also, we consider nC_7 as a good precipitant for asphaltene.

2.3.2 Building Molecular Structure and Topology

Avogadro software [91] is a software for building, editing, and visualizing molecules. Indeed, the software is used to generate molecules. Then, the Gaussian09 software is employed to obtain the

optimal structure of each molecule at the ground state and their atoms' partial charge. Quantum mechanics calculation with density functional theory (B3LYP) method and 6-31g(d,p) basis set are used for structural optimization [92]. Also, the electrostatic potential, which is an accurate and common method, is used to estimate the atoms partial charge [93]. MKTOP [94] is used to generate topology files for the molecules based on the OPLS-AA force-field. MKTOP considers all bonds, non-bonds, and improper dihedrals for the aromatic ring in the output file. However, the output results usually need a few corrections on atom type and partial charge, which should be conducted manually for further use.

2.3.3 Setting Initial Configuration

We conduct two sets of simulations: 1) asphaltene-precipitant and 2) asphaltene-inhibitor-precipitant. Both single and binary types of asphaltenes are placed in the box to analyze the effect of polydispersity on inhibitor efficiency. For all simulation runs, a cubic box is made with dimensions of $15\times15\times15$ nm^3 to reduce the possibility of molecular overlap. It should be noted that the simulation cell box size will change in NPT stage based on the material type, quantity, intermolecular interactions and the thermodynamic conditions that lead to convergence and precise estimation of physical properties (such as density). Thus, the lower box size is limited by the MD estimation accuracy and the upper limit is controlled by computation time capacity.

The concentration of asphaltene in the simulation box is 7 wt%, and the asphaltene molecules are randomly distributed throughout the simulation box. For asphaltene-inhibitor-precipitant system, the concentration of asphaltene is still 7 wt% and the concentration of OP equals 7 wt% as well. The simulation pressure and temperature are assumed to be 1 bar and 300 K, respectively. Table 2-2 lists the number of molecules in each simulation and properties of each asphaltene.

Table 2-2. Asphaltene characteristics and the number of asphaltene and inhibitor molecules in simulation box.

Asphaltene type	Number of asphaltene molecules	Number of OP molecules
A1	50	0, 303
A2	50	0, 164
A3	50	0, 176
A1+A2	25 + 25	0, 240
A2+A3	25 + 25	0, 177

2.3.4 Running Molecular Dynamics Simulation

All molecular dynamics (MD) simulations in this study are conducted with GROMACS 2019 [95, 96] and OPLS-AA force-field. Figure 2-2 describes the algorithm to conduct MD simulation runs for asphaltene-inhibitor aggregation. The initial configuration is minimized by the steepest descent method for 10000 steps to relax the system. A velocity rescaling thermostat [97] is used in NVT for 100 ps to reach the desired temperature. Velocity rescaling thermostat and Berendsen barostat [98] are used in NPT for 1 ns to adjust the box size and density at the designed pressure. The production runs are conducted by utilizing the Nose-Hoover thermostat [99, 100] and Parrinello−Rahman barostat [101] to maintain the system temperature and pressure for 120 ns. Leapfrog algorithm [102] is used to integrate the equation of motion for all NVT, NPT, and production runs. The time step is fixed at 2 fs as an optimal time step in all simulation runs [41]. The outputs, including the atom position, energy, temperature, pressure, and density, are recorded every 10 ps. The long-range electrostatic interactions are governed by particle-mesh Ewald (PME) algorithm [103, 104] for which the cutoff radius of the van der Waals and Coulomb interactions is fixed at 1.2 nm. Periodic boundary conditions are employed to approximate a large system and all bond lengths are kept rigid using the LINCS algorithm [105].

We script a python code using MDAnalysis package to define the asphaltene aggregates in each time step and to obtain the aggregation number, aggregate size, aggregate shape, and aggregate density. It is worth noting that after the MD simulation run, we remove the periodic boundary conditions for post-processing; otherwise, the aggregate characteristics are prone to uncertainties such as a part of molecules or aggregates being on each side of the adjacent boxes. The accuracy and reliability of the scripted code are verified using the GROMACS built-in tools in the next section. Figure 2-3 depicts the flowchart of the python script that is used for post-processing.

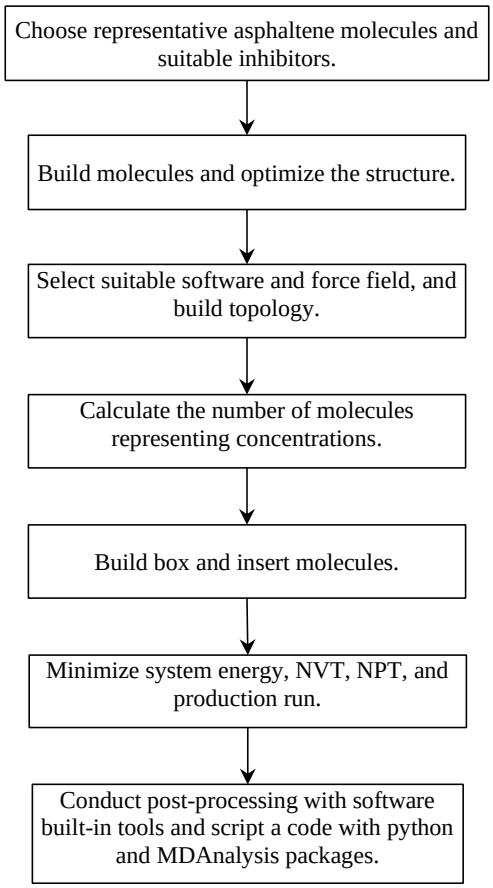

Figure 2-2. A flowchart to simulate asphaltene-inhibitor interactions using MD.

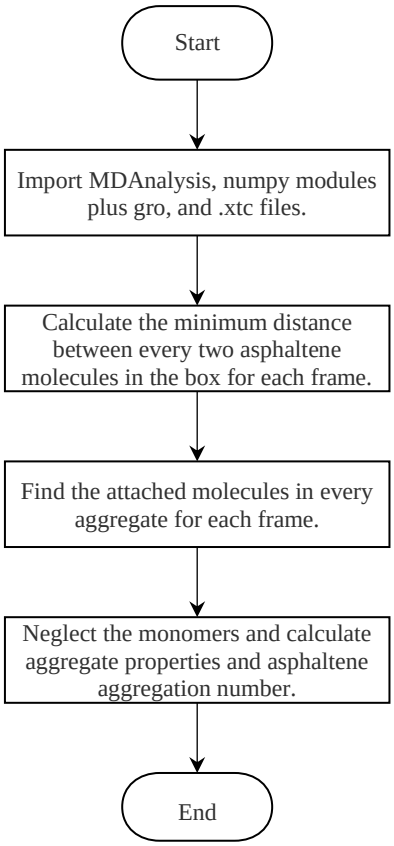

Figure 2-3. A flowchart of python scripted code that is used for post-processing.

2.3.5 Challenges and Limitations

One of the main challenges in molecular-scale simulation of asphaltene systems is to discover the dominant asphaltene structure for a target oil. Also, the intramolecular forces should be defined in the selected force-field for the asphaltene structure chosen for MD simulation; alternatively, the relative parameters can be found in the literature and inserted into force-field manually. Constructing the topology file is commonly challenging in MD analysis; researchers simplify this stage by developing computer codes such as MKTOP. However, the code might not always be accurate for different systems, and usually needs fine-tuning. Another challenge is analyzing the MD outputs. There are built-in tools in MD software packages such as GROMACS that enable a preliminary analysis. Auxiliary packages (or software) such as MDAnalysis or MDtraj are developed to help with detailed analysis of the MD outputs.

Although the MD simulation has a huge benefit in terms of understanding molecular-level interaction mechanisms, it is limited by system size, simulation time, and computational costs. The periodic boundaries are suggested to cope with the limitations in the system size. The simulation time is on the scale of nanosecond, which is far from an industrial perspective. The MD simulation strategy is considered an advanced chemistry computation; however, the MD computation time usually is long, and depends on the number of atoms in the system, simulation run time, and computer storage capacity (and speed).

2.4 RESULTS AND DISCUSSION

2.4.1 Result Validation and Code Verification

Result validation: Headen et al.[31] simulated an asphaltene similar to A1 and A3, using *n*C_7 as a precipitant. Similar to the case study by Headen et al., we use asphaltene concentration of 7 wt%. However, we increase the number of asphaltene from 27 molecules (in their study) to 50

molecules. The simulation time is also increased from 80 ns to 120 ns in our study. Figure 2-4 compares the average aggregate gyration radius for A1 and A3 in both studies. As it is evident, there is an overall similarity between the trends. The reason for the differences is due to the longer simulation time for a larger system (in terms of number of molecules and volume), causing bigger aggregates over the simulation run time, and eventually a higher probability of forming aggregates with a certain size.

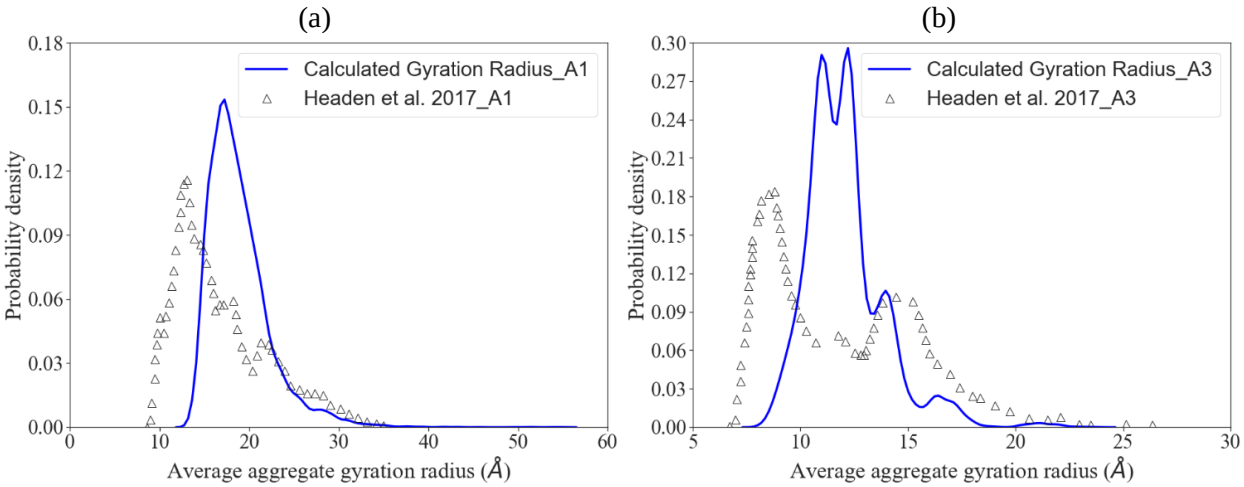

Figure 2-4. A comparison between the results of our modelling and the study by Headen et al.[31]; (a) average aggregate gyration radius of A1-*n*C_7, and (b) average gyration radius of A3-*n*C_7.

Verification of scripted code: As mentioned in the previous section, the simulation outputs are recorded every 10 ps in this work. Since the aggregates can be formed and dissociated, the average aggregation number can fluctuate in short time steps. Therefore, we only report data every 500 ps in all average aggregation number plots to decrease the number of fluctuations and make them more understandable. The scripted code enables us to determine the average aggregation number, aggregate size, aggregate shape, and aggregate density. In Figure 2-5, the average aggregation number is shown using both scripted code (indicated with scatter data points) and the built-in *gmx clustsize* module in GROMACS. Since both match each other, the code can recognize the aggregates perfectly; the code is valid for using in any calculations related to the aggregates. It

should be mentioned that the *gmx clustsize* considers the asphaltene monomers in the calculation of average aggregation number; we do not consider monomers in our calculations except to verify the code in this section.

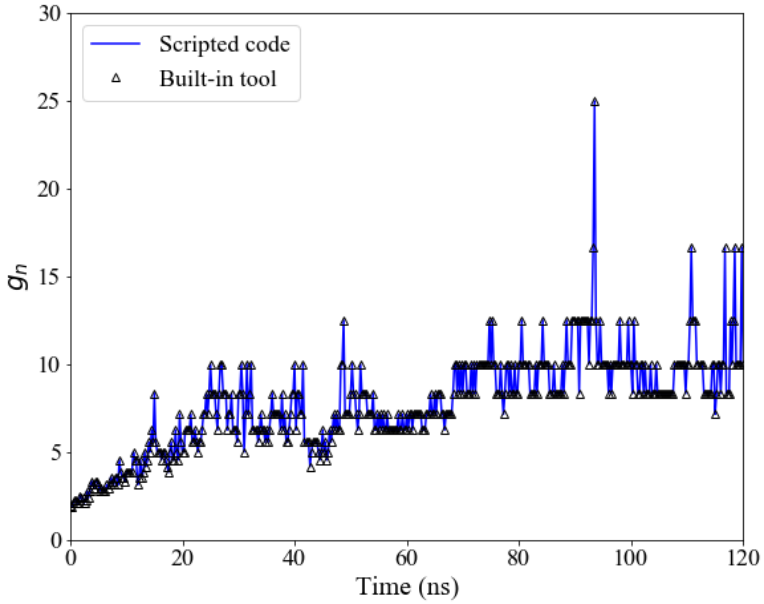

Figure 2-5. Comparison of average aggregation numbers using GROMACS and python scripted code for A3 without inhibitor.

2.4.2 Asphaltene Aggregation

Single-type asphaltenes: Six MD simulation runs are considered for three single-type asphaltenes (only one among A1, A2, and A3) for 120 ns, with and without the inhibitor (OP). The *z*-average aggregation number (g_z) is used as a preliminary analysis of the asphaltene aggregation. Figure 2-6 demonstrates the aggregation intensity for three different simulations. Without the inhibitor, the asphaltene A1 molecules aggregate and dissociate during the simulation, showing agreement with previous research works [31]; the OP addition reduces the asphaltene aggregation (see Figure 2-6(a)). The main interaction energy for self-aggregation of A1 and A1-OP is aromatic stacking, which is characterized with LJ and Coulomb energy. The average values for Asp-Asp, Asp-OP, and OP-OP interaction energies for the final 20 ns simulations are presented in Table 2-3. The

negative values in Table 2-3 show the attraction energy, and positive values represent the repulsion energy. The LJ energy among the asphaltenes is an attraction type, and the Coulomb energy is a repulsion type, which is nearly twice the value of the LJ. The high repulsive energy between the asphaltene molecules causes the A1 to exhibit a low aggregation tendency, for which the asphaltene aggregates dissociate during the simulation even without OP. Upon the addition of OP, the LJ energy between the Asp-Asp significantly decreases, and the LJ energy between Asp-OP becomes considerably high. Moreover, the Coulomb energy accounting for the repulsion between Asp-Asp pair increases significantly after adding OP (becomes more repulsive). The energy changes due to OP addition verify the efficient inhibitory effect of OP for A1. Figure 2-7 illustrates frames at 60 ns and 120 ns for both the pure asphaltene and asphaltene-OP simulations. The asphaltenes do not aggregate appreciably; nevertheless, the aggregation rate decreases after OP addition, confirming that the inhibitors reduce the asphaltene aggregation rate.

In the simulation of A2, the *z*-average aggregation number is calculated (Figure 2-6(b)). Although the asphaltene aggregates dissociate over time, the aggregates grow and eventually reach the maximum number of asphaltenes in the simulation box. The addition of OP lowers the asphaltene aggregation significantly at the beginning of the simulation, until 80 ns; after that, the *z*-average aggregation number increases and eventually becomes stable. The asphaltene A2 can form hydrogen bonds with itself and with OP due to having hydroxyl and nitrogen in its chemical structure. Table 2-3 reports the values of Asp-Asp, Asp-OP, and OP-OP interaction energies. Furthermore, Table 2-4 lists the average hydrogen bond number of Asp-Asp and Asp-OP in three-time spans. Because both LJ and Coulomb energies are the attraction types between the asphaltenes, the asphaltene A2 molecules aggregate gradually and persistently. In addition, the average number of hydrogen bonds of Asp-Asp increases over the simulation. The OP addition

reduces the LJ attraction energy between the asphaltenes; also, the LJ energy for Asp-OP is higher than that for OP-OP. The Coulomb energy of Asp-Asp is slightly reduced after the addition of OP, but it is comparable with Asp-OP Coulomb energy. The addition of OP dramatically reduces the average number of hydrogen bonds between adjacent asphaltenes, while it monotonically increases the average number of hydrogen bonds for Asp-OP. Therefore, OP enables aromatic stacking and hydrogen bonds with asphaltene A2; consequently, OP can be considered an effective inhibitor. The hydrogen bonds are formed in the peripheral of the asphaltene molecules due to the orientation of the hydroxyl group and nitrogen; also, the aromatic stacking force for Asp-OP is weaker than the Asp-Asp force due to the small aromatic core in OP. Hence, OP prefers to form hydrogen bonds with asphaltene and can only postpone the asphaltene aggregation, as seen in Figure 2-6(b), which is in agreement with previous results by Goual et al. [10]. Figure 2-8 verifies that the existence of OP in the system decreases aggregation at 60 ns; however, aggregation eventually is increased during the simulation, and there is no difference in the aggregation behavior with and without OP at 120 ns. As it is obvious, at 120 ns, the OP will be inside and around the aggregates. It means that OP reduces the aggregation of A2 at the beginning; but, the A2 and OP agglomerate and form larger aggregates. In this case, OP will not reduce deposition; in fact, it will cause more severe asphaltene deposition.

In the system of A3/*n*C_7, the molecules of asphaltene A3 can aggregate and dissociate during the simulation (Figure 2-6(c)). Hence, the Asp-Asp interaction for asphaltene A3 is weaker, compared to that of A2, due to less dipole moment (Figure 2-1) and the lack of a hydroxyl group. The asphaltene A3 is more prone to self-aggregation than A1 due to having a larger aromatic core. Table 2-3 reports the LJ energy and Coulomb energy between the molecules of asphaltene A3, which are attractive and repulsive, respectively, with a similar value. The repulsive Coulomb force

is related to the absence of nitrogen in the aromatic core for asphaltene A3, compared to A2 [73]. Additionally, the lack of a hydroxyl group on the asphaltene A3 eliminates the capability to form hydrogen bonds. It explains why the asphaltene A3 has less affinity for aggregation than the asphaltene A2. Therefore, for this asphaltene type, OP is not an effective inhibitor because the LJ energy of Asp-OP is significantly lower than that of Asp-Asp; the OP addition even increases the Asp-Asp energy.

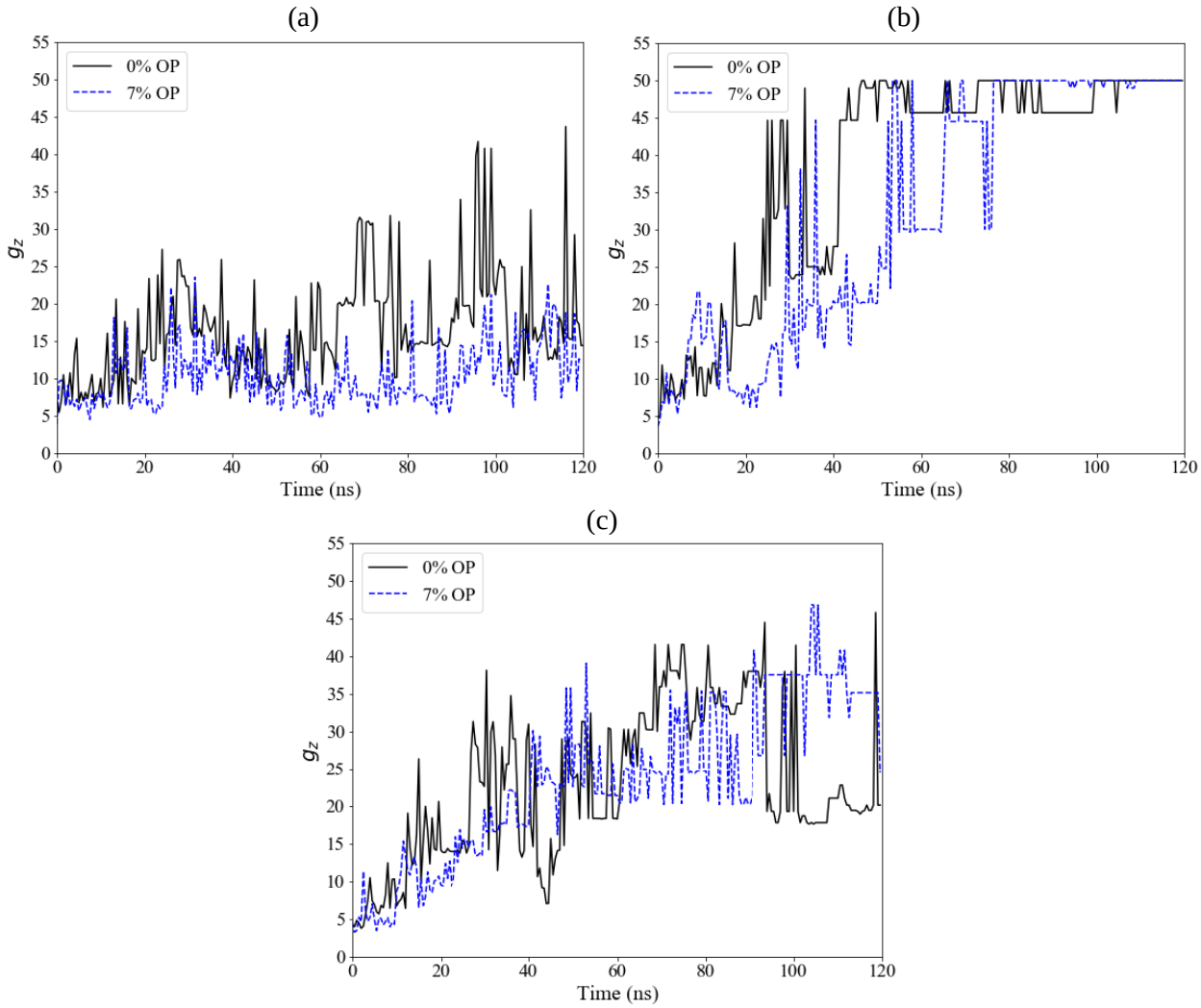

Figure 2-6. *z*-average aggregation number versus time for (a) A1, (b) A2, and (c) A3 with and without the OP.

Table 2-3. Average of LJ and Coulomb energy between asphaltenes and OP for different types of asphaltenes in the final 20 ns of simulations.

Energy (kJ/mol)	Asphaltene system	No inhibitor	With inhibitor (7% OP)		
		Asp-Asp	Asp-Asp	Asp-OP	OP-OP
LJ	A1	-10998.13	-9943.34	-3147.15	-4175.83
	A2	-9968.93	-9007.86	-3953.06	-2600.55
	A3	-8957.19	-9221.79	-1454.49	-2463.85
Coulomb	A1	17395.80	17414.50	-147.63	-1057.64
	A2	-2499.03	-2137.00	-1475.26	-616.43
	A3	8903.77	8938.92	-101.68	-623.29

Table 2-4. Average number of hydrogen bonds for Asp-Asp and Asp-OP for three time spans.

Time span (ns)	No inhibitor	With inhibitor (7% OP)		
	A2-A2	A2-A2	A2-OP	OP-OP
0–50	14.3	7.1	46.7	16.0
50–100	22.7	12.7	51.5	15.3
100–120	22.7	9.7	58.7	15.3

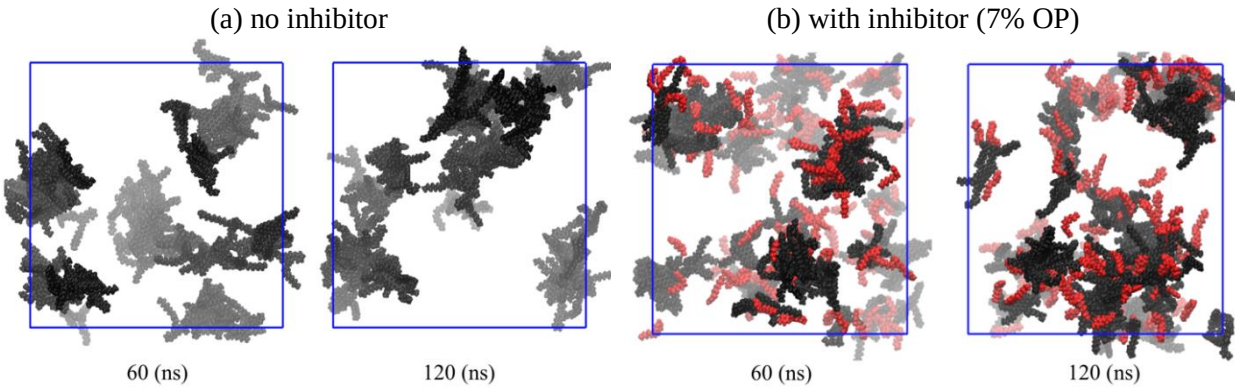

Figure 2-7. Visualization of molecular coordination for asphaltene A1 (black) with and without inhibitor (OP, in red) after 60 ns and 120 ns. The precipitant (nC_7) molecules and OP molecules with more than 6 Å distance from asphaltenes are not shown for clarity.

Binary-type asphaltenes: In the binary system, consisting of asphaltenes of two different types (from A1, A2, and A3), the asphaltene molecules can aggregate with each other. Figure 2-9 shows the *z*-average aggregation number for binary-type asphaltenes with and without the inhibitor (OP). Based on Figure 2-9 (a), OP does not significantly change the aggregation intensity for a system including asphaltenes A1 and A2 , which is reasonable in regards to the energy changes (Table 2-5

and Table 2-6). The LJ and Coulomb energies of Asp-Asp decrease slightly after OP addition, especially between similar types of asphaltene. The Asp-OP interaction is attractive and comparable with Asp-Asp energy, which gives asphaltenes a choice to bond with either asphaltene molecules or OP. The average number of hydrogen bonds between the asphaltenes decreases significantly after OP addition over the simulation time, and has an increasing trend for Asp-OP. It is thus confirmed that the addition of OP can postpone asphaltene aggregation because it decreases the Asp-Asp aromatic stacking and Asp-Asp hydrogen bonds. Figure 2-10 illustrates that in the case of OP addition, the aggregates become smaller at 60 ns compared to the case without OP, but this trend is reversed at 120 ns. The comparison of Figure 2-6(a), Figure 2-6(b), and Figure 2-9(a) shows that the *z*-average aggregation number for the mixed asphaltene types lies between the *z*-average aggregation number for pure components, which is in good agreement with previous research 31. The OP appears less effective, which can be due to decreased asphaltene molecules that can form hydrogen bonds.

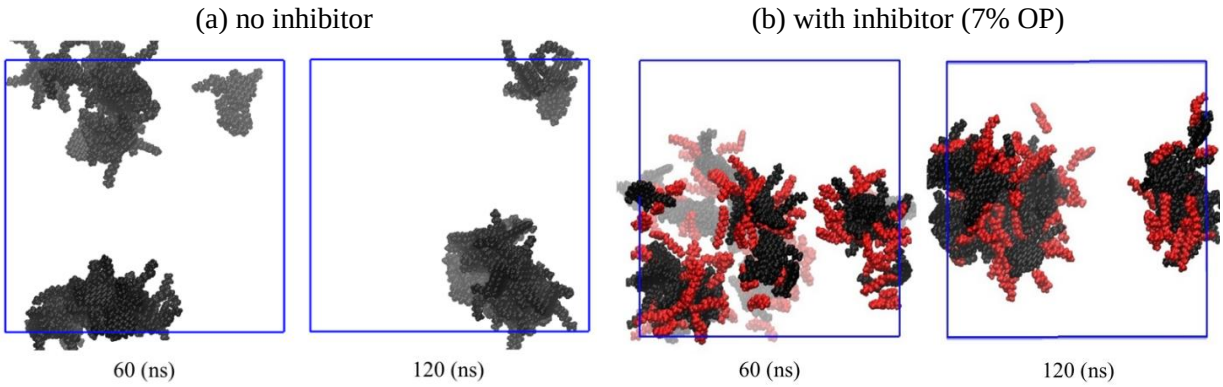

Figure 2-8. Visualization of molecular coordination for asphaltene A2 (black) with and without inhibitor (OP, in red) after 60 ns and 120 ns. The precipitant (nC_7) molecules and OP molecules with more than 6 Å distance from asphaltenes are not shown for clarity.

Figure 2-9(b) depicts the *z*-average aggregation number for the system with asphaltenes A2 and A3. The aggregation number trends are similar for both cases with and without OP up to 60 ns.

The *z*-average aggregation number has a monotonic trend for the second half of the simulation (60–120 ns) without the inhibitor OP, but fluctuates sharply when OP is present. Although the presence of OP does not change the Coulomb energy between the molecules, it reduces the LJ energy between asphaltenes A2 and A3 (Table 2-5). Additionally, in the presence of OP, the average number of hydrogen bonds for A2-A2 reduces (compared to the case without OP) and fluctuates (Table 2-6), which can be the main reason for the considerable fluctuations in *z*-average aggregation after OP addition. Figure 2-11 visualizes the Asp-OP coordination, which shows less aggregation with adding OP compared to the system without the inhibitor. Comparing Figure 2-6(b), Figure 2-6(c), and Figure 2-9(b) reveals that OP has a greater efficiency when asphaltenes A2 and A3 are mixed rather than that with either of these asphaltenes (alone). Based on the results, there are several possibilities that could be improved with a combination of asphaltenes A2+A3; A2 brings the advantage of forming hydrogen bonds with OP, and A3 could restrict the attraction between A2-OP pairs. In addition, as the number of A2 molecules becomes half when mixed, OP can curb the aggregation much more effectively. A system containing a mixture of asphaltenes is inherently more complex than that containing a pure component; therefore, extensive mechanistic investigations are required for a realistic interpretation of the system.

Table 2-5. Average of LJ and Coulomb energy for the binary mixture of asphaltenes with and without OP in the final 20 ns of simulations (x is 1 and 3 in A1+A2 and A3+A2 systems, respectively).

Energy (kJ/mol)	Asphaltene system	No inhibitor			With inhibitor (7 wt% OP)				
		Ax-Ax	A2-A2	Ax-A2	Ax-Ax	A2-A2	Ax-A2	Ax-OP	A2-OP
LJ	A1+A2	-4386.93	-3269.26	-3205.80	-3990.97	-2717.82	-3109.27	-1972.84	-1524.17
	A3+A2	-2937.30	-3291.42	-3580.24	-3347.67	-3344.04	-2170.49	-895.92	-1551.06
Coulomb	A1+A2	8722.58	-1114.84	-57.27	8710.41	-954.15	-42.67	-78.72	-738.20
	A3+A2	4470.21	-1055.21	-66.03	4463.20	-951.56	-40.87	-54.70	-683.06

Table 2-6. Average number of hydrogen bonds of Asp-Asp and Asp-OP for binary mixture of asphaltenes with and without OP in three time spans.

Time span (ns)	Asphaltene system	No inhibitor	With inhibitor (7 wt% OP)	
		A2-A2	A2-A2	A2-OP
0–50	A1+A2	3.1	1.5	23.5
	A3+A2	2.3	3.2	21.9
50–100	A1+A2	5.9	1.9	24.8
	A3+A2	4.9	1.6	28.9
100–120	A1+A2	8.0	1.3	29.3
	A3+A2	5.5	1.4	27.1

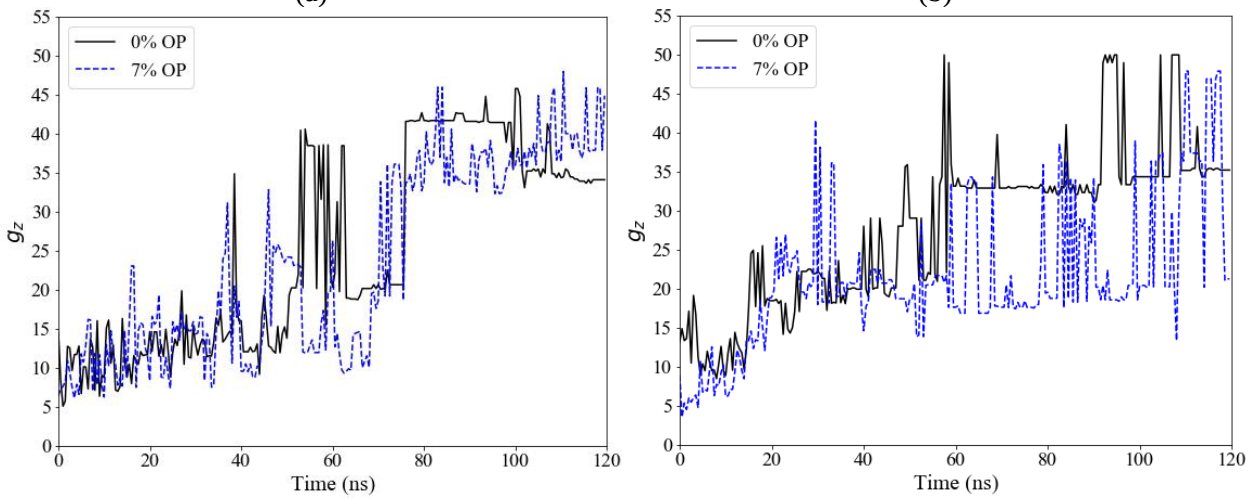

Figure 2-9. *z*-average aggregation number for a binary mixture of asphaltenes with and without OP: (a) A1 and A2, (b) A2 and A3.

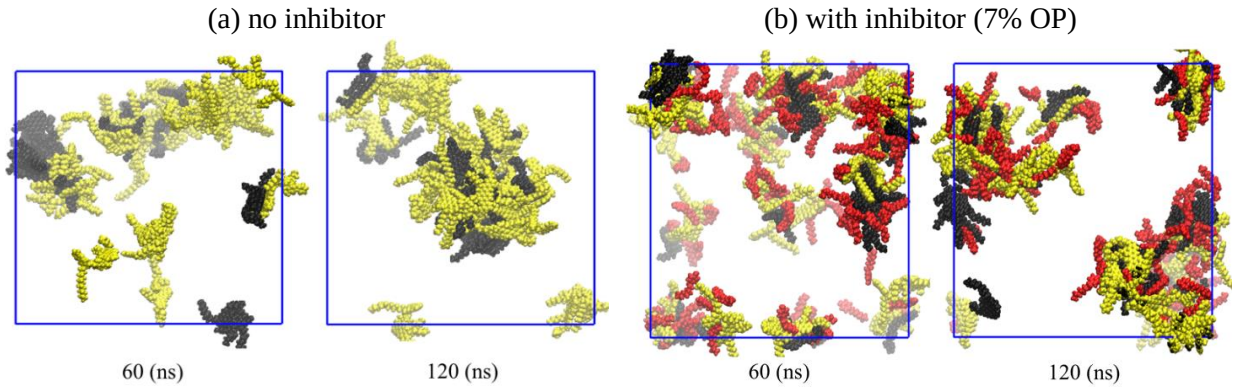

Figure 2-10. Visualization of molecular coordination for asphaltenes A1 (yellow)-A2 (black) with and without inhibitor (OP, in red) after 60 ns and 120 ns. The precipitant (nC_7) molecules and OP molecules with more than 6 Å distance from asphaltenes are not shown for clarity.

(a) no inhibitor (b) with inhibitor (7% OP)

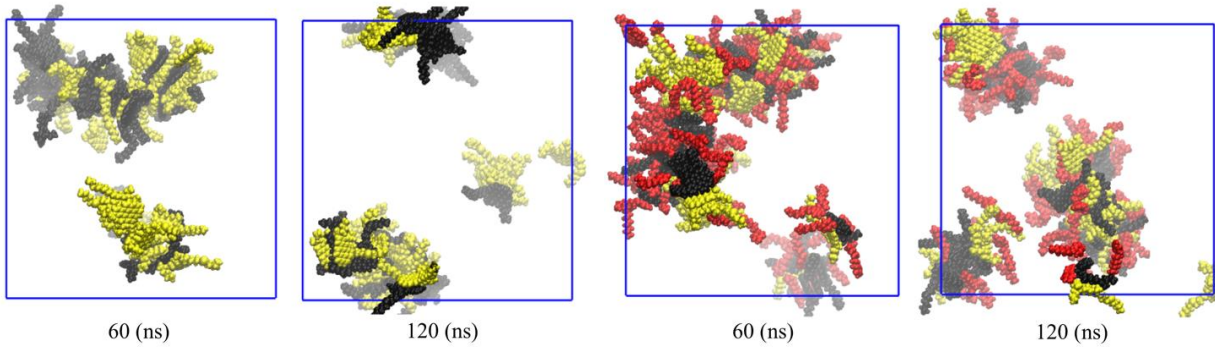

Figure 2-11. Visualization of molecules coordination for asphaltenes A2 (black)-A3 (yellow) with and without inhibitor (OP, in red) after 60 ns and 120 ns. The precipitant (nC_7) molecules and OP molecules with more than 6 Å distance from asphaltenes are not shown for clarity.

2.4.3 Aggregate characteristics

Single-type asphaltene: In this section, the effect of OP on the gyration radius, and density and shape of the aggregates is investigated. Based on Figure 2-12(a), the gyration radius for the asphaltene A1 aggregates is unimodal and has the maximum probability at 17 Å before adding the inhibitor. After OP addition, the probability of the aggregates is increased and the gyration radius slightly decreases, indicating that the aggregates are either squeezed or broken. If the aggregates were squeezed, the aggregates volume would have reduced, and the aggregate density would have increased. However, Figure 2-12(b) reveals that the aggregate density not only reduces, but that the probability of the aggregates with lower density increases, which verifies the aggregates break down hypothesis due to OP addition. Figure 2-12(c) and Figure 2-12(d) illustrate that the asphaltene aggregates are more prone to be prolate either with or without OP—the OP addition only reduces the variety of asphaltene shapes.

Figure 2-13 shows the changes in the A2 asphaltene aggregate characteristics due to the addition of OP. A2 forms multimodal aggregate size at 13, 17, and 26 Å without OP; it changes to a bimodal curve with peaks at 11 and 28 Å, having a wider aggregate size distribution (Figure 2-13(a)). Hence, the addition of OP can reduce the size of some aggregates but increase the size of others.

Since the average aggregate size is plotted over the simulation time, it can be interpreted that the aggregates with a lower gyration radius belong to the earlier stage of OP addition, while the aggregates with a larger gyration radius are related to the later stage of the simulation. The aggregate density plot (Figure 2-13(b)) demonstrates a lower aggregate density with OP; it follows that the OPs break down the aggregates in early time and the small Asp-OP aggregates are attached to each other later; this causes the large aggregates to be relaxed because of OP involvement.

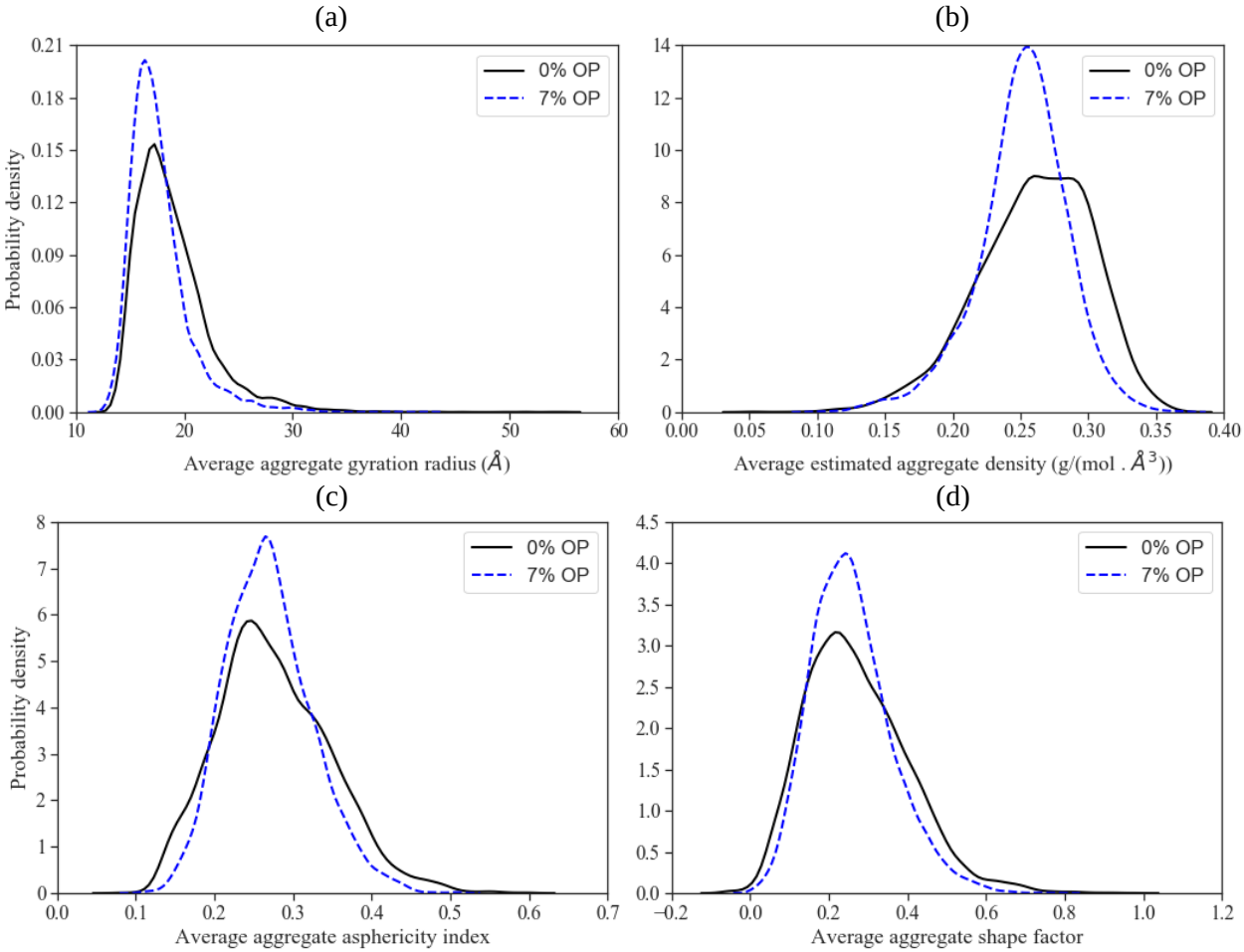

Figure 2-12. Probability of aggregate average (a) gyration radius, (b) density, (c) asphericity, and (d) shape factor over the simulation run of A1.

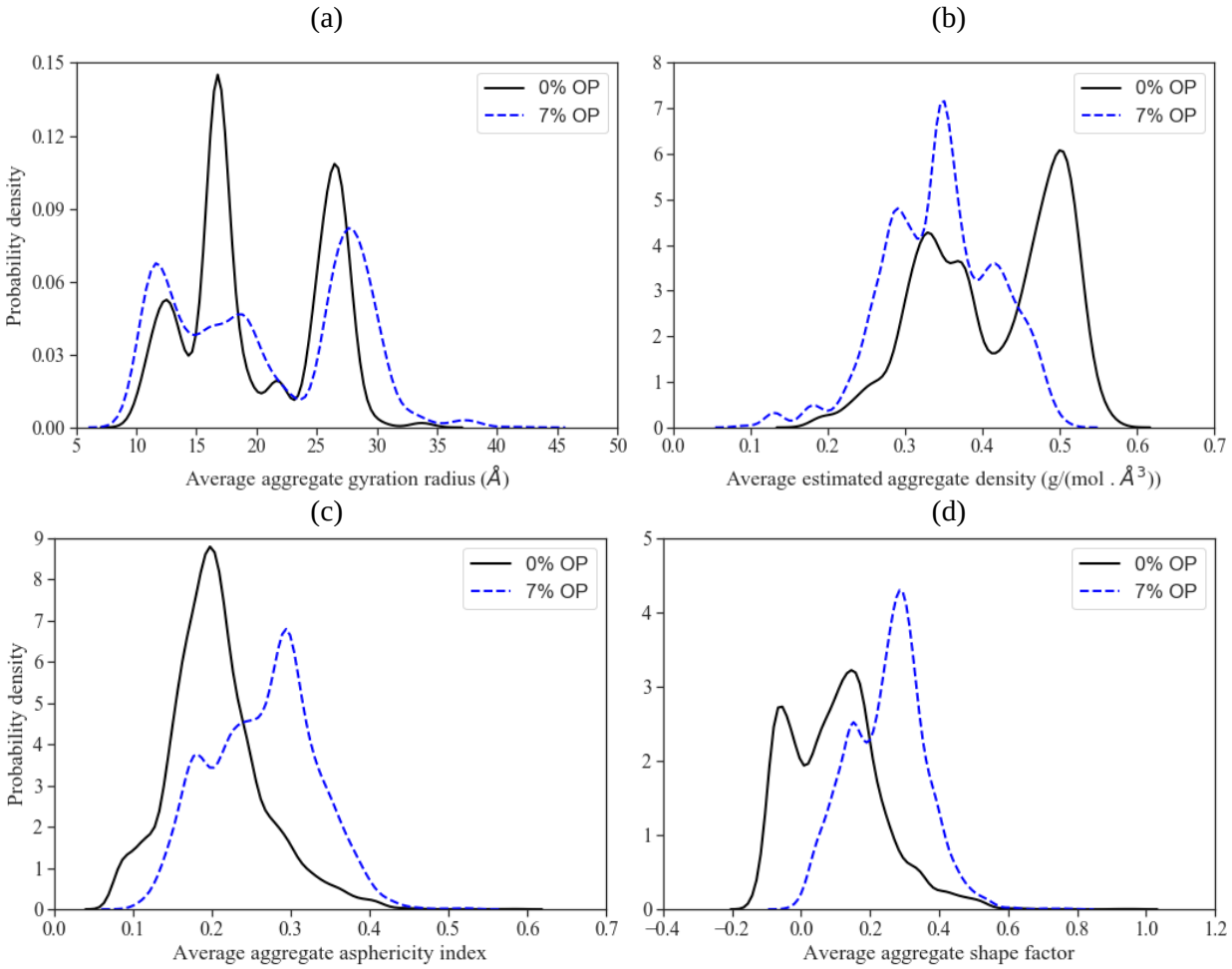

Figure 2-13. Probability of aggregate average; (a) gyration radius, (b) density, (c) asphericity, and (d) shape factor over the simulation run of A2.

According to Figure 2-13(c), the asphaltene aggregates are nearly spherical in the absence of OP, and the addition of OP makes them mainly linear. Figure 2-13(d) reveals that the aggregates can be oblate, spherical, and prolate in the absence of OP, while the aggregates mostly become prolate after OP addition. This conclusion regarding the aggregate shapes being affected by the hydrogen bond is consistent with the results of a previous research study [73]. Figure 2-14 displays r_2 vs. r_1 in a color-coded comparison: blue represents a low density of data, and red represents a high density of data. Figure 2-14(a) verifies the multimodality of aggregate shape in the absence of OP

and Figure 2-14(b) shows that the shape of most aggregates is changed from oblate (r_1=1 and r_2≠1) and spherical (r_1=1 and r_2=1) to prolate shape as the r_2 value approaches 1 and r_1 varies widely.

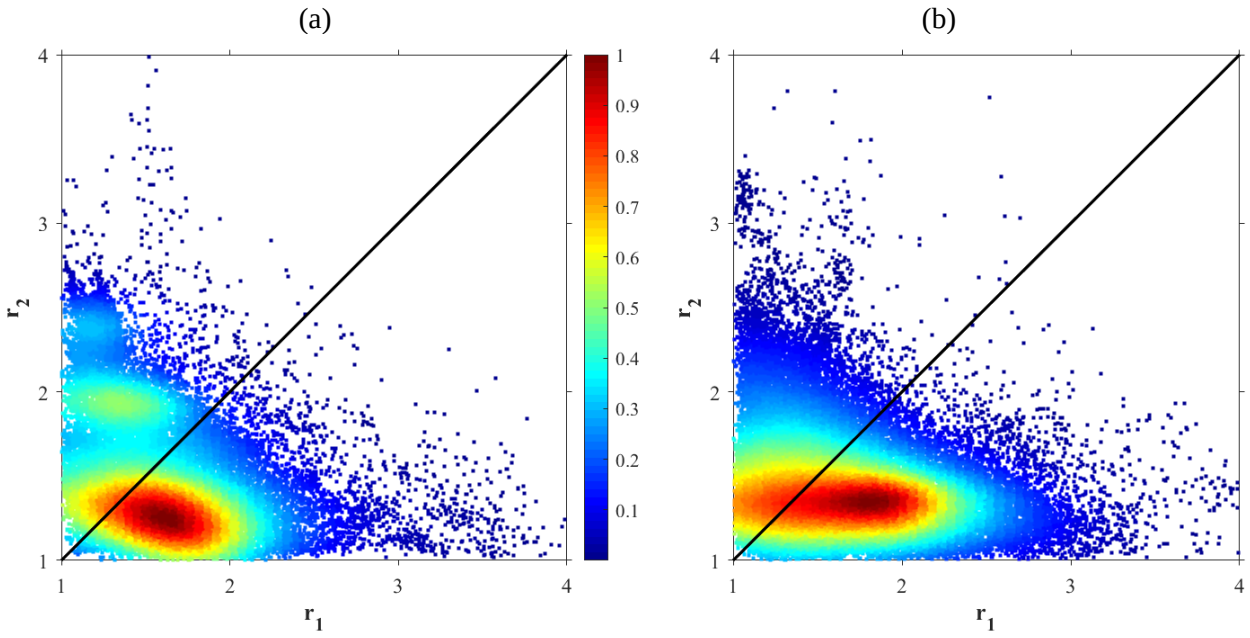

Figure 2-14. Aggregate shape index over the simulation for A2: (a) 0 wt% OP, and (b) 7 wt% OP. The color bar shows the repetition of aggregates with similar shape index: the red and blue represent the high and low intensity, respectively.

Figure 2-15 shows the average values of aggregate size, density, and shape factor over the simulation for asphaltene A3. In the absence of OP, the average size of aggregates is between 10–15 Å and unimodal; but after the OP addition, the average size becomes bimodal, with one peak between 10–15 Å and one peak at 18 Å. Furthermore, the average density of aggregates reduces after adding OP (Figure 2-15(b)). The increasing asphaltene aggregate size and decreasing density imply that the OP penetrates into the asphaltene aggregates and expands them. Based on Figure 2-15(c), the aggregate shape of A3 is unimodal and mainly spherical, and the OP addition makes the aggregates more asymmetrical. This claim is verified in Figure 2-15(d), revealing that the asphaltene aggregates shape is unimodal and close to zero in the absence of OP; it becomes more prolate after OP addition.

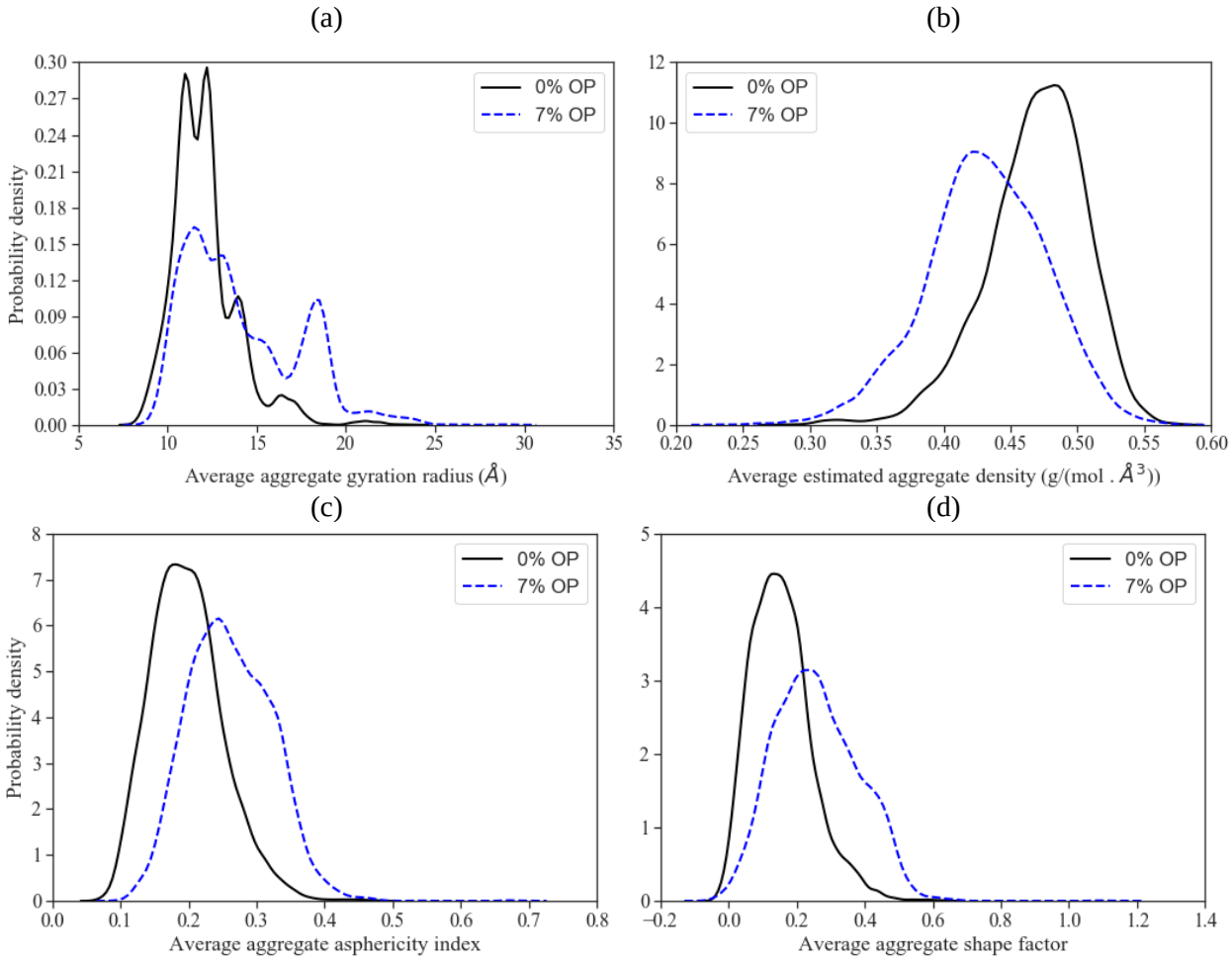

Figure 2-15. Probability of aggregate average (a) gyration radius, (b) density, (c) asphericity, and (d) shape factor over the simulation run of A3.

Binary-asphaltene type: In the systems with binary asphaltene structure, the aggregates can form with either single type asphaltene or mixed. Figure 2-16(a) depicts the average gyration radius of aggregates for asphaltenes A1 and A2. The radius is between 12–20 Å in the case without inhibitor. However, it becomes bimodal upon addition of OP, with a secondary peak between 25–30 Å, showing that the aggregate size increases. According to Figure 2-16(b), OP addition reduces the aggregate density. It follows that the OP molecules penetrate into the asphaltene aggregates, increasing the aggregate size and volume, and consequently reducing the aggregate density. In the case with OP, the asphaltene aggregates take wider range of shape since the bell curves in Figure

2-16(c) and Figure 2-16(d) become shorter and fatter. At the same time, the aggregates with linear and prolate shape become more dominant since the peak shifts to the right in both panels (c and d) of Figure 2-16.

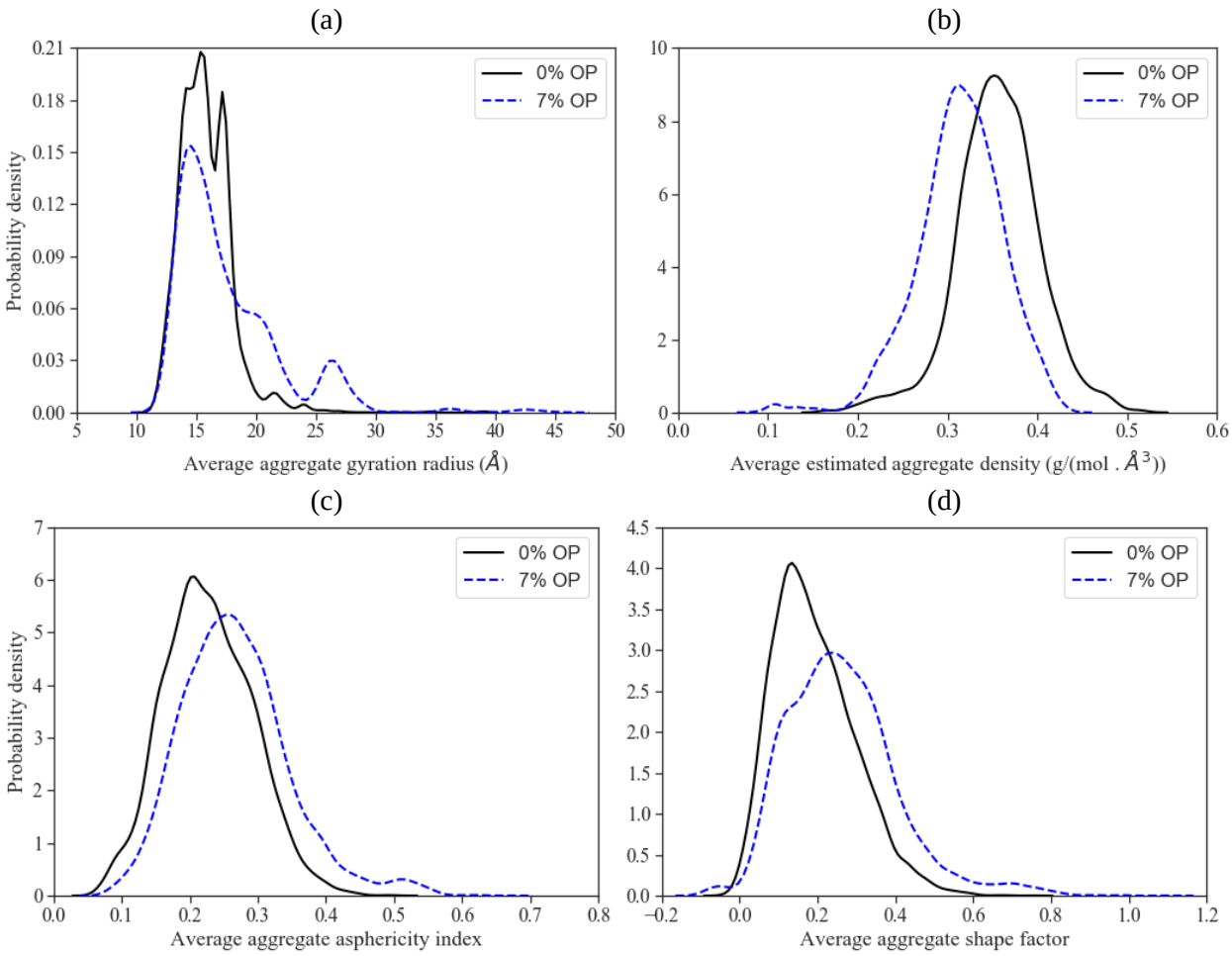

Figure 2-16. Probability of aggregate average (a) gyration radius, (b) density, (c) asphericity, and (d) shape factor over the simulation run of A1 and A2 binary mixture.

Figure 2-17(a) shows the average gyration radius of the aggregates for asphaltenes A2 and A3. Without OP, the aggregate radius is multimodal with three peaks: 15 Å, 20 Å, and 27–40 Å. The addition of OP decreases the aggregate size and the aggregate density (Figure 2-17(b)), showing that the asphaltene aggregates are broken down. Having smaller aggregates (upon OP addition), the aggregate shape becomes more uniform with less diversity; and they are still in the form of

prolate (see Figure 2-17(c) and Figure 2-17(d)). Based on Figure 2-18(a), the aggregate shape is mostly prolate since $r_1 \neq 1$ and $r_2 = 1$, while the aggregates become more spherical ($r_1 = 1$ and $r_2 = 1$) when OP is added (Figure 2-18(b)). The color bar shows the intensity of data repetition.

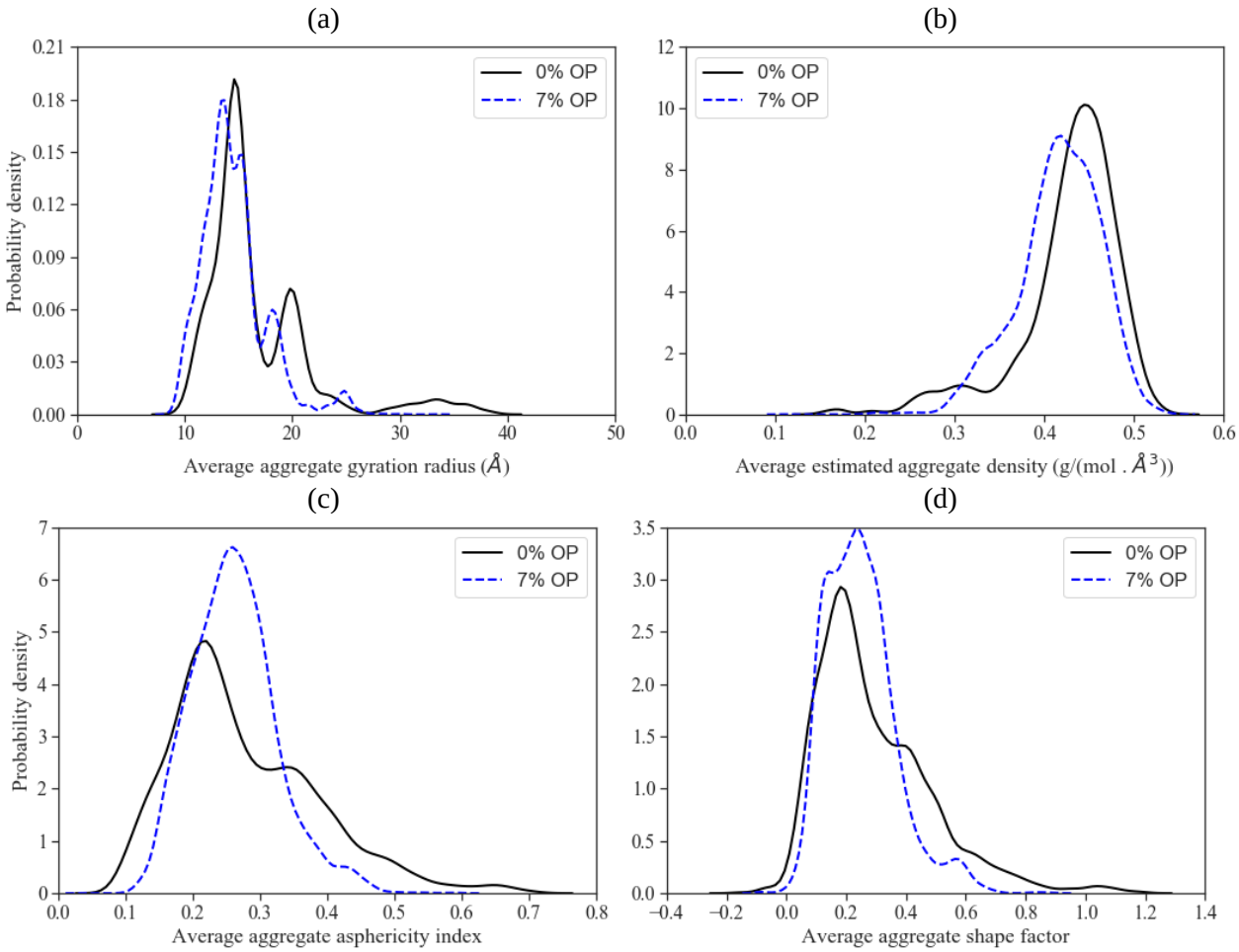

Figure 2-17. Probability of aggregate average (a) gyration radius, (b) density, (c) asphericity, and (d) shape factor during the simulation run of asphaltenes A2 and A3 binary mixture.

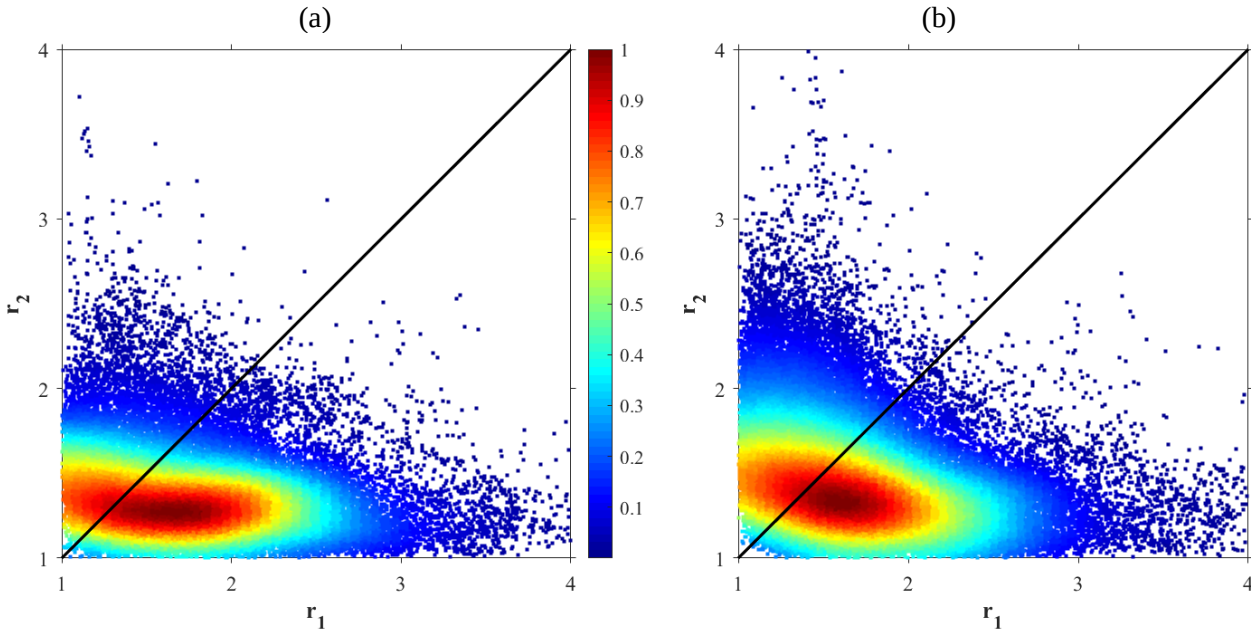

Figure 2-18. Aggregate shape index over the simulation for a binary mixture of asphaltenes A2 and A3: (a) 0 wt% OP, and (b) 7 wt% OP. The color shows the repetition of aggregates with a similar shape index: red and blue indicate the high and low intensities, respectively.

2.4.4 Discussions

In 2010, Mullins modified the Yen and Chilingarian model[106] and introduced a hierarchical paradigm for asphaltene aggregation at three levels: nanoaggregate, cluster, and flocculate [107]. In the nanoaggregates, the asphaltene molecules bond non-covalently from their polar side, and their tail will point out the aggregates and provide the steric hindrance around the aggregates. The number of asphaltene molecules in nanoaggregates depends on asphaltene structure, and it is lower than ten with a gyration radius of less than 30 Å[107]. The nanoaggregates can bond and form larger aggregates, which are known as cluster(s). The binding energy of a cluster is much lower than the nanoaggregate binding energy. Based on the literature review, there is not a certain range of the number of asphaltene molecules for cluster formation, while their gyration radius is between 30–100 Å [32, 107]. Flocculates can be formed by cluster aggregation, and their gyration radius is

more than 300 nm to one micrometer[107]. Based on this theory, the cluster size for all the simulations in our study is in the range of nanoaggregation except for the mixture of asphaltenes A2 and A3.

According to the modified Yen-Mullins theory, the main driving force for the asphaltene aggregation is induced dipole-induced dipole, dipole-dipole, and quadrupole-quadrupole (aromatic stacking) interactions between the asphaltene aromatic cores. The quadrupole-quadrupole interactions include face-to-face, T-shape, and offset π-stacked arrangements, which are repulsive, attractive, and attractive, respectively. Gray et al. [108] claimed that the combination of binding forces including brønsted acid-base interactions, hydrogen bonding, metal coordination complexes, and the interactions between cycloalkyl and alkyl groups as well as the aromatic stacking cause asphaltene aggregation. The asphaltene molecule considered in MD simulation should have required features for formation of various bonding types. The asphaltenes A1 and A3 are only able to form aromatic stacking, while A2 has a hydroxyl group and a pyridine ring that enable it to form hydrogen bonds besides the aromatic stacking. Based on our results, hydrogen bond formation is effective and important with and without an inhibitor. Therefore, our findings are in agreement with the theory of Gray et al. [108]. In the MD model, it is important to introduce the asphaltene structure that can form various bonding types including acid–base interaction (brønsted acidic species), hydrogen bond, coordination complexes, the association of a polar, cycloalkyl, and alkyl groups, and aromatic stacking [108].

The Gaoul's research group at the University of Wyoming confirmed the hierarchical paradigm of asphaltene aggregation through investigating z-average aggregation number for asphaltenes with different structures [29, 42, 107]. However, Headen et al. [31] were not able to verify the Yen-Mullins theory by studying five different asphaltene structures in two solvents. They determined

the average aggregation number and gyration radius in their study. To observe the hierarchical paradigm in a MD simulation run, an adequate number of asphaltene and precipitant molecules, and also sufficient run time are required; furthermore, the hypothesized asphaltene structure should be capable of forming different bonding types. Although the *z*-average aggregation number can predict the asphaltene aggregation trend, we suggest considering a gyration radius as the main criterion since it relies on the experimental observations. For instance, Sedghi et al. [32] simulated the same asphaltene structure for the same time span from two different studies, and used the *z*-average aggregation number measurement to confirm the hierarchical paradigm. They simulated 36 asphaltene molecules (named as A04) in nC_7 as a precipitant, as shown in Figure 2-19(a) [42]; 200 asphaltene molecules (named as AN) in CO_2 (as a precipitant) were employed, as demonstrated in Figure 2-19(b) [29]. Referring to Figure 2-19(a), the criteria are proposed for different levels of aggregation based on the *z*-average aggregation number in which the nanoaggregates have g_z between 8–10, the clusters have g_z between 14–16, and the flocculates have g_z over 25. However, these criteria do not comply with the results of the second study in which the g_z less than 100 can be considered as nanoaggregates, g_z around 150 can be attributed to clusters, and g_z of 200 can be considered as flocculates (see Figure 2-19(b)). Therefore, there is a controversy in classification of aggregates based on g_z; neither of them can be confirmed unless the gyration radius of aggregates is investigated.

Headen et al. [31] used 27 asphaltene molecules with a structure similar to those examined by the Wyoming research group (asphaltene A3), but without a pyridine group. The lack of a pyridine group reduced the dipole moment of the asphaltene molecules; therefore, the asphaltene molecules had less polarizability and, consequently, less aggregation attraction. They did not notice any hierarchical paradigm, which is logical since the average gyration radius of aggregates was less

than 30 Å during the simulation. It was found that the chosen box size and simulation time limit their simulation capability. In this study, we simulate the same asphaltene structure and with the same asphaltene concentration where the number of asphaltene molecules in the simulation box is twice; we also allow for longer simulation runs. Based on Figure 2-6(c) and Figure 2-15(a), the hierarchical paradigm cannot be seen yet, which is related to the limited number of asphaltene molecules, in addition to the inability of asphaltene structure to form bonding interactions (instead of the aromatic stacking).

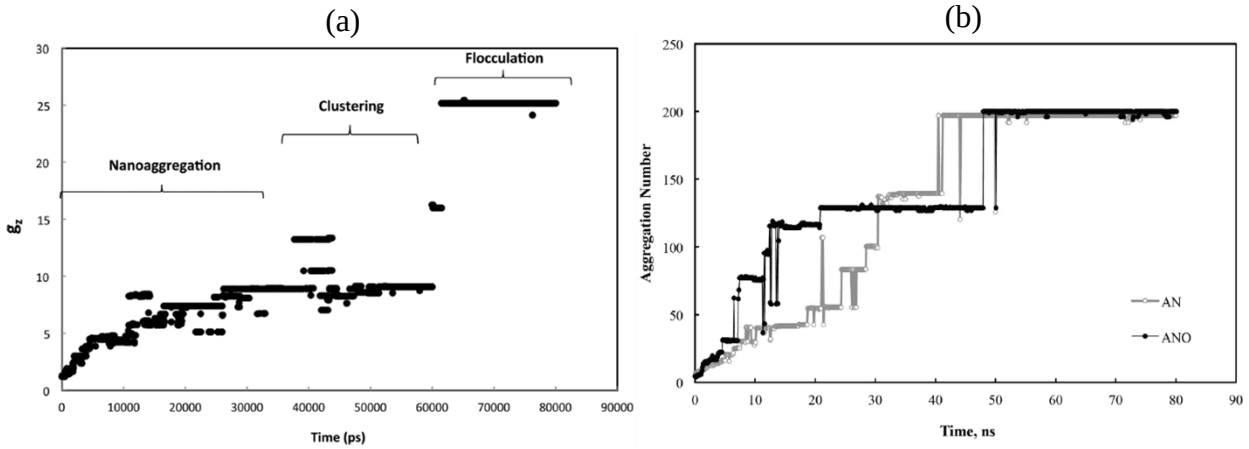

Figure 2-19. a) *z*-average aggregation number for A04 [42], and b) *z*-average aggregation number for AN and ANO [29].

As mentioned earlier, three different criteria can be applied to consider two molecules as an aggregate. Two of these criteria are more commonly used in the literature: 1) the distance between the closest atoms of two molecules, and 2) the distance between the COM of two molecules. Based on the type of bonding force, the path through which the molecules approach each other, and the arrangement of attached molecules, both methods can be useful and valid. A fundamental study is needed to find the suitable criteria that predict aggregates for a certain type of molecules. However, the first method has a greater chance of successfully predicting aggregates for the molecules, which are able to form bonds from different angles. Therefore, there might be no difference for asphaltene

A3 to use either the distance between closest atoms of molecules or the distance between the COM; however, there can be flaws if the latter method is used for A1 and A2 due to having a flexible structure and hydroxyl group, respectively. For instance, Figure 2-20 shows the aggregation of five A2 molecules, which are close to each other in two continuous frames. If the COM distance is considered as an aggregation criterion, five molecules are considered as one aggregate in frame 479. In frame 480, asphaltenes 1–3 do not move significantly, and asphaltenes 4–5 are distorted less compared with frame 479; the COM method considers them as two separate aggregates. However, there is a hydrogen bond between asphaltene 2 and asphaltene 5, and they still should be considered as one aggregate.

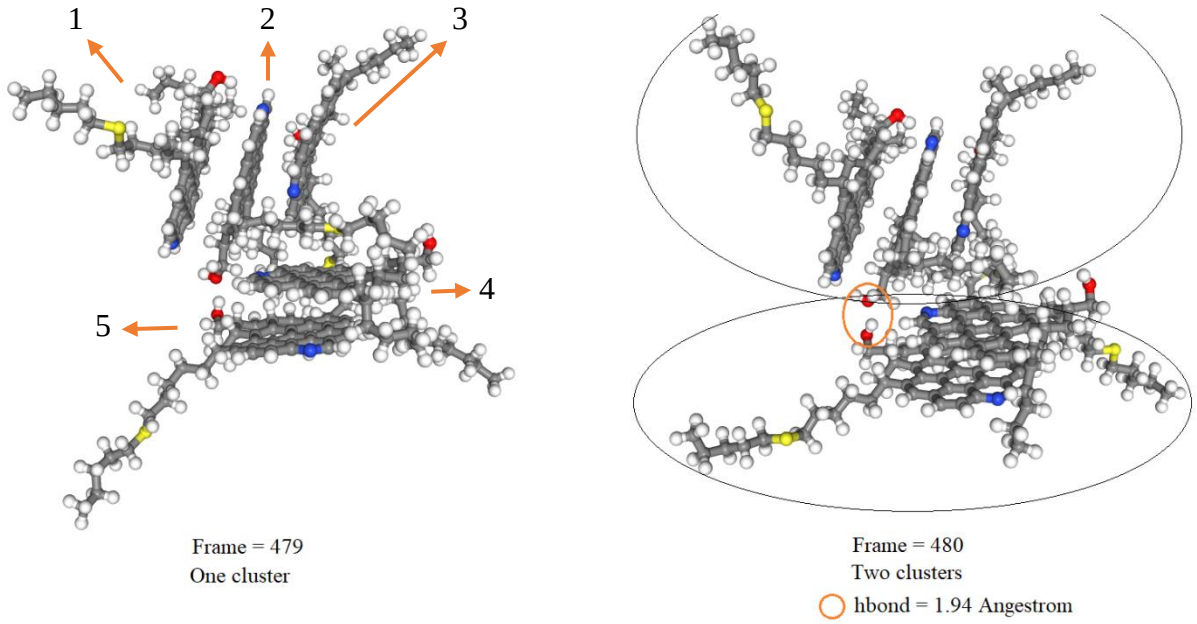

Figure 2-20. Aggregation of A2 molecules in two consecutive frames.

2.5 CONCLUSIONS

Asphaltene precipitation and deposition are critical issues that challenge the oil and gas industries for many years. They generally use different chemical and physical methods, such as the addition of chemical inhibitors, to restrict or postpone asphaltene aggregation. Recently, molecular

dynamics (MD) technique has been used to study the asphaltene-asphaltene and asphaltene-inhibitor interactions at the molecular level and understand inhibition mechanisms. Nevertheless, there are only a few research investigations on asphaltene-inhibitors, particularly surfactant types of inhibitors. In this work, MD is employed to study the effect of *n*-octylphenol (OP), as a surfactant inhibitor, on the aggregation of three asphaltene structures: archipelago asphaltene (A1), continental asphaltene with the ability to form hydrogen bonding (A2), and continental asphaltene without capability to form hydrogen bonding (A3). We perform the MD simulations of pure and mixtures of asphaltenes and analyze asphaltene aggregation and aggregate characteristics such as aggregates' gyration radius, shape, and density.

The archipelago asphaltene (A1) molecules show low self-aggregation in the n-heptane as a precipitant. Nevertheless, OP can break the asphaltene aggregates to postpone their deposition. Using the average gyration radius criterion, the aggregates (for A1) never pass the nanoaggregate level with or without the inhibitor OP. A2 has the highest dipole moment, implying that it is more polarizable and has a stronger aromatic stacking than other types. The asphaltene A2 can form hydrogen bonds due to its hydroxyl and pyridine functional groups. Hence, A2 can severely aggregate; nevertheless, the average gyration radius for the aggregates is lower than 30 Å. Therefore, the A2 aggregates are only in the nanoaggregate scale. OP breaks the asphaltene aggregates at the early stage and then penetrates into the aggregates. The aggregation of A3 is less than A2 due to its lower polarizability and the lack of the ability to make hydrogen bonds. Based on the results, OP is not able to break A3 aggregates, but it can penetrate into the asphaltene aggregates and reduce their density. Hence, the comparison of OP effects on A2 and A3 confirms that the ability of asphaltene structure to form hydrogen bonds, affecting the aggregate characteristics significantly. This is in agreement with the Gray Theory that highlights the

importance of considering different types of interactions other than aromatic stacking in asphaltene aggregation studies. In the case of the asphaltene mixture of A1 and A2, OP is not effective, and the aggregates are at cluster-level in the simulation box. In the case of the asphaltene mixture of A2 and A3, asphaltene aggregates are in cluster level without OP; the inhibitor is able to break the aggregates effectively. Therefore, OP has a different level of effectiveness (as an inhibitor), depending on the type of asphaltene structure and the heterogeneity in asphaltene structure. We conclude that the number of asphaltenes in the aggregates is not a good criterion to distinguish the aggregation levels because, in the experimental tests, many other molecules might have been involved in an aggregate to change the aggregate arrangement even with a few asphaltene molecules. Therefore, we confirm the hierarchical paradigm for asphaltene aggregation; the gyration radius of aggregates is suggested to be used as a criterion for distinguishing aggregates. It is recommended to investigate the effect of pressure, temperature, and inhibitor concentration on asphaltene aggregation and asphaltene-inhibitor interactions. As another recommendation, using combination of different types of inhibitors might be an interesting topic for future work. This approach might increase the overall effectiveness of inhibitors while lowering their individual effective concentrations, since each inhibitor has a potential of forming a specific type of interaction with asphaltene molecules.

ACKNOWLEDGEMENTS

We greatly appreciate the financial assistance of Equinor Canada, InnovateNL, Memorial University, and the Natural Sciences and Engineering Research Council of Canada (NSERC) throughout this project.

NOMENCLATURES

Acronyms	
Asp	Asphaltene
A1	Archipelago asphaltene
A2	Continental asphaltene with hydroxyl and pyridine groups
A3	Continental asphaltene
CO_2	Carbon dioxide
COM	Molecules' center of mass
DBSA	Dodecyl benzenesulfonic acid
DETPMP	Diethylene triamine-penta methylene phosphonic acid
EOR	Enhanced oil recovery
EoS	Equations of state
ES	Electrostatic
HB	Hydrogen bond
IOR	Improved oil recovery
LJ	Lennard-Jones
MD	Molecular dynamics
nC_7	*n*-heptane
OP	*n*-octylphenol
OPLS-AA	All-atom optimized potentials for liquid simulations
QMR	Quantitative molecular representation
PME	Particle-mesh Ewald
PPCA	Poly-phosphino carboxylic acid
PVAc	Polyvinyl acetate
vdW	Van der Waals
VMD	Visual Molecular Dynamics
English letters/variables	
g_i	Number of monomers in an aggregate
g_n	Average aggregation number
g_z	*z*-average aggregation numbers
k, k_{ij}, k_{ijk}, and k_{ijkl}	Force constant for bond, angle, and dihedral atomic potential energy, repectively.
m_i	Mass of each atom of asphaltene molecules
n_i	Number of aggregates
Q *and* r_{ij}	Charge of each atom and Distance between charges
r_1 and r_2	Shape indices
r_0	Initial bond length
R_g	Radius of gyration
S	Shape factor
$V_{aggregate}$	Volume of an aggregate
Greek letters/variables	
δ	Adjustment parameter for phase degree in the dihedral potential
ε_0	Permittivity of vacuum
ε_{ij}	Potential well depth
θ_0	Initial angle size
κ^2	Relative shape anisotropy
λ_1, λ_2, and λ_3	Principal moments of the gyration tensor
$\rho_{aggregate}$	Density of an aggregate
σ	Distance in which the potential is zero
$m\varphi$	Initial dihedral size

REFERENCES

1. IEA, World Energy Outlook 2019, IEA, Paris. 2019. https://www.iea.org/reports/world-energy-outlook-2019. 8th Aug.
2. Zendehboudi, S., Chapter 3 | Asphaltenes Review: Characterization and Modeling. In Totten, G.; Shah, R.; Forester, D., Eds. ASTM International: West Conshohocken, PA, 2019; pp 39-77.
3. Al-Qasim, A.; Al-Anazi, A.; Omar, A. B.; Ghamdi, M. In Asphaltene Precipitation: A Review on Remediation Techniques and Prevention Strategies, Abu Dhabi International Petroleum Exhibition & Conference, 2018; Society of Petroleum Engineers: 2018.
4. Chang, C.-L.; Fogler, H. In Asphaltene stabilization in alkyl solvents using oil-soluble amphiphiles, SPE International Symposium on Oilfield Chemistry, 1993; Society of Petroleum Engineers: 1993.
5. Chang, C.-L.; Scott Fogler, H., Peptization and coagulation of asphaltenes in apolar media using oil-soluble polymers. Fuel Science and Technology International 1996, 14 (1-2), 75-100.
6. Zendehboudi, S.; Shafiei, A.; Bahadori, A.; James, L. A.; Elkamel, A.; Lohi, A., Asphaltene precipitation and deposition in oil reservoirs–Technical aspects, experimental and hybrid neural network predictive tools. Chemical Engineering Research and Design 2014, 92 (5), 857-875.
7. Allenson, S. J.; Walsh, M. A. In A novel way to treat asphaltene deposition problems found in oil production, International Symposium on Oilfield Chemistry, 1997; Society of Petroleum Engineers: 1997.

8. Schantz, S.; Stephenson, W. In Asphaltene deposition: development and application of polymeric asphaltene dispersants, SPE Annual Technical Conference and Exhibition, 1991; Society of Petroleum Engineers: 1991.

9. Karambeigi, M.; Kharrat, R., An investigation of inhibitors performance on asphaltene precipitation due to CO2 injection. Petroleum science and technology 2014, 32 (11), 1327-1332.

10. Goual, L.; Sedghi, M.; Wang, X.; Zhu, Z., Asphaltene aggregation and impact of alkylphenols. Langmuir 2014, 30 (19), 5394-5403.

11. Lowry, E.; Sedghi, M.; Goual, L., Polymers for asphaltene dispersion: Interaction mechanisms and molecular design considerations. Journal of Molecular Liquids 2017, 230, 589-599.

12. Tazikeh, S.; Amin, J. S.; Zendehboudi, S.; Dejam, M.; Chatzis, I., Bi-fractal and bi-Gaussian theories to evaluate impact of polythiophene-coated Fe3O4 nanoparticles on asphaltene precipitation and surface topography. Fuel 2020, 117535.

13. Hu, Y.-F.; Guo, T.-M., Effect of the structures of ionic liquids and alkylbenzene-derived amphiphiles on the inhibition of asphaltene precipitation from CO2-injected reservoir oils. Langmuir 2005, 21 (18), 8168-8174.

14. Chang, C.-L.; Fogler, H. S., Stabilization of asphaltenes in aliphatic solvents using alkylbenzene-derived amphiphiles. 1. Effect of the chemical structure of amphiphiles on asphaltene stabilization. Langmuir 1994, 10 (6), 1749-1757.

15. Permsukarome, P.; Chang, C.; Fogler, H. S., Kinetic study of asphaltene dissolution in amphiphile/alkane solutions. Industrial & engineering chemistry research 1997, 36 (9), 3960-3967.

16. Goual, L.; Sedghi, M., Role of ion-pair interactions on asphaltene stabilization by alkylbenzenesulfonic acids. Journal of colloid and interface science 2015, 440, 23-31.

17. Clarke, P. F.; Pruden, B. B., Asphaltene precipitation from Cold Lake and Athabasca bitumens. Petroleum science and technology 1998, 16 (3-4), 287-305.

18. Gonzalez, G.; Middea, A., Peptization of asphaltene by various oil soluble amphiphiles. Colloids and Surfaces 1991, 52, 207-217.

19. León, O.; Contreras, E.; Rogel, E., Amphiphile adsorption on asphaltene particles: adsorption isotherms and asphaltene stabilization. Colloids and Surfaces A: Physicochemical and Engineering Aspects 2001, 189 (1-3), 123-130.

20. León, O.; Rogel, E.; Urbina, A.; Andújar, A.; Lucas, A., Study of the adsorption of alkyl benzene-derived amphiphiles on asphaltene particles. Langmuir 1999, 15 (22), 7653-7657.

21. Leon, O.; Contreras, E.; Rogel, E.; Dambakli, G.; Espidel, J.; Acevedo, S., The influence of the adsorption of amphiphiles and resins in controlling asphaltene flocculation. Energy & Fuels 2001, 15 (5), 1028-1032.

22. Kashefi, S.; Shahrabadi, A.; Jahangiri, S.; Lotfollahi, M. N.; Bagherzadeh, H., Investigation of the performance of several chemical additives on inhibition of asphaltene precipitation. Energy Sources, Part A: Recovery, Utilization, and Environmental Effects 2016, 38, (24) 3647-3652.

23. Al-Taq, A. A.; Alfakher, B. M.; Al-Muhaish, S. A.; Alrustum, A. A. In From Lab to Field: An Integrated Approach to Successfully Restore The Productivity of Damaged Wells with Organic Deposition, Abu Dhabi International Petroleum Exhibition & Conference, 2016; Society of Petroleum Engineers: 2016.

24. Sigma-Aldrich website, 4-octylphenol price. 2020. https://www.sigmaaldrich.com/catalog/product/supelco/442850?lang=en&region=CA. 8th Aug.

25. Sigma-Aldrich website, 4-nonylphenol price. 2020. https://www.sigmaaldrich.com/catalog/product/supelco/442873?lang=en&region=CA. 8th Aug.

26. Chamkalani, A.; Zendehboudi, S.; Bahadori, A.; Kharrat, R.; Chamkalani, R.; James, L.; Chatzis, I., Integration of LSSVM technique with PSO to determine asphaltene deposition. Journal of Petroleum Science and Engineering 2014, 124, 243-253.

27. Rogel, E., Studies on asphaltene aggregation via computational chemistry. Colloids and Surfaces A: Physicochemical and Engineering Aspects 1995, 104 (1), 85-93.

28. Headen, T. F.; Boek, E. S., Molecular dynamics simulations of asphaltene aggregation in supercritical carbon dioxide with and without limonene. Energy & fuels 2011, 25 (2), 503-508.

29. Sedghi, M.; Goual, L. In Molecular dynamics simulations of asphaltene dispersion by limonene and PVAc polymer during CO 2 flooding, SPE International Conference and Exhibition on Formation Damage Control, 2016; Society of Petroleum Engineers: 2016.

30. Tirjoo, A.; Bayati, B.; Rezaei, H.; Rahmati, M., Molecular dynamics simulations of asphaltene aggregation under different conditions. Journal of Petroleum Science and Engineering 2019, 177, 392-402.

31. Headen, T.; Boek, E.; Jackson, G.; Totton, T.; Müller, E., Simulation of asphaltene aggregation through molecular dynamics: Insights and limitations. Energy & Fuels 2017, 31 (2), 1108-1125.

32. Javanbakht, G.; Sedghi, M.; Welch, W. R.; Goual, L.; Hoepfner, M. P., Molecular polydispersity improves prediction of asphaltene aggregation. Journal of Molecular Liquids 2018, 256, 382-394.

33. Headen, T. F.; Hoepfner, M. P., Predicting Asphaltene Aggregate Structure from Molecular Dynamics Simulation: Comparison to Neutron Total Scattering Data. Energy & Fuels 2019, 33, (5) 3787-3795.

34. Sheu, E. Y., Self-association of asphaltenes. In Structures and dynamics of asphaltenes, Springer: 1998; pp 115-144.

35. Rogel, E., Simulation of interactions in asphaltene aggregates. Energy & Fuels 2000, 14 (3), 566-574.

36. Pacheco-Sánchez, J.; Zaragoza, I.; Martínez-Magadán, J., Asphaltene aggregation under vacuum at different temperatures by molecular dynamics. Energy & fuels 2003, 17 (5), 1346-1355.

37. Pacheco-Sánchez, J.; Zaragoza, I.; Martínez-Magadán, J., Preliminary study of the effect of pressure on asphaltene disassociation by molecular dynamics. Petroleum science and technology 2004, 22 (7-8), 927-942.

38. Takanohashi, T.; Sato, S.; Tanaka, R., Structural relaxation behaviors of three different asphaltenes using MD calculations. Petroleum science and technology 2004, 22 (7-8), 901-914.

39. Carauta, A. N.; Seidl, P. R.; Chrisman, E. C.; Correia, J. C.; Menechini, P. d. O.; Silva, D. M.; Leal, K. Z.; de Menezes, S. M.; de Souza, W. F.; Teixeira, M. A., Modeling solvent effects on asphaltene dimers. Energy & fuels 2005, 19 (4), 1245-1251.

40. Kuznicki, T.; Masliyah, J. H.; Bhattacharjee, S., Molecular dynamics study of model molecules resembling asphaltene-like structures in aqueous organic solvent systems. Energy & Fuels 2008, 22 (4), 2379-2389.

41. Headen, T. F.; Boek, E. S.; Skipper, N. T., Evidence for asphaltene nanoaggregation in toluene and heptane from molecular dynamics simulations. Energy & Fuels 2009, 23 (3), 1220-1229.

42. Sedghi, M.; Goual, L.; Welch, W.; Kubelka, J., Effect of asphaltene structure on association and aggregation using molecular dynamics. The Journal of Physical Chemistry B 2013, 117 (18), 5765-5776.

43. Jian, C.; Tang, T.; Bhattacharjee, S., Probing the effect of side-chain length on the aggregation of a model asphaltene using molecular dynamics simulations. Energy & fuels 2013, 27 (4), 2057-2067.

44. Gao, F.; Xu, Z.; Liu, G.; Yuan, S., Molecular dynamics simulation: the behavior of asphaltene in crude oil and at the oil/water interface. Energy & fuels 2014, 28 (12), 7368-7376.

45. Ungerer, P.; Rigby, D.; Leblanc, B.; Yiannourakou, M., Sensitivity of the aggregation behaviour of asphaltenes to molecular weight and structure using molecular dynamics. Molecular Simulation 2014, 40 (1-3), 115-122.

46. Silva, H. S.; Sodero, A. C.; Bouyssiere, B.; Carrier, H.; Korb, J.-P.; Alfarra, A.; Vallverdu, G.; Bégué, D.; Baraille, I., Molecular dynamics study of nanoaggregation in asphaltene mixtures: Effects of the N, O, and S heteroatoms. Energy & Fuels 2016, 30 (7), 5656-5664.

47. Sodero, A. C.; Santos Silva, H.; Guevara Level, P.; Bouyssiere, B.; Korb, J.-P.; Carrier, H.; Alfarra, A.; Begue, D.; Baraille, I., Investigation of the effect of sulfur heteroatom on asphaltene aggregation. Energy & Fuels 2016, 30 (6), 4758-4766.

48. Liu, B.; Li, J.; Qi, C.; Li, X.; Mai, T.; Zhang, J., Mechanism of asphaltene aggregation induced by supercritical CO 2: insights from molecular dynamics simulation. RSC advances 2017, 7 (80), 50786-50793.

49. Fang, T.; Wang, M.; Li, J.; Liu, B.; Shen, Y.; Yan, Y.; Zhang, J., Study on the asphaltene precipitation in CO2 flooding: a perspective from molecular dynamics simulation. Industrial & Engineering Chemistry Research 2018, 57 (3), 1071-1077.

50. Mehana, M.; Fahes, M.; Huang, L., Asphaltene Aggregation in Oil and Gas Mixtures: Insights from Molecular Simulation. Energy & Fuels 2019, 33 (6), 4721-4730.

51. Murgich, J.; Rodríguez, J.; Aray, Y., Molecular recognition and molecular mechanics of micelles of some model asphaltenes and resins. Energy & Fuels 1996, 10 (1), 68-76.

52. Murgich, J.; Strausz, O. P., Molecular mechanics of aggregates of asphaltenes and resins of the Athabasca oil. Petroleum science and technology 2001, 19 (1-2), 231-243.

53. Headen, T. F.; Boek, E. S., Potential of mean force calculation from molecular dynamics simulation of asphaltene molecules on a calcite surface. Energy & fuels 2011, 25 (2), 499-502.

54. Mohammed, S.; Gadikota, G., The role of calcite and silica interfaces on the aggregation and transport of asphaltenes in confinement. Journal of Molecular Liquids 2019, 274, 792-800.

55. Mohammed, S.; Gadikota, G., The influence of CO2 on the structure of confined asphaltenes in calcite nanopores. Fuel 2019, 236, 769-777.

56. Mikami, Y.; Liang, Y.; Matsuoka, T.; Boek, E. S., Molecular dynamics simulations of asphaltenes at the oil–water interface: from nanoaggregation to thin-film formation. Energy & Fuels 2013, 27 (4), 1838-1845.

57. Jian, C.; Liu, Q.; Zeng, H.; Tang, T., A molecular dynamics study of the effect of asphaltenes on toluene/water interfacial tension: surfactant or solute? Energy & fuels 2018, 32 (3), 3225-3231.

58. Lv, G.; Gao, F.; Liu, G.; Yuan, S., The properties of asphaltene at the oil-water interface: A molecular dynamics simulation. Colloids and Surfaces A: Physicochemical and Engineering Aspects 2017, 515, 34-40.

59. Mohammed, S.; Mansoori, G. A., Effect of CO2 on the interfacial and transport properties of water/binary and asphaltenic oils: insights from molecular dynamics. Energy & fuels 2018, 32 (4), 5409-5417.

60. Mohammed, S.; Mansoori, G. A., Molecular insights on the interfacial and transport properties of supercritical CO2/brine/crude oil ternary system. Journal of Molecular Liquids 2018, 263, 268-273.

61. Teklebrhan, R. B.; Ge, L.; Bhattacharjee, S.; Xu, Z.; Sjöblom, J., Initial partition and aggregation of uncharged polyaromatic molecules at the oil–water interface: a molecular dynamics simulation study. The Journal of Physical Chemistry B 2014, 118 (4), 1040-1051.

62. Song, S.; Zhang, H.; Sun, L.; Shi, J.; Cao, X.; Yuan, S., Molecular Dynamics Study on Aggregating Behavior of Asphaltene and Resin in Emulsified Heavy Oil Droplets with Sodium Dodecyl Sulfate. Energy & fuels 2018, 32 (12), 12383-12393.

63. Liu, J.; Zhao, Y.; Ren, S., Molecular dynamics simulation of self-aggregation of asphaltenes at an oil/water interface: formation and destruction of the asphaltene protective film. Energy & Fuels 2015, 29 (2), 1233-1242.

64. Amjad-Iranagh, S.; Rahmati, M.; Haghi, M.; Hoseinzadeh, M.; Modarress, H., Asphaltene solubility in common solvents: A molecular dynamics simulation study. The Canadian Journal of Chemical Engineering 2015, 93 (12), 2222-2232.

65. Zhang, L.; Greenfield, M. L., Relaxation time, diffusion, and viscosity analysis of model asphalt systems using molecular simulation. The Journal of chemical physics 2007, 127 (19), 194502.

66. Li, D. D.; Greenfield, M. L., Viscosity, relaxation time, and dynamics within a model asphalt of larger molecules. The Journal of chemical physics 2014, 140 (3), 034507.

67. Kondori, J.; James, L.; Zendehboudi, S., Molecular scale modeling approach to evaluate stability and dissociation of methane and carbon dioxide hydrates. Journal of Molecular Liquids 2020, 297, 111503.

68. Kondori, J.; Zendehboudi, S.; James, L., Molecular dynamic simulations to evaluate dissociation of hydrate structure II in the presence of inhibitors: A mechanistic study. Chemical Engineering Research and Design 2019, 149, 81-94.

69. Kondori, J.; Zendehboudi, S.; James, L., New insights into methane hydrate dissociation: Utilization of molecular dynamics strategy. Fuel 2019, 249, 264-276.

70. Yaseen, S.; Mansoori, G. A., Molecular dynamics studies of interaction between asphaltenes and solvents. Journal of Petroleum Science and Engineering 2017, 156, 118-124.

71. Yaseen, S.; Mansoori, G. A., Asphaltene aggregation due to waterflooding (A molecular dynamics study). Journal of Petroleum Science and Engineering 2018, 170, 177-183.

72. Yaseen, S.; Mansoori, G. A., Asphaltene aggregation onset during high-salinity waterflooding of reservoirs (a molecular dynamic study). Petroleum Science and Technology 2018, 36 (21), 1725-1732.

73. Khalaf, M. H.; Mansoori, G. A., Asphaltenes aggregation during petroleum reservoir air and nitrogen flooding. Journal of Petroleum Science and Engineering 2019, 173, 1121-1129.

74. Lowry, E.; Sedghi, M.; Goual, L., Novel dispersant for formation damage prevention in CO2: a molecular dynamics study. Energy & Fuels 2016, 30 (9), 7187-7195.

75. Wang, W.; Taylor, C.; Hu, H.; Humphries, K. L.; Jaini, A.; Kitimet, M.; Scott, T.; Stewart, Z.; Ulep, K. J.; Houck, S., Nanoaggregates of diverse asphaltenes by mass spectrometry and molecular dynamics. Energy & Fuels 2017, 31 (9), 9140-9151.

76. Khalaf, M. H.; Mansoori, G. A., A new insight into asphaltenes aggregation onset at molecular level in crude oil (an MD simulation study). Journal of Petroleum Science and Engineering 2018, 162, 244-250.

77. Fu, C.-F.; Tian, S. X., A comparative study for molecular dynamics simulations of liquid benzene. Journal of chemical theory and computation 2011, 7 (7), 2240-2252.

78. Jorgensen, W. L.; Maxwell, D. S.; Tirado-Rives, J., Development and testing of the OPLS all-atom force field on conformational energetics and properties of organic liquids. Journal of the American Chemical Society 1996, 118 (45), 11225-11236.

79. Jorgensen, W. L.; Tirado-Rives, J., The OPLS [optimized potentials for liquid simulations] potential functions for proteins, energy minimizations for crystals of cyclic peptides and crambin. Journal of the American Chemical Society 1988, 110 (6), 1657-1666.

80. Allen, M. P., Introduction to molecular dynamics simulation. Computational soft matter: from synthetic polymers to proteins 2004, 23 (1), 1-28.

81. Humphrey, W.; Dalke, A.; Schulten, K., VMD: visual molecular dynamics. Journal of molecular graphics 1996, 14 (1), 33-38.

82. Nguyen, H.; Case, D. A.; Rose, A. S., NGLview–interactive molecular graphics for Jupyter notebooks. Bioinformatics 2018, 34 (7), 1241-1242.

83. Tipler, P. A.; Mosca, G., Physics for scientists and engineers. Macmillan: 2007.

84. Desiraju, G. R.; Steiner, T., The weak hydrogen bond: in structural chemistry and biology. International Union of Crystal: 2001; Vol. 9.

85. Herschlag, D.; Pinney, M. M., Hydrogen bonds: Simple after all? Biochemistry 2018, 57 (24), 3338-3352.

86. Gowers, R. J.; Linke, M.; Barnoud, J.; Reddy, T. J. E.; Melo, M. N.; Seyler, S. L.; Domanski, J.; Dotson, D. L.; Buchoux, S.; Kenney, I. M. MDAnalysis: a Python package for the rapid analysis of molecular dynamics simulations; 2575-9752; Los Alamos National Lab.(LANL), Los Alamos, NM (United States): 2019.

87. Michaud-Agrawal, N.; Denning, E. J.; Woolf, T. B.; Beckstein, O., MDAnalysis: a toolkit for the analysis of molecular dynamics simulations. Journal of computational chemistry 2011, 32 (10), 2319-2327.

88. Yen, A.; Yin, Y. R.; Asomaning, S. In Evaluating asphaltene inhibitors: laboratory tests and field studies, SPE International Symposium on Oilfield Chemistry, 2001; Society of Petroleum Engineers: 2001.

89. Boek, E. S.; Yakovlev, D. S.; Headen, T. F., Quantitative molecular representation of asphaltenes and molecular dynamics simulation of their aggregation. Energy & Fuels 2009, 23 (3), 1209-1219.

90. Strausz, O. P.; Mojelsky, T. W.; Lown, E. M., The molecular structure of asphaltene: an unfolding story. Fuel 1992, 71 (12), 1355-1363.

91. Hanwell, M. D.; Curtis, D. E.; Lonie, D. C.; Vandermeersch, T.; Zurek, E.; Hutchison, G. R., Avogadro: an advanced semantic chemical editor, visualization, and analysis platform. Journal of cheminformatics 2012, 4 (1), 17.

92. Parr, R. G., Density functional theory of atoms and molecules. In Horizons of Quantum Chemistry, Springer: 1980; pp 5-15.

93. Campañá, C.; Mussard, B.; Woo, T. K., Electrostatic potential derived atomic charges for periodic systems using a modified error functional. Journal of Chemical Theory and Computation 2009, 5 (10), 2866-2878.

94. Ribeiro, A. A.; Horta, B. A.; Alencastro, R. B. d., MKTOP: a program for automatic construction of molecular topologies. Journal of the Brazilian Chemical Society 2008, 19 (7), 1433-1435.

95. Lindahl, Abraham, Hess, & Spoel, V. D. , GROMACS 2019.3 Source code. 2019.

96. Abraham, M. J.; Murtola, T.; Schulz, R.; Páll, S.; Smith, J. C.; Hess, B.; Lindahl, E., GROMACS: High performance molecular simulations through multi-level parallelism from laptops to supercomputers. SoftwareX 2015, 1, 19-25.

97. Bussi, G.; Donadio, D.; Parrinello, M., Canonical sampling through velocity rescaling. The Journal of chemical physics 2007, 126 (1), 014101.

98. Berendsen, H. J.; Postma, J. v.; van Gunsteren, W. F.; DiNola, A.; Haak, J. R., Molecular dynamics with coupling to an external bath. The Journal of chemical physics 1984, 81 (8), 3684-3690.

99. Nosé, S., A molecular dynamics method for simulations in the canonical ensemble. Molecular physics 1984, 52 (2), 255-268.

100. Hoover, W. G., Canonical dynamics: Equilibrium phase-space distributions. Physical review A 1985, 31 (3), 1695.

101. Parrinello, M.; Rahman, A., Strain fluctuations and elastic constants. The Journal of Chemical Physics 1982, 76 (5), 2662-2666.

102. Hockney, R. W.; Goel, S.; Eastwood, J., Quiet high-resolution computer models of a plasma. Journal of Computational Physics 1974, 14 (2), 148-158.

103. Darden, T.; York, D.; Pedersen, L., Particle mesh Ewald: An N· log (N) method for Ewald sums in large systems. The Journal of chemical physics 1993, 98 (12), 10089-10092.

104. Essmann, U.; Perera, L.; Berkowitz, M. L.; Darden, T.; Lee, H.; Pedersen, L. G., A smooth particle mesh Ewald method. The Journal of chemical physics 1995, 103 (19), 8577-8593.

105. Hess, B.; Bekker, H.; Berendsen, H. J.; Fraaije, J. G., LINCS: a linear constraint solver for molecular simulations. Journal of computational chemistry 1997, 18 (12), 1463-1472.

106. Yen, T. F.; Chilingarian, G. V., Structural parameters from asphaltenes and their geochemical significance. In Developments in Petroleum Science, Elsevier: 1994; Vol. 40, pp 159-178.

107. Mullins, O. C., The modified Yen model. Energy & Fuels 2010, 24 (4), 2179-2207.

108. Gray, M. R.; Tykwinski, R. R.; Stryker, J. M.; Tan, X., Supramolecular assembly model for aggregation of petroleum asphaltenes. Energy & Fuels 2011, 25 (7), 3125-3134.

3. CHAPTER THREE

Effects of Inhibitor Concentration and Thermodynamic Conditions on *n*-Octylphenol-Asphaltene Molecular Behaviours

Preface

A version of this manuscript has been published in the Journal of Molecular Liquids (2021), 340, p. 116897. Ali Ghamartale, the first author of this paper, designed the simulations and manuscript's structure with the help of co-authors (Rezaei, N. and Zendehboudi, S.). The first author conducted the literature review, model execution, and results analysis. The first draft was prepared by Ghamartale and extensively revised by the co-authors (Rezaei, N., Chatzis, I., and Zendehboudi, S.). The concerns of journal reviewers and co-authors were addressed by the first author. The co-author, Sohrab Zendehboudi, had the supervision role and edited the manuscript.

ABSTRACT

The asphaltene stability in crude oil can be disturbed due to changes to thermodynamic conditions during production, raising flow assurance concerns. The addition of chemical inhibitors, such as surfactants, to a crude oil can improve the asphaltene stability. The impact of chemical inhibitors on the asphaltene aggregation intensity and aggregate characteristics, which is needed for design of an efficient inhibitor for a target crude oil, is poorly understood. In this paper, a molecular dynamics simulation tool is employed to simulate the molecular behaviour of the asphaltene and *n*-octylphenol (OP) at various concentrations of OP (0–15 wt%) and thermodynamic conditions (T = 300–360 K and P = 1–60 bar). To meet the objectives, the average aggregation number of different asphaltenes and asphaltene mixtures is measured besides the aggregate characteristics, including aggregate gyration radius, density, and shape. The results show that the archipelago asphaltenes (A1) do not self-aggregate severely, and the gyration radius distribution of the aggregates is similar after the OP addition. Nevertheless, the average aggregation number and the aggregate density analysis show that the aggregation intensity reduces slightly when the OP concentration is increased. Because the continental asphaltene (A2) can form hydrogen bonds, the addition of OP increases the aggregate dispersity significantly, which is identified with the highest peaks at 28 and 35 Å after the addition of 7 and 15 wt% OP, respectively. It is found that OP increases the variations in the aggregate shape and type for A2 aggregates. It is concluded that a high concentration of OP (above 7 wt%) is needed to avoid the asphaltene aggregation. The pressure increase does not change the aggregate shape both with and without the OP. However, adding OP increases the aggregate gyration radius and decreases the aggregate density at 30 bar. Increasing temperature results in a severe aggregation in the system without the inhibitor as the aggregate gyration radius increases, and aggregates become more compact and spherical.

However, by adding OP, both the average aggregation number and aggregate gyration radius decrease (especially at 360 K). According to the sensitivity analysis results, integrating GPUs with CPUs can speed up the simulation approximately three times, compared to the system processing with only CPUs. Outcomes from this research work can help for a better understanding of the molecular behaviour of asphaltene and inhibitors in various thermodynamic situations, leading to the improvement of inhibitor design. This paper highlights the competence of molecular dynamics for exploring the optimal inhibitor concentration and the thermodynamic conditions in which the inhibitor has the highest impact on asphaltene aggregation.

***Keywords*:** Asphaltene inhibitor, Molecular dynamics; Inhibitor concentration; Thermodynamic conditions; Asphaltene aggregation; Hydrogen bond

3.1 INTRODUCTION

Asphaltene is a heavy portion of crude oil, consisting of various molecule structures that are soluble in aromatic solvents but insoluble in aliphatic solvents. The pressure, temperature, and crude oil composition can change upon production, causing asphaltene aggregation. Based on the modified Yen-Mullins theory [1], the asphaltene aggregation mechanism follows a three-level hierarchical paradigm, starting from nanoaggregates, growing to form clusters, and eventually forming flocculates. The asphaltene flocculates can deposit inside the reservoir and onto transportation pipeline, lowering flow rate along with pressure drop increment. The asphaltene removal methods are usually costly and need production interruption [2]. To avoid such serious issues, different chemical inhibitors (or mitigators) are added to the downhole and production pipeline to delay the asphaltene precipitation (and/or deposition) [3, 4]. The inhibitors shift the onset of asphaltene precipitation and/or maintain asphaltenes suspended in the crude oil (by lowering or stopping their growth) in a wider range of pressure and temperature. Asphaltene

chemical inhibitors can be surfactants, polymers, nanoparticles, ionic liquids, and other organic solvents [5]. Fundamentally, the chemical inhibitors should have a polar moiety that attaches to the asphaltene molecules or adsorbs onto the asphaltene molecules, and providing steric hindrance to suspend the asphaltene molecules [6]. To the best of our knowledge, surfactants (in particular, phenols-based) are known as a potential type of inhibitors based on techno-economic perspectives. Inhibitor screening studies show that octylphenol, nonylphenol, and ethoxylated nonylphenol are the most effective surfactants for prevention of asphaltene aggregation [7]. For a given crude oil and inhibitor, temperature, pressure, and the inhibitor concentration are three important parameters that control the efficiency of asphaltene inhibitors. Molecular dynamics (MD) simulation is an advanced modeling approach to study various phenomena at molecular level [8-13]. Thus, it can be employed to assess the effects of inhibitor concentration, temperature, and pressure during asphaltene aggregation as well as inhibition process of asphaltene aggregation. In 2014, Goual et al. [14] evaluated the impact of *n*-octylphenol (OP) concentration on the inhibition phenomenon at the atmospheric condition for 150 ns simulation time. They used GROMACS 4.5.5 software and OPLS-AA force-field to investigate the influence of 6.6 and 33 wt% OP addition on the nanoaggregation and cluster formation of asphaltene molecules. It was revealed that adding 33 wt% OP breaks the asphaltene clusters, while adding 6.6 wt% OP is not effective to break the clusters. However, addition of 6.6 wt% OP to the asphaltene system prevented the nanoaggregates to form clusters. Sedghi and Goual [15] studied limonene and polyvinyl acetate (PVAc) as the asphaltene inhibitors in a range of concentrations for both individual and mixed asphaltenes at 308 K and 300 bar. They used GROMACS 5.1.0 and OPLS-AA force-field to simulate asphaltene (4 wt%) in CO2 without and with 10–30 wt% of limonene and 1–5 wt% of PVAc for 80 ns. Both inhibitors reduced the asphaltene aggregation and the reduction extent was directly affected by the

inhibitor concentration. The effect of limonene concentration in the presence of 5 wt% PVAc was also investigated. In such a system, limonene acted as a co-solvent and also limited the aggregation of asphaltene-PVAc pair, which was enhanced by increasing the limonene concentration. Lowry et al. [16] studied the effectiveness of PVAc, polydimethylsiloxane (PDMS), and PDMS-g-propyl acetate as the asphaltene aggregation inhibitors with 5–10 wt% concentration. PDMS was not effective to prevent asphaltene aggregation in all concentrations, which is due to its low interaction energy with asphaltene and the lack of a side chain in its chemical structure. PVAc was initially efficient, but the inhibitory effect was not stable as its hydrocarbon backbone caused PVAc to self-aggregate [15, 16]. PDMS-g-propyl acetate significantly decreased the asphaltene aggregation for all three asphaltene structures, owing to the potential of asphaltene-inhibitor hydrogen bonds formation. In 2017, Lowry et al. [17] investigated three polymeric inhibitors: two succinimide-based structures and a maleic anhydride derived co-polymer, with a concentration range of 1–10 wt%. All three inhibitors prevented asphaltene aggregation at an optimal concentration of 5 wt% [17]. Tirjoo et al. [18] employed COMPASS force-field in Material Studio 6.0 software to investigate the influence of limonene and various acidic inhibitors such as linear dodecyl benzenesulfonic acid, on the aggregation of a continental asphaltene structure. They included five asphaltene molecules in toluene (at 14.3 wt%), at 298 K and 100 bar for 100 ps, to determine the optimum concentration of the inhibitors. The optimum numbers of inhibitors for dodecyl benzenesulfonic acid, oleic acid, poly-phosphino carboxylic acid, and diethylene triamine-penta methylene phosphonic acid are five molecules; it is three molecules for limonene; and the optimal number is ten molecules for stearic acid. It was found that adding more inhibitor molecules beyond the optimum values results in the inhibitor self-aggregation upon hydrogen bonding.

The effect of thermodynamic conditions on inhibitor effectiveness has also been studied in the literature, using the MD simulation. For instance, Pacheco-Sanchez et al. [19] used MD simulation (Discover 4.2.1 module, COMPASS force filed) to investigate the aggregation of a hypothetical asphaltene structure at different temperatures (273–368 K). They considered 96 asphaltene molecules in the simulation box under vacuum condition, using 100–300 ps simulation run time. Their results confirmed that the number of asphaltene aggregates reduces when the temperature is increased. In a follow-up research, Pacheco-Sanchez et al. [20] used the similar technique to explore the pressure impacts on asphaltene precipitation. They considered 32 asphaltene molecules in pentane and toluene at a broad range of pressure (10–10000 bar). It was concluded that the dominant configuration of asphaltene aggregation in pentane is off-set π stacking at high pressures (4400 bar), while at low pressures (130 bar), the configuration could be face-to-face, T-shape or off-set π stacking [20]. Takanohashi et al. [21] employed Cerius2 software and DREIDING 2.02 method to calculate force-field and to model three asphaltene types derived from vacuum residues of various crude oils (Khafji, Maya, and Iranian-Light) in a temperature range 373–673 K. It was found that increasing temperature dissociates the asphaltene aggregates for Khafji and Iranian-Light cases, while it is ineffective for the Maya asphaltene. Carauta et al. [22] studied the influence of temperature on asphaltene aggregation where asphaltene dimers were dissolved in different solvents, including toluene, n-butane, and isobutane. They used Accelrys Discover Program, CVFF force-field, and simulation run time of 100 ps at 323–573 K. The distance between the monomers decreased with increasing temperature, implying that increasing temperature did not effectively dissociate the asphaltene aggregates. In 2009, Headen et al. [23] investigated the average aggregation number of asphaltene in toluene and n-heptane when temperature was increased from 300 K to 350 K. They used OPLS-AA force-field in GROMACS, and concluded

that the aggregation time decreases by half in heptane after increasing temperature, while the average asphaltene aggregation slightly lowers. Fang et al. [24] used Material Studio to analyze the pressure impact on asphaltene precipitation in the presence of carbon dioxide (CO2). It was found that the free energy for the formation of asphaltene dimers decreases from 34.47 kJ/mol to 25.41 kJ/mol when pressure is increased from 200 bar to 400 bar, which disorders the asphaltene stacks. Headen et al. [25] simulated the asphaltene aggregation of two different asphaltene structures in 1-methylnaphthalene at 300–453 K. Using radial distribution function, they concluded that for all cases, the aggregation intensity decreases with increasing temperature. Mehana et al. [26] studied the effect of pressure and temperature on asphaltene aggregation upon addition of CO2 for two asphaltene structures, in pressure range 300–500 bar and temperature range 285–400 K. The size of aggregates increased upon an increase in pressure, and decreased with increasing temperature. Headen et al. [27] evaluated the limonene impact as an asphaltene inhibitor in temperature range 300–400 K and pressure range 100–200 bar. They selected OPLS-AA force-field in GROMACS for simulating 7 wt% asphaltene in CO2 for 20 ns with and without limonene. It was claimed that the limonene has the highest inhibitory efficiency at 350 K and 150 bar.

Our comprehensive literature review shows that although the effects of pressure and temperature on asphaltene aggregation and aggregate characteristics are studied, these effects have not been studied in the presence of inhibitors and specifically *n*-octylphenol (OP) as an inhibitor (Figure 3-1). Also, there are a few studies that evaluate the inhibitor concentration effect on asphaltene aggregation, while there is no study that is particularly related to phenol-based inhibitors to investigate the aggregate size, density and shape using MD simulation. In our previous study [28], we investigated the inhibitory effects of OP for three asphaltene structures at atmospheric

condition; it was concluded that OP is a proper inhibitor for two asphaltene structures, featuring: (1) an archipelago type chemical structure (named as A1), and (2) a continental type with a hydroxyl functional group that can form hydrogen bonding with the inhibitor (named as A2). We conduct a sensitivity analysis to study the effects of the inhibitor concentration, pressure, and temperature on inhibition performance for single and mixed asphaltene structures in this study: OP concentration (0 wt%, 3.5 wt%, 7 wt%, and 15 wt%), temperature (300 K, 330 K, and 360 K), and pressure (1 bar, 30 bar, and 60 bar). The asphaltene average aggregation, aggregate size, aggregate density and aggregate shape along with the bonding and nonbonding energies are the main analysis used to evaluate the results of MD simulation.

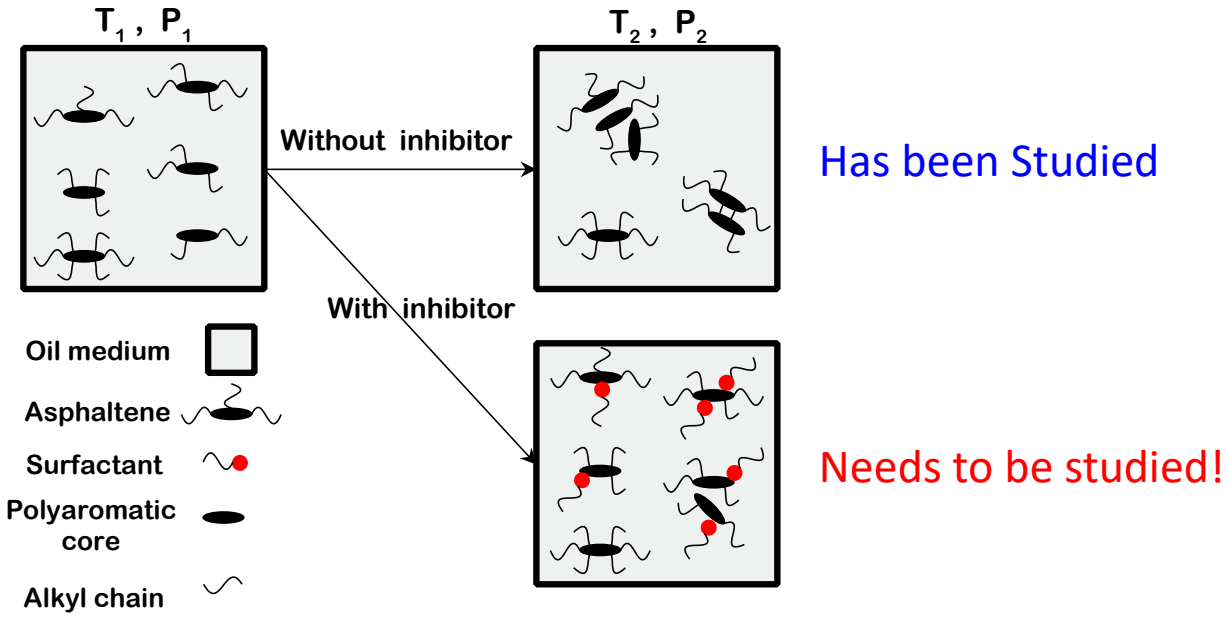

Figure 3-1. The research gap that is focused on in this study.

This paper is organized as follows: After a comprehensive literature review, in Section 3.2, the theory of MD approach is briefly reviewed along with the description of methodology and conditions used in this study. Section 3.3 presents the steps and analysis that will be followed for post-processing. Section 3.4 covers the results and discussions in three subsections: 1- inhibitor concentration sensitivity analysis for single and mixture of asphaltenes, 2- pressure impact for

mixture of asphaltenes, and 3- temperature sensitivity analysis for mixture of asphaltenes. Both the asphaltene aggregation and aggregate characterization analysis are discussed in all simulation scenarios. Also, the hardware sensitivity analysis is conducted in the last part of the results and discussion. Finally, Section 3.5 is dedicated to summarizing the main findings of our study. The results highlighted in this paper can benefit researchers to determine effective inhibitor concentration for asphaltene aggregation of crude oil systems in various thermodynamic conditions.

3.2 THEORY AND SIMULATION/MODELING METHODOLOGY

Molecular dynamics (MD) simulation is a powerful analytical tool for studying physical, chemical, and biochemical systems at molecular scale, with applications such as thermodynamics, transport phenomena, reaction kinetics, and bulk and interfacial properties of the fluids. Recently, MD has been applied to explore the effects of saline water [29-31], gas [32, 33], and chemical materials [14-18, 27, 34] on hydrocarbon fluids. The core architecture of MD simulation is the force-field that defines forces between atoms and molecules. To simulate systems of hydrocarbons, researchers commonly use GROMOS96 force-field [26, 35-42], and all-atom optimized potentials for liquid simulation (OPLS-AA) force-field [14-17, 23, 25, 27, 29-32, 34, 43-51]. Simulating the liquid benzene thermodynamic properties, OPLS-AA force-field was found to be more accurate based on a comparison of simulation results and experimental data [52]. The general equation of force-field is given in Appendix A. Although MD simulation is a valuable tool to study the interaction mechanisms at a molecular scale, a realistic simulation suffers from several limitations and challenges. One of the main challenges is lack of respective parameters between particular atoms in the selected force-field. The MD software packages continuously improve their force-field and data bank; however, the relative parameters of non-bond or dihedral interactions can be

missing that must be introduced to the software manually from literature. Another challenge is related to the preparation of topology files. The topology files can be prepared manually, with online servers and provided code for specific force-field such as MKTOP for AMBER and OPLSAA force-fields. The online servers and provided code may need changes manually, specifically atom charge column, which can be achieved using quantum mechanic simulation. The post-processing of MD simulation results can be challenging if the built-in toolboxes are not able to calculate target properties. The auxiliary package or software, such as MDAnalysis Package in Python, can be used to resolve this issue. Finally, the system size, simulation size and computation cost are three vital factors that need to be carefully taken care of along the MD simulation. Also, the computational burden limits the number of molecules and simulation run time that can be considered in the MD simulation.

The OPLS-AA force-field and GROMACS 2019 [53, 54] are employed in this study, to evaluate the impacts of OP concentration, temperature, and pressure on the asphaltene aggregation in nC_7 with and without OP. The asphaltenes include an archipelago and a continental asphaltene structure for which OP is considered as an effective inhibitor [28] (Figure 3-2). The asphaltene sample with the archipelago chemical structure is shown as A1 (in Figure 3-2(a)) and that with a continental chemical structure and a hydroxyl functional group is indicated with A2 (see Figure 3-2(b)). The effect of inhibitor concentration is investigated in three main systems including A1/OP/nC_7, A2/OP/nC_7, and (A1+A2)/OP/nC_7. The effects of temperature and pressure on the asphaltene aggregation are analyzed while dealing with the (A1+A2)/OP/nC_7. The molecular structures are developed using Avogadro software [55]; Gaussian09 software is utilized to optimize the chemical structures at the ground state, using density functional theory; the basis set

of 6-31g(d,p). MKTOP [56] is employed to generate molecule topology files; and corrections on atom names and partial charges are applied on the generated topology files.

(a) A1 with Mw of 1250 g/mol and dipole moment of 3.64 Debye.

(b) A2 with Mw = 730 g/mol and dipole moment of 4.44 Debye.

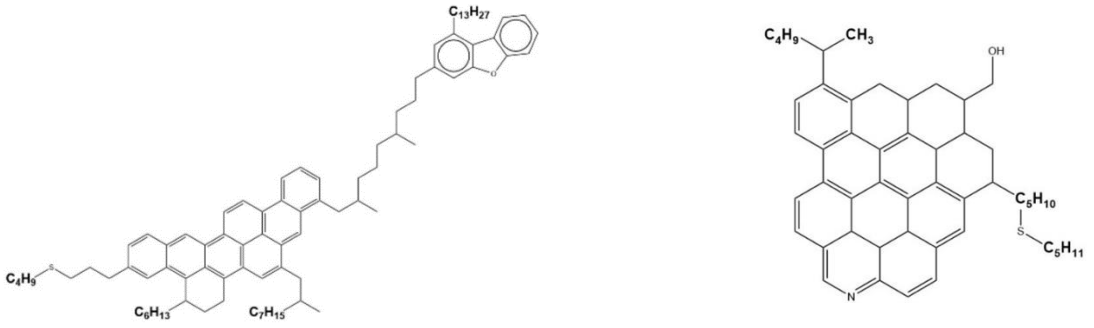

Figure 3-2. The asphaltene structure employed in the present study: (a) A1 is an archipelago-type and (b) A2 is a continental-type.

Three sets of simulation runs are conducted in this work: 1) Asp/OP/nC$_7$ with 0, 3.5, 7, and 15 wt% OP concentration for both single (A1 or A2) and mixture (A1+A2) of asphaltenes at 1 bar and 300 K ; 2) (A1+A2)/OP/nC$_7$ with 0 and 7 wt% OP at 300 K and 1–60 bar; and 3) (A1+A2)/OP/nC$_7$ with 0 and 7 wt% of OP at 1 bar and 300–360 K. The asphaltene concentration is set to be 7 wt% in all simulation runs. Table 3-1 lists the properties of different systems including the number of asphaltenes (and their types), inhibitor, and precipitant as well as the operating conditions. The steepest descent method is utilized to minimize and relax the initial system configuration for 10000 steps. The NVT step is performed to reach the required temperature for 100 ps by the velocity rescaling thermostat [57]. The NPT step is executed to adjust the pressure by altering the box size and density for 1 ns with the velocity rescaling thermostat and the Berendsen barostat [58]. The production runs are carried out for 120 ns at the design temperature and pressure by applying the Nose-Hoover thermostat [59, 60], and the Parrinello−Rahman barostat [61]. The rest of the force-field and simulation settings/procedures, along with the

simulation flowchart, are the same as our previous paper [28]. The outputs from our simulation tests include the atom position and energy, which are recorded every 10 ps. The validity of our simulation results for the system of A1/nC_7 was compared with Headen et al. [43] and proved in our previous study [28].

Table 3-1. The number of asphaltene, inhibitor, and precipitant molecules at targeted thermodynamic conditions for different asphaltene systems.

System	Name	No. of molecules				Temperature (K)	Pressure (bar)
		A1	A2	OP	nC_7		
1	A1/OP/nC_7	50	0	0–649	6950–7975	300	1
2	A2/OP/nC_7	0	50	0–379	4059–4657	300	1
3	(A2+A1)/OP/nC_7	25	25	0–514	5505–6316	300–360	1–60

3.3 POST-PROCESSING ANALYSIS

Figure 3-3 shows a workflow for the analyses followed in this paper. The interaction energy and molecules configuration are two main features of MD outputs. The van der Waals (vdW), electrostatic, and hydrogen bonding are three focal interaction energies for Asp-Asp and Asp-OP. The geometry and polarizability of molecules are two key parameters affecting the vdW force. Molecules with a large electron cloud, such as asphaltene with a benzenic core, have higher polarizability, which gives them a higher opportunity to form vdW bonds. The electrostatic force is due to heteroatoms (such as sulfur) on the asphaltene molecular structure, affecting the polarity of interacting molecules [62]. Hydrogen bond is stronger than vdW bond but, weaker than covalent bond [63]. The interaction energy and spatial coordination of molecules are obtained, using the provided modules in GROMACS. The molecule configuration includes the average aggregation and aggregate characteristics of molecules, calculated using the MDAnalysis package in Python. The accuracy and reliability of the written code were confirmed by comparing the code results

with the results of the modules available in GROMACS , as described in our previous research work [28]. The *z*-averaged aggregation number is employed to compute the aggregation intensity. The distance between the closest atoms of molecules is considered as the aggregation criterion by imposing 0.35 nm as a cut-off limit [28]. The aggregate characterization analysis focuses on the aggregate gyration radius, density, and shape. The gyration radius is utilized to measure the aggregate size; and the relative shape anisotropy and shape factor are used to determine the 3D shape of aggregates. The density of aggregates is used as a criterion for the aggregates from which the efficiency of inhibitor is inferred. For brevity, we include the mathematical expressions of *z*-average aggregation number, aggregate gyration radius, density, relative shape anisotropy, and shape factor in Appendix A.

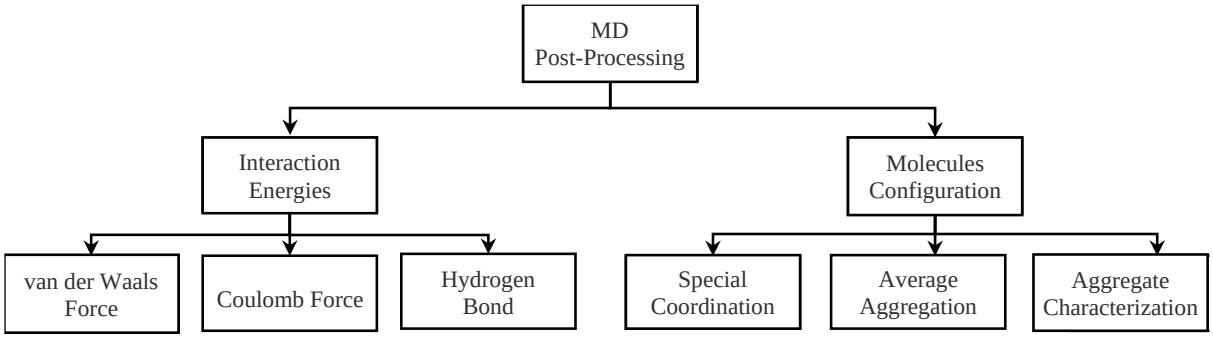

Figure 3-3. The post-analyses of MD analysis outputs.

3.4 RESULTS AND DISCUSSION

3.4.1 Effect of OP Concentration

Asphaltene aggregation: Since OP is an effective inhibitor for both A1 and A2 asphaltenes, this part of the research work focuses on the sensitivity analysis of OP concentration (0–15 wt%) for A1/OP/nC$_7$, A2/OP/nC$_7$, and (A1+A2)/OP/nC$_7$ systems at 1 bar and 300 K. Figure 3-4 shows *z*-average aggregation number (g_z) for A1/OP/nC$_7$ system at different OP concentrations: without OP (panel a), 3.5 wt% (panel b), 7 wt% (panel c), and 15 wt% (panel d). The addition of 3.5 wt%

OP postpones the aggregation before 80 ns relatively, compared to panel (a), but the low concentration of OP and the archipelago structure of A1 make OP ineffective, after 80 ns the average aggregation number continuously increases. However, the addition of 7 wt% OP lowers the average aggregation significantly. Table 3-2 lists the LJ and Coulomb energies for the A1/OP/nC$_7$ case at different inhibitor concentrations. Comparison the case with 7 wt% OP and that without OP shows a significant reduction in Asp-Asp LJ energy and an increase in Asp-OP LJ and Coulomb energy, confirming the effectiveness of OP as the asphaltene inhibitor at a concentration of 7 wt%. Figure 3-4(d) reveals that the addition of 15 wt% OP does not change the g_z compared to the case of 7 wt% OP. Increasing the inhibitor concentration from 7% to 15% causes both the LJ and Coulomb energy to decrease for Asp-Asp and increase for Asp-OP. The reason is that the asphaltene aggregates are highly unstable when 7 wt% OP exists in the system; additionally, asphaltenes have limitations in available sites to bond with OP. Therefore, increasing the inhibitor concentration will only promote the inhibitor self-aggregation which is evident by the substantial increase of non-covalent energies for OP-OP (see Table 3-2). Therefore, although the interaction energy between the asphaltene and OP increases at 15 wt% OP, the g_z does not change meaningfully.

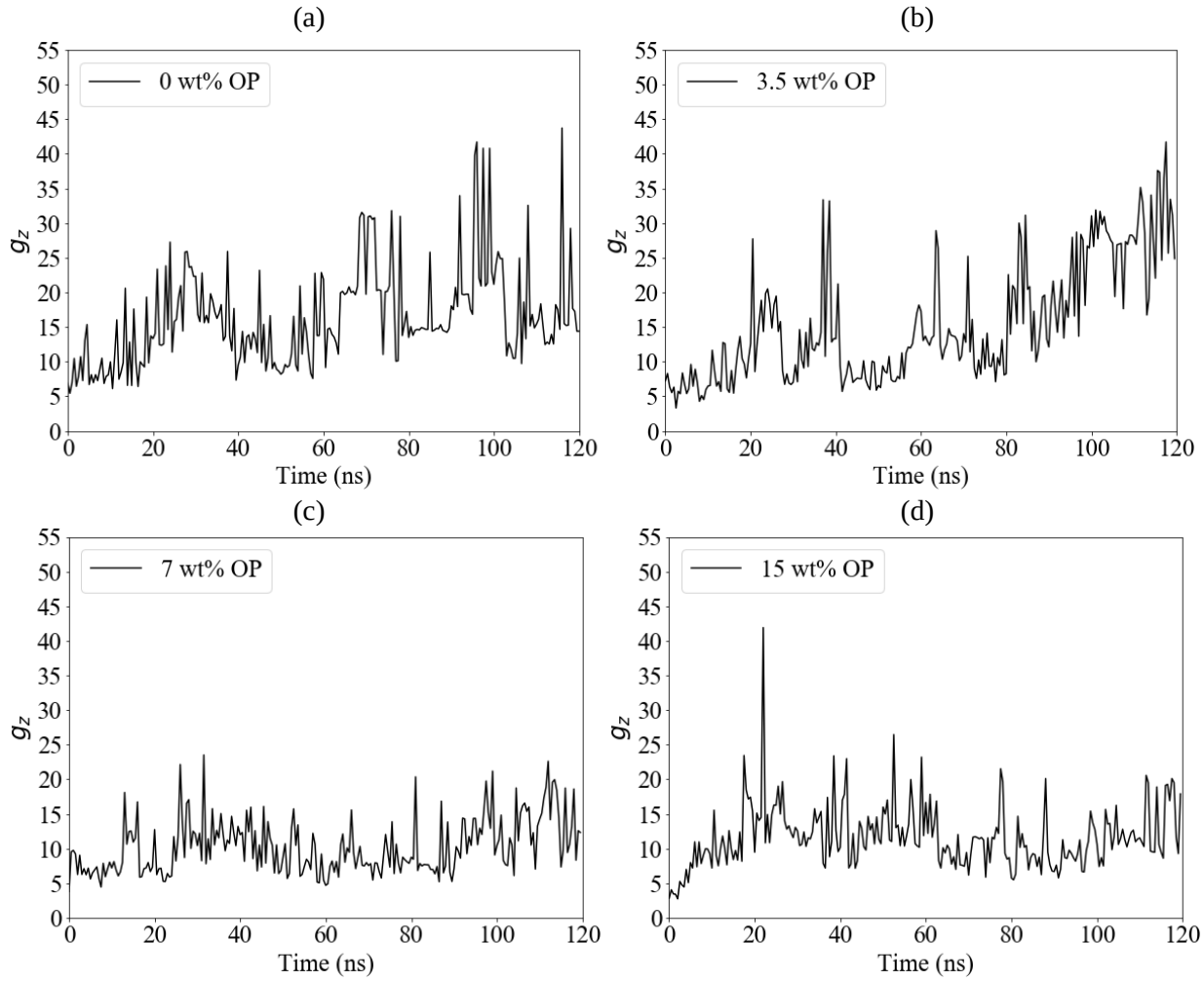

Figure 3-4. Plots of *z*-average aggregation number for A1/OP/nC$_7$ system at 1 bar and 300 K.

Figure 3-5 depicts the g_z for A2/OP/nC$_7$ system in the OP concentration range 0–15 wt%. Comparison of Figure 3-5(a) and Figure 3-5(b) shows that the aggregation rate increases after adding 3.5 wt% OP; however, the final average aggregation is less than the case without OP. As shown in Table 3-2, the LJ interaction energy for Asp-Asp is nearly four times of that for Asp-OP at 3.5 wt% inhibitor, confirming the dominancy of asphaltene aggregation. The addition of 7 wt% OP mitigates the asphaltene aggregation in early time, while the final g_z approaches a plateau at the maximum possible g_z (Figure 3-5(c)). According to Table 3-2, although the addition of 7 wt% OP increases the Asp-OP LJ and Coulomb energies; they are still significantly lower than those for Asp-Asp interactions. The addition of 15 wt% OP to the asphaltene increases the fluctuation

in g_z, which can be explained since the interaction energies for Asp-OP become similar to those for Asp-Asp (see Table 3-2). The number of hydrogen bonds for Asp-Asp and Asp-OP molecules is reported in Table 3-3. When the OP concentration increases from 0 to 15 wt%, the number of hydrogen bonds for Asp-Asp and Asp-OP cases decreases and increases, respectively. By increasing the OP concentration, the number of OP molecules increases in the simulation box while the available number of active sites on asphaltene stays the same. At a high OP concentration (15 wt% OP), the addition of inhibitor molecules causes them to self-aggregate (OP-OP), leading to a substantial increase in the number of hydrogen bonds in OP-OP (Table 3-3).

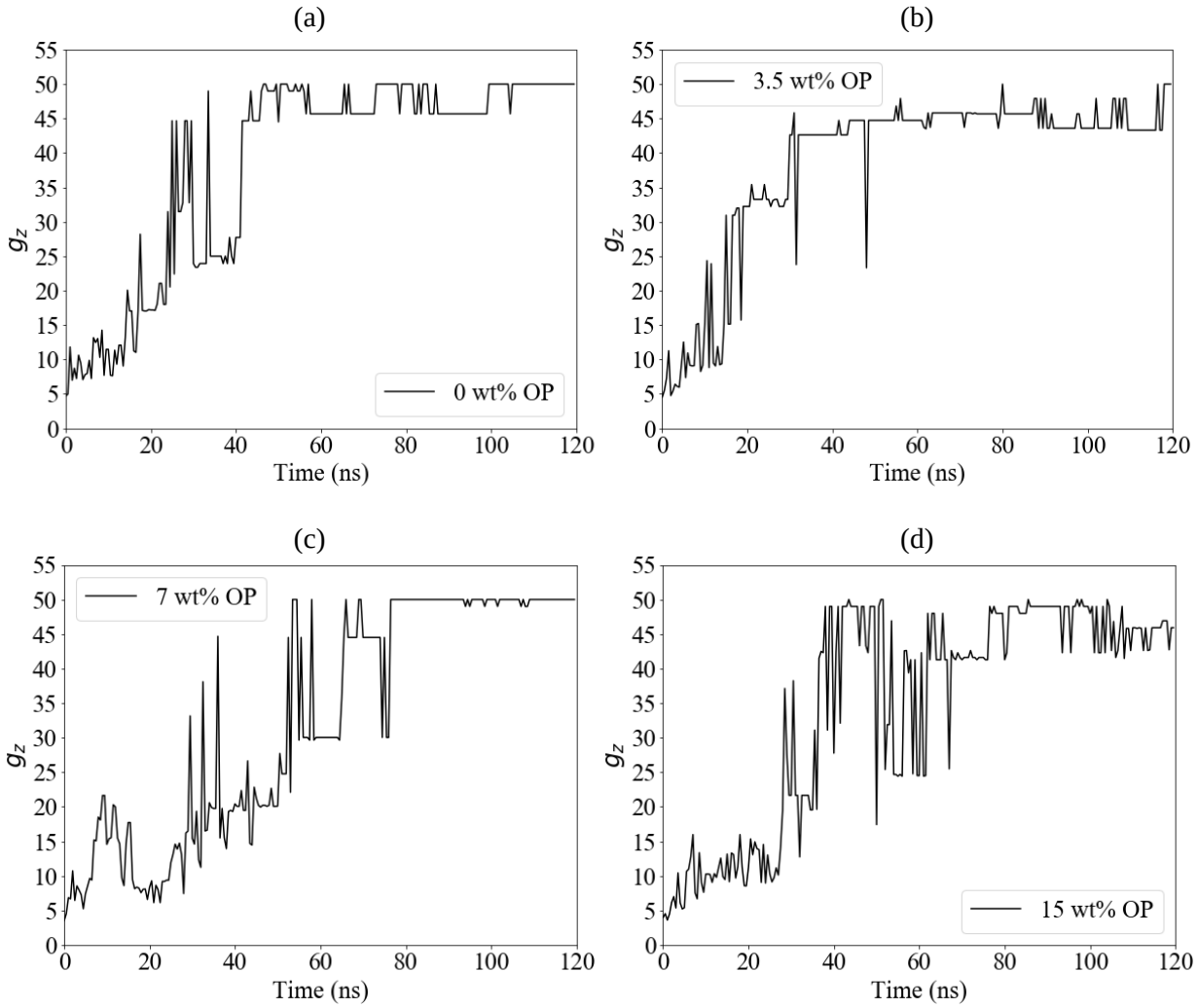

Figure 3-5. *z*-average aggregation number for A2/OP/*n*C_7 system versus time at 1 bar and 300 K.

Figure 3-6 demonstrates the trend in g_z for the system (A1+A2)/OP/nC$_7$ with varying ranges of OP concentrations (0–15 wt%). Compared to the baseline case without inhibitor, the addition of 3.5 wt% OP alters the g_z behavior for the asphaltene aggregates, but no significant change in the aggregates size is noticed compared to the baseline case without OP. At higher concentrations of OP, the asphaltene aggregation decreases considerably over the simulation run which is more pronounced for the case of 15 wt% OP. For example, the g_z values for asphaltene aggregates are below 25 for more than 80% of the simulation time, using 15 wt% OP. Table 3-4 reports the interaction energies between molecules for (A1+A2)/OP/nC$_7$ system. By increasing the OP concentration, the interaction energies of A1-OP and A2-OP increase, while the interaction energies of asphaltenes self-aggregation (A1-A1 and A2-A2) decrease. The LJ attraction energy between A1-A2 increases after the adding a small amount of OP, while it decreases sharply when the OP concentration is increased to 7 wt% and 15 wt%. The trends of LJ energy change verify that the inhibitor becomes more effective upon an increase in the concentration of the inhibitor in the range 7–15 wt% (Table 3-4). The Coulomb energy between asphaltene molecules does not change appreciably by increasing the OP concentration, while it increases slightly for A1-OP and A2-OP (Table 3-4). The average numbers of hydrogen bonds are tabulated in Table 3-5. The number of hydrogen bonds between Asp-Asp within all three time spans decreases when the concentration of OP increases. When the OP concentration increases from 3.5 wt% to 7 wt%, the number of hydrogen bonds for A2-OP increases; however, it decreases when the OP concentration is increased to 15 wt%. This implies that increasing the OP concentration does not necessarily cause more hydrogen bonds between the asphaltene and OP. This is expected since the asphaltene's capacity to form hydrogen bonding is limited, beyond which self-interactions of OPs increase.

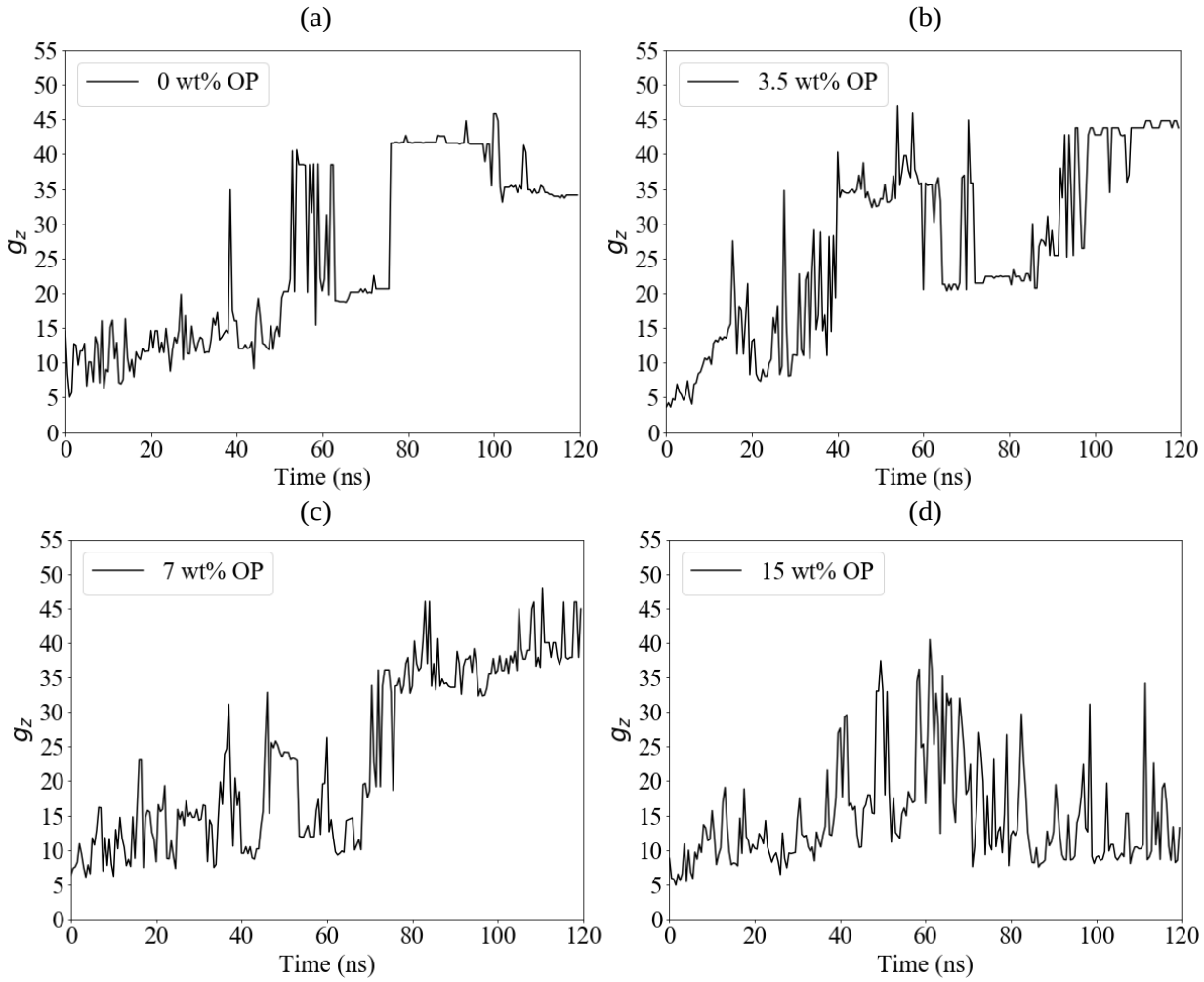

Figure 3-6. Variations of *z*-average aggregation number for (A1+A2)/OP/nC_7 system at 1 bar and 300 K.

Table 3-2. Effect of inhibitor concentration on average LJ and Coulomb energy for A1/OP/nC_7 and A2/OP/nC_7 systems in the last 20 ns of simulations.

Asphaltene system	Energy (kJ/mol)	No inhibitor	With inhibitor (3.5% OP)			With inhibitor (7% OP)			With inhibitor (15% OP)		
		Asp-Asp	Asp-Asp	Asp-OP	OP-OP	Asp-Asp	Asp-OP	OP-OP	Asp-Asp	Asp-OP	OP-OP
A1	LJ	-10998.13	-10579.51	-1408.79	-1692.73	-9943.34	-3147.15	-4175.83	-8996.22	-6019.65	-12634.97
	Coulomb	17395.80	17408.80	-64.32	-396.95	17414.50	-147.63	-1057.64	17444.95	-252.82	-3385.69
	Sum*	6397.67	6829.29	-1473.11	-2089.68	7471.16	-3294.78	-5233.47	8448.73	-6272.47	-16020.66
A2	LJ	-9968.93	-8763.27	-2513.03	-1211.91	-9007.86	-3953.06	-2600.55	-7787.35	-6997.42	-8227.19
	Coulomb	-2499.03	-2204.49	-916.81	-292.09	-2137.00	-1475.26	-616.43	-1979.74	-2226.8	-2044.36
	Sum*	-12467.96	-10967.76	-3429.84	-1504	-11144.86	-5428.32	-3216.98	-9767.09	-9224.22	-10271.55

* The summation of LJ and Coulomb energy contributions to intermolecular forces

Table 3-3. Impact of inhibitor concentration on average number of hydrogen bonds for A2/OP/nC_7 case.

Time span (ns)	No inhibitor	With inhibitor (3.5% OP)			With inhibitor (7% OP)			With inhibitor (15% OP)		
	A2-A2	A2-A2	A2-OP	OP-OP	A2-A2	A2-OP	OP-OP	A2-A2	A2-OP	OP-OP
0–50	14.3	12.8	31.3	6.5	7.1	46.7	16.0	4.6	73.0	66.5
50–100	22.7	16.3	35.5	7.3	12.7	51.5	15.3	5.8	80.9	64.7
100–120	22.7	14.3	36.3	6.5	9.7	58.7	15.3	4.8	85.0	65.0

Table 3-4. Effect of inhibitor concentration on average LJ and Coulomb energy for (A1+A2)/OP/nC_7 system in the last 20 ns of simulation runs.

Asphaltene system	Energy (kJ/mol)	No inhibitor			With inhibitor (3.5 wt% OP)					With inhibitor (7 wt% OP)					With inhibitor (15 wt% OP)				
		A1-A1	A2-A2	A1-A2	A1-A1	A2-A2	A1-A2	A1-OP	A2-OP	A1-A1	A2-A2	A1-A2	A1-OP	A2-OP	A1-A1	A2-A2	A1-A2	A1-OP	A2-OP
A1+A2	LJ	-4386.9	-3269.3	-3205.8	-4164.9	-3165.9	-3335.6	-1178.3	-866.5	-3991	-2717.8	-3109.3	-1972.8	-1524.2	-3113.8	-2564.3	-2333	-3747.5	-2864
	Coulomb	8722.58	-1114.84	-57.27	8724.4	-1001.71	-67.1	-46.85	-523.9	8710.41	-954.15	-42.67	-78.72	-738.20	8719.07	-961.77	-39.9	-135.26	-1022.5
	Sum*	4335.68	-4384.14	-3263.1	4559.5	-4167.61	-3402.7	-1225.1	-1390.4	4719.41	-3672	-3152	-2051.5	-2262.4	5605.27	-3526.1	-2372.9	-3882.8	-3886.5

* The summation of LJ and Coulomb energy contributions to intermolecular forces

Table 3-5. Effect of inhibitor concentration on average number of hydrogen bonds for (A1+A2)/OP/nC_7 case.

Time span (ns)	Asphaltene system	No inhibitor	With inhibitor (3.5 wt% OP)		With inhibitor (7 wt% OP)		With inhibitor (15 wt% OP)	
		A2-A2	A2-A2	A2-OP	A2-A2	A2-OP	A2-A2	A2-OP
0–50	A1+A2	3.1	1.5	15.9	1.5	23.5	1.3	18.6
50–100	A1+A2	5.9	2.2	23.7	1.9	24.8	2.2	18.4
100–120	A1+A2	8.0	3.1	21.6	1.3	29.3	2.5	18.4

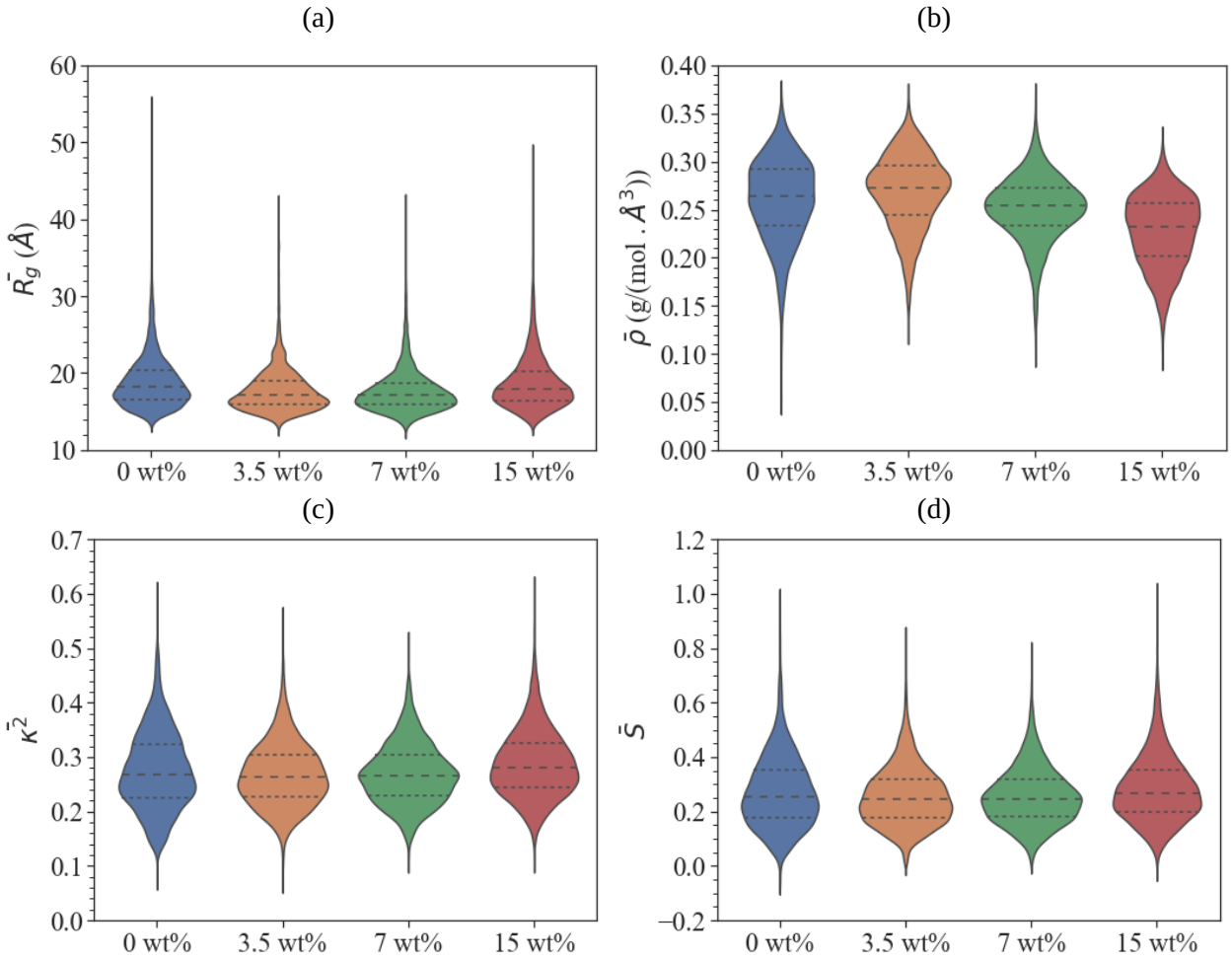

Figure 3-7. The effect of OP concentration on aggregate average (a) radius of gyration, (b) density, (c) relative shape anisotropy, and (d) shape factor for A1/OP/nC$_7$ system at 1 bar and 300 K.

Aggregate characteristics: Figure 3-7 shows the aggregate characteristics of A1 with 0–15 wt % OP concentration. Based on Figure 3-7(a), the average gyration radius does not change considerably with increasing OP. All four plots in Figure 3-7 have peaks between 15 and 25 Å. As shown in Figure 3-4, A1 does not aggregate vigorously without OP. Therefore, the aggregates are mostly built from few asphaltene molecules such as dimer, trimer, and tetramer regardless of the OP presence. Panel b of Figure 3-7 reveals that the aggregate density decreases when OP concentration is increased. The reduction in density without a significant change in the gyration radius implies that when one molecule separates out of dimers or trimers, this reduces the aggregate

mass to half or one-third while the volume does not alter considerably since A1 is flexible. According to Panels c and d of Figure 3-7, the aggregate shape has a similar trend for 0–15 wt% OP concentration, confirming that the volume of aggregates does not vary significantly.

Figure 3-8 displays the aggregate characteristics for A2/OP/*n*C_7 at different OP concentrations. For the baseline case without OP, the average gyration radius has three peaks at 13, 17, and 26 Å. The distribution becomes bimodal with peaks at 17 and 20 Å after adding 3.5 wt% OP, indicating that the aggregate size distribution has become more homogenous. However, by adding further OP, the aggregate dispersity increases with the highest peak at 28 and 35 Å for 7 and 15 wt%, respectively. The average aggregate density follows a bimodal distribution in the baseline case without inhibitor, with the peaks located at 0.32 and 0.5 g/(mol.Å^3). The addition of 3.5 and 7 wt% OP deforms the average density probability distribution to unimodal with a distinct peak at 0.4 and 0.35 g/(mol.Å^3), respectively. The density changes indicate that the aggregates have become less dense, larger, and more uniform; this indicates OP penetration into the asphaltene aggregates. When 15 wt% OP is added to A2/OP/*n*C_7 system, the probability of average aggregate density changes to a bimodal distribution with a peak at 0.1 and 0.39 g/(mol.Å^3). The extremely low aggregate density is interpreted as the reformation of broken aggregates with a relatively large gap between them due to the OP presence. Therefore, using high inhibitor concentrations has positive and negative effects, such as breaking and reforming aggregates, respectively, for asphaltene structure with potential to make hydrogen bonds. Based on Figure 3-8(c), the aggregates become more linear other than spherical after adding 3.5 wt% OP since the relative shape anisotropy distribution and peak change toward one, revealing the penetration of the inhibitor molecules into the structure of the asphaltene aggregates. At 7 wt% OP, the aggregates become more spherical again; this confirms that at 7 wt% OP, the inhibitor can break the aggregates partially. However,

the aggregate shape distribution becomes more versatile after the addition of 15 wt% OP. This approves the controversial effect of OP on asphaltene aggregate, implying that the aggregates break and reform at this concentration. Figure 3-8(d) demonstrates that without the inhibitor, the aggregates can be prolate, spherical, and oblate during the simulation. Adding 3.5 to 7 wt% of OP eliminates the oblate shape and substantially reduces the probability of observing spherical aggregates. The addition of 15 wt% OP again increases the probability of the aggregates having different shapes.

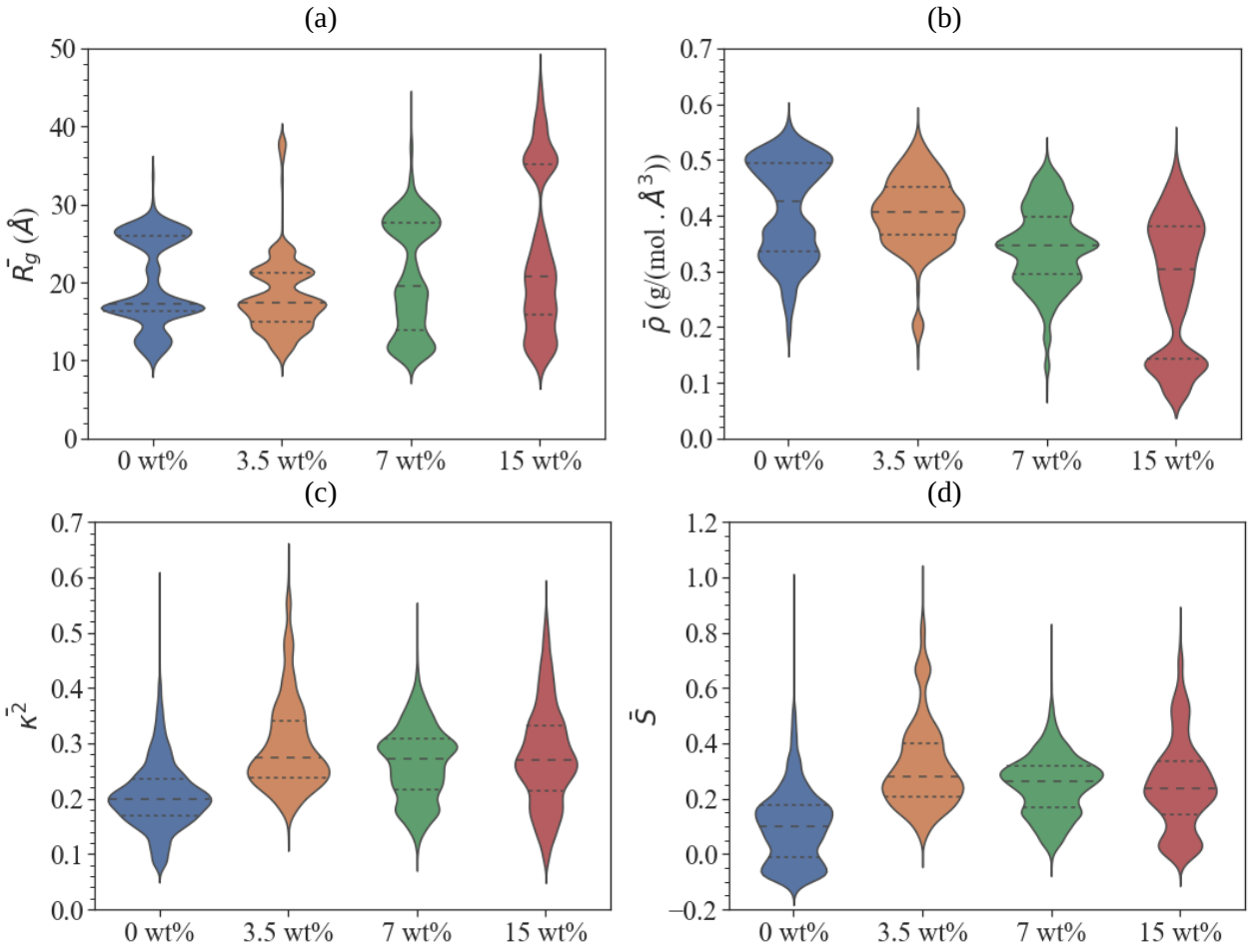

Figure 3-8. The impact of OP concentration on aggregate average (a) radius of gyration, (b) density, (c) relative shape anisotropy, and (d) shape factor for A2/OP/nC$_7$ case at 1 bar and 300 K.

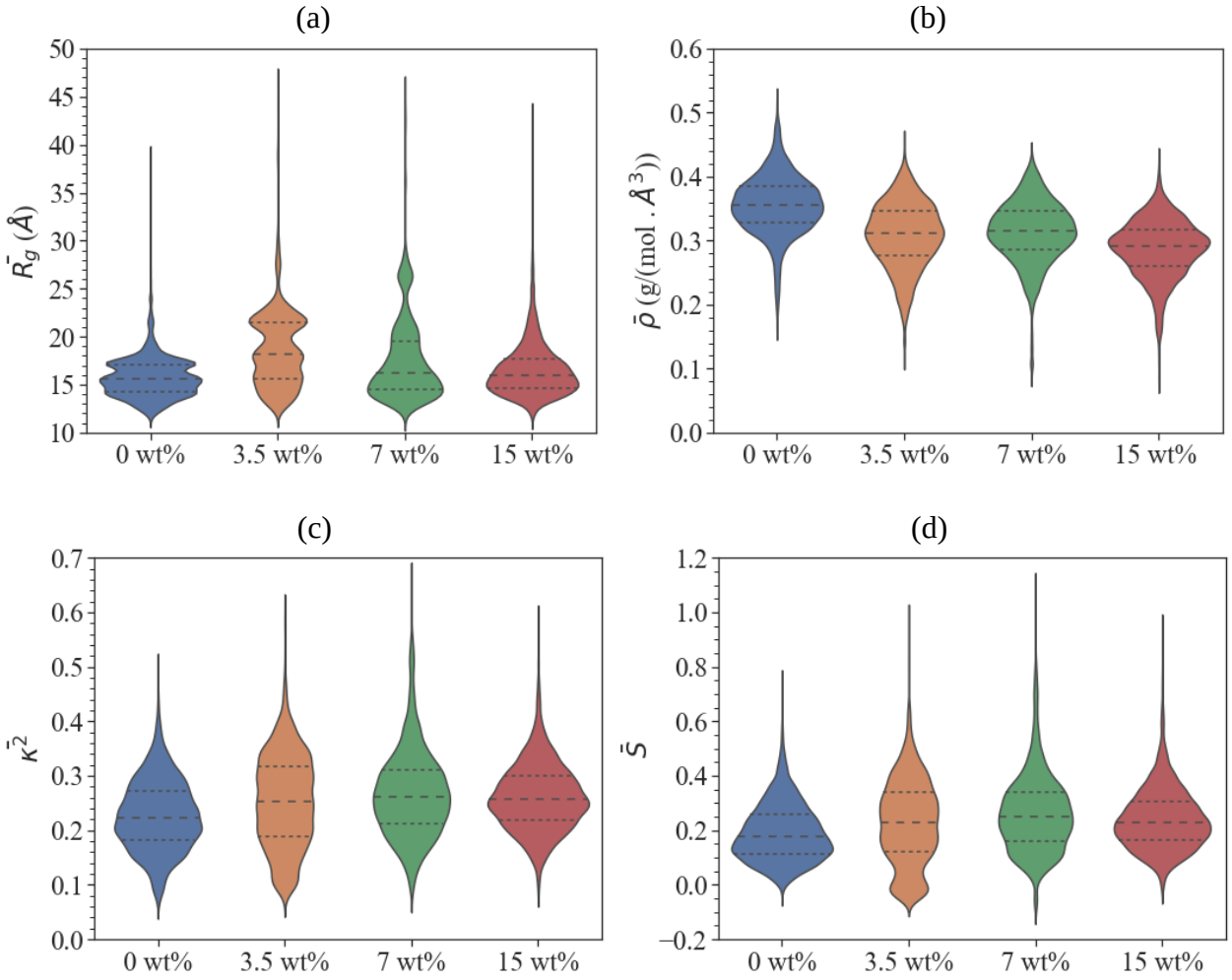

Figure 3-9. The influence of OP content on aggregate average (a) radius of gyration, (b) density, (c) relative shape anisotropy, and (d) shape factor for (A1+A2)/OP/*n*C_7 system at 1 bar and 300 K.

Figure 3-9 depicts the aggregate gyration radius, density, and shape variations for the (A1+A2)/OP/*n*C_7 system at various inhibitor concentrations. Figure 3-9(a) shows a peak between 12–20 Å for the aggregate gyration radius without OP; the distribution changes to bimodal with a broader variation in the gyration radius by adding 3.5 and 7 wt% OP. At 15 wt% OP, the aggregates become more uniform, and the average gyration radius features a peak at 15 Å. According to Figure 3-9(b), the density of the aggregates decreases upon an increase in the concentration of OP. The behaviors of gyration radius and density confirm that the OP starts to diffuse into the asphaltene

aggregate structure at low concentrations of OP, while it breaks the aggregates at 15 wt% OP. Figure 3-9(c) and Figure 3-9(d) reveal that the addition of 3.5 wt% OP increases the heterogeneity in aggregate shape; some aggregates turn to oblate and spherical, while they become more uniform and prolate at higher OP concentrations, confirming the break down hypothesis for the asphaltene aggregates.

3.4.2 Effect of Pressure

Asphaltene aggregation: Pressure change significantly affects the asphaltene precipitation and deposition phenomena. In this part, we study the impact of pressure on the asphaltene aggregation with and without the inhibitor in (A1+A2)/OP/nC$_7$ system. Figure 3-10 describes the g_z of asphaltene with and without OP when the pressure is increased from 0 to 60 bar and temperature is kept constant at 300 K. Without OP, increasing pressure increases the fluctuation in g_z; this implies that the associated asphaltene molecules that form aggregates are not stable and dissociate (panel a). Therefore, pressure incremental decreases asphaltene aggregation affinity and postpones asphaltene aggregation. Table 3-6 confirms that without the inhibitor, the LJ interaction energy for Asp-Asp decreases when pressure is increased. The coulomb energy does not change significantly with increasing pressure compared to LJ interaction energy as it is clear in Table 3-6. Figure 3-11 demonstrates nC$_7$ phase envelope [64] and the hypothetical asphaltene onset envelope. Fundamentally, the asphaltene starts to precipitate below the upper onset point and above lower onset point with the highest precipitation at the bubble point curve. AB line shows a thermodynamic process in which the pressure is increased (1–60 bar) at 300 K. The AB process confirms that the mixture condition tends toward liquid only when the pressure is increased since the thermodynamic conditions change toward upper onset point from liquid-solid at 1 bar and 300 K. This confirms the observation in Figure 3-10(a): aggregation reduction as a result of increasing

pressure when OP is absent. Figure 3-10(b-d) demonstrates the g_z changes with increasing pressure for both scenarios (with and without inhibitor) in (A1+A2)/OP/nC$_7$ system; thus, we can assess the impact of pressure on inhibitor effectiveness based on Figure 3-10. Comparing panels b, c, and d of Figure 3-10 shows that the OP has the most inhibition effect on the asphaltene aggregation at 30 bar. The reason is that the aggregates are tight and dense with a high self-aggregation affinity at 1 bar that does not allow the OP molecules to interfere in the aggregation process. Also, at 60 bar, the thermodynamic condition is changed toward less asphaltene aggregation even when the OP is absent (Figure 3-11), and OP cannot be effective enough. Table 3-6 reports the interaction energies between asphaltene and OP molecules. This is expected as Asp-Asp LJ energy significantly drops upon OP addition at 30 bar with high Asp-OP LJ interaction energy. The Coulomb energy between the molecules is not affected by pressure.

Table 3-7 lists the average number of hydrogen bonds when pressure is increased from 1 to 60 bar. According to the results, the number of hydrogen bonds does not depend on pressure. Thus, it does not change considerably by increasing pressure, which is in agreement with the literature [29].

Table 3-6. Effect of pressure on average LJ and Coulomb energy in the last 20 ns of simulation runs for (A1+A2)/OP/nC$_7$ system in the absence and presence of 7 wt% inhibitor.

Pressure	Asphaltene system	Energy (kJ/mol)	No inhibitor			With inhibitor				
			A1-A1	A2-A2	A1-A2	A1-A1	A2-A2	A1-A2	A1-OP	A2-OP
30 bar	A1+A2	LJ	-4077.2	-3308.4	-4258.7	-3664.5	-2747.8	-3712.4	-2237.6	-1480.7
		Coulomb	8725	-1018.4	-68.6	8714.0	-958.5	-48.1	-83	-774.8
		Sum*	4647.8	-4326.8	-4327.3	5049.5	-3706.3	-3760.5	-2320.6	-2255.5
60 bar	A1+A2	LJ	-3779.6	-3155.7	-3431.4	-4061.5	-2791.1	-2741.4	-1978.6	-1804.0
		Coulomb	8735.0	-1059.1	-62.5	8728	-993.6	-49.8	-70.8	-743.9
		Sum*	4955.4	-4214.8	-3493.9	4666.5	-3784.7	-2791.2	-2049.4	-2547.9

* The summation of LJ and Coulomb energy contributions to intermolecular forces

Table 3-7. Impact of pressure on average number of hydrogen bonds for (A1+A2)/OP/nC$_7$ case with and without 7 wt% inhibitor.

Pressure	Time span (ns)	No inhibitor	With inhibitor		
		A2-A2	A2-A2	A2-OP	OP-OP
30 bar	0–50	2.5	2.3	23.9	21.1
	50–100	2.7	1.8	27.3	22.2
	100–120	2.6	2.2	31.4	21.6
60 bar	0–50	3.1	2.8	23	21.3
	50–100	4.6	3.5	28.5	23. 7
	100–120	5.7	2.4	28.4	22.8

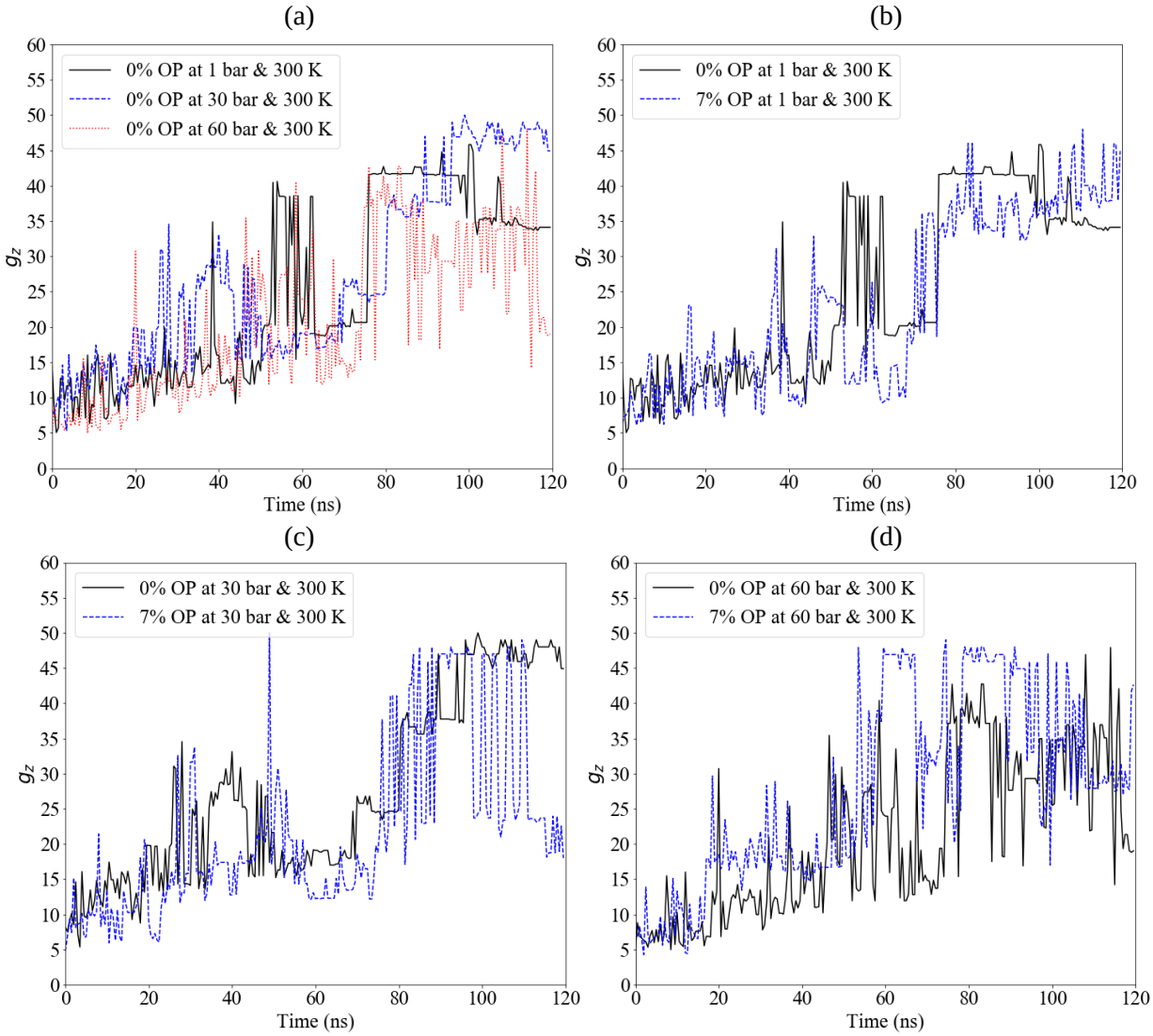

Figure 3-10. Plots of z-average aggregation number for (A1+A2)/OP/nC$_7$ at 1 bar, 30 bar and 60 bar, and 300 K without and with OP.

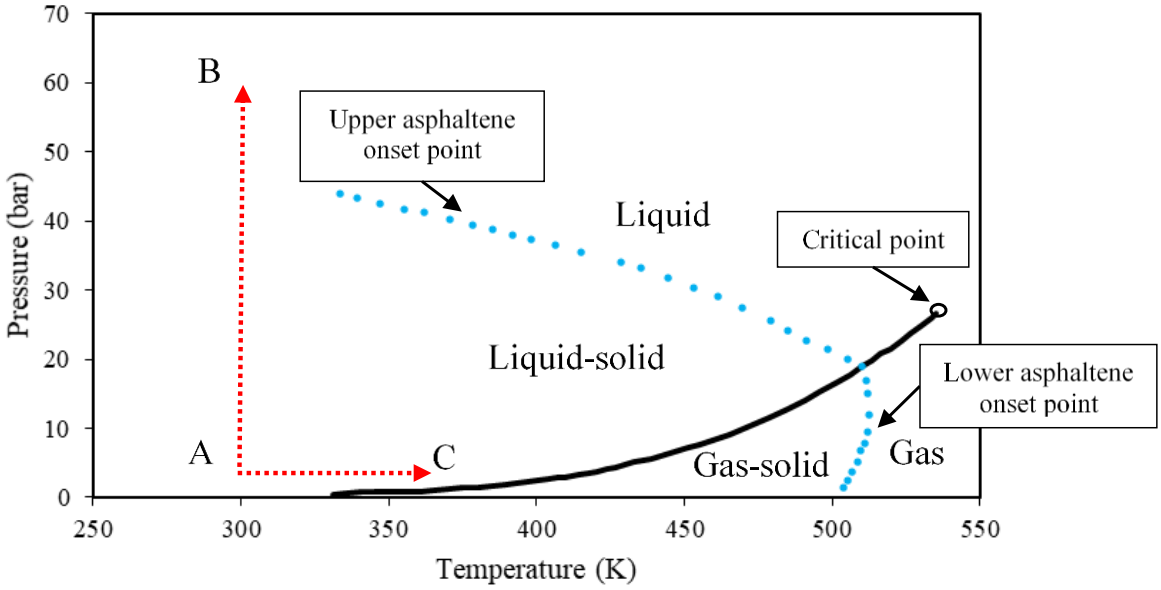

Figure 3-11. Pressure and temperature changes for *n*-heptane in the form of the P-T diagram (black line) [64] and hypothetical asphaltene onset envelope (blue dots): AB isothermal compression and AC isobaric temperature variation.

Aggregate characteristics: Figure 3-12 displays the aggregate characteristics of the (A1+A2)/OP/nC_7 system with and without OP. In fact, the average gyration radius and the average aggregate density for the aggregates are shown in Figure 3-12(a) and Figure 3-12(b), respectively. According to the results, the aggregates are compact and dense at 1 bar without OP, and the presence of OP cannot significantly deform the structure of the aggregates. On the contrary, at 30 bar, the aggregates are more relaxed compared to atmospheric conditions without OP. Thus, the presence of OP gives them the opportunity to penetrate into the structure of the asphaltene aggregates. The OP weakens the aggregates, and also detaches the loose asphaltene molecules from the aggregate peripheral. At a pressure of 60 bar, the aggregates feature a high variation in the gyration radius and density regardless of OP presence; this confirms the instability of aggregates due to thermodynamic conditions, as described in Figure 3-11. Panels c and d of Figure 3-12 show that increasing pressure does not influence the asphaltene aggregate shape in the

absence and presence of inhibitor. The OP addition alters the aggregate shape toward the linear chain and prolate shape at all pressures to the same extent. This means that the aggregate shape is not sensitive to pressure, though it is strongly affected by the OP concentration.

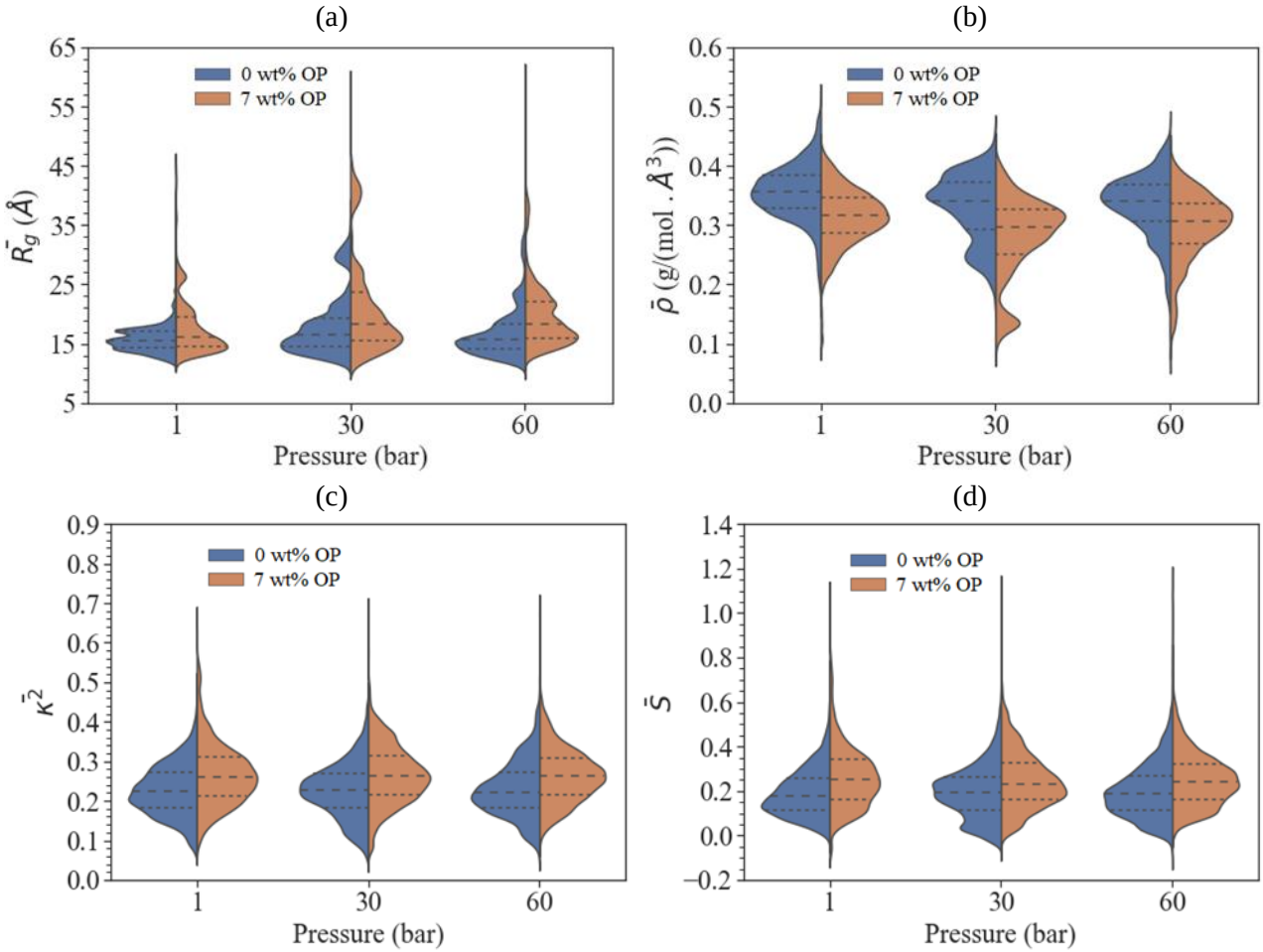

Figure 3-12. The impact of pressure on aggregate average (a) radius of gyration, (b) density, (c) relative shape anisotropy, and (d) shape factor for (A1+A2)/OP/nC$_7$ system.

3.4.3 Effect of Temperature

Asphaltene aggregation: Pacheco et al. [19] and Carauta et al. [22] used MD strategy to evaluate the temperature effect on asphaltene aggregate size. Pacheco et al. [19] reported that the aggregate size is reduced when the temperature is increased, while Carauta et al. [22] concluded that the aggregate size is increased with increasing temperature. Takanahshi et al. [21] claimed that the

types of asphaltene and precipitant are two parameters that correlate with the temperature effect on asphaltene aggregation. In most past research investigations, researchers have considered only very few asphaltene molecules and no precipitant molecules in MD simulation runs due to computational limitations. The contradictory results can be due to computation/simulation limitations, assumptions, and various thermodynamic conditions in different studies.

Figure 3-13 presents the g_z for (A1+A2)/OP/nC$_7$ system with and without OP in the temperature range 300–360 K and at a pressure of 1 bar. In the baseline case without the inhibitor, the g_z increases when temperature is increased (Panel a of Figure 3-13). Increasing temperature from 300 to 360 K enhances the molecules movement. Since nC$_7$ has repulsion interactions with asphaltene molecules, the asphaltene molecules have a higher chance to move closer to each other and form aggregation. Also, the LJ and Coulomb interaction energies between the asphaltenes are increased at 360 K, compared to the temperatures of 300 K and 330 K (see Table 3-8), which confirms the primary claim. The thermodynamic viewpoint of temperature effect on asphaltene-nC$_7$ interactions is shown with line AC in Figure 3-11. According to Figure 3-11, the thermodynamic state of the mixture stays in liquid-solid, and it becomes closer to the bubble-dew point curve when temperature is increased. Based on the literature [65], the asphaltene precipitation increases as the thermodynamic condition approaches the bubble point curve. The comparison of panel b, c, and d of Figure 3-13 illustrates that the inhibitor exhibits the highest efficiency at 360 K. According to Table 3-8, the LJ energy of A1-A1 and A1-A2 expressively decreases at 360 K after the addition of OP, such that the increase in LJ energy for A2-A2 is negligible. The LJ energy between Asp-OP decreases when the temperature is increased; however, the change is not considerable relative to the asphaltene LJ energies. Hence, the Coulomb energy and number of hydrogen bonds are not considered as the game changer in temperature variation (Table 3-9).

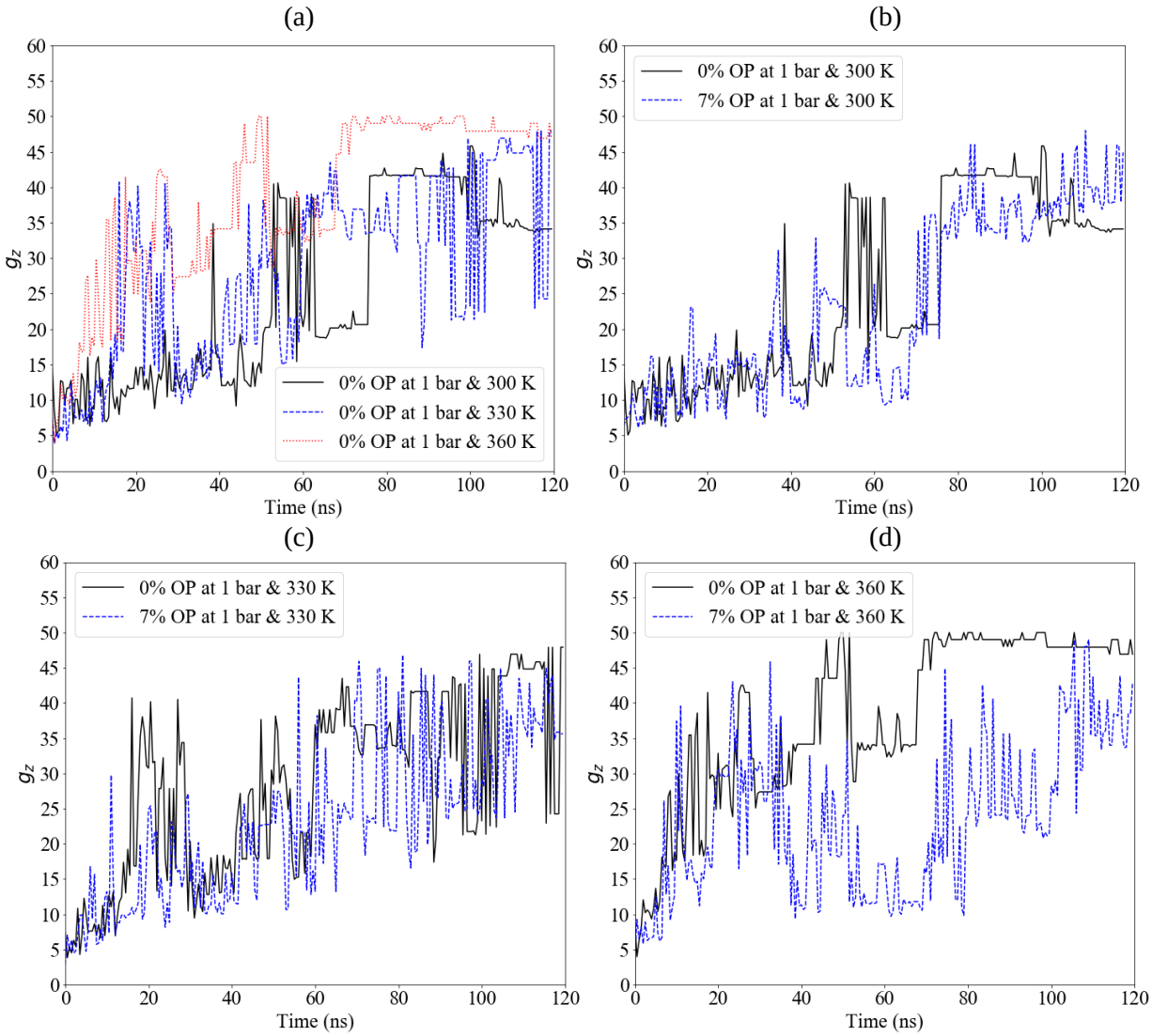

Figure 3-13. *z*-average aggregation number for (A1+A2)/OP/nC_7 system at 300–360 K and 1 bar with and without OP.

Table 3-8. Effect of temperature on average LJ and Coulomb energy in the last 20 ns of simulation runs for (A1+A2)/OP/nC_7 system in the absence and presence of 7 wt% inhibitor.

Temperature	Asphaltene system	Energy (kJ/mol)	No inhibitor			With inhibitor				
			A1-A1	A2-A2	A1-A2	A1-A1	A2-A2	A1-A2	A1-OP	A2-OP
330 K	A1+A2	LJ	-4047.5	-3053.2	-3991.4	-3584.6	-3551.2	-2129.3	-1691.9	-1285.3
		Coulomb	8712.4	-960.8	-76.9	8724.2	-1003.8	-29.8	-56.2	-521.7
		Sum*	4664.9	-4014	-4068.3	5139.6	-4555	-2159.1	-1748.1	-1807
360 K	A1+A2	LJ	-4470.6	-3341.5	-4781.9	-3861.3	-3633.2	-2561.4	-1327.1	-1070.5
		Coulomb	8727.0	-1046.3	-79.7	8710.5	-999.3	-40.5	-40.7	-344.2
		Sum*	4256.4	-4387.8	-4861.6	4849.2	-4632.5	-2601.9	-1367.8	-1414.7

* The summation of LJ and Coulomb energy contributions to intermolecular forces

Table 3-9. Average number of hydrogen bonds for (A1+A2)/OP/*n*C_7 case with and without 7 wt% inhibitor as a function of temperature.

Thermodynamics	Time span (ns)	No inhibitor	With inhibitor		
		A2-A2	A2-A2	A2-OP	OP-OP
1 bar & 330 K	0–50	1.2	1.4	15.8	11
	50–100	2.7	2.6	18.5	11.2
	100–120	1.5	2.6	19.8	2.6
1 bar & 360 K	0–50	3.2	1.2	10	6.2
	50–100	4.4	2.9	11	6.2
	100–120	5.3	3	13.3	6.5

Aggregate characteristics: Figure 3-14 depicts the properties of the asphaltene aggregates in the (A1+A2)/OP/*n*C_7 system with and without the inhibitor when temperature is increased, and pressure is fixed at 1 bar. Without OP, the gyration radius increases with increasing temperature, while the average aggregate density is not affected considerably by temperature. At 300 K and 330 K, the aggregate gyration radius has a unimodal distribution with a peak between 14 and 17 Å, while, at 360 K, it is bimodal with an additional peak at 28 Å. Nevertheless, the density distribution for all temperature levels is unimodal, with a peak that is located between 0.3 and 0.4 g/(mol.Å^3). This means that increasing temperature does not expand the aggregate's volume by increasing a void area; and the aggregates become relatively larger with mass incremental. Figure 3-14(c) and Figure 3-14(d) demonstrate that without the inhibitor, the aggregates are nearly spherical at 360 K. For the case of 7 wt% OP, the average gyration radius distribution confirms that the inhibitor penetrates into the asphaltene aggregates at 300 K and 330 K, while it breaks the aggregates at 360 K since the average gyration radius becomes unimodal with a peak at 15 Å at 360 K (Figure 3-14(a)). In the presence of inhibitor, the aggregates' shape at 360 K tends to be linear chain and prolate rather than spherical, as demonstrated in Figure 3-14(panels c and d). Therefore, the OP molecules either break or detach the asphaltene molecules surrounded the aggregates.

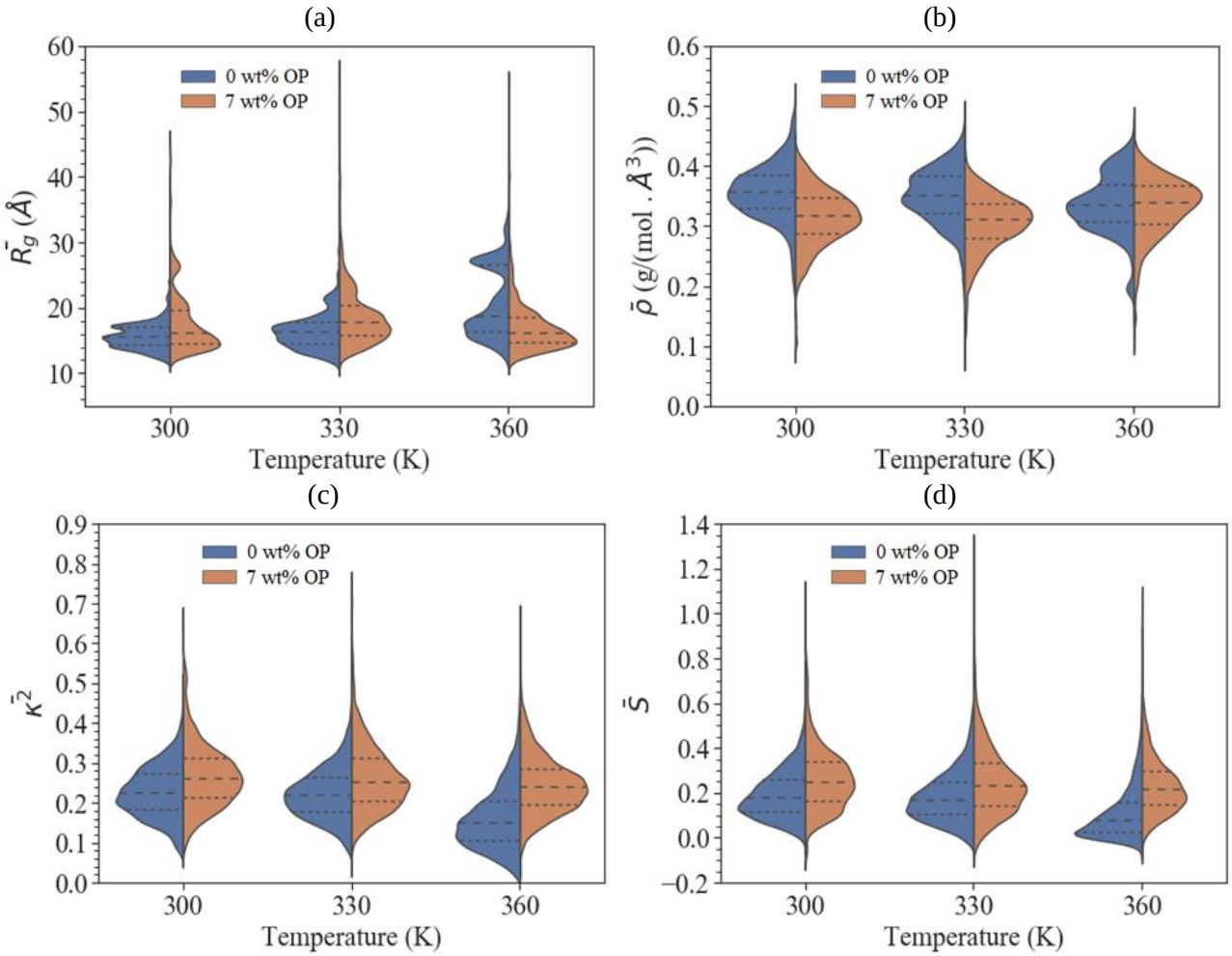

Figure 3-14. Influence of temperature on aggregate average (a) radius of gyration, (b) density, (c) relative shape anisotropy, and (d) shape factor for (A1+A2)/OP/nC$_7$ system.

3.4.4 Sensitivity analysis of hardware efficiency

The advanced MD simulation technique involves complex computation, which results in a very long run time. The common method to cope with this issue is coupling multiple CPUs to reduce the run time. Although the mentioned strategy is effective, the run time can still be relatively long, depending on the simulation length. Recently, the technology of GPU-Accelerated GROMACS has been introduced that can boost the calculation three-times when NVIDIA GPUs are coupled with CPUs compared with the case of CPU only. In this study, the run times of the sampling

simulation for 120 ns of the A2/*n*C_7 are compared for these two cases: when the only CPU is used and when both CPU and GPU are linked. In both cases, 40 CPU cores of Intel Gold 6148 Skylake @ 2.4 GHz are utilized; in case of having GPU, 4 NVidia V100SXM2 GPU is coupled with CPUs. The run time for the first case is 84.89 h with the 99.55% CPU efficiency and 842.90 MB memory usage, while the run time for the second case is reduced to 32.04 h with 99.37% CPU efficiency and 3.75 GB memory usage. Thus, the run time is reduced almost three times with similar CPU efficiency; however, the memory usage in the case of involving GPU is increased ~4 times because of parallel calculations. It can be concluded the incorporation of GPU in simulation reduces the run time significantly. As memory is not a limiting factor in this level of computation, using a few more gigabytes memory is worth saving time.

3.5 SUMMERY AND CONCLUSIONS

The asphaltene can be a stable part of the crude oil at initial thermodynamic conditions in a hydrocarbon reservoir. The oil production processes usually change the thermodynamic conditions and cause compositional changes, which trigger asphaltene precipitation and deposition. Surfactants are one of the potential types of inhibitors for asphaltene aggregation. The investigation of inhibitor concentration and thermodynamic conditions on asphaltene-inhibitor interactions in molecular level can provide valuable information to design efficient asphaltene inhibitors. In this paper, the molecular dynamics (MD) simulation is utilized to evaluate the impact of inhibitor (OP) concentration (0–15 wt%), temperature (300–360 K), and pressure (1–60 bar) on both archipelago (A1) and continental (A2) structures of asphaltenes.

The A1 does not aggregate vigorously when there is no OP, though the average aggregation number increases slightly after the addition of 3.5 wt% OP. However, the addition of 7 wt% OP significantly lowers the average aggregation number compared to the cases of 0 wt% and 3.5 wt%

OP; addition of more OP is considered useless since there is no more aggregation reduction. A2 has high polarizable aromatic core and hydrogen bond sites compared to A1, causing higher aggregation intensity when OP is absent. The low concentration of OP homogenizes the aggregates in terms of size and shape, implying that OP separates the loose asphaltenes from the side of aggregates. However, the high concentration of OP causes OP molecules to penetrate into asphaltene aggregates and break them. Nevertheless, due to the high potential of both asphaltene and OP to form hydrogen bonds, the aggregates can reform unstably with a very low density at the extremely high concentrations of OP (15 wt%). In the case of considering both archipelago and continental asphaltenes, the OP appears to be an effective inhibitor at a concentration higher than 7 wt%. Also, the results show that the 15 wt% of OP does not lead to reformation of the aggregates due to the existence of A1 in the system. Investigating the effect of thermodynamic conditions, we consider the variations in pressure and temperature for A1/A2/*n*C_7 system without and with 7 wt% of OP. In the absence of OP, increasing pressure and temperature, respectively, reduces and increases the asphaltene aggregation. The comparison of noncovalent energies between the cases with and without OP at various pressures reveals that the interaction energies between Asp-Asp and Asp-OP, respectively, drop and increase meaningfully at 30 bar. The reason is that, at 1 bar, the aggregates are very compact, and OP can not be fully efficient, while at 60 bar the aggregates are already unstable due to the favorable thermodynamic state. Therefore, OP exhibits a greater efficiency at 30 bar compared with other cases. The comparison of asphaltene aggregation between 300 and 360 K shows that the most effective temperature for OP to inhibit asphaltene aggregation is 360 K in which OP occupies the peripheral of asphaltene aggregates. Also, OP alters the aggregate shape to linear chain and prolate at 360 K, though the aggregate shape is extremely spherical when there is no OP in the system.

It is recommended to include different types of inhibitors such as polymer and ionic liquids with various functional groups in both inhibitor and asphaltene structures to disclose all possible inhibitory mechanisms. Also, it will be valuable to study the effect of inhibitors' mixture on asphaltene aggregation. We also recommend evaluating the OP efficiency in mitigating the asphaltene aggregation in contact with different types of rocks such as silica and calcite. This approach will make the simulation more practical, close to the real conditions. Also, it would be interesting to analyze the configurations of asphaltenes that approach and attach to each other in the presence of inhibitor, which has been conducted mostly without inhibitor and can be π-π stacking, π-π offset stacking, and T-shape stacking.

APPENDIX A

The total energy in OPLS-AA force-field is determined as follows [66]:

$$k = \left\{ \sum_{bond} \frac{1}{2} k_{ij} (r - r_0)^2 + \sum_{angle} \frac{1}{2} k_{ijk} (\theta - \theta_0)^2 + \sum_{dihedral} k_{ijkl} (1 + \cos(m\varphi - \delta)) \right\}_{\text{Intramolecular}} + \left\{ \sum_{LJ} 4\varepsilon_{ij} \left[\left(\frac{\sigma_{ij}}{r_{ij}} \right)^{12} - \left(\frac{\sigma_{ij}}{r_{ij}} \right)^{6} \right] + \sum_{Coulomb} \frac{q_i q_j}{4\pi\varepsilon_0} \frac{1}{r_{ij}} \right\}_{\text{Intermolecular}} \quad \text{(A-3.1)}$$

In Eq. (A-1), k represents the atomic potential energy; k_{ij}, k_{ijk}, and k_{ijkl} symbolize the force constants for bond, angle, and dihedral angle; r_0 is the initial bond length; θ_0 introduces the initial angle; mφ refers to the initial dihedral; the parameter δ is an adjustable parameter for phase degree of the dihedral potential; σ denotes the radial distance from a molecule at which the potential energy is equal to zero; r_{ij} stands for the distance of two separate charges; q indicates the charge of each atom; ε_0 resembles the permittivity of vacuum; and ε_{ij} signifies the potential well depth.

The z-average aggregation number (g_z) is defined as follows:

$$g_z = \frac{\sum_i n_i g_i^3}{\sum_i n_i g_i^2} \tag{A-3.2}$$

in which, the number of aggregates containing g_i monomers is denoted by n_i. It should be mentioned that i starts from 2, which implies that the smaller aggregates are dimers, and monomers are not considered as aggregates.

The definition for the radius of gyration (R_g) is given below:

$$R_g^2 = \frac{1}{N}\sum_{k=1}^{N}(r_k - r_{cm})^2 \tag{A-3.3}$$

In Eq. (A-3), r_k stands for the coordination of atom k; and r_{cm} refers to the coordination of the aggregate center of mass.

The following equation introduces the relative shape anisotropy (κ^2):

$$\kappa^2 = 1 - 3\frac{(\lambda_1\lambda_2 + \lambda_2\lambda_3 + \lambda_3\lambda_1)}{(\lambda_1 + \lambda_2 + \lambda_3)^2} \tag{A-3.4}$$

where κ^2 identifies the dimensionality and symmetry of the aggregates. κ^2 can vary from zero to one. Zero means the aggregate is a perfectly spherical chain, while one corresponds to the condition that the aggregate is a linear chain. λ_1, λ_2, and λ_3 are the principal moments of the gyration tensor.

The shape factor (S) is obtained as follows:

$$S = 27\frac{\prod_{i=1}^{3}(\lambda_i - \lambda)}{(\sum_{i=1}^{3}\lambda_i)^3} \tag{A-3.5}$$

S can be between -0.25 and 2. The aggregates are oblate shape if S<0; the aggregates appear in prolate shape if S>0; and the aggregates are spherical if S=0.

The aggregate density ($\rho_{aggregate}$) and aggregate volume ($V_{aggregate}$) can be calculated by the following equations:

$$\rho_{aggregate} = \frac{\sum_i m_i}{V_{aggregate}} \quad \text{(A-3.6)}$$

$$V_{aggregate} = \frac{4}{3}\pi\sqrt{5^3\lambda_1\lambda_2\lambda_3} \quad \text{(A-3.7)}$$

Here, m_i introduces the mass of every single atom of asphaltene molecules which are included in an aggregate.

CONFLICTS OF INTEREST

There are no conflicts to declare.

ACKNOWLEDGMENTS

The authors would like to thank Memorial University, InnovateNL, and the Natural Sciences and Engineering Research Council of Canada (NSERC) for the financial assistance of this research project.

REFERENCES

1. Mullins, O.C., The modified Yen model. Energy & Fuels, 2010. 24(4): p. 2179-2207.
2. Zendehboudi, S., et al., Asphaltene precipitation and deposition in oil reservoirs–Technical aspects, experimental and hybrid neural network predictive tools. Chemical Engineering Research and Design, 2014. 92(5): p. 857-875.
3. Allenson, S.J. and M.A. Walsh. A novel way to treat asphaltene deposition problems found in oil production. in International Symposium on Oilfield Chemistry. 1997. Society of Petroleum Engineers.

4. Schantz, S. and W. Stephenson. Asphaltene deposition: development and application of polymeric asphaltene dispersants. in SPE Annual Technical Conference and Exhibition. 1991. Society of Petroleum Engineers.
5. Ghamartale, A., et al., Asphaltene Deposition Control by Chemical Inhibitors: Theoretical and Practical Prospects. 2021: Elsevier Science.
6. Chang, C.-L. and H.S. Fogler, Stabilization of asphaltenes in aliphatic solvents using alkylbenzene-derived amphiphiles. 1. Effect of the chemical structure of amphiphiles on asphaltene stabilization. Langmuir, 1994. 10(6): p. 1749-1757.
7. Clarke, P.F. and B.B. Pruden, *Asphaltene precipitation from Cold Lake and Athabasca bitumens.* Petroleum science and technology, 1998. **16**(3-4): p. 287-305.
8. Ahmadi, M. and Z. Chen, Comprehensive molecular scale modeling of anionic surfactant-asphaltene interactions. Fuel, 2021. 288: p. 119729.
9. Bai, Y., et al., Effects of the N, O, and S heteroatoms on the adsorption and desorption of asphaltenes on silica surface: A molecular dynamics simulation. Fuel, 2019. 240: p. 252-261.
10. Fallah, F., et al., Molecular dynamics modeling and simulation of bituminous binder chemical aging due to variation of oxidation level and saturate-aromatic-resin-asphaltene fraction. Fuel, 2019. 237: p. 71-80.
11. Tazikeh, S., et al., Molecular dynamics simulation to investigate the effect of polythiophene-coated Fe3O4 nanoparticles on asphaltene precipitation. Chemical Engineering Science, 2021: p. 116417.

12. Qu, H., et al., Dissolution of polycyclic aromatic hydrocarbons in subcritical and supercritical water: A molecular dynamics simulation study. Chemical Engineering Science, 2019. 195: p. 958-967.
13. Sappidi, P., B.D. Rabideau, and C.H. Turner, Molecular simulation of the separation of toluene and p-xylene with the thermally-robust ionic liquid triphenyl-p-phenyl sulfonyl phenyl phosphonium. Chemical Engineering Science, 2020. 224: p. 115790.
14. Goual, L., et al., Asphaltene aggregation and impact of alkylphenols. Langmuir, 2014. 30(19): p. 5394-5403.
15. Sedghi, M. and L. Goual. Molecular dynamics simulations of asphaltene dispersion by limonene and PVAc polymer during CO 2 flooding. in SPE International Conference and Exhibition on Formation Damage Control. 2016. Society of Petroleum Engineers.
16. Lowry, E., M. Sedghi, and L. Goual, Novel dispersant for formation damage prevention in CO2: a molecular dynamics study. Energy & Fuels, 2016. 30(9): p. 7187-7195.
17. Lowry, E., M. Sedghi, and L. Goual, Polymers for asphaltene dispersion: Interaction mechanisms and molecular design considerations. Journal of Molecular Liquids, 2017. 230: p. 589-599.
18. Tirjoo, A., et al., Molecular dynamics simulations of asphaltene aggregation under different conditions. Journal of Petroleum Science and Engineering, 2019. 177: p. 392-402.
19. Pacheco-Sánchez, J., I. Zaragoza, and J. Martínez-Magadán, Asphaltene aggregation under vacuum at different temperatures by molecular dynamics. Energy & fuels, 2003. 17(5): p. 1346-1355.

20. Pacheco-Sánchez, J., I. Zaragoza, and J. Martínez-Magadán, Preliminary study of the effect of pressure on asphaltene disassociation by molecular dynamics. Petroleum science and technology, 2004. 22(7-8): p. 927-942.

21. Takanohashi, T., S. Sato, and R. Tanaka, Structural relaxation behaviors of three different asphaltenes using MD calculations. Petroleum science and technology, 2004. 22(7-8): p. 901-914.

22. Carauta, A.N., et al., Modeling solvent effects on asphaltene dimers. Energy & fuels, 2005. 19(4): p. 1245-1251.

23. Headen, T.F., E.S. Boek, and N.T. Skipper, Evidence for asphaltene nanoaggregation in toluene and heptane from molecular dynamics simulations. Energy & Fuels, 2009. 23(3): p. 1220-1229.

24. Fang, T., et al., Study on the asphaltene precipitation in CO2 flooding: a perspective from molecular dynamics simulation. Industrial & Engineering Chemistry Research, 2018. 57(3): p. 1071-1077.

25. Headen, T.F. and M.P. Hoepfner, Predicting Asphaltene Aggregate Structure from Molecular Dynamics Simulation: Comparison to Neutron Total Scattering Data. Energy & Fuels, 2019. 33(5): p. 3787-3795.

26. Mehana, M., M. Fahes, and L. Huang, Asphaltene Aggregation in Oil and Gas Mixtures: Insights from Molecular Simulation. Energy & Fuels, 2019. 33(6): p. 4721-4730.

27. Headen, T.F. and E.S. Boek, Molecular dynamics simulations of asphaltene aggregation in supercritical carbon dioxide with and without limonene. Energy & fuels, 2011. 25(2): p. 503-508.

28. Ghamartale, A., S. Zendehboudi, and N. Rezaei, New Molecular Insights into Aggregation of Pure and Mixed Asphaltenes in the Presence of n-Octylphenol Inhibitor. Energy & Fuels, 2020.

29. Yaseen, S. and G.A. Mansoori, Molecular dynamics studies of interaction between asphaltenes and solvents. Journal of Petroleum Science and Engineering, 2017. 156: p. 118-124.

30. Yaseen, S. and G.A. Mansoori, Asphaltene aggregation due to waterflooding (A molecular dynamics study). Journal of Petroleum Science and Engineering, 2018. 170: p. 177-183.

31. Yaseen, S. and G.A. Mansoori, Asphaltene aggregation onset during high-salinity waterflooding of reservoirs (a molecular dynamic study). Petroleum Science and Technology, 2018. 36(21): p. 1725-1732.

32. Khalaf, M.H. and G.A. Mansoori, Asphaltenes aggregation during petroleum reservoir air and nitrogen flooding. Journal of Petroleum Science and Engineering, 2019. 173: p. 1121-1129.

33. Zhang, W., et al., CO2-regulated octane flow in calcite nanopores from molecular perspectives. Fuel. 286: p. 119299.

34. Goual, L. and M. Sedghi, Role of ion-pair interactions on asphaltene stabilization by alkylbenzenesulfonic acids. Journal of colloid and interface science, 2015. 440: p. 23-31.

35. Silva, H.S., et al., Molecular dynamics study of nanoaggregation in asphaltene mixtures: Effects of the N, O, and S heteroatoms. Energy & Fuels, 2016. 30(7): p. 5656-5664.

36. Song, S., et al., Molecular Dynamics Study on Aggregating Behavior of Asphaltene and Resin in Emulsified Heavy Oil Droplets with Sodium Dodecyl Sulfate. Energy & fuels, 2018. 32(12): p. 12383-12393.

37. Sodero, A.C., et al., Investigation of the effect of sulfur heteroatom on asphaltene aggregation. Energy & Fuels, 2016. 30(6): p. 4758-4766.

38. Lv, G., et al., The properties of asphaltene at the oil-water interface: A molecular dynamics simulation. Colloids and Surfaces A: Physicochemical and Engineering Aspects, 2017. 515: p. 34-40.

39. Kuznicki, T., J.H. Masliyah, and S. Bhattacharjee, Molecular dynamics study of model molecules resembling asphaltene-like structures in aqueous organic solvent systems. Energy & Fuels, 2008. 22(4): p. 2379-2389.

40. Jian, C., et al., A molecular dynamics study of the effect of asphaltenes on toluene/water interfacial tension: surfactant or solute? Energy & fuels, 2018. 32(3): p. 3225-3231.

41. Jian, C., T. Tang, and S. Bhattacharjee, Probing the effect of side-chain length on the aggregation of a model asphaltene using molecular dynamics simulations. Energy & fuels, 2013. 27(4): p. 2057-2067.

42. Gao, F., et al., Molecular dynamics simulation: the behavior of asphaltene in crude oil and at the oil/water interface. Energy & fuels, 2014. 28(12): p. 7368-7376.

43. Headen, T., et al., Simulation of asphaltene aggregation through molecular dynamics: Insights and limitations. Energy & Fuels, 2017. 31(2): p. 1108-1125.

44. Headen, T.F. and E.S. Boek, Potential of mean force calculation from molecular dynamics simulation of asphaltene molecules on a calcite surface. Energy & fuels, 2011. 25(2): p. 499-502.

45. Sedghi, M., et al., Effect of asphaltene structure on association and aggregation using molecular dynamics. The Journal of Physical Chemistry B, 2013. 117(18): p. 5765-5776.

46. Khalaf, M.H. and G.A. Mansoori, A new insight into asphaltenes aggregation onset at molecular level in crude oil (an MD simulation study). Journal of Petroleum Science and Engineering, 2018. 162: p. 244-250.

47. Mikami, Y., et al., Molecular dynamics simulations of asphaltenes at the oil–water interface: from nanoaggregation to thin-film formation. Energy & Fuels, 2013. 27(4): p. 1838-1845.

48. Mohammed, S. and G. Gadikota, The role of calcite and silica interfaces on the aggregation and transport of asphaltenes in confinement. Journal of Molecular Liquids, 2019. 274: p. 792-800.

49. Mohammed, S. and G. Gadikota, The influence of CO2 on the structure of confined asphaltenes in calcite nanopores. Fuel, 2019. 236: p. 769-777.

50. Mohammed, S. and G.A. Mansoori, Effect of CO2 on the interfacial and transport properties of water/binary and asphaltenic oils: insights from molecular dynamics. Energy & fuels, 2018. 32(4): p. 5409-5417.

51. Mohammed, S. and G.A. Mansoori, Molecular insights on the interfacial and transport properties of supercritical CO2/brine/crude oil ternary system. Journal of Molecular Liquids, 2018. 263: p. 268-273.

52. Fu, C.-F. and S.X. Tian, A comparative study for molecular dynamics simulations of liquid benzene. Journal of chemical theory and computation, 2011. 7(7): p. 2240-2252.

53. Lindahl, Abraham, Hess, & Spoel, V. D. , GROMACS 2019.3 Source code. 2019.

54. Abraham, M.J., et al., GROMACS: High performance molecular simulations through multi-level parallelism from laptops to supercomputers. SoftwareX, 2015. 1: p. 19-25.

55. Hanwell, M.D., et al., Avogadro: an advanced semantic chemical editor, visualization, and analysis platform. Journal of cheminformatics, 2012. 4(1): p. 17.

56. Ribeiro, A.A., B.A. Horta, and R.B.d. Alencastro, MKTOP: a program for automatic construction of molecular topologies. Journal of the Brazilian Chemical Society, 2008. 19(7): p. 1433-1435.

57. Bussi, G., D. Donadio, and M. Parrinello, Canonical sampling through velocity rescaling. The Journal of chemical physics, 2007. 126(1): p. 014101.

58. Berendsen, H.J., et al., Molecular dynamics with coupling to an external bath. The Journal of chemical physics, 1984. 81(8): p. 3684-3690.

59. Nosé, S., A molecular dynamics method for simulations in the canonical ensemble. Molecular physics, 1984. 52(2): p. 255-268.

60. Hoover, W.G., Canonical dynamics: Equilibrium phase-space distributions. Physical review A, 1985. 31(3): p. 1695.

61. Parrinello, M. and A. Rahman, Strain fluctuations and elastic constants. The Journal of Chemical Physics, 1982. 76(5): p. 2662-2666.

62. Tipler, P.A. and G. Mosca, Physics for scientists and engineers. 2007: Macmillan.

63. Desiraju, G.R. and T. Steiner, The weak hydrogen bond: in structural chemistry and biology. Vol. 9. 2001: International Union of Crystal.

64. Danesh, A., PVT and phase behaviour of petroleum reservoir fluids. 1998: Elsevier.

65. Karan, K., et al., Evaluation of asphaltene instability and a chemical control during production of live oils. Petroleum science and technology, 2003. 21(3-4): p. 629-645.

66. Allen, M.P., Introduction to molecular dynamics simulation. Computational soft matter: from synthetic polymers to proteins, 2004. 23(1): p. 1-28.

4. CHAPTER FOUR

Impact of Chemical Inhibitors on Asphaltene Binding Arrangement: Molecular Dynamics Simulation Strategy

Preface

A version of this manuscript is in the review process to be submitted to a reputable journal. Ali Ghamartale is the first author of this manuscript. Along with the insights from co-authors (Rezaei, N. and Zendehboudi, S.), the first author designed the simulation and the manuscript structures. The literature review, concept development, model execution, and results evaluation/comparison were conducted by the first author. The first author prepared the first draft of the manuscript and applied the comments from the co-authors. Both co-authors (Rezaei, N. and Zendehboudi, S.) had the supervision role and edited the manuscript.

ABSTRACT

Asphaltene deposition is one of the challenging issues in petroleum production and transportation. Chemical inhibitors are commonly employed to postpone the asphaltene aggregation, which is the primary stage of asphaltene deposition. Design and introduction of an effective chemical inhibitor have always been a challenge for the industry, considering substantial variations in characteristics and structures of asphaltene and petroleum. The binding arrangement of asphaltene is a factor of bond strength and stability, which depends on asphaltene structure. This feature alters in the presence of chemical inhibitors. In this work, molecular dynamics (MD) simulation is employed as a cost-effective and accurate method to study the binding arrangement of two continental asphaltene structures in the presence of chemical inhibitors. The chemical inhibitors are Octylphenol (OP), 1-Butyl-3-methylimidazolium bromide ([BMIM][Br]), and 1-Butyl-3-methylimidazolium chloride ([BMIM][Cl]). OP cannot stop the quadrupole-quadrupole interaction between the asphaltenes since the force between OP's benzene ring and asphaltene polyaromatic core is weaker than the force between two polyaromatic cores. Nevertheless, OP forms a hydrogen bond with the asphaltene and prevents asphaltene molecules from approaching each other by providing steric hindrance around the molecules. As a result, OP does not show a promising potential to reduce the parallel stacking especially for the asphaltene with no hydrogen bond potential, while it reduces the T-shape arrangement relatively for both asphaltene structures. The ionic liquids (ILs) beat the quadrupole-quadrupole interaction between the asphaltene cores with cation-quadrupole force and notably reduce the parallel stacking. They also lower the number of T-shape binding arrangement between the asphaltene molecules. The shape and binding arrangement of polyaromatic compounds (such as asphaltene) are not only important in the petroleum industry, but these features also play a crucial role in designing optical and electronic

nanodevices. The introduced approach is a new pathway to improve the design of chemical inhibitors that affects the aggregation arrangement of polyaromatic compounds.

Keywords: Continental asphaltene; Chemical inhibitor; Ionic liquids; Binding interaction; Molecular dynamics simulation.

4.1 INTRODUCTION

Resins initially stabilize the asphaltene molecules in crude oils; however, changes in the thermodynamic conditions can destabilize the asphaltenes, resulting in asphaltene aggregation. The aggregate formation disrupts oil production and transport by changing the fluid properties such as solubility, density, and viscosity [1]. Commonly, chemical inhibitors are added to the crude oil to improve the asphaltene suspension stability and to avoid asphaltene aggregation [2, 3]. Chemical inhibitors have been utilized in the oil industry for decades; however, design and synthesis of an efficient inhibitor for a target crude oil have always been challenging. Self- and cross-association energies between the asphaltene and inhibitor molecules are critical in designing of an inhibitor for a given crude oil composition and reservoir conditions. Although the π-π stacking is considered one of the main mechanisms for asphaltene binding [4], other driving forces and mechanisms are also hypothesized for the asphaltene binding for different asphaltene chemical structures and crude oil compositions [5, 6]. Due to the presence of various functional groups in the asphaltene structure, combination of van der Waals, Coulombic, exchange-repulsion interactions, and induction forces (such as hydrogen bond and π-π stacking) is responsible for the asphaltene binding behavior [1, 7]. Adequate understanding of the asphaltene binding with itself and with the inhibitor molecules is imperative for the design of chemical inhibitors for prevention

of asphaltene aggregation. Chemical inhibitors usually bind to the asphaltene molecules, providing steric hindrance and disrupting the asphaltene self-interaction [8].

The asphaltene binding arrangement is a quantitative measure of the aggregate formation potential [9]; it depends on the number of aromatic rings in the polyaromatic core [4], the type and number of functional groups [10], the type, number, and location of heteroatoms [4, 11], and the length, number, and location of alkyl chains [6]. For instance, asphaltenes with a larger aromatic core, or with nitrogen atoms in their aromatic core, have a higher self-aggregation tendency [4], while the presence of sulfur atoms in the asphaltene aromatic core reduces the asphaltene self-aggregation [11]. There are three main arrangements proposed for the asphaltene aggregation: face-to-face (also called parallel stacked or π-π stacked), offset stacked (offset parallel stacked, offset π-stacked, or parallel displaced), and T-shape (π-σ stacked, perpendicular stacked, or edge-on stacked) [12-14]. The number of aromatic rings in the asphaltene polyaromatic core plays a major role in the asphaltene binding arrangement [6]. For instance, molecules with a single aromatic ring, such as benzene, form T-shape bonding to minimize the repulsion force [15, 16]. In contrast, molecules with multiple aromatic rings such as asphaltenes prefer parallel arrangements [12, 17-19], including the face-to-face [17] and offset stacked [12, 18, 20]. Arrangements different than the parallel types are packed much looser and have an irregular outward form, which greatly impacts the final aggregate shape [21].

Molecular dynamics (MD) simulation has been used to understand the asphaltene binding arrangements and to analyze the influence of various parameters, including: aromatic core size [4], functional groups [22], heteroatoms position [11], side chain (lengths and number) [4, 6, 23], solvent properties [24-26], and thermodynamic conditions [12, 19]. In the previous studies, the asphaltene behavior was investigated both in the bulk medium [1, 4, 6, 10, 11, 19, 23, 24, 27] and

the water-oil interface [10, 22, 28-32]. In the following, we review the studies that used MD to analyze the asphaltene binding arrangements. Zhang and Greenfield [19] were the first researchers to investigate the angle between asphaltene molecules as a measure of the asphaltene binding arrangement for two different asphaltene structures. They used an asphaltene structure with long side chains and a small aromatic core, and another asphaltene structure with short side chains and a large aromatic structure. The asphaltene with a small aromatic core formed mostly parallel and perpendicular aggregation arrangements at high and low temperatures, respectively. In contrast, the asphaltene with the large aromatic core favored the parallel arrangement at low temperatures and perpendicular arrangement at high temperatures [19]. Sedghi et al. [4] adopted different asphaltene structures and studied the asphaltene arrangements in the dimerization process. They considered the potential mean force versus binary distances between asphaltene molecules to analyze the binding arrangements. Potential mean force curves showed a drop at 0.5 nm for all asphaltene structures, which represented the offset parallel stacking. The T-shape dimerization arrangement was explained by observing a minimum at 0.7–0.8 nm in the potential mean force curves for various asphaltene structures, although the minimum vanished for asphaltene structures with side chains. Jian et al. [6] used the minimum distance and angle between asphaltenes to study the effect of side-chain size on the aggregation mechanisms in water. The Violanthrone-78 asphaltene with 16, 12, 8 and 4 carbons alkyl side chains were tested. The asphaltene with the side chain length of 4- and 16-carbon had a similar aggregation severity and trend but through different mechanisms. They claimed that the polyaromatic core stacking is the dominant aggregation mechanism for the asphaltene with a short side chain. However, the alkyl side chains interacted with themselves for the asphaltene structure having a long side chain, and resulted in a similar aggregation rate. The T-shape arrangement was observed at equilibrium stage; the aggregates were

rod-like [6]. Jian and Tang [24] studied the importance of asphaltene medium properties on asphaltene aggregate shape and arrangement by considering water, toluene, and *n*-heptane as the bulk fluid. In water, polyaromatic compounds minimized the contact with water, and the aggregates were spherical. Using *n*-heptane, its molecules interacted with the asphaltene side chains and minimized the interactions between the polyaromatic cores and side chains. Therefore, parallel stacking was considered as the dominant aggregation mechanism and led to large rod-shape aggregates. Using toluene, the parallel stacking was also dominant; however, the aggregates were smaller than those in *n*-heptane [24]. The importance of bulk fluid was also noted by Takanohashi et al. [33, 34], who studied the dissociation of asphaltene aggregates in benzene, methanol, and pyridine. Pyridine was the only fluid that could dissociate the asphaltene aggregates because it could form both hydrogen bonds and parallel stacking. Gao et al. [10] compared the aggregation arrangements for an asphaltene structure with an anionic asphaltene structure in crude oil through an MD simulation. The neutral asphaltene was more prone to form face-to-face aggregates, while the anionic asphaltene had both face-to-face and T-shape arrangements. They also confirmed the argument by the quantum mechanics simulation. Sodero et al. [11] used the minimum distance and the angle between the asphaltene molecules to probe the effect of heteroatom location on asphaltene aggregation. They found parallel stacking to be the main aggregation force; the location of heteroatoms affected the strength of the binding interaction. For instance, the presence of sulfur atoms in an asphaltene core reduced the asphaltene parallel stacking, while the presence of a sulfur atom in the asphaltene alkyl branch enhanced the aggregate stability due to interaction with carboxylic group [11]. Wang et al. [23] studied the effect of length and number of side chains on the most plausible aggregation arrangement for continental asphaltenes with 5 to 8 aromatic rings in a vacuum environment. They concluded that the

asphaltene chemical structures with short or no side branches prefer face-to-face stacking as the dominant aggregation arrangement, while the long side branch leads to a mixture of parallel stacking and T-shape arrangements. Teklebrhan et al. [1] used a similar analysis and studied the asphaltene aggregation when naphthenic acid was incorporated in the asphaltene-toluene mixture. The naphthenic acid restricted the formation of hydrogen bonding between the asphaltenes and forced asphaltenes to form longer parallel stacking. The shorter naphthenic acid was more impactful than the longer ones in restricting the asphaltene self-aggregation through hydrogen bonds [1].

Despite the strong desire to develop (and introduce) a reliable inhibitor, there is no systematic research to study the asphaltene binding arrangement with an asphaltene inhibitor and to elaborate on the asphaltene aggregation mechanisms and asphaltene-inhibitor interactions. Lack of molecular knowledge on the binding arrangements and intermolecular network formation between the asphaltenes and inhibitors limits the design and preparation of chemical inhibitors. In this study, we use the radial distribution function, the aggregate shape index, the angle and distance between the molecules to explore the asphaltene binding arrangement manipulation in the presence of different inhibitors. We also improve the criteria to distinguish various types of asphaltene binding arrangements. To achieve these objectives, two different continental-type asphaltene structures with and without functional groups (in their chemical structures) in the presence of three different inhibitors are considered. The inhibitors include a surfactant, *n*-octylphenol (OP), and two ionic liquids (ILs), 1-butyl-3-methylimidazolium bromide ([BMIM][Br]), and 1-butyl-3-methylimidazolium chloride ([BMIM][Cl]). We also use *n*-heptane as a precipitant.

The paper is structured as follows: after the introduction, the methodology and the analysis methods are elaborated in detail in section 4.2. In section 4.3, the reliability of simulation runs is

verified, and the results are discussed. The last part is dedicated to concluding remarks. The highlighted results of this paper help to further understand the molecular interaction between asphaltene and asphaltene-inhibitor, and provide valuable guidance for future inhibitor design.

4.2 METHODOLOGY

4.2.1 SIMULATION AND MODELING FRAMEWORK

Molecular scale simulation is divided into three main categories: molecular mechanics, quantum mechanics, and molecular dynamics (MD). Among them, MD considers the parameter dynamically, while the other two methods have no time dimension. Molecular mechanics and quantum mechanics are accompanied by complex and demanding computation, limiting the number of atoms in the system and necessitating large CPU/GPU resources. The other differences are that the covalent bonds are fixed, and the molecule structures do not change in the MD simulation, while the covalent bonds can break and form in the two other methods. MD is a beneficial tool in chemistry, biochemical, and drug discovery research to probe mechanisms. MD applications have been recently expanded into engineering and petroleum research with a mechanistic approach. In this study, we employ MD method using the GROMACS software [35, 36]. Based on our previous experiences, we use OPLS-AA force-field due to its accuracy in calculating thermodynamic properties of hydrocarbons such as benzene [37].

There is a debate whether the continental or archipelago structures are the most dominant representatives of asphaltenes. Mikami et al. [28] simulated three types of asphaltenes: the continental, archipelago, and resin types. They compared properties of the oil generated from the simulation with experiments and theoretical studies, and confirmed that the continental type has the best match. In 2017, Wang et al. [23] summarized experimental studies and recommended the continental asphaltene structure as the main and dominant structure for asphaltenes. Also,

Ghamartale et al. [38] studied the aggregation of an archipelago asphaltene with and without inhibitor in *n*-heptane as a precipitant; they did not observe a severe aggregation for the archipelago-type asphaltene even in the absence of inhibitors. Therefore, we consider two continental asphaltene structures that were used in our previous study [38], as shown in Figure 4-1 (a)-(b), to study the potential effect of hydrogen bond in the presence of chemical inhibitors. The chemical inhibitors include octylphenol (OP), 1-butyl-3-methylimidazolium bromide ([BMIM][Br]), and 1-butyl-3-methylimidazolium chloride ([BMIM][Cl]), as depicted in Figure 4-1(c). The structures are built with Avogadro software [39] and optimized with Gaussian09 software, using 6-31g(d,p) basis set.

Four boxes of *n*-heptane are made for each asphaltene type. 50 asphaltene molecules (with 7 wt % concentration) are distributed in each *n*-heptane box. One box is simulated with no additives as a control system, while in each of the three other boxes, 7 wt% of one inhibitor is added. The number of the inhibitor molecules is 177 for OP, 167 for [BMIM][Br], and 209 for [BMIM][Cl] [38].

The simulation algorithm involves four steps. The first step includes the minimization of system energy by avoiding the molecules' overlapping or very close positioning between the atoms in the initial configuration. The steepest descent method is applied for energy minimization. In the following, the system temperature adjusts to 300 K by running the NVT simulation for 100 ps. The velocity rescaling thermostat is considered for the NVT simulation. In the third step, the pressure adjusts to 1 bar at the adjusted temperature by running the NPT simulation for 1 ns. The velocity rescaling thermostat and the Berendsen barostat are considered for the NPT simulation. The last step is data sampling at the target temperature and pressure (300 K and 1 bar, respectively), by running the simulation for 120 ns. The Nose-Hoover thermostat [40, 41] and the Parrinello−Rahman barostat [42] are employed for the data sampling. In the sampling step, the

positions of molecules are recorded every 10 ps and used in the post-analysis. More details about the simulation settings and steps can be found in our previous work [38].

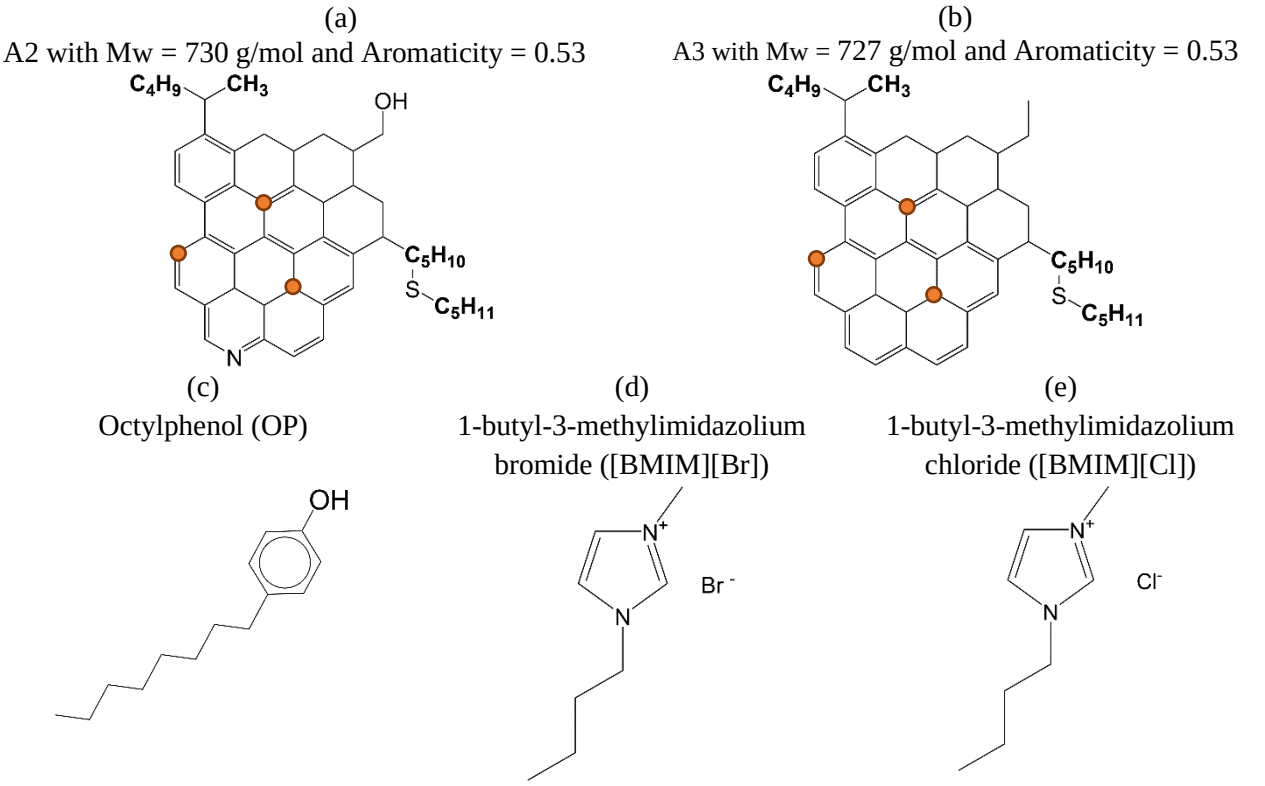

Figure 4-1. The chemical structures of: (a) A2 continental-type asphaltene with the potential to form hydrogen bonds; (b) A3 continental-type asphaltene with no potential to form hydrogen bonds; (c) surfactant inhibitor: octylphenol (OP); (d) ionic liquid inhibitor: 1-butyl-3-methylimidazolium bromide ([BMIM][Br]); (e) ionic liquid inhibitor: 1-butyl-3-methylimidazolium chloride ([BMIM][Cl]). Orange filled circles in panels (a) and (b) show the selected atoms to describe polyaromatic plane in the analysis.

4.2.2 ANALYSIS METHODS

Radial distribution function (RDF): The RDF or *g(r)* shows the probability of observing two types of molecules within a distance over the adjusted period. This function identifies the intensity of molecules' binary interactions. In this study, RDF is calculated between the centre-of-mass (COM) for asphaltene molecules in the last 60 ns of the simulation using the trajectory file. This analysis is conducted with a built-in tool in GROMACS, *gmx rdf*.

Aggregate Shape: As a result of the asphaltene non-covalence bond, the asphaltene aggregates have various shapes during the simulation; the asphericity index is employed to analyze the aggregate shapes in this study. The asphericity index varies between zero and one. The asphericity index of zero represents a spherical shape; as the index approaches one, the aggregates become rod-like [38]. In this study, the average asphericity index for the aggregates in each frame is determined, and its probability density is plotted in the adjusted period. MDAnalysis package in Python is employed to conduct this analysis. The aggregate shape is compared in the last 60 ns of the simulation in this study.

Angle-distance analysis: Commonly, asphaltene pairs with a distance less than 0.5 nm are classified as the face-to-face stacked in the literature; those with a distance between 0.5 to 0.75 nm are considered as the offset stacked; and the ones with a larger distance up to 1.5 nm are considered as the T-shape [6, 10, 30, 32, 43]. However, Jian and Tang [24] showed that the asphaltenes could form a parallel arrangement at a pair distance of 0.45, 0.75, 1.1, and 1.5 nm, which was also confirmed by Teklebrhan el al. [1]. Therefore, classifying the asphaltene aggregate mechanisms solely based on the pair distance is inconclusive. For an accurate analysis, both angle and distance criteria should be considered in such a classification. In this study, the distance between the COM of asphaltene molecules is measured using *gmx distance*, a built-in tool in GROMACS. The angle between two asphaltenes' polyaromatic cores is calculated using *gmx gangle* by measuring the angle between the polyaromatic planes. The aromatic plane is defined by considering a plane, which connects three carbon atoms in the asphaltene core. The carbon atoms in each structure are shown by orange dots in Figure 4-1 (a)-(b). The angle between two planes is measured by the angle between the normal vectors to the planes. In Figure 4-2 (a), two planes are shown with grey diamonds. If the normal of planes are concurrent (n_1 and n_2), the θ-angle is between 0 and 90

degrees; if they are countercurrent (n_1 and n_2'), the θ-angle is in the range of 90 - 180 degrees (Figure 4-2 (b)). In this study, the θ-angle is assigned to distinguish the T-shape arrangement from the face-to-face and offset stacking. For the angle $60 < \theta < 120$ degrees, the T-shape arrangement is considered for asphaltene binding, while for $\theta < 30$ or $\theta > 150$, the parallel stacked (either face-to-face or offset stacked) arrangement is considered. To differentiate between the face-to-face and offset arrangements, we employ α-angle between a vector which connects the center of two planes, $\overrightarrow{AB}$, and the resultant vector of plane normals ($\vec{R}$), as depicted in Figure 4-2 (c). The $\vec{R}$ is either the summation of normal vectors ($0 < \theta < 30$) or subtraction of them ($150 < \theta < 180$). Different types of parallel stacked arrangements can be distinguished through α-angle*;* if the α-angle is less than 45 degrees, the plane arrangement is considered face-to-face, and if the deviation is larger than 45 degrees, the arrangement is considered offset stacked. Figure 4-3 exhibits two scenarios in which the θ-angle is lower than 30 degrees, and the α-angle is either less than 45 degrees (Figure 4-3, left) or more than 45 degrees (Figure 4-3, right). In Figure 4-3, the black dash line is $\overrightarrow{AB}$ and the red arrow is $\vec{R}$.

In this study, the angle and distance criteria are used, and three types of the analysis are conducted. One analysis presents the probability density function versus angle. This plot shows the probability of the θ-angles regardless of the distance between the molecules for the selected period (the last 60 ns of simulation in this study). The second plot illustrates the number of each intermolecular contact along the simulation time for a certain range of distances (less than 1.2 nm in this study). The last plot demonstrates the cumulative number of intermolecular contacts between molecules versus the simulation time in different ranges of molecule distance.

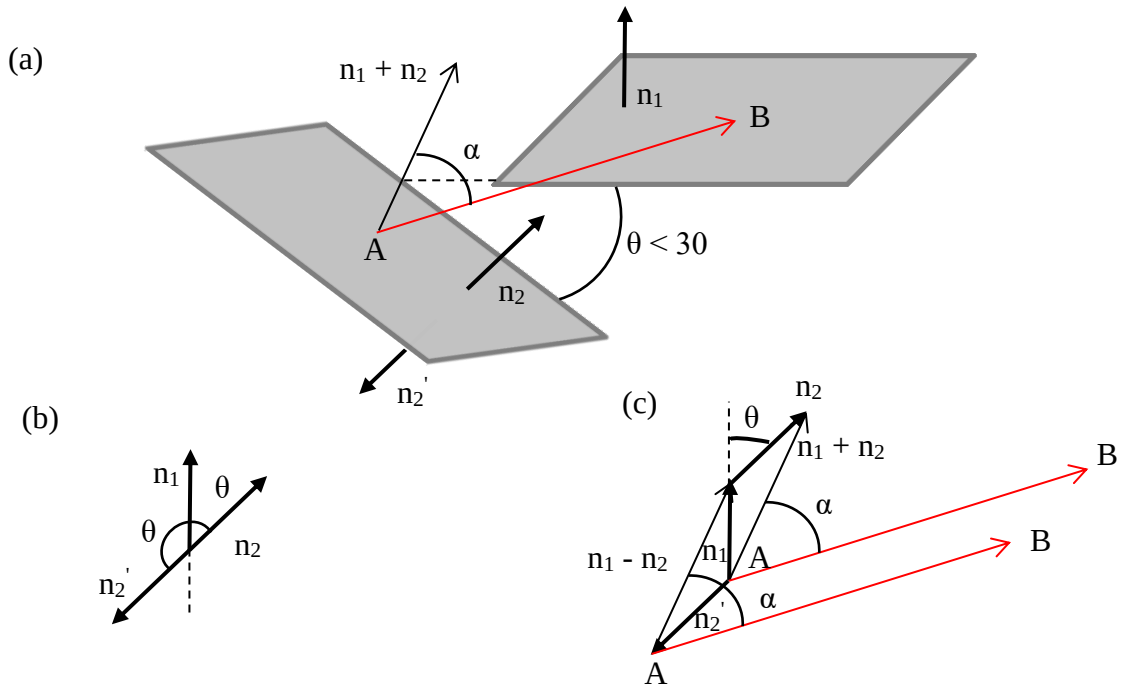

Figure 4-2. The angle between two planes: (a) the θ- and α-angle between two planes with normal of n_1 and n_2, (b) the θ-angle for co-current and counter-current planes' normal, and (c) the α-angle for both cases of having plane with co-current and counter-current normals.

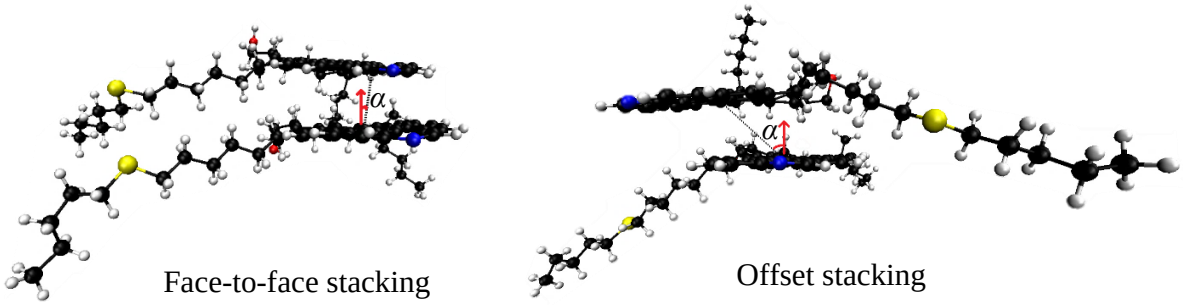

Figure 4-3. Example of asphaltene arrangements for parallel stacking and offset stacking.

4.3 RESULTS AND DISCUSSION

4.3.1 Repeatability of MD Tests

In both experimental and simulation studies, it is important to have reliable and accurate results. Repeatability is a key step toward reliability. Therefore, we repeat the simulation system of A3/*n*-

heptane and compare the aggregate shape characteristics. Figure 4-4 shows the probability distribution of the average aggregate asphericity index for three simulation sets in the last 60 ns. Data set 2 shows a lower probability at the peak than data set 1, while data set 3 indicates the highest probability at the peak, showing a more uniform shape. This variation in the *y*-direction is because of the random distribution of asphaltene molecules in the box and the molecules' freedom to move in any direction based on the imposed forces from other molecules. Nevertheless, all three sets are unimodal, with a peak at 0.15–0.18. The similar aggregate shape distribution for three simulations means that regardless of random molecule distribution and movement freedom, the molecule's position and trajectory (the main output of simulations) are similar for three simulations. Thus, the consistency in the output of replicated MD simulations makes the study's conclusion more valuable and trustworthy. The statistical analysis also proves the high similarity between the three simulations as the averages of asphericity for simulation runs 1–3 are 0.189 ± 0.052, 0.209 ± 0.068, and 0.174 ± 0.044.

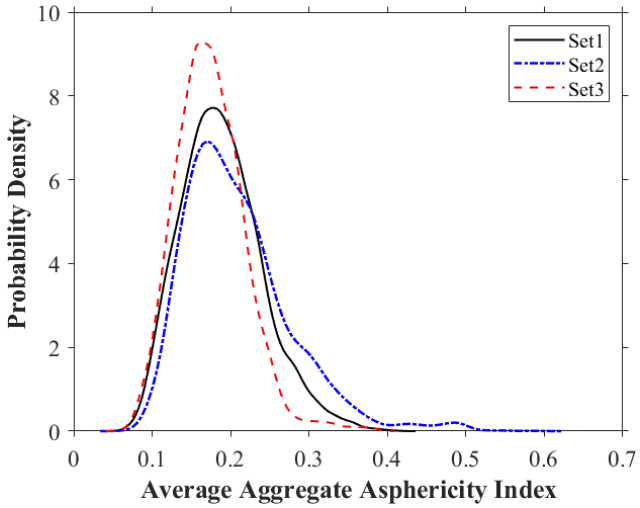

Figure 4-4. The replication of A3/*n*-heptane simulation, shown by analyzing the aggregate shape in the last 60 ns of the simulations.

4.3.2 Asphaltene Aggregate Shape in the Presence of Different Inhibitors

This section discusses the asphaltene aggregation shape for four asphaltene systems with and without inhibitors. In the first system, the 7 wt% of asphaltene is randomly distributed in *n*-heptane, without any inhibitor. In the other three systems, 7 wt% of one inhibitor type, either OP, [BMIM][Br] or [BMIM][Cl], is distributed in the system in addition to the asphaltene/*n*-heptane. We use RDF, angular probability density, and aggregate shape index analyses to study the asphaltene aggregation behavior. In the first two analyses, the arrangements of every asphaltene pair molecules are analyzed, using their distance and angle, respectively. The third analysis is based on the aggregate shape, which varies from zero (spherical) to one (rod-like).

Figure 4-5 shows the RDF, θ-angle probability density, and the aggregate shape index for A2 asphaltene in the last 60 ns of the simulation. A close look at Figure 4-5 (a) reveals that the OP is not able to manipulate the asphaltene interaction within a short distance, whereas [BMIM][Cl] and [BMIM][Br] strongly decrease the *g(r)* peak at 0.5 nm, which is known as a sign of face-to-face arrangement. The [BMIM][Cl] decreases *g(r)* peak between 1 and 1.2 nm substantially, which is a sign of the T-shape arrangement. Therefore, based on the RDF plot, all three inhibitors reduce the asphaltene aggregation for pairs of asphaltenes such that the ILs of [BMIM][Cl] and [BMIM][Br] lower both the parallel and T-shape stacking for A2, while OP is more impactful at long distance interactions. Figure 4-5 (b) shows the θ-angle probability density between the polyaromatic cores of the asphaltene pairs regardless of their distances with and without the inhibitors. The presence of inhibitor decreases the probability of the asphaltene pairs with angles ranging from 60 to 120 degrees, which is a sign of T-shape arrangement. According to Figure 4-5, OP and [BMIM][Cl] have a similar impact on the asphaltene aggregation, which agrees with the RDF results (Figure 4-5 (a)). Based on Figure 4-5 (c), the probability of the aggregate shape index

shifts toward higher values (more rod-shape) with significantly more differences in the distribution in the presence of inhibitors. This implies that the inhibitors make the aggregates more rod-like shape compared to the inhibitor-free case, in which the aggregates are more spherical and single modal. In addition, the changes regarding OP and [BMIM][Cl] are similar and in agreement with the angle distribution function (Figure 4-5 (b)), while [BMIM][Br] drastically alters the aggregate asphericity, which is in match with the RDF graph (Figure 4-5 (a)). The RDF analysis does not include angles, and the distance is not considered in angle distribution analysis; hence, it is challenging to elaborate the binding arrangement and connect the binding arrangement to the aggregate shape. For example, the ILs reduce the face-to-face stacking based on the RDF analysis, which only considers the parallel arrangements and within short distances. However, the parallel arrangement does not change appreciably based on the angle distribution density, which implies the long-distance parallel arrangement is increased, such as sandwiching one molecule between two parallel molecules. Moreover, the angle distribution density does not distinguish between the face-to-face and offset stacked, and considers both as parallel stacking. Therefore, it is necessary to incorporate distance and angle factors to classify binding arrangements and study the inhibitor impact on them.

Figure 4-6 shows the binary arrangements and the asphericity index for A3 in the last 60 ns of the simulation in both cases: without inhibitor and with three different inhibitors. Based on Figure 4-6(a), the addition of OP does not because the significant changes to the RDF graph, while [BMIM][Cl] and [BMIM][Br], respectively, reduce the intensity of *g(r)* peak at 0.5 nm, which means less face-to-face stacking occurs. Figure 4-6(b) confirms the reduction of parallel stacking with ILs (as the inhibitors) because the probability of θ-angle between 0 - 30 degrees and 150 - 180 degrees is less than the case of asphaltene without the inhibitors. It is noted that the addition

of [BMIM][Br] and OP increases and decreases the probability of θ-angles between 60 and 120, respectively. These behaviors can dictate the aggregate shape to become more spherical in the presence of [BMIM][Br] and more rod-like in the presence of OP.

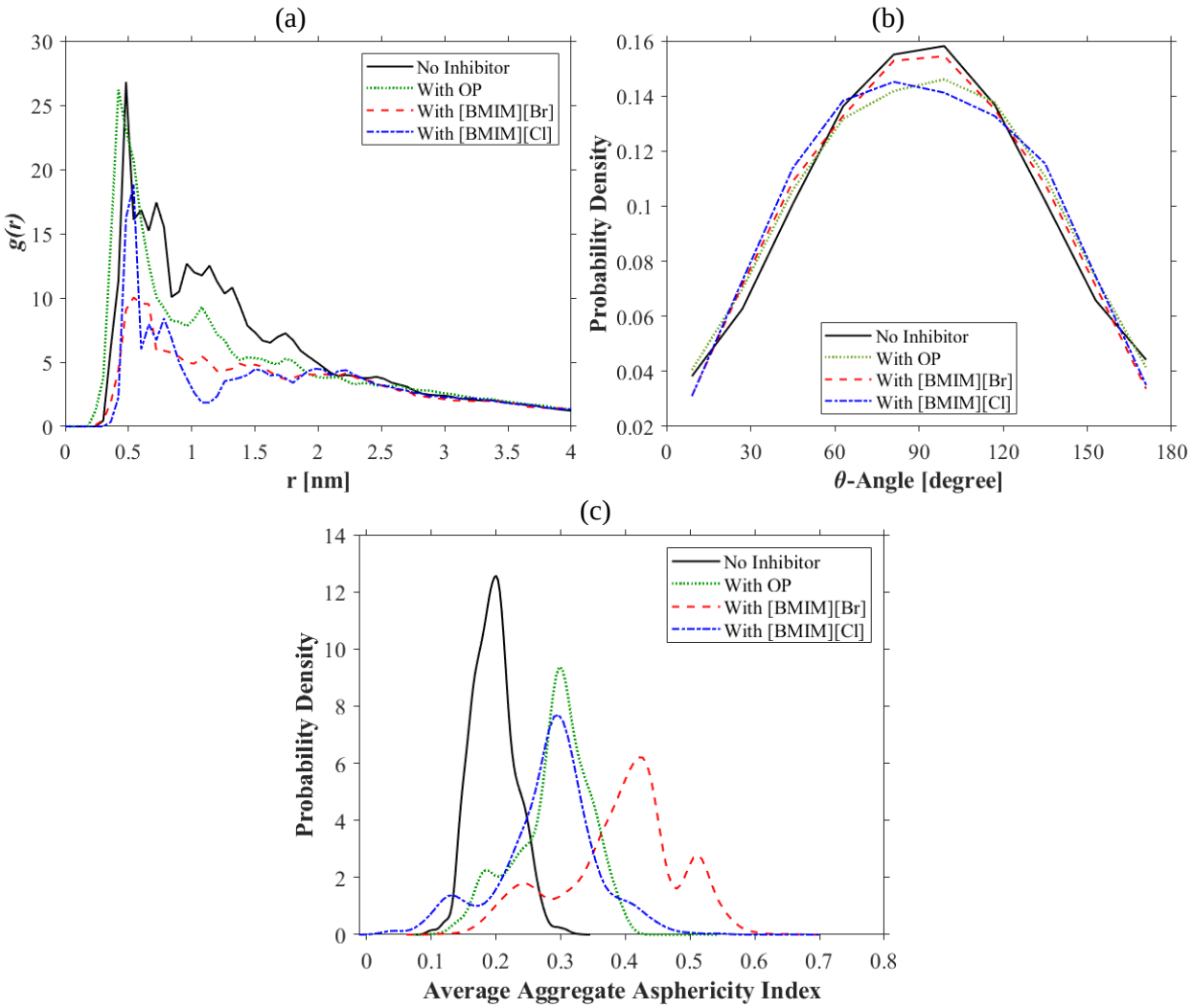

Figure 4-5. (a) radial distribution function, (b) θ-angle probability density, (c) asphericity index probability density for A2/nC$_7$ without and with inhibitors for last 60 ns.

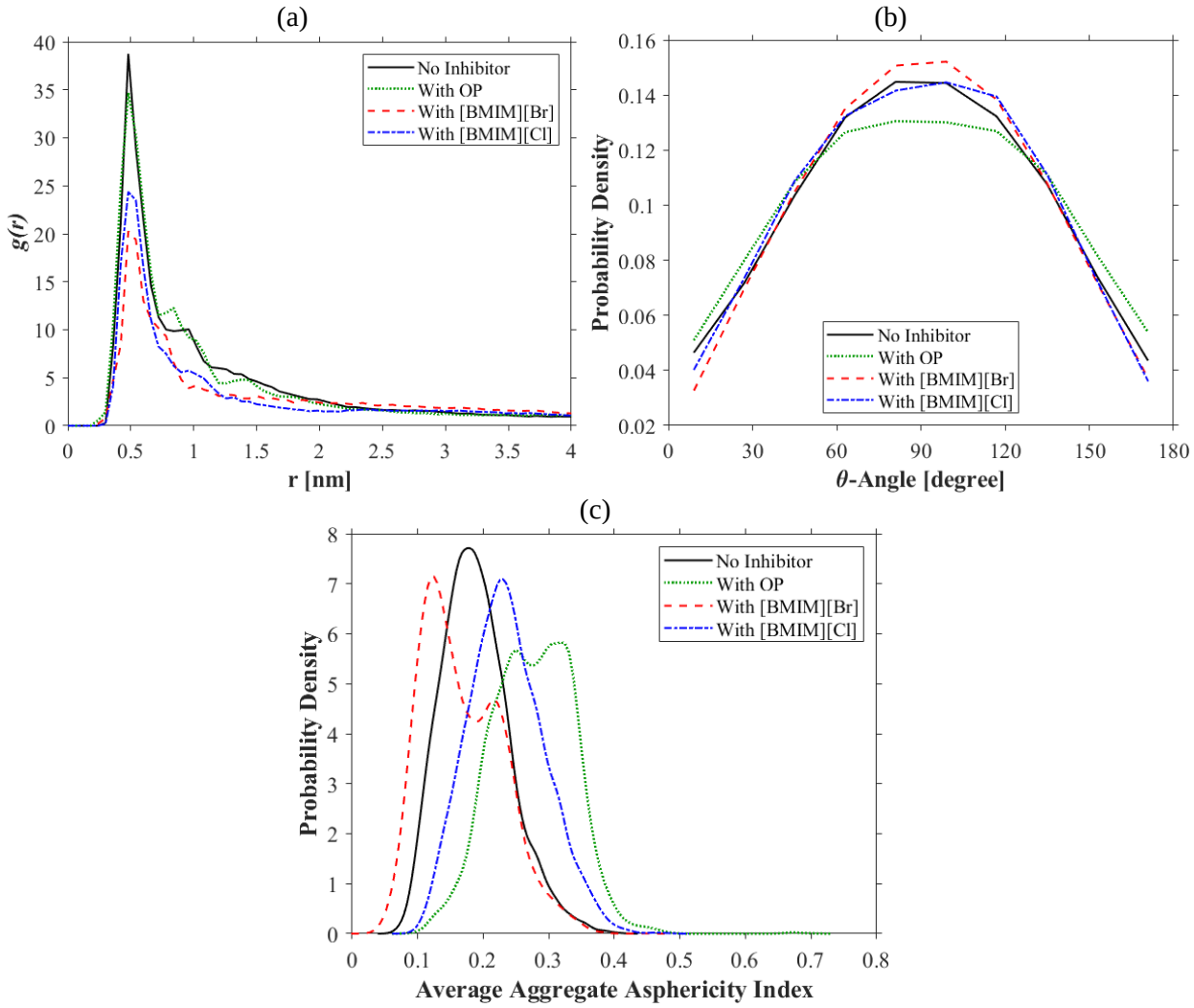

Figure 4-6. (a) radial distribution function, (b) θ-angle probability density, and (c) asphericity index probability density for A3/nC$_7$ without and with inhibitors for last 60 ns.

Figure 4-6(c) confirms the prediction for asphaltene aggregate shape using [BMIM][Br] and OP inhibitors. The inhibitor-free system has a strong single peak at asphericity index of 0.2. [BMIM][Br] changes the aggregate shape probability distribution to a bimodal distribution with a higher peak at 0.12, meaning that the aggregates are more spherical than the system without the inhibitor. OP changes the probability distribution to bimodal with peaks shifting to 0.25 and 0.32, implying that the aggregate shape is altering to rod-like. The asphericity index in asphaltene system containing [BMIM][Cl] is between the OP and [BMIM][Br] effects. The asphericity probability

distribution in the presence of [BMIM][Cl] is unimodal and it is slightly shifting from the case with no inhibitor toward rod-like aggregate shape, which was not noticed in RDF or angle distribution density plots. Again, the misinterpretation and lack of conclusion in RDF and angle distribution density graph highlight the necessity of distance and angle coupling to study the aggregation interaction, which will be discussed in the next sections.

4.3.3 Effect of Inhibitors on the Asphaltene Binding Mechanisms

There are three main binding arrangements in asphaltene aggregation: face-to-face, offset stacked, and T-shape stacked. In most research studies in the literature, the COM distance is used to distinguish the aggregation types. However, we believe that considering only distance may result in a false conclusion. For example, identifying T-shape arrangement mistakenly, rather than offset stacked, if the displacement is large enough that the distance between the molecules' COM falls into the T-shape category. Additionally, an offset stacked arrangement might be misidentified as face-to-face if there is an arrangement with the distance between the COM less than 0.5 nm. Furthermore, the angle between two molecules alone can not be used as an independent variable to differentiate between the aggregations arrangements as mentioned in section 4.3.2. Therefore, we propose considering the distance between the molecules' COM, the angle between two asphaltene polyaromatic cores (θ), and the angle between the vector, connecting the centre of polyaromatic cores and the resultant vector of polyaromatic plane normals (α).

Figure 4-7 displays the number of intermolecular contacts between the asphaltene molecules versus time for the systems without (Figure 4-7(a)) and with inhibitors (Figure 4-7(b)-(d)) when the distance between molecules' COM is less than 1.2 nm. The cut off threshold of 1.2 nm is chosen because the vdW and Coulombic energy contributions are neglected beyond this cut off distance in the simulation. Also, this value is the maximum limit used for distinguishing the

aggregation mechanisms that is commonly used based on the distance between the molecules [32]. Figure 4-7(a) reveals that the face-to-face and T-shape are two main arrangements for A2 binding, and the offset stacked has the lowest contribution to asphaltene binding without an inhibitor. The system containing OP follows a similar order, while the T-shape contribution is significantly lower than the face-to-face such that the face-to-face arrangement is the primary binding mechanism (Figure 4-7(b)). In the presence of [BMIM][Br], face-to-face is the most probable, and the offset stacked is the least probable arrangement for asphaltene binding, which is similar to the case with OP or that without an inhibitor. However, when ILs are used as the inhibitor, the number of intermolecular contacts for face-to-face drops significantly from 40–45 to 16 (three times) at 120 ns in the presence of [BMIM][Br] compared to the cases with no inhibitor and OP (Figure 4-7(c)). The reduction of face-to-face intermolecular contacts vanishes the dominancy of face-to-face arrangement, and no arrangement is dominant when [BMIM][Br] is added. Figure 4-7(d) demonstrates that adding [BMIM][Cl] decreases both the face-to-face and T-shape binding arrangements significantly compared to an inhibitor-free system. The offset stacked and T-shape arrangements have similar ranges of fluctuations with an average value of 5 contacts at 120 ns. In contrast, using [BMIM][Cl] as the inhibitor, the number of intermolecular contacts for the face-to-face arrangement is 20, and this mechanism dominates the asphaltene aggregation behavior.

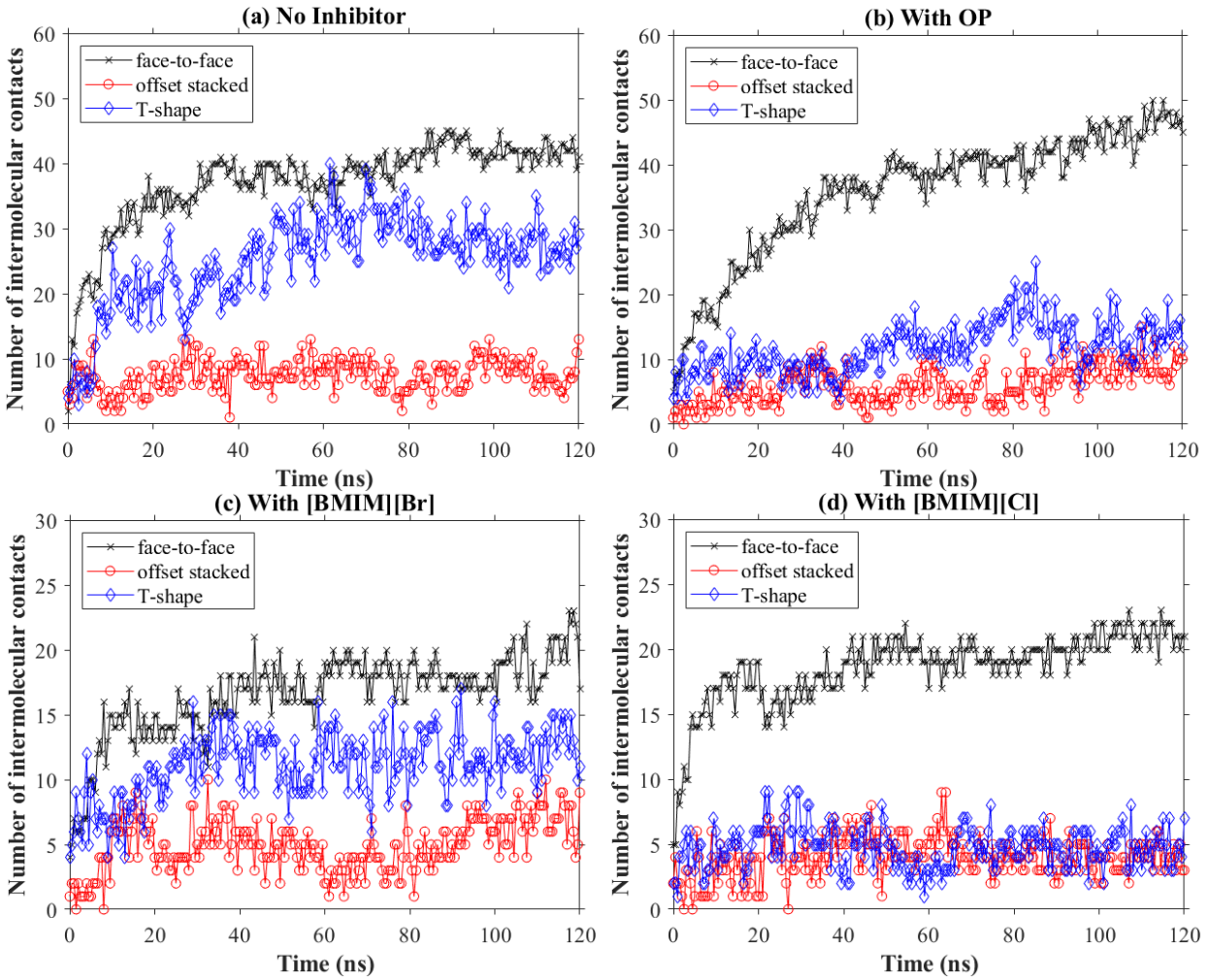

Figure 4-7. The number of intermolecular contacts for A2/nC$_7$: (a) no inhibitor, (b) OP addition, (c) [BMIM][Br] addition, and (d) [BMIM][Cl] addition.

Figure 4-8 shows the number of intermolecular contacts between A3 molecules for the systems without (Figure 4-8(a)) and with an inhibitor (Figure 4-8(b)-(d)) when the distance between the molecules' COM is less than 1.2 nm. In the inhibitor-free system, face-to-face has the highest number of contacts, following by offset stacked and T-shape, as shown in Figure 4-8(a). Comparing the binding arrangements for A2 and A3 shows that the face-to-face and T-shape are the dominant binding arrangements for A2, while for A3 only the face-to-face is the main binding arrangement. Hence, the order of aggregation mechanisms for A3 is slightly different from A2,

due to the capability of A2 for formation of hydrogen bonds. According to Figure 4-8(b), adding OP only increases the number of face-to-face contacts and does not change the offset stacked and T-shape arrangement order. On the contrary, adding the IL inhibitors decreases the number of face-to-face arrangements to approximately half and reduces the aggregation by offset stacked to a similar occurrence for the T-shape contact.

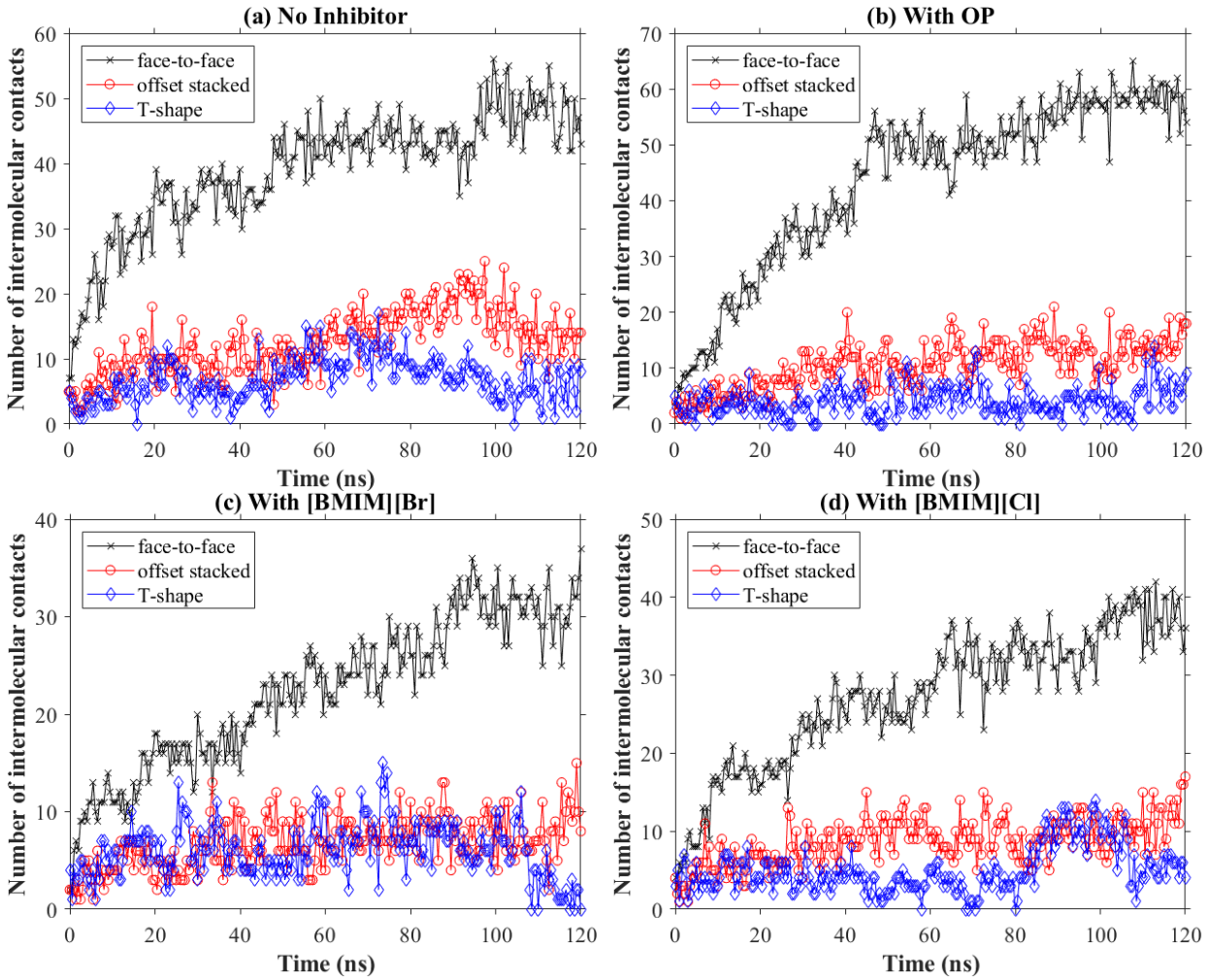

Figure 4-8. The number of intermolecular contacts for A3/nC$_7$: (a) no inhibitor, (b) OP addition, (c) [BMIM][Br] addition, and (d) [BMIM][Cl] addition.

Therefore, the trend and order of binding arrangements are different for two different asphaltene structures with and without inhibitor; the binding arrangements are also affected by the type of inhibitor because of the variations in the type of interaction forces for the asphaltene-asphaltene

and asphaltene-inhibitors. Gray et al. [5] introduced various forces between the asphaltene molecules based on their chemical structures. The two asphaltene structures employed in this study have quadrupole-quadrupole interaction force, while A2 can form hydrogen bonds. OP has one benzene ring, which is relatively smaller than the asphaltene polyaromatic core with nine aromatic rings. The quadrupole-quadrupole attraction force between the electron cloud in OP and that in the asphaltene polyaromatic is less than the attraction force between the electron clouds of two polyaromatic cores. Therefore, there is no effective binding between the OP and A3 molecules to stop asphaltene aggregation. Nevertheless, the OP molecules have a hydroxyl group, which results in forming hydrogen bonds with highly electronegative atoms such as oxygen and nitrogen that are available in A2. Therefore, OP forms hydrogen bonding with A2, provides steric effects with alkyl tail, and reduces the asphaltene binding. Although OP is still incapable of stopping quadrupole-quadrupole interactions between the asphaltene polyaromatic cores, it prevents the asphaltene molecules to form hydrogen bonding with themselves, and reduces the number of asphaltene T-shape arrangements (Figure 4-7(b)). ILs are strong electron donor-acceptors that play a crucial role in their inhibitory effect. The interaction forces between the IL inhibitor and asphaltene are dispersive, hydrogen bond, charge transfer, dipolar, and Coulombic [44]. One of the main interactions between the asphaltene and ILs is cation-quadrupole interaction, which is stronger than quadrupole-quadrupole interaction. The cation-quadrupole interactions increase if the anion part of ILs acts as an electron donor, and binds with the electron cloud of the asphaltene polyaromatic core. This mechanism significantly reduces the number of face-to-face contacts for both asphaltenes in the presence of ILs (as inhibitors). The anion electron donation capacity is directly related to the anion charge density, which increases by increasing the anion charge and decreasing the anion radius. Chloride has a higher anion charge density than bromide because of

smaller anion size with a similar charge. While both ILs similarly affect the face-to-face binding arrangement for both asphaltenes, [BMIM][Cl] reduces the T-shape binding more for A2, owing to its higher electron charge density (as an electron donor).

4.3.4 Inhibitors Effect on the Asphaltene Stacking Model

In this section, the alteration of each arrangement type is discussed in three ranges of distance including 0–0.5 nm, 0.5–0.75 nm, and 0.75–1.2 nm when asphaltenes aggregate in the presence and absence of inhibitors. This analysis shows the possibility of occurring different stacking model in the above-mentioned distance ranges. In this section, the cumulative number of intermolecular contacts is considered rather than the number of intermolecular contacts because of overlapping between graphs, resulting in a misleading conclusion.

Figure 4-9 shows the binding arrangements for A2 with different inhibitors where COM distance is less than 0.5 nm. Although both face-to-face and offset arrangement are observed for all scenarios, T-shape arrangement is not observed due to the lack of space for molecule rotation at this distance. Figure 4-9(a) demonstrates that the cumulative number of face-to-face arrangements is increased with steep slope in the presence of OP compared to the inhibitor-free system, which implies that the OP promotes face-to-face arrangements at short COM distances. A similar impact is noticed for the offset stacked arrangement, while the OP effect is delayed to the last 20 ns of the simulation (Figure 4-9(b)). ILs show their significant impacts by reducing parallel binding at short distances with a more reduction when [BMIM][Br] is used (Figure 4-9(a)-(b)).

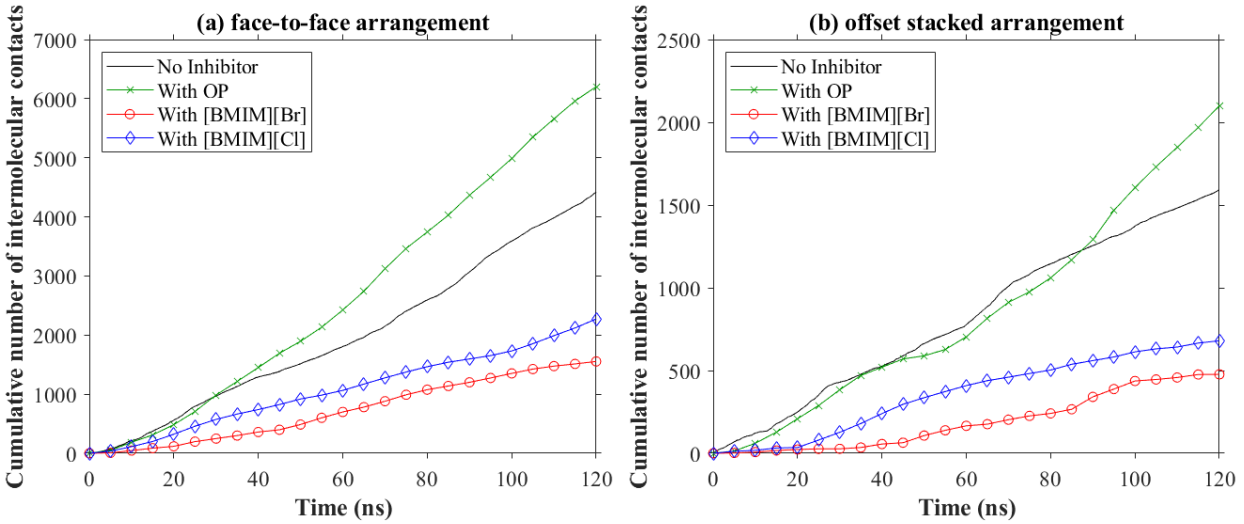

Figure 4-9. The parallel stacking arrangement for A2/nC$_7$ in the COM distance range of less than 0.5 nm: (a) face-to-face arrangement, and (b) offset stacked arrangement.

Figure 4-10 shows the A2 binding arrangement in the distance range of 0.5 to 0.75 nm. In this distance range, the face-to-face arrangement is reduced when an inhibitor is added compared to the inhibitor-free system. Figure 4-10(a) illustrates that the cumulative number of interaction contacts for the face-to-face arrangement decreases with the following order: the inhibitor-free system (the highest), with OP, with [BMIM][Cl], and with [BMIM][Br] (the lowest). While [BMIM][Br] does not change the frequency of the offset stacking occurrences (compared to the inhibitor-free system), OP and [BMIM][Cl] decrease the cumulative number of orderly offset stacked arrangements (Figure 4-10(b)). Based on Figure 4-10(c) and comparing the behavior in this panel (c) with those in panels (a) and (b), it can be concluded that the T-shape binding arrangement effectively decreases by adding the inhibitors. The reduction of the T-shape arrangement proves that the aggregate shape changes toward rod-like. The significant reductions of both the face-to-face and T-shape asphaltene arrangements using [BMIM][Br] as the inhibitor result in a wider range of aggregate shapes (section 4.3.2).

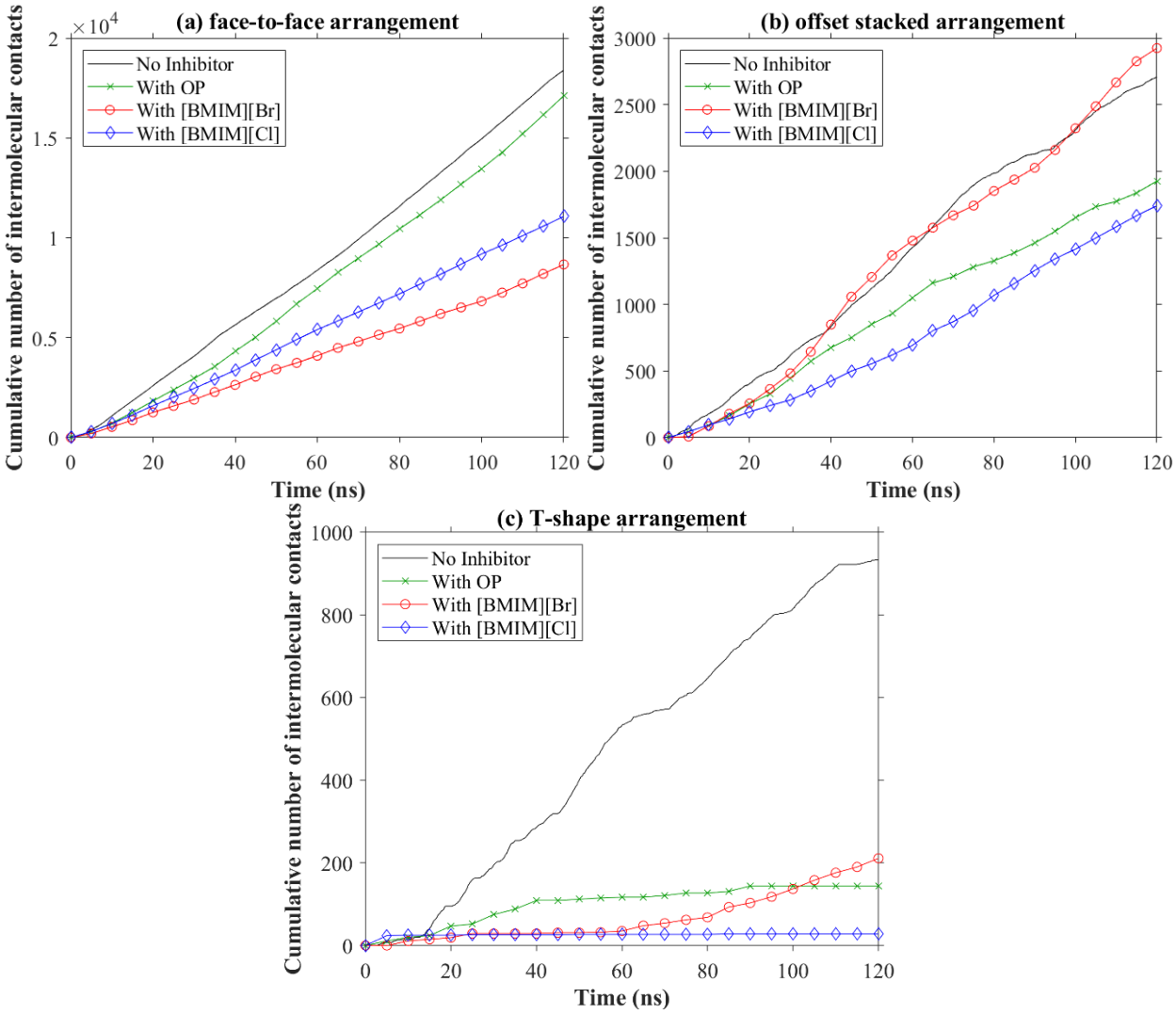

Figure 4-10. The binding arrangement for A2/nC$_7$ in the COM distance range of 0.5 to 0.75 nm: (a) face-to-face arrangement, (b) offset stacked arrangement, and (c) T-shape arrangement.

Figure 4-11 shows the asphaltene binding arrangement for A2 when the COM distance range is between 0.75–1.2 nm. For the face-to-face and offset stacked arrangements, the trends and order of the interaction contact number are similar to the 0.5–0.75 nm distance range, except that [BMIM][Br] also reduces the offset stacked arrangement (Figure 4-11(a)-(b)). Although the ILs eliminate the T-shape binding arrangement for asphaltenes at this distance range, there is a relatively greater extent of T-shape arrangement in the presence of OP (Figure 4-11(c)). Comparing the T-shape arrangement for OP in the distance range of 0.5–0.75 nm with that in the

range of 0.75–1.2 nm reveals that OP controls the asphaltene T-shape binding only at lower distances.

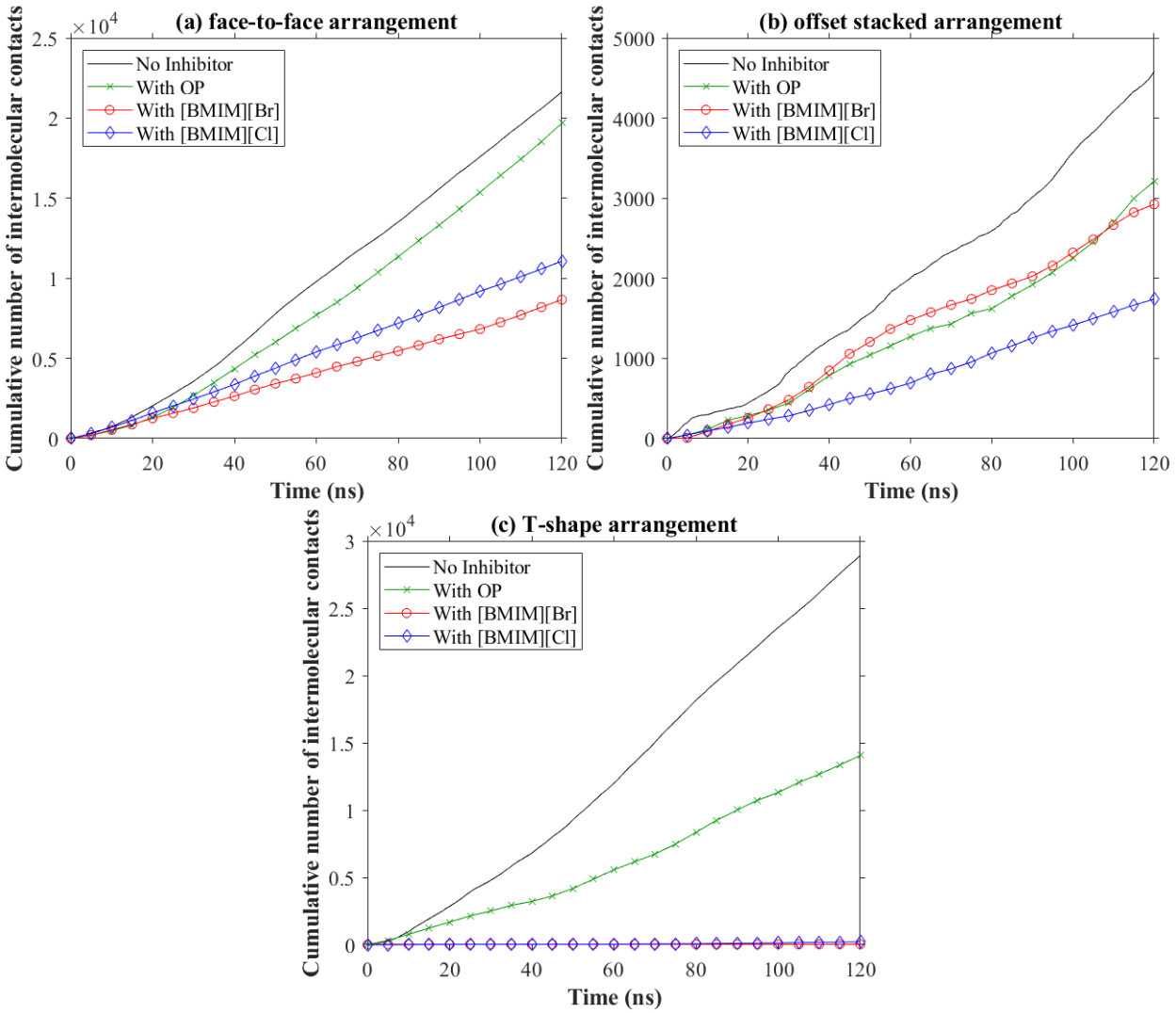

Figure 4-11. The binding arrangement for A2/nC$_7$ in the COM distance range of 0.75 to 1.2 nm: (a) face-to-face arrangement, (b) offset stacked arrangement, and (c) T-shape arrangement.

Figure 4-12 demonstrates the parallel stacking arrangement changes for A3 by adding inhibitors when asphaltene COM distance is less than 0.5 nm. Unlike for A2, all inhibitors reduce the frequency of parallel stacking for A3 at this distance range. The ILs the most reduction in the frequency for both binding arrangements; [BMIM][Br] reduces the offset stacked more than

[BMIM][Cl]. Similar to A2, no T-shape arrangement is observed in this range due to the lack of space for the asphaltene molecules to rotate.

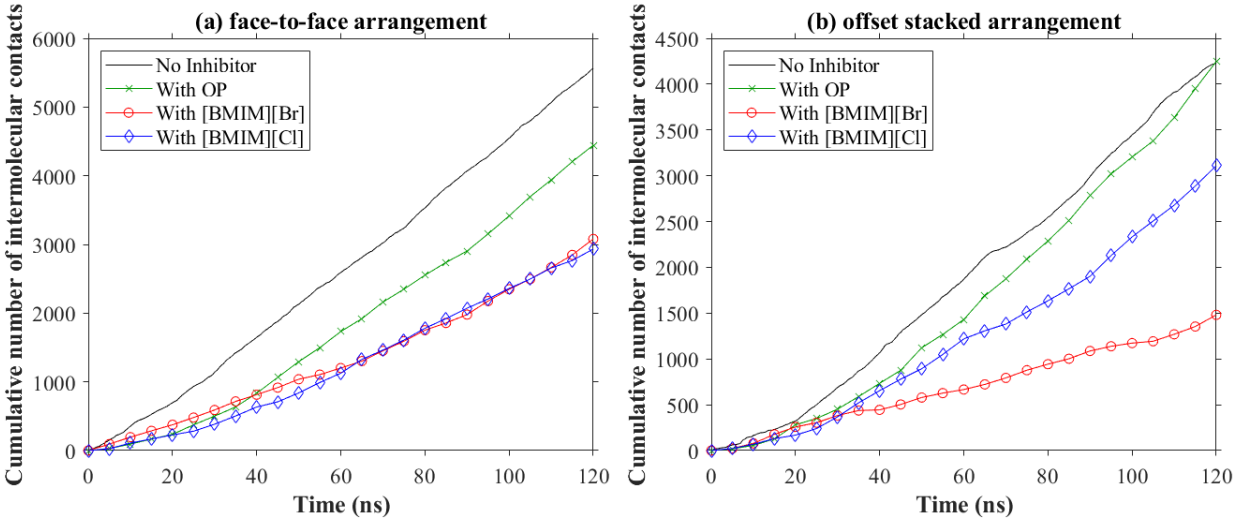

Figure 4-12. The parallel stacking arrangement for A3/nC_7 in the COM distance range of less than 0.5 nm: (a) face-to-face arrangement, and (b) offset stacked arrangement.

Figure 4-13 displays the A3 binding arrangement at a distance 0.5–0.75 nm; comparing that with A2 at the same conditions (Figure 4-10) reveals that the inhibitors are less effective for A3 because A3 has no functional groups in its chemical structure. For example, the inhibitors change the T-shape arrangement for A3 (Figure 4-13(c)) less than that for A2 (Figure 4-6 (c)).

Figure 4-14 depicts the A3 binding arrangements for COM distance range 0.75–1.2 nm. The inhibitors' low impact on parallel stacking in 0.5–0.75 nm distance range is changed to a negative impact in this distance range such that OP promotes the face-to-face, and [BMIM][Cl] enhances the cumulative number of offset stacking compared to the inhibitor-free system. It follows that adding the inhibitors may even promote the asphaltene parallel stacking on some occasions, which has been claimed in the literature [44, 45]. Figure 4-14(c) shows that all three inhibitors decrease the T-shape arrangement, which is more noticeable for IL/A3 systems.

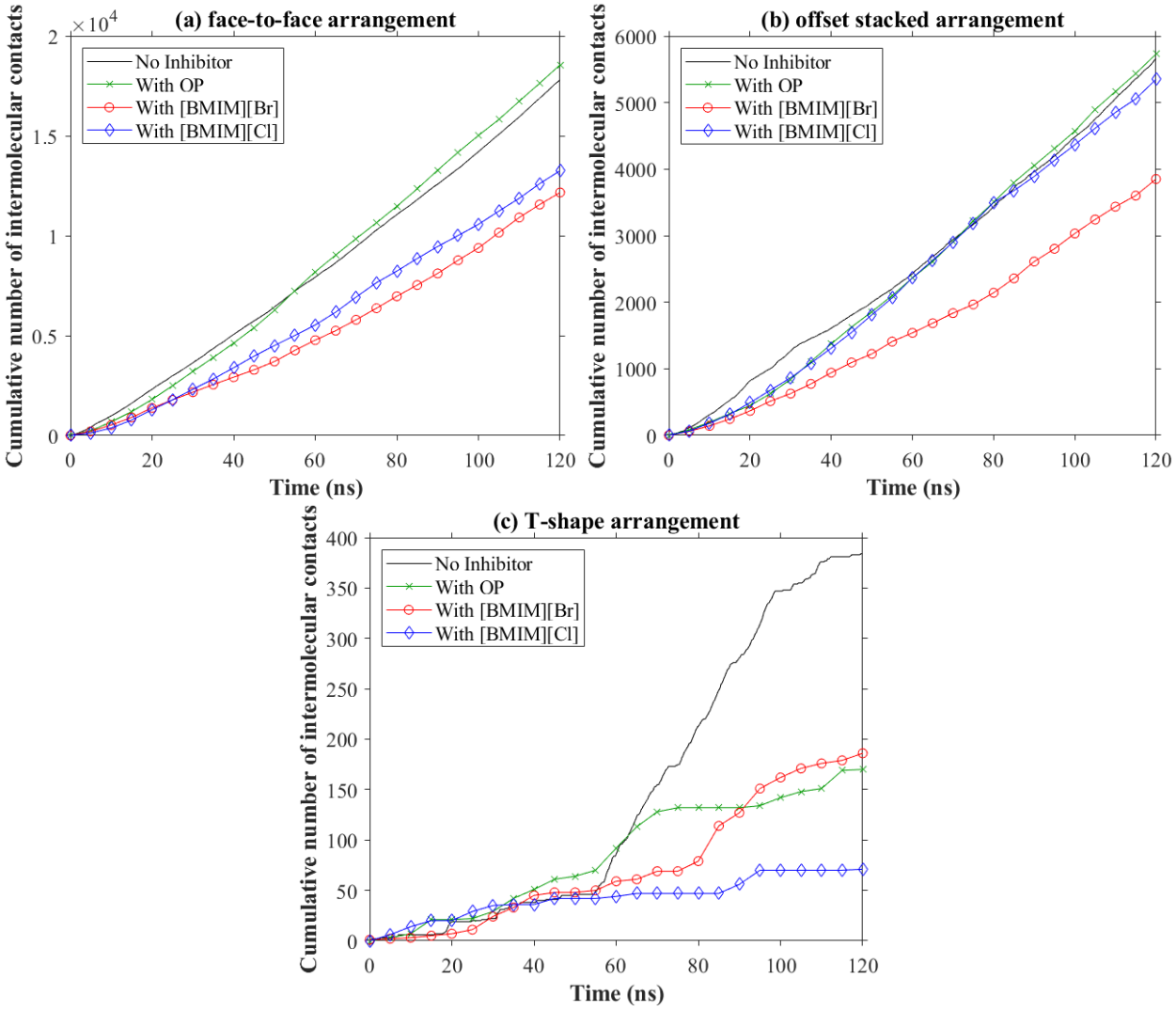

Figure 4-13. The binding arrangement for A3/*n*C_7 in the COM distance range of 0.5 to 0.75 nm; (a) face-to-face arrangement, (b) offset stacked arrangement, and (c) T-shape arrangement.

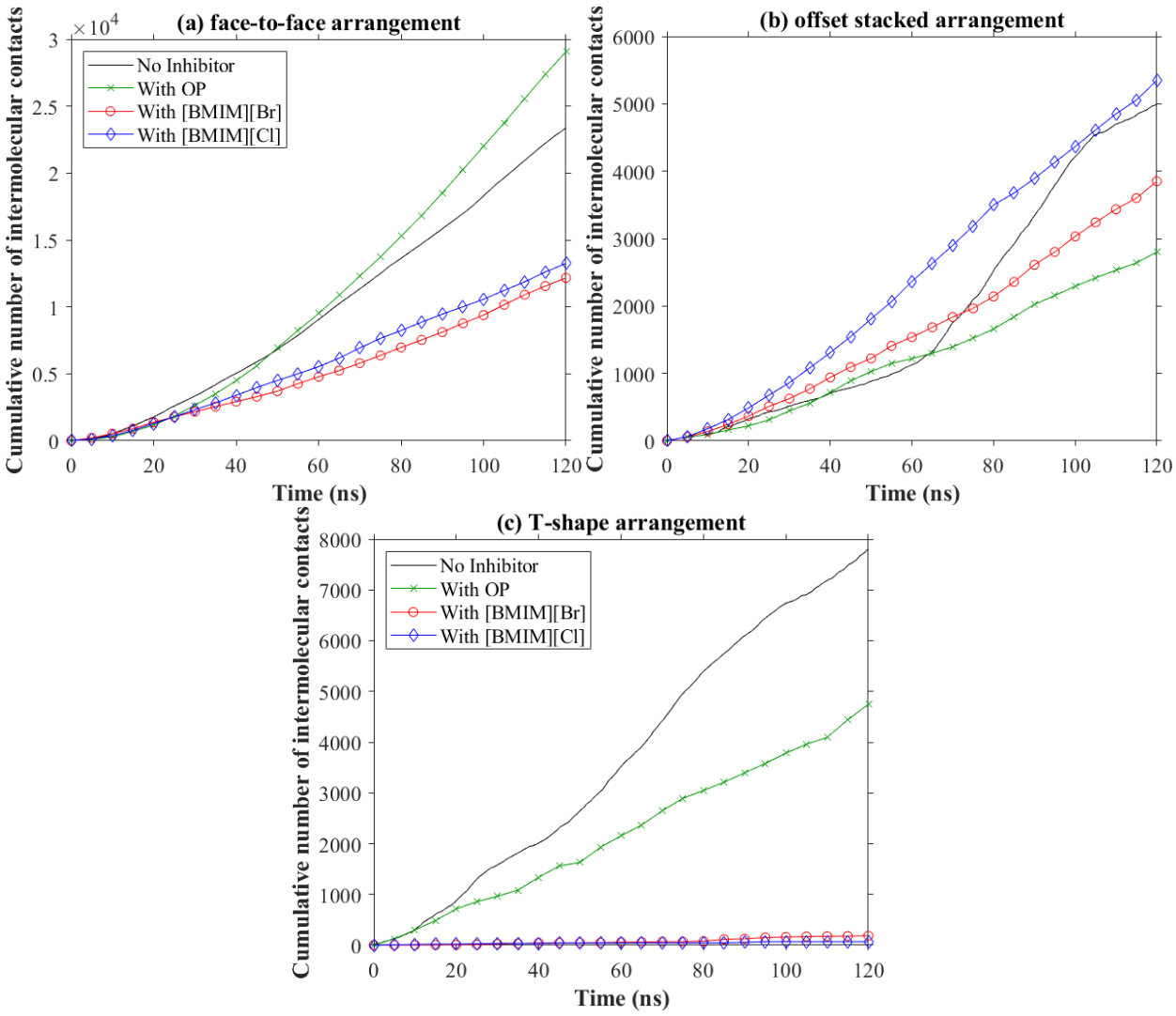

Figure 4-14. The binding arrangement for A3/nC_7 in the COM distance range of 0.75 to 1.2 nm: (a) face-to-face arrangement, (b) offset stacked arrangement, and (c) T-shape arrangement.

4.4 CONCLUSIONS

Naturally, resins are responsible for maintaining the asphaltene suspension in the crude oil during production and transportation. However, changes in the thermodynamic conditions during the production disrupt the asphaltene stability, leading to asphaltene aggregation and deposition. To cope with these problems, chemical inhibitors can be added to keep asphaltene suspended and improve the asphaltene stability before asphaltene aggregation occurs. The binding arrangement between the asphaltene molecules strongly relates to the stability of the aggregates, and chemical

inhibitors can alter the binding arrangements because of interactions between the functional groups in their structures and asphaltene structures. Improving molecular-level knowledge about the bonding orientation between asphaltenes and between asphaltene-inhibitor can help to design more effective inhibitors.

The asphaltene molecules bind together using three arrangements: face-to-face, offset stacked, and T-shape. Usually, the distance between the molecules' centre of mass (COM) is used to identify the different binding arrangements; using only this feature can result in a false conclusion in some occasions. We propose an improved framework to differentiate between the binding arrangements by including two angular criteria besides the COM. The angular criteria include the angle between the polyaromatic cores of two molecules and the angle between a vector connecting the centres of polyaromatic cores and resultant vector of plane normals ($\vec{R}$). This method avoids false identification of the binding arrangements for face-to-face stacking with a long separation distance (sandwich arrangement) or for confusing offset stacked with T-shape arrangement. In this study, the effects of *n*-octylphenol (OP) and two IL inhibitors, including 1-Butyl-3-methylimidazolium bromide [BMIM][Br], and 1-Butyl-3-methylimidazolium chloride [BMIM][Cl] are investigated on the shape and binding arrangements for two different asphaltene structures. The A2 asphaltene has hydroxyl and pyridine groups, while A3 asphaltene does not have either of them. The results imply that OP and [BMIM][Cl] have similar impacts on the aggregate shape for both asphaltenes. However, [BMIM][Br] increases the variations in the aggregate shape for A2 with more probability of forming rod-like aggregates while making the A3 aggregates more spherical. The differences in the behavior of asphaltenes and inhibitors are related to their chemical structures and the presence of functional groups that result in interplay between competitive intermolecular forces between the asphaltenes and asphaltene-inhibitors. For instance, the primary inhibitory

mechanism of OP is through forming hydrogen bonds with the asphaltene molecules, followed by preventing the growth of asphaltene aggregate. However, OP does not reduce nor prevent quadrupole-quadrupole force between the asphaltene polyaromatic cores. In contrast, ILs cause cation-quadrupole interactions with polyaromatic cores, which is stronger than quadrupole-quadrupole force. Therefore, they reduce the number of parallel bindings (especially face-to-face) between the asphaltene molecules. It is also found that the inhibitors have different impacts on asphaltene binding mechanisms at different distance ranges. We expect our results to provide and improve a scientific pathway to design and synthesize more effective asphaltene inhibitors under production conditions. For follow-up studies, we recommend considering the effect of asphaltene deposition on various surfaces (in terms of type, morphology, and composition) in the presence of chemical inhibitors.

ACKNOWLEDGEMENTS

Financial supports of Memorial University, Canada; the Natural Sciences and Engineering Research Council (NSERC) of Canada; and Equinor Canada are greatly acknowledged.

REFERENCES

1. Teklebrhan, R.B., et al., *Role of naphthenic acids in controlling self-aggregation of a polyaromatic compound in toluene.* The Journal of Physical Chemistry B, 2016. **120**(14): p. 3516-3526.
2. Allenson, S.J. and M.A. Walsh. *A novel way to treat asphaltene deposition problems found in oil production*. in *International Symposium on Oilfield Chemistry*. 1997. Society of Petroleum Engineers.

3. Schantz, S. and W. Stephenson. *Asphaltene deposition: development and application of polymeric asphaltene dispersants*. in *SPE Annual Technical Conference and Exhibition*. 1991. Society of Petroleum Engineers.

4. Sedghi, M., et al., *Effect of asphaltene structure on association and aggregation using molecular dynamics.* The Journal of Physical Chemistry B, 2013. **117**(18): p. 5765-5776.

5. Gray, M.R., et al., *Supramolecular assembly model for aggregation of petroleum asphaltenes.* Energy & Fuels, 2011. **25**(7): p. 3125-3134.

6. Jian, C., T. Tang, and S. Bhattacharjee, *Probing the effect of side-chain length on the aggregation of a model asphaltene using molecular dynamics simulations.* Energy & fuels, 2013. **27**(4): p. 2057-2067.

7. Murgich, J., *Intermolecular forces in aggregates of asphaltenes and resins.* Petroleum science and technology, 2002. **20**(9-10): p. 983-997.

8. Chang, C.-L. and H.S. Fogler, *Stabilization of asphaltenes in aliphatic solvents using alkylbenzene-derived amphiphiles. 1. Effect of the chemical structure of amphiphiles on asphaltene stabilization.* Langmuir, 1994. **10**(6): p. 1749-1757.

9. Javanbakht, G., et al., *Molecular polydispersity improves prediction of asphaltene aggregation.* Journal of Molecular Liquids, 2018. **256**: p. 382-394.

10. Gao, F., et al., *Molecular dynamics simulation: the behavior of asphaltene in crude oil and at the oil/water interface.* Energy & fuels, 2014. **28**(12): p. 7368-7376.

11. Sodero, A.C., et al., *Investigation of the effect of sulfur heteroatom on asphaltene aggregation.* Energy & Fuels, 2016. **30**(6): p. 4758-4766.

12. Pacheco-Sánchez, J., I. Zaragoza, and J. Martínez-Magadán, *Asphaltene aggregation under vacuum at different temperatures by molecular dynamics.* Energy & fuels, 2003. **17**(5): p. 1346-1355.

13. Hunter, C.A. and J.K. Sanders, *The nature of. pi.-. pi. interactions.* Journal of the American Chemical Society, 1990. **112**(14): p. 5525-5534.

14. Boek, E.S., D.S. Yakovlev, and T.F. Headen, *Quantitative molecular representation of asphaltenes and molecular dynamics simulation of their aggregation.* Energy & Fuels, 2009. **23**(3): p. 1209-1219.

15. Narten, A., *X-ray diffraction pattern and models of liquid benzene.* The Journal of Chemical Physics, 1977. **67**(5): p. 2102-2108.

16. Evans, D. and R. Watts, *On the structure of liquid benzene.* Molecular Physics, 1976. **32**(1): p. 93-100.

17. Alvarez-Ramirez, F., E. Ramirez-Jaramillo, and Y. Ruiz-Morales, *Calculation of the interaction potential curve between asphaltene− asphaltene, asphaltene− resin, and resin− resin systems using density functional theory.* Energy & Fuels, 2006. **20**(1): p. 195-204.

18. Headen, T.F., E.S. Boek, and N.T. Skipper, *Evidence for asphaltene nanoaggregation in toluene and heptane from molecular dynamics simulations.* Energy & Fuels, 2009. **23**(3): p. 1220-1229.

19. Zhang, L. and M.L. Greenfield, *Molecular orientation in model asphalts using molecular simulation.* Energy & fuels, 2007. **21**(2): p. 1102-1111.

20. Rodríuez, J., et al., *Molecular aggregation of polycyclic aromatic hydrocarbons. A theoretical modelling of coronene aggregation.* Journal of Molecular Structure: THEOCHEM, 1992. **254**: p. 429-441.

21. Mullins, O.C. and E.Y. Sheu, *Structures and dynamics of asphaltenes*. 2013: Springer Science & Business Media.

22. Teklebrhan, R.B., et al., *Probing structure–nanoaggregation relations of polyaromatic surfactants: a molecular dynamics simulation and dynamic light scattering study.* The Journal of Physical Chemistry B, 2012. **116**(20): p. 5907-5918.

23. Wang, W., et al., *Nanoaggregates of diverse asphaltenes by mass spectrometry and molecular dynamics.* Energy & Fuels, 2017. **31**(9): p. 9140-9151.

24. Jian, C. and T. Tang, *One-dimensional self-assembly of polyaromatic compounds revealed by molecular dynamics simulations.* The Journal of Physical Chemistry B, 2014. **118**(44): p. 12772-12780.

25. Shi, M.-M., et al., *π− π interaction among violanthrone molecules: Observation, enhancement, and resulting charge transport properties.* The Journal of Physical Chemistry B, 2011. **115**(4): p. 618-623.

26. Pacheco-Sánchez, J., F. Alvarez-Ramirez, and J. Martínez-Magadán, *Morphology of aggregated asphaltene structural models.* Energy & fuels, 2004. **18**(6): p. 1676-1686.

27. Khalaf, M.H. and G.A. Mansoori, *A new insight into asphaltenes aggregation onset at molecular level in crude oil (an MD simulation study).* Journal of Petroleum Science and Engineering, 2018. **162**: p. 244-250.

28. Mikami, Y., et al., *Molecular dynamics simulations of asphaltenes at the oil–water interface: from nanoaggregation to thin-film formation.* Energy & Fuels, 2013. **27**(4): p. 1838-1845.

29. Liu, J., Y. Zhao, and S. Ren, *Molecular dynamics simulation of self-aggregation of asphaltenes at an oil/water interface: formation and destruction of the asphaltene protective film.* Energy & Fuels, 2015. **29**(2): p. 1233-1242.

30. Song, S., et al., *Molecular Dynamics Study on Aggregating Behavior of Asphaltene and Resin in Emulsified Heavy Oil Droplets with Sodium Dodecyl Sulfate.* Energy & fuels, 2018. **32**(12): p. 12383-12393.

31. Lv, G., et al., *The properties of asphaltene at the oil-water interface: A molecular dynamics simulation.* Colloids and Surfaces A: Physicochemical and Engineering Aspects, 2017. **515**: p. 34-40.

32. Yaseen, S. and G.A. Mansoori, *Asphaltene aggregation due to waterflooding (A molecular dynamics study).* Journal of Petroleum Science and Engineering, 2018. **170**: p. 177-183.

33. Takanohashi, T., M. Iino, and K. Nakamura, *Evaluation of association of solvent-soluble molecules of bituminous coal by computer simulation.* Energy & fuels, 1994. **8**(2): p. 395-398.

34. Takanohashi, T., M. Iino, and K. Nakamura, *Simulation of interaction of coal associates with solvents using the molecular dynamics calculation.* Energy & fuels, 1998. **12**(6): p. 1168-1173.

35. Lindahl, Abraham, Hess, & Spoel, V. D. , *GROMACS 2019.3 Source code.* 2019.

36. Abraham, M.J., et al., *GROMACS: High performance molecular simulations through multi-level parallelism from laptops to supercomputers.* SoftwareX, 2015. **1**: p. 19-25.

37. Fu, C.-F. and S.X. Tian, *A comparative study for molecular dynamics simulations of liquid benzene.* Journal of chemical theory and computation, 2011. **7**(7): p. 2240-2252.

38. Ghamartale, A., S. Zendehboudi, and N. Rezaei, *New Molecular Insights into Aggregation of Pure and Mixed Asphaltenes in the Presence of n-Octylphenol Inhibitor.* Energy & Fuels, 2020.

39. Hanwell, M.D., et al., *Avogadro: an advanced semantic chemical editor, visualization, and analysis platform.* Journal of cheminformatics, 2012. **4**(1): p. 17.

40. Nosé, S., *A molecular dynamics method for simulations in the canonical ensemble.* Molecular physics, 1984. **52**(2): p. 255-268.

41. Hoover, W.G., *Canonical dynamics: Equilibrium phase-space distributions.* Physical review A, 1985. **31**(3): p. 1695.

42. Parrinello, M. and A. Rahman, *Strain fluctuations and elastic constants.* The Journal of Chemical Physics, 1982. **76**(5): p. 2662-2666.

43. Silva, H.S., et al., *Molecular dynamics study of nanoaggregation in asphaltene mixtures: Effects of the N, O, and S heteroatoms.* Energy & Fuels, 2016. **30**(7): p. 5656-5664.

44. Boukherissa, M., et al., *Ionic liquids as dispersants of petroleum asphaltenes.* Energy & Fuels, 2009. **23**(5): p. 2557-2564.

45. Barcenas, M., et al., *Study of medium effect on asphaltene agglomeration inhibitor efficiency.* Energy & Fuels, 2008. **22**(3): p. 1917-1922.

5. CHAPTER FIVE

A Mechanistic Study on Chemical Inhibitors for Control of Asphaltene Deposition in Calcite Pore

Preface

A version of this manuscript has been accepted to be published in the Journal of Industrial & Engineering Chemistry Research. Ali Ghamartale is the primary author who conducted the literature review, executed the simulation runs, and discussed the results. The conceptual model and manuscript structure were developed by the first author with insights from co-authors (Mohamadi-Baghmolaei, M., and Zendehboudi, S.). Both draft and revised versions of the manuscript were prepared by the first author based on the feedback from the co-authors. The co-author, Sohrab Zendehboudi, had the supervision role and edited the manuscript.

ABSTRACT

Asphaltene deposition is a major problem during oil production and transportation that imposes extra treatment costs and reduces oil production. Historically, various chemical inhibitors have been developed to resolve the asphaltene deposition issue. However, the inhibitors are usually effective for a specific type of crude oil and asphaltene since the asphaltene's nature is different for various oil samples. To develop a proper chemical inhibitor, the interaction between inhibitor and asphaltene needs to be explored. This work employs a molecular dynamics (MD) simulation strategy to study asphaltene deposition on a calcite surface, considering chemical inhibitors. Two asphaltene structures with potential to form hydrogen bond (A2) and without potential to form hydrogen bond (A3) are considered in this study. The selected inhibitors, including *n*-octylphenol (OP) and 1-Butyl-3-methylimidazolium chloride (as an ionic liquid (IL)), can form van der Waals, Coulomb, and hydrogen bonds with the asphaltene molecules. The results show that the OP reduces the asphaltene aggregation by attaching to the asphaltene through hydrogen bonds. In the presence of OP, the Lennard-Jones (LJ) and Coulomb energies between A2 and calcite are reduced by 400 and 1000 kJ/mol units, leading to the asphaltene deposition reduction by adsorbing on the calcite surface and providing a hindrance layer. The IL is able to cope with the quadrupole-quadrupole interaction between asphaltene polyaromatic cores and reduce the asphaltene face-to-face aggregation. However, IL cannot provide a hindrance layer near the calcite surface since it does not have a long hydrocarbon tail. Therefore, the combination of inhibitors can benefit the inhibition process as both prevention mechanisms will be active. The 3:1 OP-IL ratio shows the optimum efficiency. At this ratio, inhibitors reduce the aggregation from 20 to less than 10 and deposition rate from 1 to 0.8 compared to the case without inhibitors. Also, the deposited aggregates have low compaction with a spherical shape which is easy to dislodge in the dynamic

situation. This research aims to demystify the asphaltene-inhibitor behaviors during asphaltene deposition, which can be a useful practice for designing chemical inhibitors for flow assurance issues.

Keywords: Asphaltene deposition; Pore blockage; Chemical inhibitor; Molecular dynamics simulation; Calcite pore.

5.1 INTRODUCTION

Asphaltene deposition is a challenging issue that impacts hydrocarbon production from reservoirs and flow assurance through production wells and transportation pipelines. Asphaltene deposition occurs due to changes in reservoir fluid properties and composition over natural depletion and enhanced oil recovery (EOR) processes [1]. Asphaltene deposition in the reservoir alters the rocks' wettability and reduces oil recovery by blocking the pores and flow path [2, 3]. Removing asphaltene deposition carries economic burdens, considering production loss and labor works. Thus, preventing asphaltene deposition is vital for sustainable production [3].

Generally, chemical inhibitors, such as surfactants and ionic liquids (ILs), are utilized to prevent/reduce asphaltene deposition [3]. Understanding the asphaltene precipitation/deposition mechanisms is useful for choosing proper chemical inhibitors. It is essential to assess the behavior and interaction of asphaltene with various chemical inhibitors to design effective inhibitors and introduce new treatment workflows. Understanding the asphaltene-inhibitor interactions/behaviors relies on several experiments in core systems [4-8], packed columns [9-13], and microfluidics [14, 15]. For instance, Karambeigi et al. [5] tested IR95 as an asphaltene inhibitor in a carbonate core. Using the inhibitor, they observed a lower pressure drop across the core (≈100 psi), which indicated asphaltene deposition prevention compared to the case without inhibitor addition [5].

Hashemi et al. [6] studied the application of NiO nanoparticles as an asphaltene inhibitor during CO_2 EOR in a coreflooding operation. The results revealed that CO_2 solo-injection reduces the core permeability by 20%, while injecting CO_2 and NiO_2 nanoparticles results in only 2% permeability reduction. The positive effect of NiO_2 as an asphaltene inhibitor was confirmed where the oil recovery from the core was increased by 7% [6]. Another experimental study on the utilization of inhibitors was performed by Madhi et al. [7], who used CTAB and SDS as the inhibitors during the coreflooding of a limestone core with two crude oils. The inhibitors increased the relative permeability and reduced the rate of asphaltene damage [7]. It is not guaranteed that inhibitors prevent asphaltene deposition in different oil cases [16-18]. Inhibitor concentration [19], chemical structure of inhibitor/asphaltene, and operating conditions [17] are the main factors that determine the success or failure of inhibitor application. Although the laboratory experiment is the primary tool to study and examine the inhibitor-asphaltene efficiency, conducting a mechanistic experimental study needs special high-tech devices, which is expensive and time-consuming.

The mechanistic study requires detailed experimental and modeling investigations. To the best of our knowledge, a limited number of research works have been dedicated to the mechanistic study of the asphaltene-inhibitor in pore-scale systems [20]. Considering the limitations of laboratory studies, the pore-scale simulation can help scientists fully understand the active mechanisms during asphaltene deposition and treatment. Over the past decade, molecular dynamics (MD) simulation has been employed to study complicated molecular-scale phenomena in different scientific fields [3, 21-23]. MD simulation is a powerful tool that uses Newton's second law and the developed forcefields based on the experiments to model the phenomena at a molecular scale. Although the asphaltene-inhibitor interaction in a bulk of fluid has been studied using MD simulation during the asphaltene precipitation [24-27], this matter has not been addressed during

the deposition process. In comparison, asphaltene deposition has been studied in various conditions near silica and calcite surfaces [28-32], which is also important before studying asphaltene deposition in the presence of chemical inhibitors. In the following, we will review the studies with the focus on disclosing the asphaltene deposition mechanisms. Lan et al. [28] studied the deposition of a continental asphaltene, Violanthrone-79, in different organic solvents near the quartz surface using GROMACS software. They considered 24 asphaltene molecules surrounded by heptane, toluene, and heptol (heptane:toluene = 1:3, 1:1, 3:1). The results showed that the adsorption rate and adsorption amount are significantly dependent on the solvent type. They explored that the asphaltene deposited in 20 and 120 ns in the presence of heptane and toluene, respectively. They also claimed that the asphaltene monomers adsorb on the silica surface with the parallel orientation while the aggregates adsorb with the oblique orientation [28]. The asphaltene structure and surface texture are two important criteria for asphaltene deposition. Mohammed et al. [30] studied the adsorption of two continental asphaltenes on the calcite and silica surfaces in a heptol (1:1) solution while employing GROMACS software. They reported that the asphaltene molecules initially aggregate in the bulk and deposit at the pore entrance and inside the pore. The asphaltene with a larger aromatic core showed faster adsorption due to higher van der Waals (vdW) force. Moreover, it was found that asphaltene diffusivity in the presence of a solid surface (i.e., calcite and silica) is reduced compared with the case of asphaltene in the bulk, which was due to the asphaltene adsorption on the surface [30]. The type of heteroatoms and their location in the asphaltene structure are two key factors that can play a role in asphaltene deposition. Bai et al. [31] explored the heteroatom's effect on the asphaltene structure during the asphaltene deposition on silica using GROMACS software. The type and location of heteroatoms were two effective factors affecting the interaction forces between the asphaltene and silica surface. Therefore, ten different

asphaltene structures with heteroatoms, such as nitrogen, oxygen, and sulfur, were hypothesized and studied. Among the three terminal groups (i.e., amino, carboxyl, and thiol), the carboxyl group significantly impacted the electrostatic force between the asphaltene and silica. It was also concluded that the strength of heteroatom's bond is reduced if the heteroatom locates in the terminal, inside the chain, and in the polyaromatic core orderly [31]. Ji et al. [29] studied the importance of surface wettability during asphaltene deposition by investigating the C5Pe asphaltene orientation near the silica surface with five different ranges of hydrophobicity using GROMACS software and GROMOS forcefield. The hydrophobicity was altered by considering the different ratios of hydroxyl group over carbon, including 0, ¼, ½, ¾ and 1, attached to the silica surface terminal. They specifically examined the morphology of deposited asphaltene molecules and demonstrated how asphaltene was predominantly adsorbed on the surface parallelly when 25% of silica interface was hydrophobic, unlike in other cases. Asphaltene deposition can occur after water flooding, in which the type of salt ions in the water can play an important role during asphaltene deposition. Wang et al. [33] studied the salinity effect of two ions, including Ca^{2+} and SO_4^{2-}, on the interaction of polyaromatic component (bitumen) with calcite surface. They concluded that the Ca^{2+} ion acts as a bridge between the calcite and bitumen molecules and enhances the adsorption of bitumen on the calcite surface. However, unlike Ca^{2+}, the attached SO_4^{2-} to the calcite surface was reluctant to bond with the bitumen, preventing bitumen from attaching to the calcite.

As mentioned earlier, various theoretical and practical factors affect the deposition process. Lack of knowledge about the inhibitor impact on asphaltene behavior near the surface particularly carbonate rock limits the design of chemical inhibitors that will be efficient for this type of reservoir that severely suffers from asphaltene deposition [34, 35]. This work aims to conduct a

mechanistic study to assess the impact of inhibitors (e.g., *n*-octylphenol (OP) and 1-butyl-3-methylimidazolium chloride ([BMIM][Cl])) on two different continental-type asphaltene structures in a calcite pore. The current research outcomes are interpreted based on the molecular analysis, such as *z*-averaged aggregation number, deposition rate, deposited aggregate compaction, and deposit shape.

The rest of the paper is structured as follows: Section 5.2 elaborates the methodology, including the materials, designed system, and software settings. This is followed by the description of the basics and theoretical aspects of molecular analysis and challenges/limitations in the simulation. Section 5.3 provides the results with adequate discussions in two sub-categories; the effect of the asphaltene type and inhibitor composition during the aggregation and deposition on the calcite surface. Finally, the paper includes the main conclusions, and recommendations in section 5.4. Our findings are the beginning of the path to reveal the inhibitor impact on asphaltene behavior near a surface, which provides valuable data/trends to design suitable chemical inhibitors.

5.2 METHODOLOGY AND COMPUTATIONAL APPROACH

5.2.1 Molecular Dynamics Simulation

MD simulation is a useful tool for studying biochemical, biomedical, physical, and chemical mechanisms. MD approach can dynamically determine thermodynamics properties, reaction kinetics, and fluid properties in the bulk and at the interface [36]. Recently, different MD tools such as GROMACS, LAMMPS, and Materials Studio have been used to reveal interaction mechanisms in engineering and science cases. In this study, GROMACS is employed for the MD simulation since it is open-source software that includes reliable forcefields (e.g. OPLS/AA forcefield) developed for organic systems such as oil [37].

Molecular model and initial configuration: A calcite slab is formed by splitting calcite along the (104) crystallographic surface of a calcite unit cell using Materials Studio software. The dimensions of the calcite slab are 11.477 nm × 9.275 nm × 2.240 nm, and the developed forcefield by Xiao and co-workers is used to model the calcite surfaces [38]. The pore is constructed by placing one layer of slab on top of the other with a 10 nm pore opening (Figure 5-1). In this research, two asphaltene structures with the continental structure, a dominant type of asphaltene structure [39], are adopted from our previous studies to investigate the formation of hydrogen bonds [40]. Asphaltene 2 (A2) is a continental asphaltene with the potency to form hydrogen bonds due to having hydroxyl and pyridine groups, while asphaltene 3 (A3) is a similar continental asphaltene with no potential for forming hydrogen bonds (Figure 5-2). Also, the impact of two inhibitors, including a surfactant, namely *n*-octylphenol (OP), and an ionic liquid (IL), namely 1-Butyl-3-methylimidazolium chloride, on the asphaltene deposition in the asphaltene/*n*-heptane solution is studied. Avogadro software is used to build the asphaltenes, OP, IL, and *n*-heptane. Similar to our previous studies [40], OPLS/AA forcefield governs the interactions between the atoms. The initial configuration of the molecules in the calcite pore is created using the PACKMOL package by randomly placing the molecules in the calcite pore, considering a 5 Å distance from each slab.

This study considers three sets of simulation runs. The first set comprises a calcite pore with 45 randomly distributed A2 molecules (equal to a 7 wt % concentration) filled with *n*-heptane. Three scenarios, including (1) no inhibitor, (2) addition of 7 wt% of OP, and (3) addition of 7 wt% of IL, are considered for this series. The inhibitor concentration is selected based on the literature review [36, 41-45] and it is realistic since *n*-heptane, a strong asphaltene precipitator, is the only carrying fluid for the asphaltene. The second set of simulations is the same as the first set but A3 is used

instead of A2. The third set of simulations focuses on the A2 and different combinations of OP and IL (i.e., OP-IL = 1:3, 1:1, 3:1). Table 5-1 presents the features/specifications for each run of the simulation run. Note that the number of asphaltene molecules and box dimensions are set to maintain the pressure and temperature at 1 bar and 300 K.

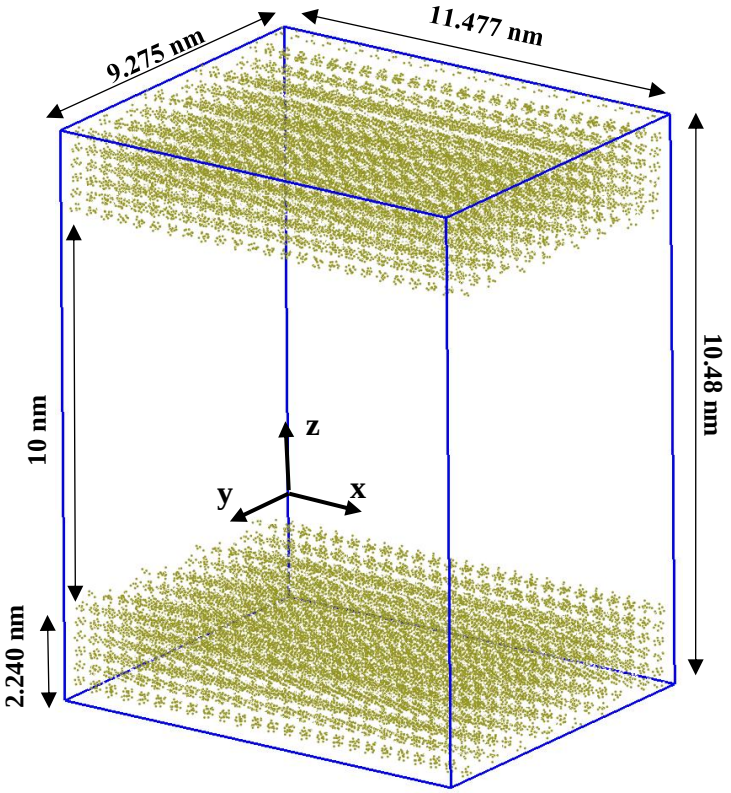

Figure 5-1. The simulation box including the calcite pore (calcite slabs are yellow).

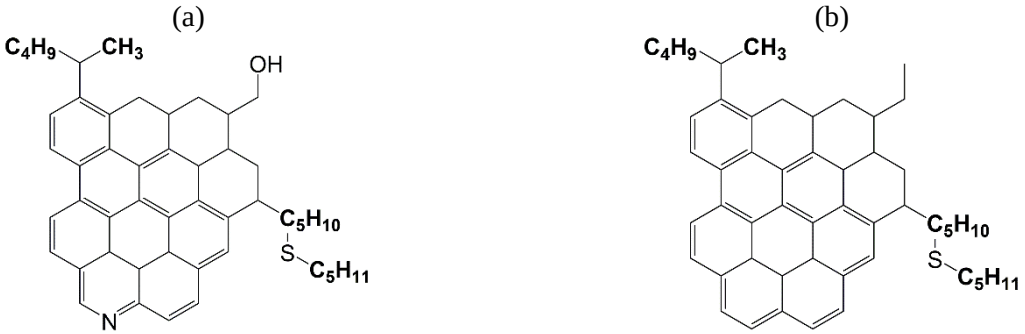

Figure 5-2. Asphaltene structures; (a) asphaltene 2 (A2) with Mw = 730 g/mol and Aromaticity = 0.53, and (b) asphaltene 3 (A3) with Mw = 727 g/mol and Aromaticity = 0.53.

Table 5-1. The number of asphaltene, inhibitor, and precipitant molecules for different systems in a calcite pore.

No.	System name	Number of molecules				
		A2	A3	OP	IL	*n*-heptane
1	A2	45	0	0	0	4356
2	A2/OP	45	0	159	0	4011
3	A2/IL	45	0	0	188	4028
4	A3	0	45	0	0	4338
5	A3/OP	0	45	159	0	4011
6	A3/IL	0	45	0	187	4011
7	A2/OP/IL (1:3)	45	0	40	141	4028
8	A2/OP/IL (1:1)	45	0	80	94	4028
9	A2/OP/IL (3:1)	45	0	119	47	4028

MD simulation process: The simulation begins with the energy minimization of the initial configuration while the calcite molecules are restrained. At this stage, the steepest descent method is adopted for 10000 steps to relax the system by changing the coordination of atoms and avoiding overlap or close placement of the atoms. Then, NVT simulation using velocity rescaling thermostat is run for 100 ps to adjust system temperature to 300 K. Calcite molecules are confined during the NVT simulation. Data sampling based on the NVT and velocity rescaling thermostat at 300 K for 60 ns is the last step. The molecules' position and energy are logged every 10 ps for further analysis at this stage. As an optimal value, the time step is set to 2 fs in the simulations [45]. The particle-mesh Ewald (PME) algorithm governs long-range electrostatic interactions with a cutoff radius of 1.2 nm for both vdW and Coulomb short-range interactions. The flowchart of the simulation workflow is shown in Figure 5-3.

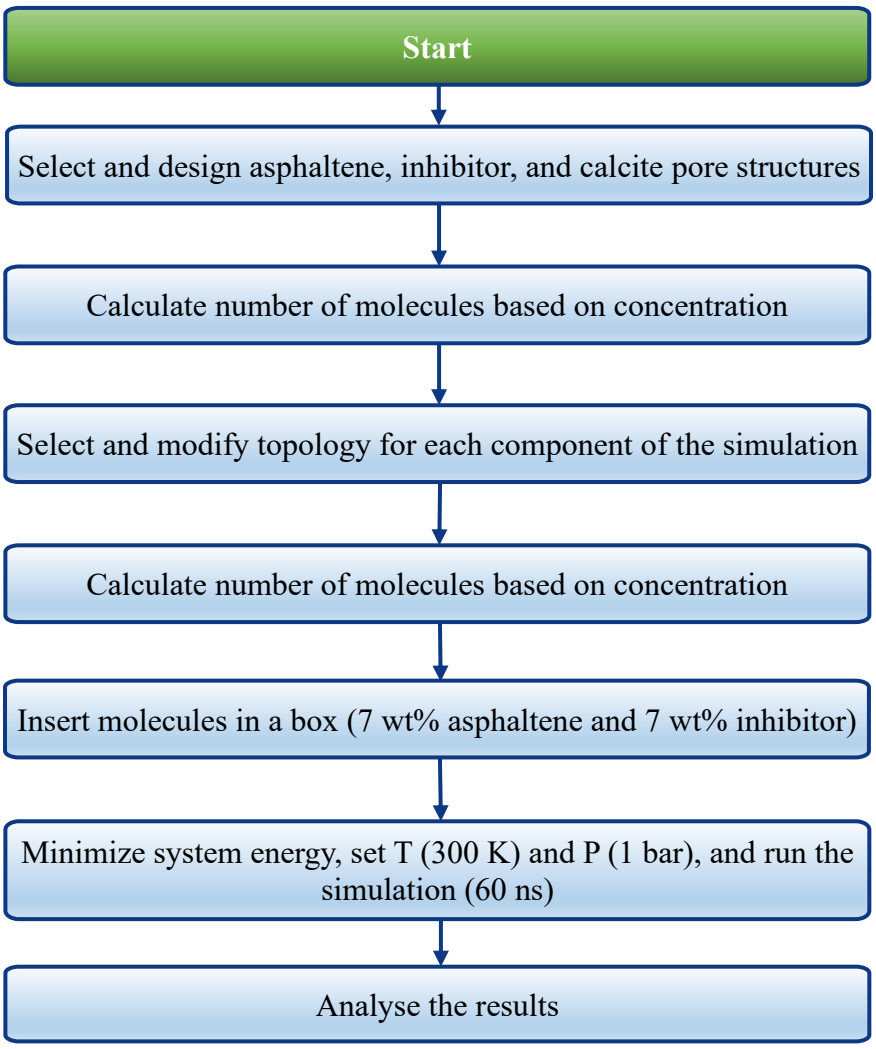

Figure 5-3. The MD simulation workflow.

5.2.2 Statistical and Post-Analysis

This section will describe the methods and tools used to analyze the MD outputs for investigation of the asphaltene-inhibitor behaviors. The primary assessments include but are not limited to asphaltene aggregation, asphaltene deposition rate, deposit compaction, and deposit shape. The GROMACS built-in toolbox and the MDAnalysis package are employed to implement the post-analysis.

Root Mean Square Deviation (RMSD): This parameter compares the location of certain atoms in a molecule to a reference structure and shows how fast the system reaches an equilibrium state

[28]. This parameter can be calculated with a build-in GROMACS toolbox using the least-square fitting of the whole asphaltene structures to the reference structures of the asphaltenes. Equation (1) is used to compute the $RMSD$ [46]:

$$RMSD(t_1, t_2) = \left[\frac{1}{M}\sum_{i=1}^{N} m_i \left|\left|r_i(t_1) - r_i(t_2)\right|\right|^2\right]^{\frac{1}{2}} \quad (5.1)$$

where $M = \sum_{i=1}^{N} m_i$, m shows the atom mass; and $r_i(t)$ denotes the position of atom *i* at the time *t*.

Energy Evaluation: The non-bonded energies between atoms include a repulsion term, a dispersion term, and a Coulomb term. The Lennard-Jones (LJ) energy represents the repulsion and dispersion terms, and the Coulomb energy corresponds to the force between (partially) charged atoms. The reported energies have two parts: sign and magnitude. The negative sign implies the attraction force between substances, and the positive sign means the repulsion force between substances. The magnitude of the energy shows how strong the force is.

Aggregation: The aggregation of the asphaltene molecules can be measured and defined by setting up a criterion for the distance between the asphaltene molecules. The distance between the closest atoms with a cutoff threshold of 0.35 nm is considered the aggregation criterion for asphaltene [40]. The *z*-averaged aggregation number (g_z) quantifies the aggregate size along the simulation time (see Equation (2)). This analysis is implemented with an in-house python script using the MDAnalysis package and the output coordinates of asphaltene molecules after the GROMACS simulation.

$$g_z = \frac{\sum_i n_i g_i^3}{\sum_i n_i g_i^2} \quad (5.2)$$

where n_i stands for the number of the aggregates containing g_i monomers. *i* counter starts from 2 to exclude monomers that do not form an aggregate.

Deposition Rate, Deposit Compaction, and Deposit Shape: Asphaltene molecules can adsorb on the calcite surface either individually or after aggregation, called deposition. This study considers 0.25 nm as a criterion for asphaltene deposition on the surface [28], the distance between the closest atoms of the asphaltene and the calcite surface. The deposition rate is the number of molecules deposited on the surface, either individually or as a part of an aggregate, divided by the total number of asphaltene molecules. This parameter is calculated by extending the in-house prepared scripted python code.

The compaction and shape of deposited asphaltene are the influential factors that show whether the deposits are easy to dislodge, prone to block the pore or have immensely embraced the surface. In the dynamic situation, when the fluid goes through the pores, the drag force can dispatch whole/part of the deposits with low compaction. Also, the deposit shape shows if the deposits are more rounded or flatted, which impacts the rock wettability due to asphaltene deposition. The compaction parameter is calculated using the in-house script, defined as the ratio of the cumulative mass of asphaltenes to the deposited aggregate volume. The "asphericity()" function provided in the MDAnalysis package is adopted to determine the shape of deposited aggregates. The index value is between zero and one; the aggregates' shape is more spherical as the value approaches zero and becomes less spherical (or more linear) as the index value approaches 1.

Asphaltene Distribution Density: This parameter shows the asphaltene molecules' distribution between the calcite layers in each frame. This study measures the asphaltene distribution density using a build-in GROMACS toolbox. In this work, the asphaltene distribution density is reported as an average number of the asphaltene molecules distributed on the x-y plane (Figure 5-1) for the last 30 ns of the simulation time.

Visual Analysis: Observation of asphaltene interaction with surface and inhibitors provides a better understanding of the governing mechanisms. In this paper, the asphaltene molecules and calcite surface are demonstrated along with the inhibitors within a 6 Å distance of the asphaltene molecules at 60 ns. The *n*-heptane molecules are hidden for more clarity. The visual molecular dynamics (VMD) software generates the visual observation of the frames. The calcite, asphaltene, OP, and IL are shown with yellow, gray, red and blue colors in the figures, respectively.

5.2.3 Challenges and Limitations

The forcefields are continuously being enhanced to become more applicable for different molecules and scenarios. However, for particular molecules such as the adopted asphaltenes, the relative parameters (e.g., dihedral interactions) need to be introduced to the software manually from the literature, which is a challenge in our study. Another challenge in MD simulation is that the software's output is only the coordination of molecules and the energy between atoms over the simulation time. This means that any parameters, such as aggregation and deposit shape, need to be calculated using these two parameters in post-analysis. For instance, we had to compose a code in python using the auxiliary MDAnalysis package to determine the aggregation, deposition rate, and the deposits' compaction and shape. Some analyses are packaged in GROMACS software for the post-analysis, such as the calculation of asphaltene distribution density.

Although MD simulation provides vital information on the dominant molecular phenomena, it suffers from several limitations/challenges. Forcefield is the heart of the MD simulation since it defines the bonded and nonbonded forces between atoms in the simulation box. Although the forcefields are applicable for some materials in a range of temperatures and pressures, they are usually tested and reliable to be used for the MD simulation at the room condition [47], which is a limitation for MD strategy. Another barrier during the MD simulation is the computational cost.

It depends on the system size and simulation box, which limits the number of molecules and simulation run time. In this study, the simulation cost is minimized by considering the system equilibrium state and CPU time criteria.

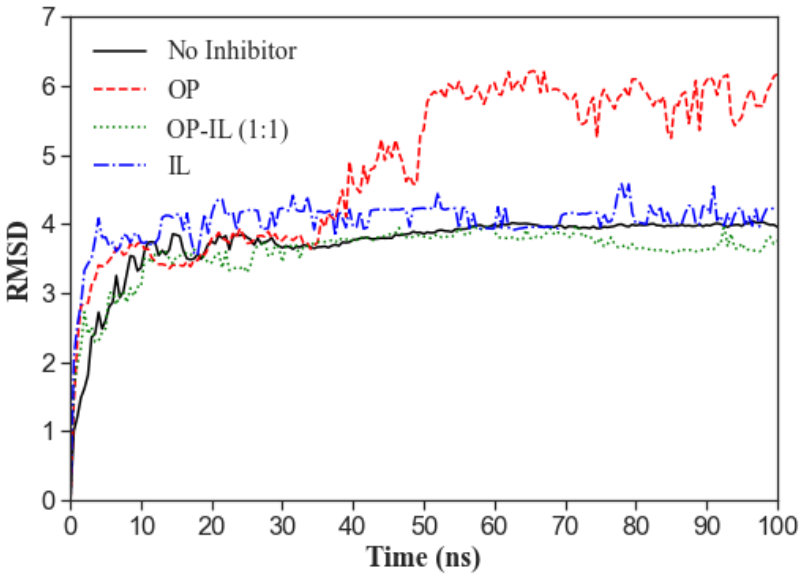

Figure 5-4. Time progression of root-mean-square deviation (RMSD) for A2 systems.

The complex computation of MD simulation requires high CPU usage. Therefore, selecting an optimum simulation time and simulation box is always necessary to reduce the computational cost while having reliable results. This study employs the root-mean-square deviations (RMSDs) analysis to assess the system's equilibrium at four representative systems of A2 in a calcite pore, including no-inhibitor, 7wt% OP, 7wt% IL, and 7wt% OP-IL(1:1). Figure 5-4 demonstrates the RMSD for the selected scenarios in 100 ns. The RMSD index is stabilized, which means the system reaches the equilibrium state after 40 ns for all cases except the one with 7wt% OP. According to Figure 5-4, RMSD for the A2/OP system is also stabilized after 60 ns. The stabilized RMSD implies that the system does not change significantly; this determines the required simulation time. The cases evaluated in Figure 5-4 cover the entire scenarios of this study. Therefore, the reliable and cost-effective simulation is limited to 60 ns for the rest of the study.

5.3 Results and Discussions

The results and discussions section is divided into two parts to study the impact of asphaltene structure and mixing ratio of asphaltene inhibitors on asphaltene deposition on the solid surface. The aggregation, deposition ratio, distribution of asphaltene molecules in the pore, and characteristics of asphaltene deposits are considered to reveal why the inhibitors sometimes behave as a preventer, and sometimes behave as a promoter of asphaltene deposition [16, 17]. In our previous study [40], we validated the application and accuracy of the simulation runs by comparing our simulation results with Headen et al. [26] results. In this study, the asphaltene diffusivity is chosen to validate our simulation results since it is a determining factor in the molecular size and aggregation size of asphaltene [48]. The self-diffusivity of asphaltene both in bulk and near calcite surface has been reported in similar MD simulations [30, 48, 49], which are in agreement with experimental data [50]. The asphaltene's diffusivity depends on the structure, molecular weight, and polarity of the molecules [30], and it reduces with increasing the asphaltene concentration [50]. The literature shows that the 2D diffusion coefficient of asphaltene near calcite surface in *n*-heptane and toluene solution is in the range of 0.19-0.93 × 10^{-10} m^2/sec [30, 49] and 0.075-1.34 × 10^{-10} m^2/sec [48], respectively. The current study reveals that the diffusion coefficient values for A2 and A3 in *n*-heptane and xy-direction are 0.85 × 10^{-10} m^2/sec and 1.1 × 10^{-10} m^2/sec, respectively, which are in acceptable ranges.

5.3.1 Impact of Asphaltene Structure on Inhibitors' Efficiency in Calcite Pore

This part is dedicated to study the impact of hydroxyl and pyridine group presence in asphaltene structure during the asphaltene deposition inhibition. Therefore, two asphaltenes with similar structures are built, one with the mentioned functional groups and the other one without the functional groups.

A2 deposition in the presence of inhibitors: Figure 5-5a shows the aggregation of asphaltene molecules during the simulation in three conditions, including no inhibitor, 7 wt% OP, and 7 wt% IL. In the absence of an inhibitor, the A2 molecules aggregate in the first few nanoseconds, and the aggregation stays stable during the simulation. The immediate surge of the deposition rate to one demonstrates rapid deposition and stability of the deposited molecules (Figure 5-5b). The visual observation of the aggregates for A2 in the last frame of the simulation (Figure 5-6) illustrates no monomer deposited on the surface, which confirms the fact that the asphaltene molecules aggregate in the fluid bulk and then deposit on the surface, as claimed by Ji et al. [29]. The LJ and Coulomb energies both show strong attraction for the asphaltene-asphaltene (LJ = -6990.39 kJ/mol and Coulomb = -1878.38 kJ/mol) and asphaltene-calcite (LJ = -1459.05 kJ/mol and Coulomb = -2223.83 kJ/mol); both are reported in Table 5-2, along with the strong asphaltene repulsion from *n*-heptane, which reveals the immediate deposition and stability of asphaltene molecules on the calcite surface.

The presence of OP in the system results in hydrogen bond formation between the asphaltene and OP. The OP tails create the hindrance layer around the asphaltenes and interfere with the quadrupole-quadrupole interaction between the asphaltene cores. Thus, asphaltene aggregation significantly decreases compared to the case without OP (Figure 5-5a). Figure 5-5b demonstrates that the deposition rate declines to less than half when OP is added. The main reason for reducing the deposition rate is the adsorption of OP molecules on the calcite surface from their polar side and the prevention of asphaltene molecules to approaching and depositing on the surface. The energy evaluation confirms that the adsorption energy between the asphaltenes does not decrease after OP addition, while the LJ and Coulomb adsorption energies for the asphaltene-calcite reduce to -1030.41 kJ/mol and -1206.29 kJ/mol (see Table 5-2). The visual observations, shown in Figure

5-6 (no inhibitor) and Figure 5-7 (with OP), prove that fewer asphaltenes are adsorbed on the surface when the inhibitor is added. Figure 5-5c presents the average distribution of asphaltene molecules between two calcite layers in the last 30 ns of the simulation. It shows that the asphaltene molecules are mostly populated near the surfaces when there is no inhibitor in the system. In contrast, adding OP decreases the possibility of asphaltene molecules to locate near the surface, and the graph becomes multi-modal with two peaks near the surface and the third peak at the middle of the pore. In other words, asphaltene aggregates stay suspended in the middle of the pore and are repelled from the surface.

Figure 5-5a illustrates that the IL reduces the asphaltene aggregation rate; however, it finally causes more aggregation compared to the case with no inhibitor addition. As expected, the IL attaches to the asphaltene cores and reduces the asphaltene self-aggregation [51], which is supported by the energy evaluation. The LJ and Coulomb adsorption energies for the asphaltene-asphaltene approximately decrease by 1500 kJ/mol and 300 kJ/mol units compared to the case without inhibitor. Although the IL molecules adsorb on the calcite surface, they do not lower the asphaltene deposition effectively (Figure 5-5b), due to the short length of their hydrocarbonic tail [52]. This claim is also supported by the energy evaluation as the LJ and Coulomb energies between the asphaltene-calcite do not change compared to the case without inhibitor (Table 5-2). Therefore, the asphaltene adsorbs on the surface before self-aggregation occurs in the pore, confirming the low aggregation at the beginning of the simulation. However, the high deposition rate and the potency of asphaltene to self-aggregate through hydrogen bond would lead to higher but unstable aggregation for the second half of the simulation (Figure 5-5a).

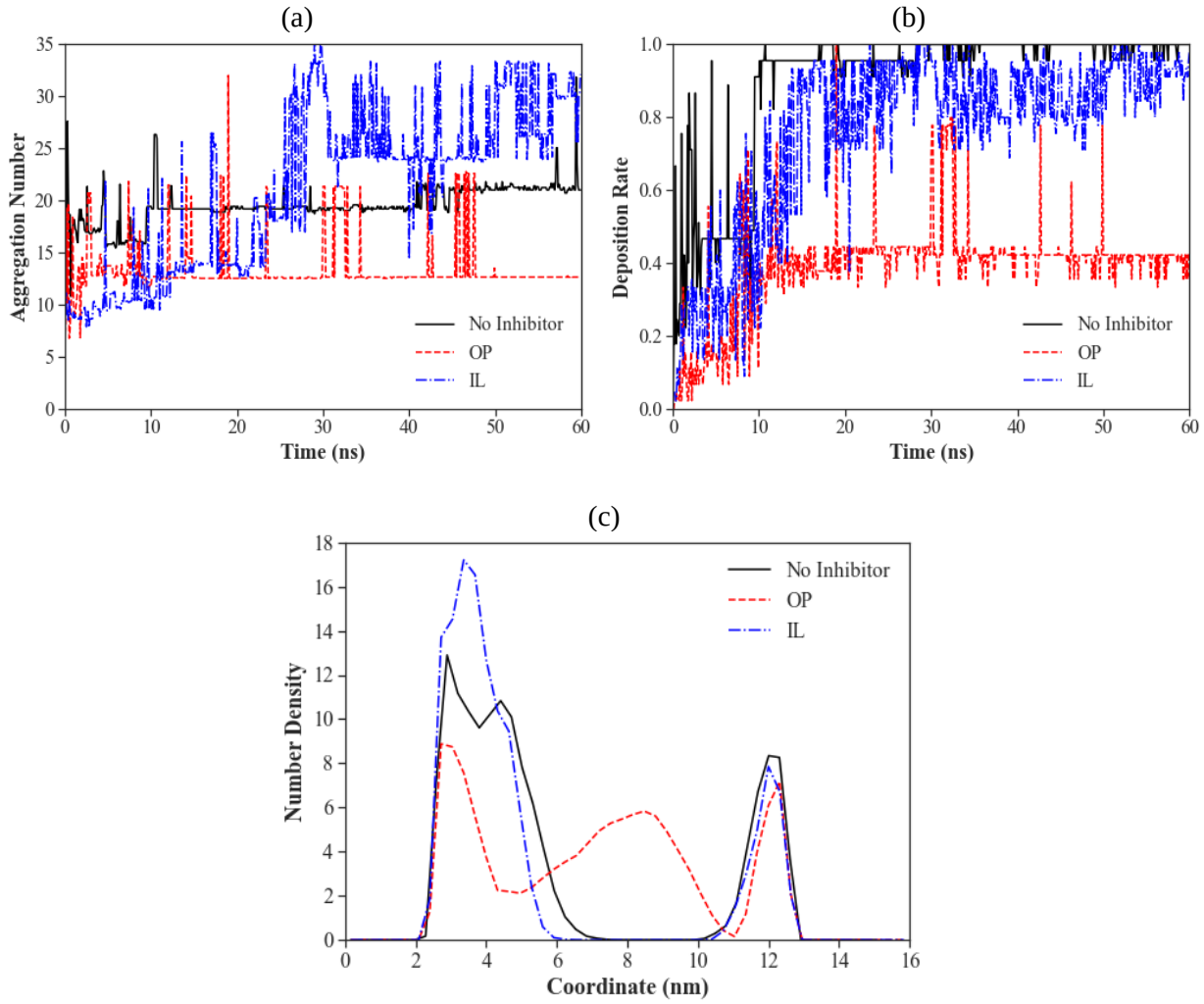

Figure 5-5. (a) aggregation and (b) deposition rates of A2, and (c) the average density distribution of A2 for the last 30 ns of the simulation.

The average distribution of the asphaltene molecules in the last 30 ns (see Figure 5-5c) demonstrates a greater population of asphaltene molecules near the calcite surface in the presence of IL compared to the case with no inhibitor. This means that the asphaltenes cover a larger surface area, compared to other cases. The deposition of the asphaltenes on the wide surface of calcite could change the calcite's wettability [34]. The deposits will hardly be dislodged, even partly in the dynamic situation when they are uniformly attached to the surface directly. Figure 5-8 displays

the asphaltene molecules in the last frame of the simulation; it confirms the high deposition of the thin asphaltene layer near the calcite surface.

The compaction and shape of deposited aggregates are the important factors to show the possibility of deposits to pile up, leading to pore closure or deposits dislodgement in a dynamic system. The probability density of the deposited aggregates compaction during the simulation shows that the deposited aggregates are denser when the OP is present in the system compared to the case with no inhibitor (Figure 5-9a). Indeed, the OP deactivates the hydrogen bonding between the asphaltene molecules, and the only active force between the asphaltene molecules is the quadrupole-quadrupole interaction, which results in the formation of denser deposits. The deposited aggregates in the presence of IL are looser than the case without an inhibitor (Figure 5-9a). This justifies the ability of IL to interfere the quadrupole-quadrupole interaction since the cation-quadrupole interaction will be dominant [34, 52]. The analysis of deposited aggregate shape (Figure 5-9b) reveals that the deposited aggregate shape does not change significantly when OP is in the system compared to the case without an inhibitor. The IL presence shifts the probability of the deposited aggregate shape toward one, meaning that the deposits are more stretched and have a lesser spherical shape. The shape analysis agrees with the previous analysis and confirms the potential of deposits to cover the calcite surface and change the surface wettability in the presence of IL.

Table 5-2. Average LJ and Coulomb energies in the last 10 ns of simulations for A2 in the presence/absence of 7wt% inhibitors.

Energy (kJ/mol)	No inhibitor		With OP		With IL	
	A2-Cal	A2-A2	A2-Cal	A2-A2	A2-Cal	A2-A2
LJ	-1459.05	-6990.39	-1030.41	-7019.36	-1390.73	-5528.09
Coulomb	-2223.83	-1878.38	-1206.29	-1903.07	-1927.28	-1598.44

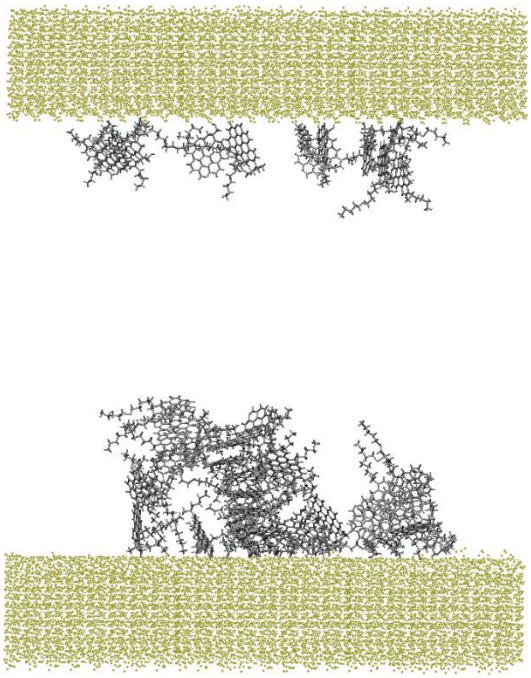

Figure 5-6. Screenshot of the asphaltene molecules' coordination for A2 without inhibitor at 60 ns.

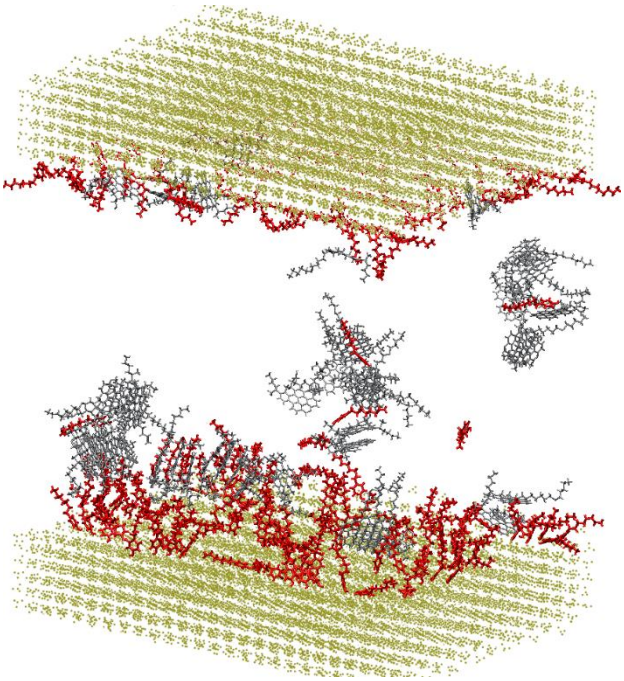

Figure 5-7. Screenshot of the asphaltene molecules' coordination for A2 with 7 wt% OP at 60 ns. All inhibitors are shown.

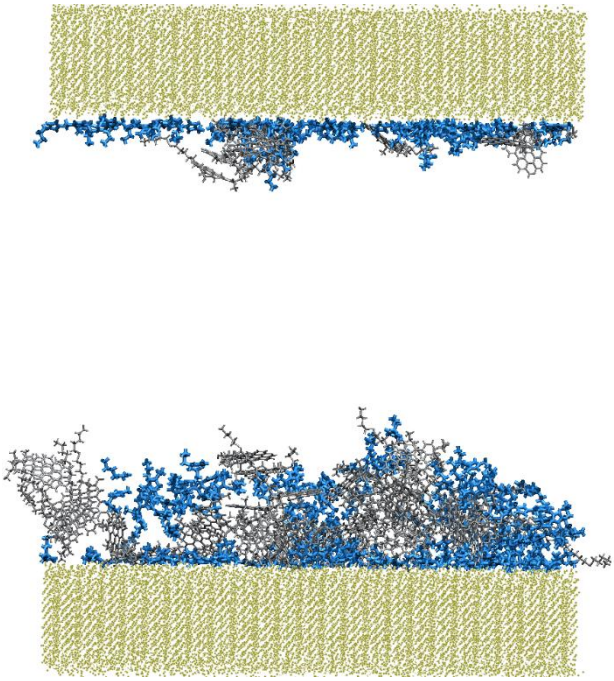

Figure 5-8. Screenshot of the asphaltene molecules' coordination for A2 with 7 wt% IL at 60 ns. All inhibitors are shown.

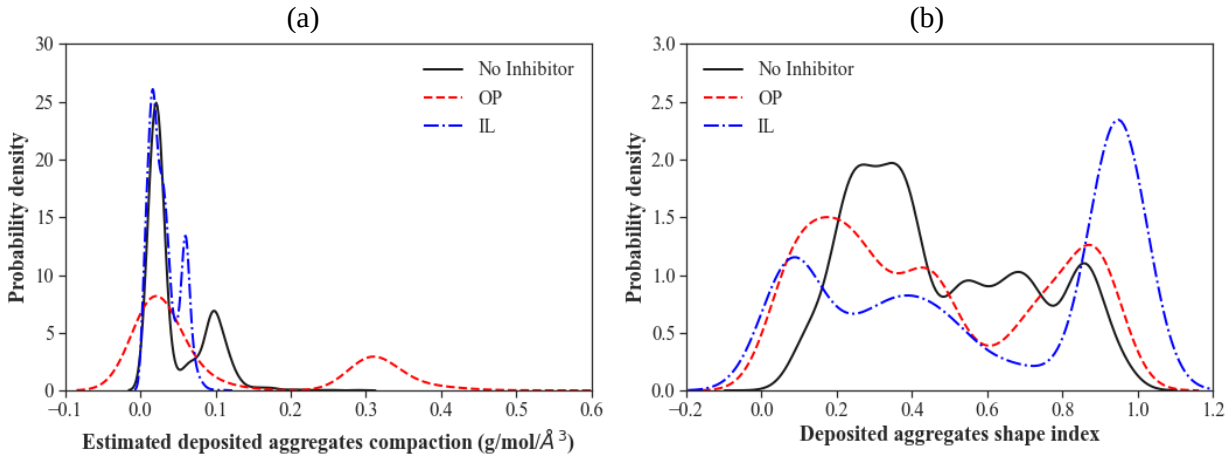

Figure 5-9. The probability density of (a) deposited aggregates compaction and (b) deposited aggregates shape for A2 in the absence/presence of inhibitors.

A3 deposition in the presence of inhibitors: A3 does not have hydroxyl and pyridine groups; it implies that the asphaltene molecules are not able to form hydrogen bonds. Thus, a lower self-aggregation rate is expected for the A3 than the A2 when no inhibitor exists in the system (black line in Figure 5-5a and Figure 5-10a). Also, the asphaltene-asphaltene energy evaluation for the A3 reveals that the LJ energy is the attraction type (negative sign), and the Coulomb energy is the repulsive type (positive sign), unlike the A2 in which both LJ and Coulomb energies are negative and in favour of asphaltene self-aggregation (Table 5-2 and Table 5-3). The deposition rate of A3 is also less than A2 due to the lack of heteroatoms in the asphaltene structure (Figure 5-5b and Figure 5-10b). Although the asphaltene-calcite LJ energy is similar for both cases, the asphaltene-calcite Coulomb energy for A3 is less than half compared to the similar energy for A2 (Coulomb asphaltene-calcite: A2=-2223.83 kJ/mol and A3= -1033.31 kJ/mol). The absence of nitrogen and oxygen in the asphaltene structure reduces the dipole moment of asphaltene molecules and the potency of hydrogen bonding. Note that the dipole moments of A2 and A3 are 4.44 and 1.2 Debye, respectively [40].

OP addition decreases the asphaltene aggregation in the early time of the simulation (Figure 5-10a). However, the OP-asphaltene bond is not stable due to the absence of hydrogen bonds. Hence, the asphaltene-asphaltene bonding eventually becomes dominant in the last 10 ns of the simulation. OPs prefer to sit on the calcite surface, provide steric hindrance layer near the surface and impact the asphaltene deposition on the surface (Figure 5-10b). The IL reduces the quadrupole-quadrupole interaction between the asphaltenes. The IL- asphaltene bond is weaker for A3 than A2 due to the lower asphaltene dipole moment [40]. Therefore, the IL cannot effectively inhibit asphaltene aggregation before deposition for the A3 case and the aggregation number for the case with IL is slightly lower than the case without inhibitor (Figure 5-10a). The asphaltene deposition rate is also high when IL is added, the reason is even if the ILs sit on the surface, they are not able to provide the steric hindrance layer considering the short length of the IL's hydrocarbonic tail (Figure 5-10b). The average distribution of asphaltene molecules in the calcite pore is illustrated in Figure 5-10c. The figure shows that asphaltene molecules are adsorbed near the calcite surfaces in all cases. OP addition has slightly reduced the asphaltene thickness near one side of the pore and shows the possibility of asphaltene presence in the middle of the pore. The reason is the Ops sit on the surface and repeal asphaltenes. The asphaltene molecules are piled up and form a thicker layer in the presence of ILs compared with two other cases. It shows that the ILs interfere the asphaltene aggregation, but they cannot effectively reduce the A3 deposition. The results of Boukherissa et al. [52] 's study also confirm that IL molecules need to have a cation equipped with an alkyl tail that has the minimum of eight carbon to effectively interrupt asphaltene aggregation. Moreover, the application of IL increases the risk of pore closure when there are enough asphaltene molecules in the system.

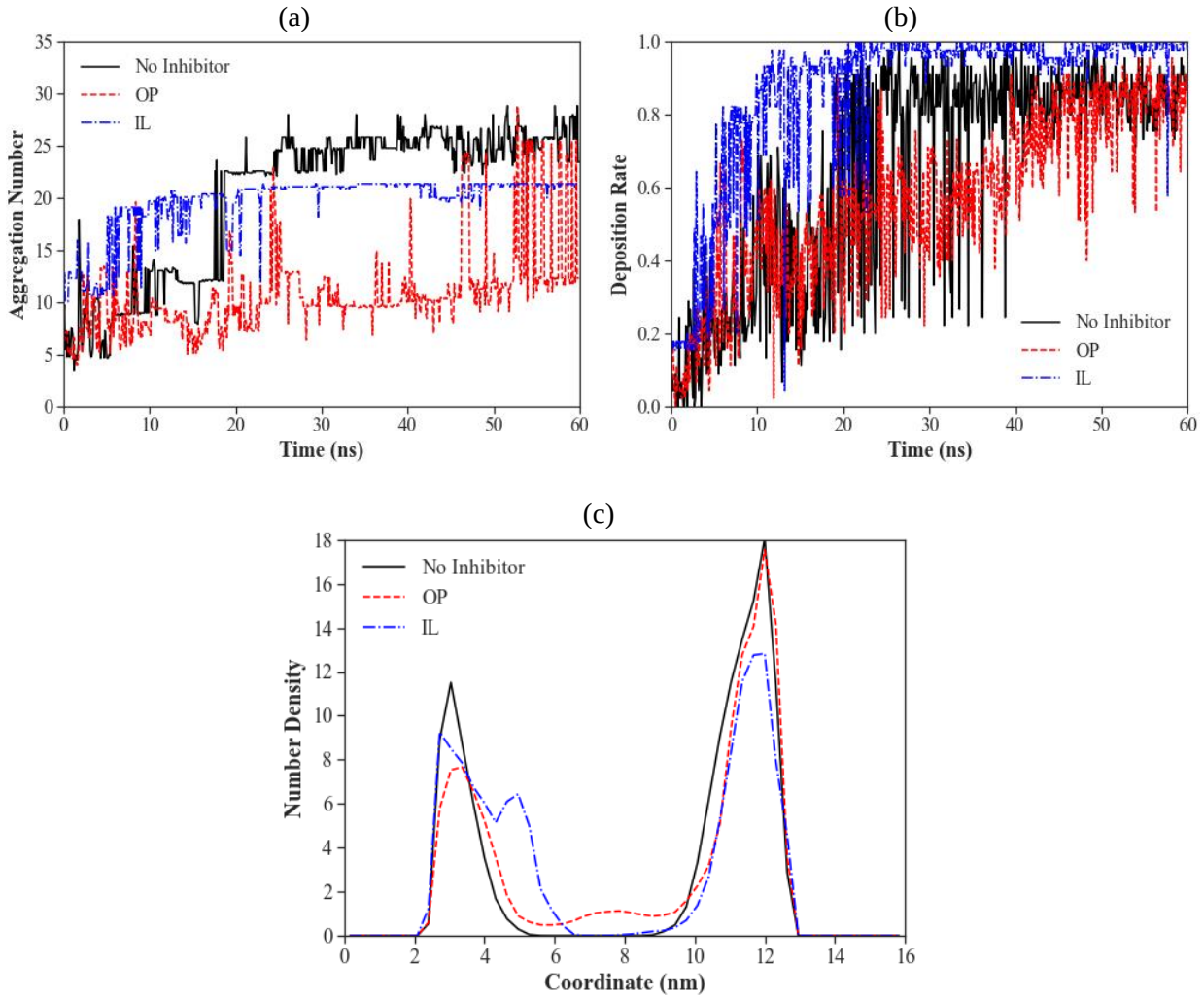

Figure 5-10. (a) aggregation and (b) deposition rate of A3 and (c) the average density distribution of A3 for the last 30 ns of the simulation.

Table 5-3. Average LJ and Coulomb energies in the last 10 ns of simulations for A3 in the presence/absence of 7wt% inhibitors.

Energy (kJ/mol)	No inhibitor		With OP		With IL	
	A3-Cal	A3-A3	A3-Cal	A3-A3	A3-Cal	A3-A3
LJ	-1509.56	-6734.79	-1724.06	-5751.63	-1612.39	-6176.21
Coulomb	-1033.31	8024.67	-1141.90	8029.72	-708.49	8000.53

Figure 5-11a depicts the probability of the deposited aggregates compaction for A3. It demonstrates that the presence of OP and IL results in forming asphaltene deposits with very low

compaction. Since the parallel stacking is the main aggregation mechanism for A3, IL can inhibit their aggregation more effectively. Therefore, the probability density of aggregate with lower compaction is higher in case of IL addition compared with the OP addition. Furthermore, although the asphaltene deposits pile up in the presence of IL, they are probable to be dispatched as a whole or part in the dynamic system due to weak connection. Figure 5-11b illustrates that the aggregates become more spherical than no inhibitor case, when the OP and IL are present in the system. ILs demonstrate higher impact on breaking the rod-like aggregates to sphere-like due to their interfering mechanisms to the asphaltene parallel stacking. As the deposits become more rounded, they have less contact with the surface and are easy to dispatch. Therefore, adding inhibitors to A3 does not reduce the deposition significantly; but, it makes the deposits unstable and fragile, which can be dragged out of the pore in a dynamic situation.

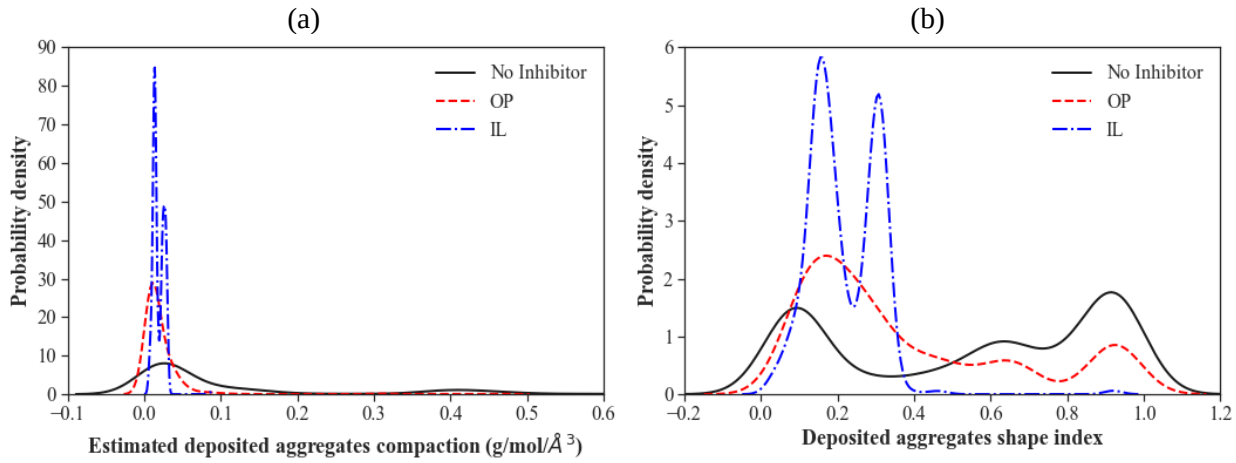

Figure 5-11. The probability density of (a) deposited aggregates compaction and (b) deposited aggregates shape for A3 in the absence/presence of inhibitors.

5.3.2 Impact of Inhibitor Combination on Asphaltene Damage in Calcite Pore

This part investigates the effect of the coexistence of inhibitors with various ratios on asphaltene aggregation and deposition. A2 is selected for further analysis as it has higher dipole moment and functional groups including hydroxyl and pyridine. A2 interacts with IL and OP more effectively

toward the aggregation prevention. Three systems which carry combined OP-IL inhibitors with 1:3, 1:1, and 3:1 ratios are simulated. The cumulative inhibitor concentration is 7 wt%, and the results are compared to 7 wt% sole OP. The detailed numbers of molecules in each system can be found in Table 5-1.

Aggregation and deposition of A2: Figure 5-12 indicates that adding a non-equal ratio of the inhibitors (OP-IL with 3:1 and 1:3) to the A2/*n*-heptane results in the lower asphaltene aggregation, even compared to the case with OP only. The deposition rate evaluation shows a high deposition rate with high instability for all cases except for the cases of 3:1 OP-IL and OP (Figure 5-13), which is also proved by visual observation (see Figure 5-16). The low aggregation and low deposition rate make the 3:1 OP-IL an effective ratio. In this case, the IL is able to interfere with the quadrupole-quadrupole force between the asphaltenes effectively, and the number of OP molecules is enough to interfere with the asphaltene self-aggregation by forming hydrogen bonds. At the same time, the rest of OP molecules attach to the calcite surface and cause the steric layer near the calcite surface to restrict asphaltene from approaching the surface.

Figure 5-12 and Figure 5-13 demonstrate that the aggregation and deposition increase significantly when the system hosts an equal ratio of the inhibitors (OP-IL, 1:1). Nevertheless, the energy evaluation noted in Table 5-4 shows that the LJ and Coulomb attraction energies for the asphaltene-calcite are reduced to -588.37 and -713.36, respectively. The low attraction energies for the asphaltene-calcite, and the high aggregation and deposition imply the indirect deposition and aggravation of the asphaltenes on the surface. The visualization of the simulation for the last frame (seen in Figure 5-17) proves the indirect deposition and aggravation. Although the aggregation and deposition reveal the inefficiency of OP-IL at an equal ratio, the presence of

inhibitors reduces the deposition forces significantly; this ratio can be efficient if the deposited aggregate experiences low compaction.

Table 5-4. Average LJ and Coulomb energies in the last 10 ns of simulations for A2 in the presence/absence of 7wt% inhibitors.

Energy	OP		OP-IL (3:1)		OP-IL (1:1)		OP-IL (1:3)	
(kJ/mol)	A2-Cal	A2-A2	A2-Cal	A2-A2	A2-Cal	A2-A2	A2-Cal	A2-A2
LJ	-1030.41	-7019.36	-1763.53	-5247.76	-588.37	-5695.61	-1469.59	-5195.00
Coulomb	-1206.29	-1903.07	-2242.33	-1501.04	-713.36	-1618.98	-1764.32	-1596.06

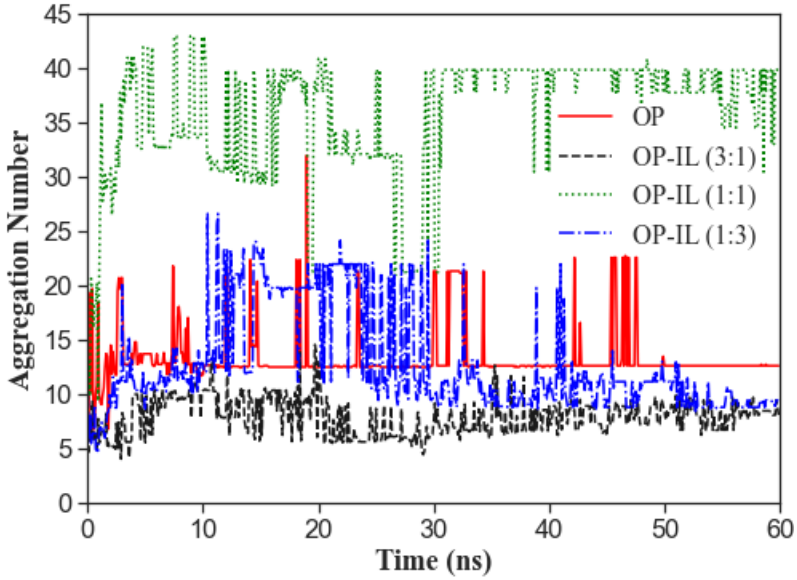

Figure 5-12. The aggregation number of A2 with various ratios of OP-IL in the calcite pore.

Figure 5-14 depicts the average distribution of the asphaltene molecules between two calcite layers for the last 30 ns of the simulation. The non-equal ratios of inhibitors show the highest possibility of asphaltene to locate near the surface. The graph for the 1:3 OP-IL is multi-modal, which displays a considerable density number drop in the middle of the pore. The graph for the 3:1 OP-IL is bi-modal with the potential of a deposit pile on one side. The big gap in the middle of the pore discards the potency of pore blockage at the 3:1 ratio. Figure 5-16 and Figure 5-18 also confirm the claim visually. The equal OP-IL ratio (1:1) shows the possibility of the asphaltene molecules presence near one surface and a monotonic density number in the range of 2 - 4 between the surfaces. In other words, the asphaltene molecules would pill up and block the pore spaces. This analysis

confirms the high aggregation and deposition with the potential pore blockage as noticed in the previous analysis.

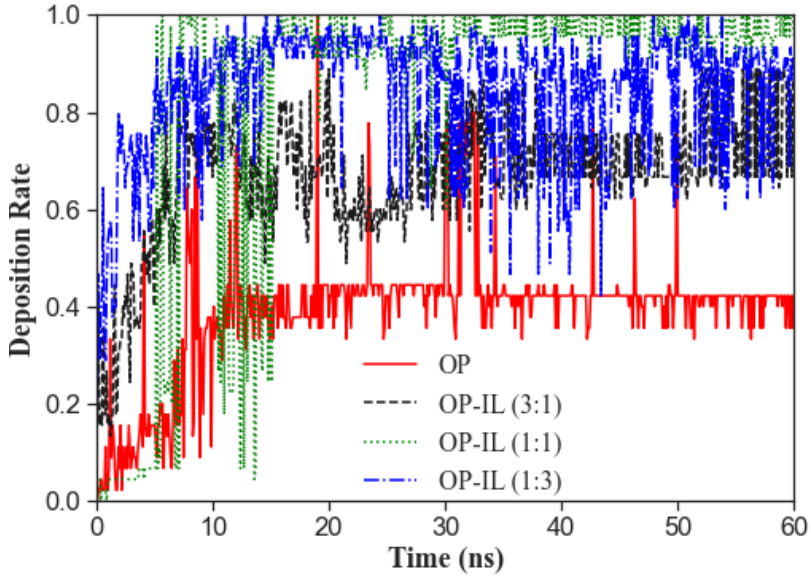

Figure 5-13. The deposition rate of A2 to the calcite pore with different ratios of OP-IL.

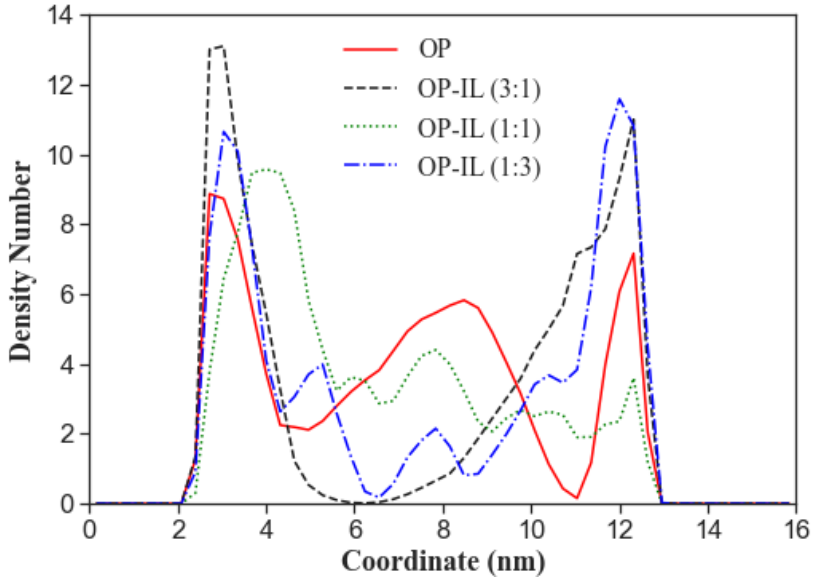

Figure 5-14. Average density distribution of A2 with various ratios of OP-IL in the last 30 ns of the simulation.

Compaction and shape of the deposited A2: Figure 5-15a displays that the compaction of deposited aggregate becomes unimodal with significantly low compaction for the 3:1 OP-IL scenario. It becomes multi-modal for the 1:3 OP-IL case with all peaks below 0.1 g/mol/Å^3.

Therefore, the deposited aggregates are not compacted when a non-eqaul ratio of OP-IL is added, which may allow the deposits to be partially separated in dynamic situations. On the other hand, the deposited aggregates compaction is bimodal for the 1:1 OP-IL, similar to the only OP with peaks at 0.045 and 0.17 g/mol/Å^3. The compacted deposits are hard to break even with the drag force. The deposited aggregate shape has a multi-modal nature in all cases, as shown in Figure 5-17. The deposits in the 3:1 OP-IL and 1:1 OP-IL cases have more tendency to become spherical, which offers the low possibility of deposits to change the calcite wettability. Nevertheless, the deposit shape for the 1:3 OP-IL is bimodal, with peaks at 0.2 and 1, showing the tendency of the deposits to be more rod-like. Therefore, the addition of 3:1 OP-IL inhibitor will make the deposits with low compaction and more spherical shape, while the rest of the cases have the disadvantage of having deposits with high compaction or deposits spread out on the surface.

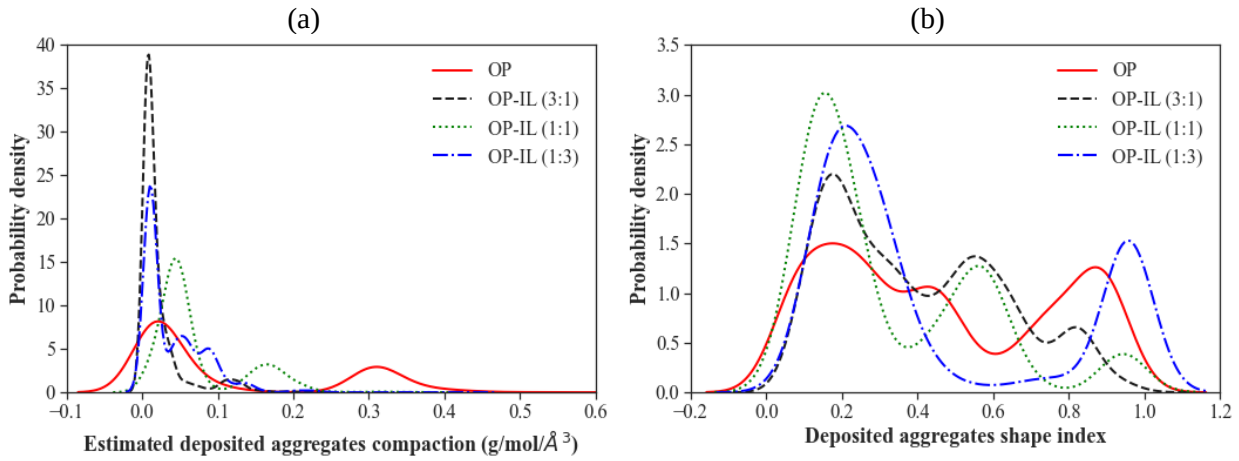

Figure 5-15. The probability density of (a) deposited aggregates compaction and (b) deposited aggregates shape for A2 with various ratios of OP-IL.

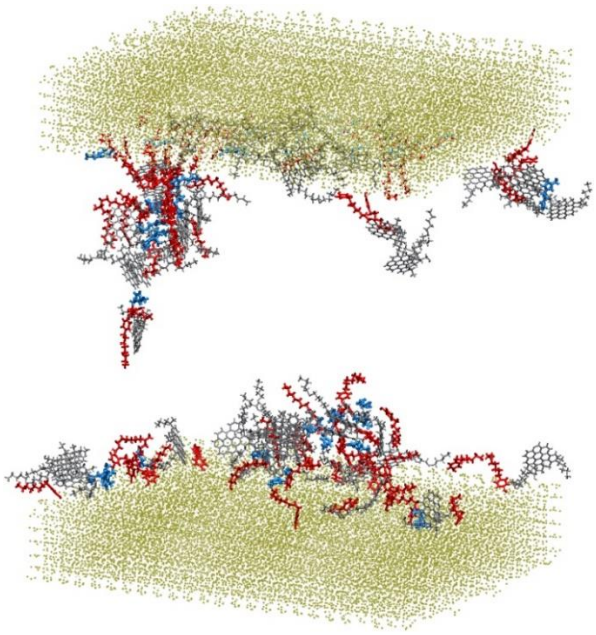

Figure 5-16. Screenshot of the asphaltene molecules' coordination for A2 with OP:IL (3:1) at 60 ns. The inhibitors with the distance of less than 6 Angstrom from A2 are shown.

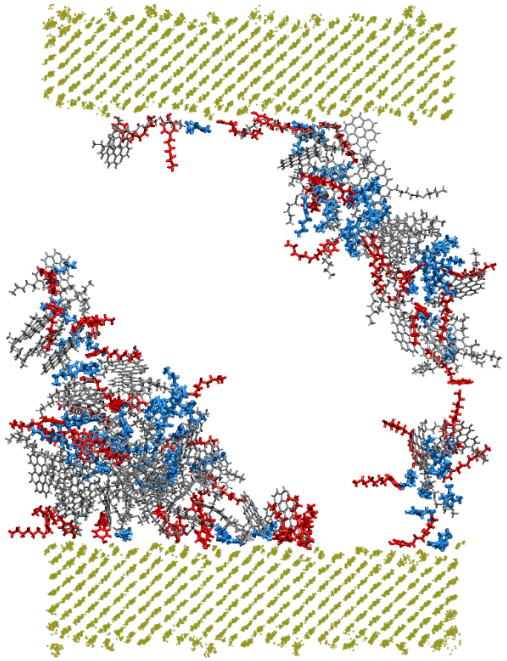

Figure 5-17. Screenshot of the asphaltene molecules' coordination for A2 with OP:IL (1:1) at 60 ns. The inhibitors with the distance of less than 6 Angstrom from A2 are shown.

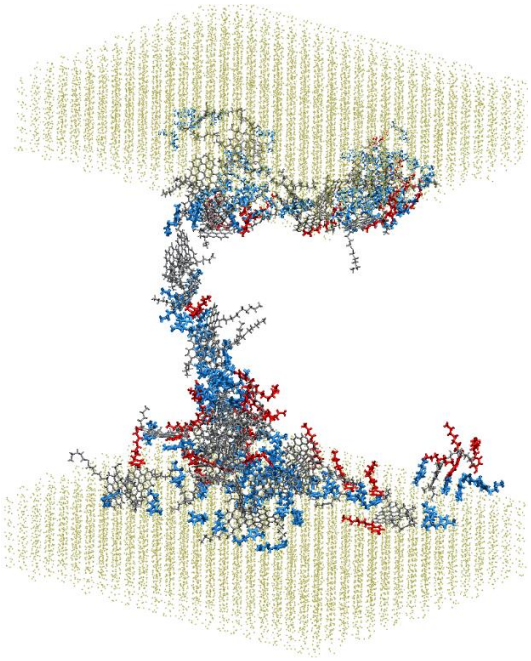

Figure 5-18. Screenshot of the asphaltene molecules' coordination for A2 with OP:IL (1:3) at 60 ns. The inhibitors with the distance of less than 6 Angstrom from A2 are shown.

5.4 CONCLUSIONS

This study explores the dominant inhibitory mechanisms considering the importance of asphaltene structure and the ratio of inhibitors' combination during the asphaltene deposition in a calcite pore. Two asphaltene structures with the difference in the potential of forming hydrogen bonds and two inhibitors, including a surfactant (*n*-octylphenol) and an ionic liquid (1-Butyl-3-methylimidazolium chloride), are adopted to accomplish the goal of this study. The principal findings of this study are summarised as follows:

- When there is no inhibitor added to the systems, the LJ and Coulomb energies for asphaltene-asphaltene are the attraction types for A2, while for A3 the Coulomb energy is a repulsive type due to lack of hydroxyl and pyridine groups.
- The lack of hydroxyl and pyridine groups in A3 compared to A2 eliminates the potency of asphaltene to form the hydrogen bonds and reduces the dipole moment of the A3.
- OP forms a hydrogen bond with asphaltenes and keeps the asphaltenes separated and suspended. The lack of hydrogen bonding potency in the asphaltene lowers the inhibitory effect of OP.
- The OP reduces the asphaltene aggregation and deposition. It forms hydrogen bonds with the asphaltenes and provides the steric layer, preventing the asphaltene self-aggregation. OP also adsorbs on the calcite surface from their polar head and prevents the asphaltene monomers/aggregates from adsorbing on the calcite surface.
- The MD simulation results show that the IL attaches to asphaltene with a different mechanism than OP. IL forms a cation-quadrupole bond with the asphaltene polyaromatic core and copes with the quadrupole-quadrupole interaction between the asphaltenes.

Although IL molecules adsorb to the calcite surface, they cannot stop the asphaltene deposition, since they do not have carbon tails with enough length.

- The lower dipole moment decreases the superiority of the cation-quadrupole interaction between the asphaltenes and IL against the quadrupole-quadrupole interaction between the asphaltene molecules.
- The potential of ILs to lower the asphaltene self-aggregation and inability of IL to completely prevent asphaltene deposition due to short alkyl tail impose the asphaltene to deposit on a vast surface of calcite. It could possibly change the wettability of the surface.
- The addition of non-equal ratios of OP-IL results in the lowest aggregation, and the addition of 3:1 OP-IL leads to a considerable deposition reduction. The deposited aggregates are spherical and loosely compacted. This implies they may separate when there is a flow.
- The addition of 1:1 OP-IL reduces the asphaltene-calcite adsorption energies to one-third compared to the case with no inhibitor, while the asphaltenes can still self-aggregate with high adsorption energy (LJ = -5695.61 kJ/mol and Coulomb = -1618.98 kJ/mol). Hence, the asphaltenes pile up with the risk of pore blockage.

The different behaviors of two asphaltene structures in the presence of inhibitors show the importance of asphaltene structure during the asphaltene deposition. This research helps further understand interactions between the asphaltene and inhibitors during asphaltene deposition. We highly recommend scholars continue this study and demystify the impact of thermodynamic condition alteration such as pressure during the inhibition process. We also recommend studying the impact of surface type on the asphaltene deposition mechanisms in the presence of inhibitors. It opens a path to use molecular-level simulation to design the chemical inhibitor and better

implement the prevention of asphaltene deposition. This method can help researchers, engineers, and companies screen the potential chemicals before conducting laboratory experiments, making the procedure cost-effective and efficient.

ACKNOWLEDGEMENTS

The financial support of InnovateNL, Memorial University, and the Natural Sciences and Engineering Research Council of Canada (NSERC) is acknowledged. We would also like to thank Dr. Sohaib Mohammed for his help in preparing the calcite surface.

REFERENCES

1. Zendehboudi, S., *Asphaltenes Review: Characterization and Modeling.* Fuels and Lubricants Handbook: Technology, Properties, Performance, and Testing, 2019: p. 39-77.
2. Tazikeh, S., et al., *Effects of asphaltene structure and polythiophene-coated magnetite nanoparticles on surface topography and wettability alteration of silica surface.* Journal of Molecular Liquids, 2022: p. 118470.
3. *Asphaltene Deposition Control by Chemical Inhibitors: Theoretical and Practical Prospects*, A. Ghamartale, et al., Editors. 2021, Gulf Professional Publishing.
4. Kashefi, S., et al., *A new polymeric additive as asphaltene deposition inhibitor in CO 2 core flooding.* Korean Journal of Chemical Engineering, 2016. **33**(11): p. 3273-3280.
5. Karambeigi, M.A., M. Nikazar, and R. Kharrat, *Experimental evaluation of asphaltene inhibitors selection for standard and reservoir conditions.* Journal of Petroleum Science and Engineering, 2016. **137**: p. 74-86.
6. Hashemi, S.I., et al., *On the application of NiO nanoparticles to mitigate in situ asphaltene deposition in carbonate porous matrix.* Applied Nanoscience, 2016. **6**(1): p. 71-81.

7. Madhi, M., R. Kharrat, and T. Hamoule, *Screening of inhibitors for remediation of asphaltene deposits: Experimental and modeling study.* Petroleum, 2017.

8. Monjezi, E., et al., *New application of henna extract as an asphaltene inhibitor: an experimental study.* Asia-Pacific Journal of Chemical Engineering, 2016. **11**(6): p. 1027-1034.

9. Piro, G., et al., *Asphaltene adsorption onto formation rock: an approach to asphaltene formation damage prevention.* SPE Production & Facilities, 1996. **11**(03): p. 156-160.

10. Betancur, S., et al., *Role of particle size and surface acidity of silica gel nanoparticles in inhibition of formation damage by asphaltene in oil reservoirs.* Industrial & Engineering Chemistry Research, 2016. **55**(21): p. 6122-6132.

11. Franco, C.A., et al., *Nanoparticles for inhibition of asphaltenes damage: adsorption study and displacement test on porous media.* Energy & Fuels, 2013. **27**(6): p. 2899-2907.

12. Kuang, J., et al., *Assessment of the performance of asphaltene inhibitors using a multi-section packed bed column.* Fuel, 2019. **241**: p. 247-254.

13. Al Sultan, A., et al., *Effect of the Surfactant on Asphaltene Deposition on Stainless-Steel and Glass Surfaces.* Energy & Fuels, 2018. **32**(4): p. 5635-5642.

14. Kazemzadeh, Y., et al., *Behavior of asphaltene adsorption onto the metal oxide nanoparticle surface and its effect on heavy oil recovery.* Industrial & Engineering Chemistry Research, 2015. **54**(1): p. 233-239.

15. Lin, Y.-J., et al., *Characterizing Asphaltene Deposition in the Presence of Chemical Dispersants in Porous Media Micromodels.* Energy & Fuels, 2017. **31**(11): p. 11660-11668.

16. Barcenas, M., et al., *Study of medium effect on asphaltene agglomeration inhibitor efficiency.* Energy & Fuels, 2008. **22**(3): p. 1917-1922.

17. Smith, D.F., et al., *Crude oil polar chemical composition derived from FT− ICR mass spectrometry accounts for asphaltene inhibitor specificity.* Energy & Fuels, 2008. **22**(5): p. 3112-3117.

18. Wang, J., et al., *The properties of asphaltenes and their interaction with amphiphiles.* Energy & Fuels, 2009. **23**(7): p. 3625-3631.

19. Alhreez, M., D. Wen, and L. Ali. *A novel inhibitor for controlling Iraqi asphaltene problems*. in *2017 International Conference on Environmental Impacts of the Oil and Gas Industries: Kurdistan Region of Iraq as a Case Study (EIOGI)*. 2017. IEEE.

20. Zendehboudi, S., N. Rezaei, and A. Lohi, *Applications of hybrid models in chemical, petroleum, and energy systems: A systematic review.* Applied energy, 2018. **228**: p. 2539-2566.

21. Alavi, S., *Molecular simulations: fundamentals and practice*. 2020: John Wiley & Sons.

22. Jian, C. and T. Tang, *One-dimensional self-assembly of polyaromatic compounds revealed by molecular dynamics simulations.* The Journal of Physical Chemistry B, 2014. **118**(44): p. 12772-12780.

23. Tazikeh, S., et al., *Molecular dynamics simulation to investigate the effect of polythiophene-coated Fe3O4 nanoparticles on asphaltene precipitation.* Chemical Engineering Science, 2021. **237**: p. 116417.

24. Mehana, M., M. Fahes, and L. Huang, *Asphaltene Aggregation in Oil and Gas Mixtures: Insights from Molecular Simulation.* Energy & Fuels, 2019. **33**(6): p. 4721-4730.

25. Jian, C., T. Tang, and S. Bhattacharjee, *Probing the effect of side-chain length on the aggregation of a model asphaltene using molecular dynamics simulations.* Energy & fuels, 2013. **27**(4): p. 2057-2067.

26. Headen, T., et al., *Simulation of asphaltene aggregation through molecular dynamics: Insights and limitations.* Energy & Fuels, 2017. **31**(2): p. 1108-1125.

27. Javanbakht, G., et al., *Molecular polydispersity improves prediction of asphaltene aggregation.* Journal of Molecular Liquids, 2018. **256**: p. 382-394.

28. Lan, T., H. Zeng, and T. Tang, *Understanding adsorption of violanthrone-79 as a model asphaltene compound on quartz surface using molecular dynamics simulations.* The Journal of Physical Chemistry C, 2018. **122**(50): p. 28787-28796.

29. Ji, D., et al., *Adsorption of C5Pe molecules on silica surfaces with different hydrophobicity studied by molecular dynamics simulation.* Applied Surface Science, 2019. **495**: p. 143624.

30. Mohammed, S. and G. Gadikota, *The role of calcite and silica interfaces on the aggregation and transport of asphaltenes in confinement.* Journal of Molecular Liquids, 2019. **274**: p. 792-800.

31. Bai, Y., et al., *Effects of the N, O, and S heteroatoms on the adsorption and desorption of asphaltenes on silica surface: A molecular dynamics simulation.* Fuel, 2019. **240**: p. 252-261.

32. Liu, F., et al., *Effects of molecular polarity on the adsorption and desorption behavior of asphaltene model compounds on silica surfaces.* Fuel, 2021. **284**: p. 118990.

33. Wang, J., et al., *Understanding the effects of salinity on bitumen-calcite interactions.* Fuel Processing Technology, 2021. **213**: p. 106668.

34. Taheri-Shakib, J., et al., *Wettability alteration by surface adsorption of asphaltene molecular in carbonate porous media.* Journal of Molecular Liquids, 2022. **345**: p. 118128.

35. AlMubarak, T., et al. *Investigation of Acid-Induced Emulsion and Asphaltene Precipitation in Low Permeability Carbonate Reservoirs*. in *SPE Saudi Arabia Section Annual Technical Symposium and Exhibition*. 2015.

36. Ghamartale, A., et al., *Effects of inhibitor concentration and thermodynamic conditions on n-octylphenol-asphaltene molecular behaviours.* Journal of Molecular Liquids, 2021. **340**: p. 116897.

37. Fu, C.-F. and S.X. Tian, *A comparative study for molecular dynamics simulations of liquid benzene.* Journal of chemical theory and computation, 2011. **7**(7): p. 2240-2252.

38. Xiao, S., S.A. Edwards, and F. Gräter, *A new transferable forcefield for simulating the mechanics of CaCO3 crystals.* The Journal of Physical Chemistry C, 2011. **115**(41): p. 20067-20075.

39. Wang, W., et al., *Nanoaggregates of diverse asphaltenes by mass spectrometry and molecular dynamics.* Energy & Fuels, 2017. **31**(9): p. 9140-9151.

40. Ghamartale, A., S. Zendehboudi, and N. Rezaei, *New Molecular Insights into Aggregation of Pure and Mixed Asphaltenes in the Presence of n-Octylphenol Inhibitor*. Energy & Fuels, 2020. **34**(10): p. 13186-13207.

41. Goual, L., et al., *Asphaltene aggregation and impact of alkylphenols.* Langmuir, 2014. **30**(19): p. 5394-5403.

42. Sedghi, M. and L. Goual. *Molecular dynamics simulations of asphaltene dispersion by limonene and pvac polymer during Co2 flooding*. in *SPE International Conference and Exhibition on Formation Damage Control*. 2016. OnePetro.

43. Lowry, E., M. Sedghi, and L. Goual, *Polymers for asphaltene dispersion: Interaction mechanisms and molecular design considerations.* Journal of Molecular Liquids, 2017. **230**: p. 589-599.

44. Lowry, E., M. Sedghi, and L. Goual, *Novel dispersant for formation damage prevention in CO2: a molecular dynamics study.* Energy & Fuels, 2016. **30**(9): p. 7187-7195.

45. Headen, T.F., E.S. Boek, and N.T. Skipper, *Evidence for asphaltene nanoaggregation in toluene and heptane from molecular dynamics simulations.* Energy & Fuels, 2009. **23**(3): p. 1220-1229.

46. Bauer, P., B. Hess, and E. Lindahl, *GROMACS 2022 Manual*. 2022.

47. Sambasivarao, S.V. and O. Acevedo, *Development of OPLS-AA force field parameters for 68 unique ionic liquids.* Journal of chemical theory and computation, 2009. **5**(4): p. 1038-1050.

48. Mohammed, S. and G. Gadikota, *The influence of CO2 on the structure of confined asphaltenes in calcite nanopores.* Fuel, 2019. **236**: p. 769-777.

49. Mohammed, S. and G. Gadikota, *Dynamic wettability alteration of calcite, silica and illite surfaces in subsurface environments: a case study of asphaltene self-assembly at solid interfaces.* Applied Surface Science, 2020. **505**: p. 144516.

50. Norinaga, K., et al., *Measurement of Self-Diffusion Coefficient of Asphaltene in Pyridine by Pulsed Field Gradient Spin− Echo 1H NMR.* Energy & Fuels, 2001. **15**(5): p. 1317-1318.

51. Atta, A.M., et al., *Effect of different families of hydrophobic anions of imadazolium ionic liquids on asphaltene dispersants in heavy crude oil.* Energy & Fuels, 2017. **31**(8): p. 8045-8053.

52. Boukherissa, M., et al., *Ionic liquids as dispersants of petroleum asphaltenes.* Energy & Fuels, 2009. **23**(5): p. 2557-2564.

6. CHAPTER SIX

Summary and Recommendations for Future Work

This study focuses on modeling and simulation of asphaltene precipitation and deposition control using the molecular dynamics (MD) method and GROMACS package. The MD approach is used to reveal important mechanisms between the asphaltene and chemical inhibitors. In each phase of this study, the influences of different key factors, such as asphaltene structure, inhibitor concentration, pressure, and temperature, on asphaltene precipitation and deposition are studied. This thesis includes six chapters: Introduction and overview (chapter one), aggregation study of pure and mixed asphaltenes in the presence of *n*-Octylphenol inhibitor at the molecular level, in which we mainly investigate the impact of asphaltene structure in systems with one and two types of asphaltene structures (chapter two). Then, the effects of inhibitor concentration and thermodynamic conditions on *n*-Octylphenol-asphaltene molecular behaviours are assessed. We study the effect of *n*-Octylphenol in 0-15 wt% concentrations for systems having various asphaltene structures for both cases when a single and a binary type of asphaltene structure exist in the system. We also further highlight the importance of pressure and temperature during the inhibition process in chapter three. In chapter four, the impact of chemical inhibitors on asphaltene binding arrangement is studied using the MD simulation strategy. In this work, the angle and distance between molecules are considered at the same time to distinguish the binding arrangement types between the asphaltene molecules in the presence of a surfactant (*n*-Octylphenol) and two ionic liquids (1-Butyl-3-methylimidazolium bromide and 1-Butyl-3-methylimidazolium chloride) (chapter four). Chapter five investigates asphaltene deposition in calcite pore in the presence of two different inhibitors individually and simultaneously. The current chapter (chapter six) contains the summary and recommendations.

6.1 New Molecular Insights into Aggregation of Pure and Mixed Asphaltenes in the Presence of *n*-Octylphenol Inhibitor (Chapter 2)

The screening and designing of an inhibitor to prevent asphaltene aggregation need further in-depth investigation and clarification. MD is a powerful method to study the mechanisms of physical phenomena at the molecular level. This work evaluates the importance of asphaltene structure and the ability of the asphaltene to form common bonds during the asphaltene aggregation, such as acid-base or hydrogen bonds, in screening and designing a chemical inhibitor. To achieve the objective, one archipelago and two continental asphaltene structures are used both individually and in combination in *n*-heptane. *n*-Octylphenol (OP) is the investigated inhibitor in this particular work. The simulation results are verified by the results of literature simulation. The main findings/conclusions of the first phase are as follows:

- The archipelago asphaltene does not aggregate significantly in the absence of OP; nevertheless, OP reduces the aggregation.
- Continental asphaltene with the potential to form hydrogen bonds (A2) has a higher aggregation rate than continental asphaltene without the capability to form hydrogen bonds (A3).
- OP effectively reduces the aggregation rate of A2 at the early stage due to the formation of strong hydrogen bonds between the asphaltene and OP.
- The A2-OP pairs can form fragile aggregates as the OP in the aggregate complex provides void spaces proved by aggregate density reduction.
- For the mixed asphaltene systems, OP considerably lowers the aggregation rate when A2 and A3 are simultaneously present; the higher relative portion of OP to A2 is the main reason for this behavior.

- Our study's results agree with the Gray’s statement, highlighting the importance of considering different interactions other than aromatic stacking in the asphaltene aggregation studies.
- OP has a different level of effectiveness (as an inhibitor), depending on the type of asphaltene structure, the relative concentration of OP to asphaltene, and the heterogeneity in the asphaltene structure.
- While the hierarchical paradigm is confirmed for asphaltene aggregation, the gyration radius of the aggregates is suggested to be considered as a criterion for differentiating between the aggregates.

6.2 Effects of Inhibitor Concentration and Thermodynamic Conditions on *n*-Octylphenol-Asphaltene Molecular Behaviours (Chapter 3)

In this research phase, MD is used to study the effect of inhibitor concentration, pressure, and temperature on asphaltene-inhibitor interaction. The asphaltene concentration is 7 wt %, while the OP concentration varies between 0 and 15 wt%. In the pressure evaluation part, the pressure changes between 1 bar and 60 bar when the temperature is constant at 300 K. In the temperature evaluation phase, the temperature varies from 300 to 360 K, while the pressure is fixed at 1 bar. The reliability of simulation results is proved by verifying the asphaltene aggregation reduction because of pressure enhancement in the isothermal process and asphaltene aggregation incremental due to increasing temperature in the isobaric process. The main outcomes of this phase are as follows:

- For A1, the average aggregation number and the aggregate density analysis show that the aggregation intensity reduces slightly when the OP concentration is increased.

- Increasing the OP concentration (above 7 wt%) results in unstable aggregates with very low density for the system that incorporates A2.
- OP increases the variations in the aggregate shape and type for A2 aggregates.
- In the system with a mixture of the archipelago and continental asphaltenes, the OP appears to be an effective inhibitor at a concentration higher than 7 wt% such that the average aggregation and aggregate gyration radius are reduced significantly at 15 wt% OP compared to the case with no inhibitor.
- Pressure evaluation shows that OP has an optimum effect at 30 bar, at which OP presence makes aggregates unstable, increases the aggregate gyration radius, and decreases the aggregate density.
- The pressure increase does not change the aggregate shape in the presence and absence of the OP.
- The result reveals that OP efficiency increases by increasing temperature.
- The hardware analysis shows that parallelizing calculation and integrating GPUs with CPUs can speed up the simulation approximately three times compared to the system processing with only CPUs.

6.3 Impact of Chemical Inhibitors on Asphaltene Binding Arrangement: Molecular Dynamics Simulation Strategy (Chapter 4)

MD is used in this research phase to study the asphaltene binding arrangement types when aggregates are formed. The binding arrangement is studied for two types of asphaltenes, one with the potency to form hydrogen bonds (A2) and one without hydrogen bonding (A3). The *n*-Octylphenol and two ionic liquids are studied to determine the impact of different inhibitor structures. In this study, we suggest incorporating two angles between asphaltene molecules in

addition to the distance between asphaltene centers to distinguish the type of binding arrangements and avoid false decisions. The asphaltene concentration is considered to be 7 wt % in *n*-heptane. Three different inhibitors, including a surfactant (*n*-Octylphenol) and two ionic liquids (1-Butyl-3-methylimidazolium bromide and 1-Butyl-3-methylimidazolium chloride), are added to the system with the concentration of 7 wt%. The key outcomes of this phase are as follows:

- The angular criteria include the angle between the polyaromatic cores of two molecules and the angle between a vector connecting the centers of polyaromatic cores and the resultant vector of plane normals ($\vec{R}$).
- OP will not stop the quadrupole-quadrupole interaction between the asphaltenes since the force between OP's benzene ring and the asphaltene polyaromatic core is weaker than the force between two polyaromatic cores.
- OP does not show a promising potential to reduce the parallel stacking, especially for the asphaltene with no hydrogen bonding potential, while it reduces the T-shape arrangement relatively for both asphaltene structures.
- The ionic liquids (ILs) beat the quadrupole-quadrupole interaction between the asphaltene cores with cation-quadrupole force and notably reduce the parallel stacking.
- ILs lower the number of T-shape binding arrangements between the asphaltene molecules, specifically for A2 in the presence of 1-Butyl-3-methylimidazolium chloride due to the higher charge density of chloride compared to bromide.
- Chloride has a higher anion charge density than bromide because of a smaller anion size with a similar charge. The higher charge density enables chloride to act as an electron donor and bind with the asphaltene electron cloud.

6.4 Mechanistic Study on Chemical Inhibitors for Control of Asphaltene Deposition in Calcite Pore (Chapter 5)

This research focuses on investigating asphaltene deposition in the calcite pore when the carrying fluid is *n*-heptane in the presence of *n*-Octylphenol and 1-Butyl-3-methylimidazolium chloride using MD. The inhibitors are used both individually and as a mixture with various ratios. The simultaneous presence of inhibitors is tested to explore if they will boost or interrupt each other's efficiency. We validate our results by assessing the asphaltene diffusivity trend in the bulk and the confined area. The asphaltene concentration and inhibitor concentration are 7 wt % each in *n*-heptane. In the case of systems with a mixture of inhibitors, the cumulative inhibitor concentration is 7 wt% with the following OP:IL ratios: 1:3, 1:1, 3:1. The major outcomes of this phase are as follows:

- OP reduces the asphaltene aggregation by attaching to the asphaltene through hydrogen bonds.
- OP reduces the Lennard-Jones (LJ) and Coulomb energies between the asphaltene and calcite by 400 and 1000 kJ/mol; respectively, leading to the asphaltene deposition reduction by adsorbing on the calcite surface and providing a hindrance layer.
- The IL copes with the quadrupole-quadrupole interaction between the asphaltene polyaromatic cores and reduces the asphaltene face-to-face aggregation.
- IL cannot provide a hindrance layer near the calcite surface since the cation's alkyl carbon tail is not long enough, according to the literature and our results.
- The systems with combined inhibitors benefit from both prevention mechanisms resulting from OP and IL.

- The 3:1 OP-IL ratio shows the optimum effect, reducing both precipitation and deposition. The average aggregation number reduces from 20 to less than 10 and the deposition rate from 1 to 0.8 compared to the case without inhibitor.

6.5 Recommendations for Future Work

In our studies, we only considered the impact of hydrogen bonding in asphaltene molecules other than the aromatic stacking, while according to the literature, asphaltene structure can form other associations such as metal coordination complex and a hydrophobic pocket as a part of aggregation mechanisms. Therefore, it is recommended to investigate the impact of different association energies between asphaltene in the presence of chemical inhibitors. In this research, we only considered the non-ionic surfactants and ionic liquids as asphaltene inhibitors, while other inhibitor types, such as ionic surfactants and nanoparticles, may follow different inhibition mechanisms. Therefore, it is recommended to study other types of inhibitors and demystify their behaviors with asphaltenes. The current study did not consider the impact of intruders or natural suspenders such as salt ions and resin during the inhibition process, which can be a potential topic for further studies. The influence of using combined types of inhibitors was addressed briefly in this study; thus, it can be interesting to combine different types of inhibitors with various inhibition mechanisms and figure out if they interrupt or boost each other's performance. The carrying fluid for asphaltene in all parts of this study was *n*-heptane. As the impact of carrying fluid is important during the asphaltene aggregation, different fluids can be considered during the inhibitors' prevention studies. We also recommend considering the effect of asphaltene deposition on various surfaces (in terms of type, morphology, and composition) such as silica and steal in the presence of chemical inhibitors. In addition, the potential chemical reaction of fluid components and surfaces at particular thermodynamic conditions can be studied by hybridizing MD and density

functional theory. We suggested new criteria for differentiation between asphaltene binding arrangements, which we believe can be improved and addressed in the follow-up studies. The result of this study can significantly contribute to designing chemical inhibitors. As another recommendation, the MD simulation may be coupled with artificial intelligence and machine learning approaches to make the designing process more efficient.

Based on the literature review, two forcefields of GROMOS and OPLS have been used and recommended in the studies of organic materials. In this research, OPLS-All Atom is also used for simulations, while evaluating different forcefields and tuning their parameters during the simulation of the asphaltene-inhibitor system may lead to interesting outcomes. The results of this study can be validated by experimental approaches such as microfluidic systems.

The mentioned follow-up research will help further understand the interactions between the asphaltene and inhibitors during asphaltene deposition. Such studies help researchers, engineers, and companies screen, design, and evaluate the potential chemicals before conducting laboratory experiments, making the procedure cost-effective and efficient.